Finanziato dall'Unione europea NextGenerationEU
Ministero dell'Università e della Ricerca
Italiadomani PIANO NAZIONALE DI RIPRESA E RESILIENZA
UNIVERSITÀ DEGLI STUDI FIRENZE

DOTTORATO DI RICERCA IN

Scienze Chimiche

CICLO XXXVIII - ex *DM 352/2022*

Identification of biologically active peptides through innovative liquid chromatography–mass spectrometry technologies in self-recoverable protein materials to be developed into active ingredient.

Settore Scientifico Disciplinare

CHEM-05 /A

Dottorando/a

Dott.ssa Margherita Marino

Margherita Marino

Supervisore

Prof.ssa Anna Maria Papini

APapini

Coordinatore

Prof.ssa Anna Maria Papini

APapini

Contents

Contents 1

Part 1 10

1. Introduction 10

1.1 Therapeutic antibodies 10

1.1.1 Example of therapeutic antibodies 12

1.1.1.1 Rituximab 12

1.1.1.2 Matuzumab 14

1.1.1.3 Trastuzumab 16

1.1.2 Design of therapeutic antibody conjugates 17

1.2 Cell-penetrating peptides 18

1.2.1 Oligoarginines 21

2. Aim of the PhD research work 23

3. Results and Discussion 28

3.1 Production of constructs of three therapeutic antibodies for intracellular delivery 28

3.1.1 Design of selected oligoarginines 28

3.1.2 Solid-phase synthesis of oligoarginine peptides 31

3.1.3 In situ modification and activation of the therapeutic antibody to form the Antibody-sulfoSMCC-Rn conjugates 36

3.1.4 Chemistry of the maleimido crosslinker 38

3.1.5 Optimization of the conjugation reactions 39

3.1.6 Impact of TFA salts on the conjugation performance 42

3.1.7 Estimation of protein concentration 44

3.1.7.1 SDS-PAGE Gel Electrophoresis 44

3.2 Purification of therapeutic antibodies screening of non-denaturing liquid chromatography techniques 47
3.2.1 Size exclusion chromatography 50
3.2.1.1 High-pressure size exclusion chromatography 51
3.2.1.2 Semi-preparative size exclusion chromatography 52
3.2.2 Hydrophobic interaction chromatography 56
3.2.2.1 High-pressure hydrophobic interaction chromatography 57
3.2.2.2 Semi-preparative hydrophobic interaction chromatography 61
3.2.3 Ion exchange chromatography 63
3.2.3.1 High-pressure ion exchange chromatography 64
3.2.3.2 Semi-preparative ion exchange chromatography 73
3.2.4 Mixed-mode chromatography (MMC) 78
3.2.4.1 Semi-preparative mixed-mode chromatography 80
3.2.5 Reversed-phase chromatography 87
3.2.5.1 High-pressure reversed phase chromatography 87
3.2.6 Final remarks 90
3.3 Multi-dimensional Liquid Chromatography (mD-LC) 92
3.3.1 Construction and validation of two-dimensional chromatography system 92
3.3.2 Two-dimensional liquid chromatography system with an online desalting step 114
3.4 Mass Spectrometry 120
4. Conclusion and future perspectives 128
5. Experimental part 133
5.1 Materials 133
5.2 Methodologies 135
5.2.1 Peptide synthesis 135

5.2.1.1 Procedure for Microwave-assisted automatic SPPS 135
5.2.1.2 Procedure of purification and characterization of the synthetic peptides 137
5.2.3 Conjugation procedure 139
5.2.4 Electrophoresis on gel.....139
5.2.5 Chromatographic operating conditions 141
5.2.5.3 Ion exchange chromatography.....141
5.2.5.4 Mixed-mode chromatography.....142
5.2.5.5 Reversed-phase liquid chromatography 142
5.2.6 Multi-dimensional liquid chromatography 142
5.2.6.1 Size-exclusion chromatography.....143
5.2.6.2 Ion-Exchange Chromatography 143
5.2.6.3 Mixed-Mode Chromatography 143
5.2.6.4 Multidimensional chromatographic workflows 144
5.2.7 Deglycosylation of monoclonal antibodies 144
5.2.8 Trypsin/Chymiotrypsin Digestion Protocol 145
5.2.9 LC-MS Analysis 145
Appendix 1-Strategy of conjugation for therapeutic monoclonal antibodies and their conjugates 147
Appendix 2- Multi dimensional liquid chromatography (mD-LC).....165
Appendix 3 - Mass spectrometry.....181
Appendix 4 - Q Exactive™ Plus Orbitrap mass spectrometer 195
Part 2 200
1. Introduction 200
1.1 Background 200
1.2 Protein Glycation and Advanced Glycation End Products (AGEs) in diabetes 201

1.2.1 Glycated peptides as biomarkers for diabetes 202
1.3 Analytical techniques to identify and characterize glycation.....204
1.3.1 Fluorescence Spectroscopy 205
1.3.2 Boronate affinity chromatography 205
1.3.2.1 Analytical and biomedical applications.....207
1.4 Analytical strategy for profiling glycated peptides in complex biological samples by LC-MS and MS tandem.....208
1.4.1 Tandem Mass Spectrometry for Glycated Peptide Analysis 211
2. Aim of PhD research work 213
3. Results and discussion 215
3.1 Preparation of solid supports for the specific capture of deoxyfructosylated peptides 215
3.1.1 Functionalization of resins varying the solid supports nature and units of phenylboronic acid 216
3.1.1.1 Preparation of bi substituted phenylboronate resins 217
3.1.1.2 Preparation of mono substituted phenylboronate resins 219
3.2 Synthesis of specific deoxyfructosylated peptide fragments 221
3.2.1 Glycation of peptides via Boratyński strategy 225
3.3 Boronate affinity chromatography 230
3.3.1 Boronate affinity chromatography: from peptide mixture to complex biological mixtures 230
3.3.1.1 Screening of Meta-Substituted resins 232
3.3.1.2 Para vs Meta Orientation: structural influence 233
3.3.1.3 Comparative evaluation with Commercial supports.....234
3.3.1.4 Application to Complex Biological Samples 235
3.4 Mass Spectrometry 240
3.4.1 MS^n for glycated peptides 240

4. Conclusion and future perspectives 244

5. Experimental part 249

5.1 ChemMatrix® Rink resin and Agarose Rink resin functionalization with boronate units 249

5.1.1 Synthesis of p-PhB-Lys(p-PhB)-ChemMatrix® Rink resin (Resin **1**) and m-PhB-Lys(m-PhB)-ChemMatrix® Rink resin (Resin **2**) 249

5.1.2 Synthesis of Ac-Lys(p-PhB)-ChemMatrix® Rink resin (Resin **3**) and Ac-Lys(m-PhB)-ChemMatrix® Rink resin (Resin **4**) 250

5.1.3 Synthesis of p-PhB-Lys(p-PhB)-Agarose Rink resin (Resin **5**) and m-PhB-Lys(m-PhB)-Agarose Rink resin (Resin **6**) 251

5.1.4 Synthesis of Ac-Lys(p-PhB)-Agarose Rink resin (Resin 7) and Ac-Lys(m-PhB)-Agarose Rink resin (Resin 8) 252

5.1.5 Loading of the new functionalized phenylboronate resins 253

5.2 Synthesis of glycated peptides 253

5.2.1 Solid-phase peptide synthesis by microwave automated synthesizer 253

5.2.1.1 Procedure for Microwave-assisted automatic SPPS 253

5.2.1.2 Boratyński protocol reaction for peptide glycation 255

5.3 Boronate affinity chromatography: from peptide to complex biological mixtures 255

5.3.1 General procedure of capturing of glycated peptides by the new functionalized resin (R1 – R8) 255

5.3.2 Experiment 1: Screening of meta-PhB-functionalized resins CMXRR (R2, R4) Resin and meta AGRR resin (R6, R8) 256

5.3.3 Experiment 2: Comparison of selected para CMXRR Resin (R3) and para AGRR resin (R7) 257

5.3.4 Experiment 3: Capturing comparison of Ac-Lys(m-PhB)-CMXRR(R4) and PBA-agarose resins 257

5.4 Trypsin/Chymiotrypsin Digestion Protocol 257

5.5 LC-MS Analysis 258
Appendix 1 - LTQ XL™ mass spectrometer 259
6. Bibliography 265

The present thesis was completed in the context of industrial PhD in partnership with PeptLab (University of Florence, Italy), Fischer Analytics GmbH (Bingen am Rhein, Germany) and Radiopharmazeutische Chemie (University Clinic Heidelberg, Germany).

Part 1

1. Introduction

1.1 Therapeutic antibodies

Therapeutic antibodies are immunoglobulin-based biopharmaceuticals engineered to bind with high specificity and affinity to disease-associated antigens and modulate pathological pathways.[1]

Since the first monoclonal antibody (mAb) approved as therapeutics in 1986.[2] This class of drugs has expanded from murine IgG to chimeric, humanized, and fully human formats, as well as to engineered derivatives such as Fc-modified antibodies, bispecific and antibody–drug conjugates (ADCs).[3,4,5] This evolution has been driven by the integration of molecular immunology, recombinant DNA technology, and structural biology, as well as by improvements in hybridoma methods and the introduction of display technologies including phage and yeast display,[6] transgenic mouse platforms, and deep sequencing of human B-cell repertoires.[7] Collectively, these advances have allowed for the rapid generation of high-affinity human antibodies against virtually any molecular target of therapeutic interest.[8]

Structurally, a typical IgG antibody is a Y-shaped glycoprotein with a molecular weight of approximately 150 kDa, composed of two identical heavy chains and two identical light chains linked by disulfide bridges.[9] The molecule is organized into two main functional regions: the fragment antigen-binding (Fab) arms and the crystallizable fragment (Fc).[10] The Fab arms contain variable regions that determine antigen specificity and affinity through complementarity-determining regions (CDRs), while the Fc portion mediates effector functions and determines pharmacokinetic behavior.

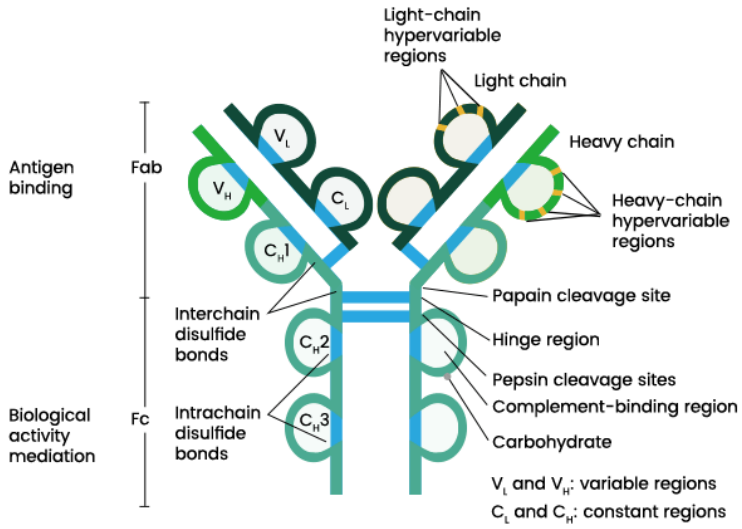

Fig. 1: Structure of an Immunoglobulin G.[11,12]

Human therapeutic antibodies primarily belong to the IgG1, IgG2, or IgG4 subclasses, each with distinct effector properties.[13] IgG1 antibodies exhibit strong binding to Fcγ receptors and are therefore suited for applications requiring immune effector recruitment,[14] such as antibody-dependent cellular cytotoxicity (ADCC) or complement-dependent cytotoxicity (CDC).[15] Conversely, IgG4 antibodies, which exhibit minimal Fc-mediated immune activation, are preferred when neutralization or receptor blockade is the desired mechanism of action.[16]

The clinical impact of therapeutic antibodies virtually connects all major domains of medicine. In oncology, antibodies serve as targeted cytostatic or cytotoxic agents, as immune checkpoint inhibitors, and as precision vehicles for drug delivery.[17,18] The introduction of immune checkpoint inhibitors targeting CTLA-4, PD-1, and PD-L1 has revolutionized cancer therapy by unleashing

endogenous antitumor immunity, resulting in durable responses in malignancies previously refractory to conventional treatments.[19]

Similarly, ADCs can deliver potent chemotherapeutics selectively to tumor cells, minimizing collateral damage to healthy tissues.[20]

In autoimmune and inflammatory diseases, antibodies targeting proinflammatory cytokines and their receptors, such as tumor necrosis factor alpha (TNF-α),[21] interleukin-6 receptor (IL-6R),[22,23] have transformed management paradigms for conditions including rheumatoid arthritis, Crohn's disease, and multiple sclerosis.[24] The COVID-19 pandemic has further demonstrated the rapid adaptability of the antibody platform, as fully human neutralizing antibodies were identified, optimized, and brought into clinical evaluation within months of pathogen identification.[25,26] Collectively, these examples illustrate the broad therapeutic versatility of antibodies across oncology, immunology, infectious diseases, and beyond.

1.1.1 Example of therapeutic antibodies

1.1.1.1 Rituximab

Rituximab is a chimeric monoclonal antibody targeting CD20. CD20 is a transmembrane protein expressed on pre-B and mature B lymphocytes, but absent on plasma cells.[27]

Rituximab has a pivotal role in therapy. Its capacity to selectively deplete CD20+ B cells, enables treatment of B-cell mediated diseases, such as non-Hodgkin's lymphoma and chronic lymphocytic leukemia (for which use Rituximab has been approved), as well as certain autoimmune diseases.[28]

The mechanism of action of Rituximab is multifaceted, primarily involving three pathways. First, antibody-dependent cellular cytotoxicity (ADCC), where

immune effector cells like natural killer (NK) cells recognize and lyse the Rituximab-coated B cells via Fcγ receptor engagement. Second, complement-dependent cytotoxicity (CDC), in which binding of Rituximab to CD20 activates the complement cascade, resulting in membrane attack complex formation and direct lysis of B cells. Third, Rituximab induces direct apoptotic signaling in the targeted B-cells and modulates B-cell receptor signaling, contributing to B-cell elimination.[29]

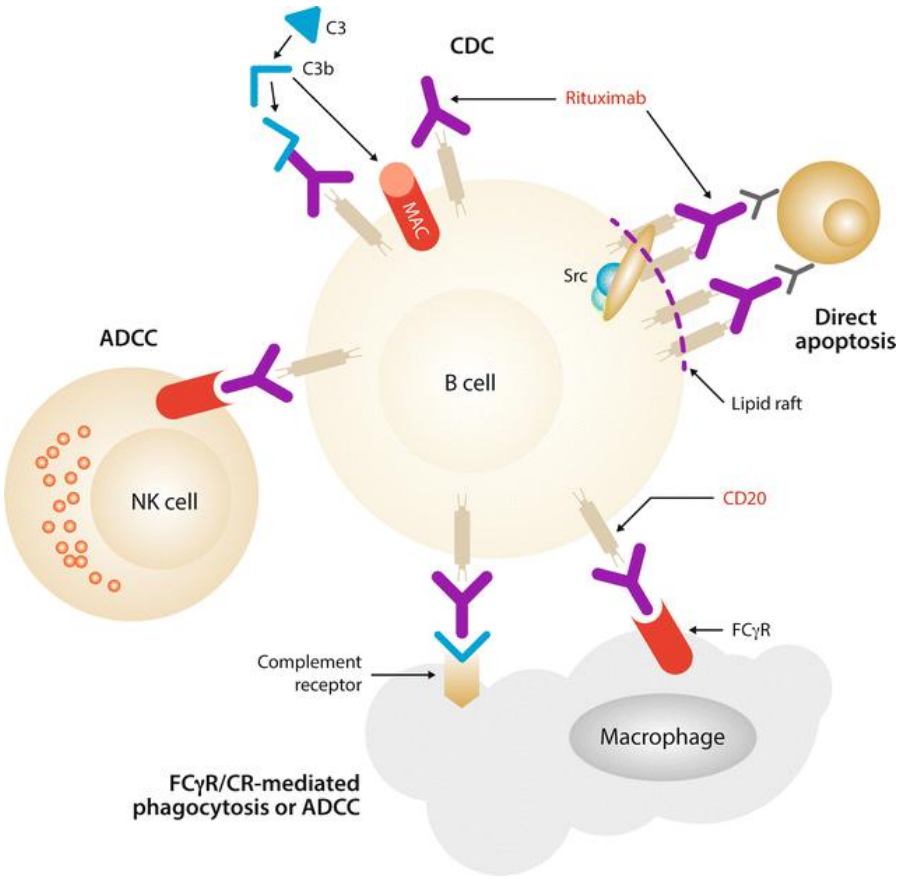

Fig. 2: Schematic representation of Rituximab's mechanism of action.[30]

Beyond oncology, Rituximab is used off-label and has been approved for autoimmune conditions such as rheumatoid arthritis, granulomatosis with polyangiitis, and microscopic polyangiitis, where B-cell depletion helps to suppress pathogenic autoimmune response. Rituximab efficacy and durable B-cell depletion have revolutionized management of these diseases by enabling targeted immune modulation with a relatively favorable safety profile.[31]

1.1.1.2 Matuzumab

Matuzumab is a humanized IgG1 monoclonal antibody targeting the epidermal growth factor receptor (EGFR), which is frequently overexpressed in various epithelial cancers.[32]

The mechanism of action of Matuzumab operates through several pathways. Primarily, it competitively inhibits the binding of natural ligands such as EGF to EGFR, hence blocking the activation of tyrosine kinase (TK) receptor, a critical step for downstream signaling pathways promoting tumor cell proliferation, survival, and migration. Matuzumab sterically prevents the EGFR conformational rearrangement required for high-affinity ligand binding and receptor dimerization, blocking indirectly the receptor activation.[33] Additionally, Matuzumab induces receptor downregulation via endocytosis and intracellular degradation, leading to prolonged inhibition of EGFR signaling. Preclinical studies also suggest that Matuzumab can mediate antibody-dependent cellular cytotoxicity (ADCC) through its IgG1 Fc region, contributing to tumor cell lysis mediated by immune effector cells.

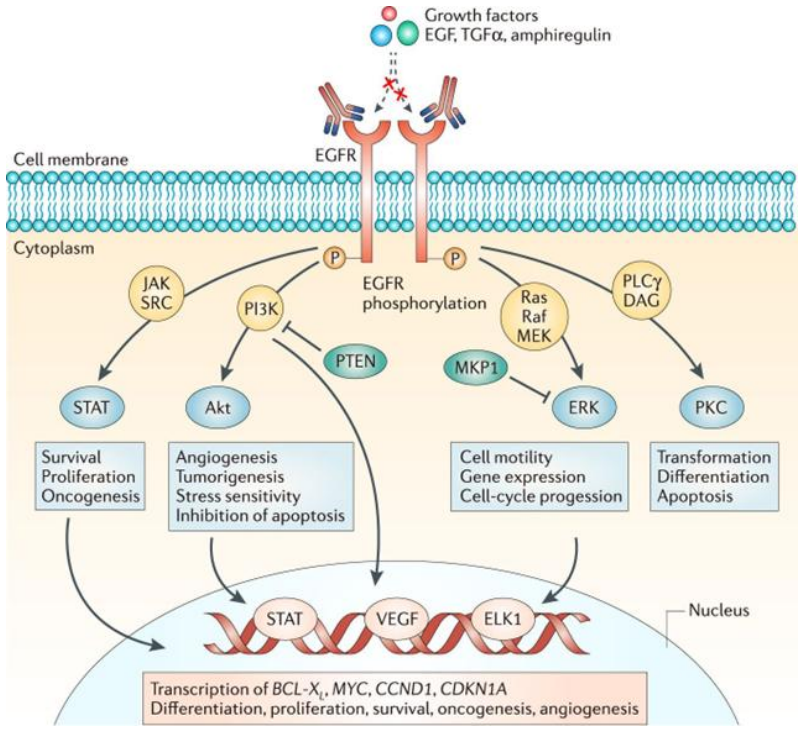

Fig.3: Schematic overview of Matuzumab mechanisms of action.[34]

Clinically, the use of Matuzumab has been investigated in several cancers including colorectal, lung, esophageal, and stomach cancers. Despite promising preclinical results and phase I data demonstrating safety and biological activity, phase II trials showed limited efficacy, leading to discontinuation of some development programs. However, Matuzumab remains a valuable example of targeting EGFR with a distinct mechanism different from tyrosine kinase inhibitors or other anti-EGFR antibodies.[35]

1.1.1.3 Trastuzumab

Trastuzumab is a humanized monoclonal antibody designed to target the HER2 receptor, which is overexpressed in approximately 15–20% of aggressive breast and gastric cancers.[36] Despite their lower prevalence, HER2-positive tumors are typically more aggressive and associated with poorer clinical outcomes, making them particularly challenging to treat.[37]

By specifically binding to domain IV of the extracellular portion of HER2, Trastuzumab effectively blocks receptor dimerization and activation, inhibiting crucial downstream signaling pathways, notably PI3K/Akt that drive tumor cell proliferation and survival. In addition to preventing HER2 activation, Trastuzumab promotes internalization and degradation of the receptor, thereby reducing HER2 levels on the tumor cell surface.

Beyond its direct inhibitory effects, Trastuzumab also recruits immune effector cells through its IgG1 Fc region, triggering antibody-dependent cellular cytotoxicity (ADCC) and facilitating targeted tumor-cell destruction.

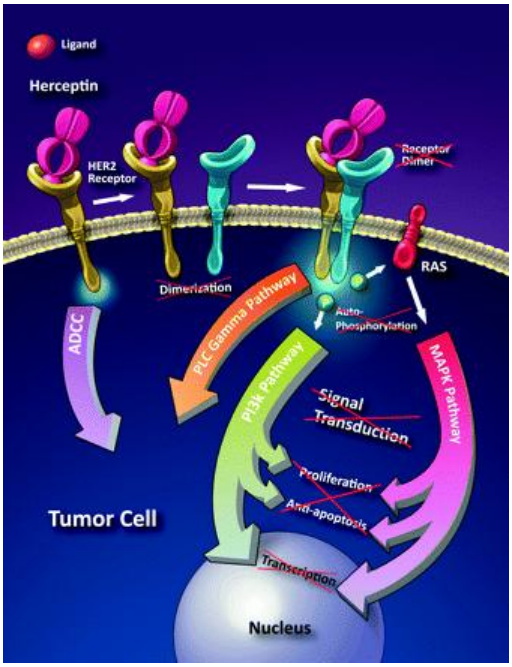

Fig. 4: Trastuzumab mechanism of action.[38]

Clinically, Trastuzumab has played a transformative role in the treatment of HER2-positive breast cancer, significantly improving patient outcomes in both early and metastatic settings when used alone or combined with chemotherapy. Its efficacy has also been extended to HER2-positive gastric and gastroesophageal cancers.[39]

With this multifaceted mechanism, combining growth signal inhibition, receptor downregulation, and immune activation, Trastuzumab exemplifies targeted cancer therapy, offering specific and durable tumor control with a favorable safety profile.[40]

1.1.2 Design of therapeutic antibody conjugates

Designing a therapeutic antibody involves the careful integration of biological and physicochemical properties to manufacturing considerations.[41] The design

must harmonize two core dimensions: biological potency[42] and molecular engineering. [42,43]

From a biological standpoint, the antibody must exhibit high specificity and sufficient affinity to ensure robust target engagement at therapeutic concentrations.[8] However, extremely high affinities can paradoxically hinder tissue distribution, particularly within solid tumors, where diffusion and target-mediated clearance can limit penetration.[44]

Concerning limitations, therapeutic antibodies can face several inherent constraints connected to their nature. One persistent concern is the immunogenicity, since even fully human antibodies can elicit anti-drug antibodies (ADAs) that neutralize therapeutic efficacy or induce hypersensitivity reactions. Studies in sequence optimization and glycoengineering are reducing these risks but do not completely eliminated them. Their large molecular size is an additional concern. The size, in fact, can restrict tissue penetration, particularly in dense or poorly vascularized tumors and in sanctuary sites such as the central nervous system. Efforts to overcome this include the development of smaller antibody fragments, engineered binding domains, and receptor-mediated transcytosis mechanisms.

In this context, the conjugation or fusion of cell-penetrating peptides (CPPs) to antibody fragments has emerged as a promising strategy to enhance intracellular delivery and tissue penetration.[45]

1.2 Cell-penetrating peptides

Cell penetrating peptides (CPPs) are a well-established class of short peptides (up to 30 amino acids) capable of crossing the cytoplasmic membrane and facilitating the intracellular delivery of various cargos, including small

molecules, proteins, nucleic acids, nanoparticles, and imaging agents, either via covalent bond or non-covalent complexation.[46]

Their significance in therapeutic and diagnostic contexts lies in their ability to circumvent the cell membrane's selective permeability barrier, thereby enhancing intracellular access to bioactive agents that otherwise exhibit poor uptake.

CPPs are produced either through chemical synthesis in solid-phase, which offers precise control over sequence and modifications, or via recombinant expression in microbial systems when delivering peptide-fusion constructs.[47]

CPP can be classified into subgroups according to their origin or sequence characteristics [48]

The most well-known group rely on positively charged sequences of amino acids, predominantly arginine and lysine residues, that at physiological pH facilitate electrostatic interactions with negatively charged cell-surface glycoproteins prior to internalization. Lysine and arginine carry the same net positive charge, but arginine residues are more effective in membrane penetration due to the presence of the guanidinium head group, since it enables the formation of hydrogen bonds with phosphate and sulfate groups of the plasma membrane, promoting the cellular uptake.[49] The number and order of basic amino acids, especially arginine, are critical factors for the efficiency.[50] Penetratin, TATp and polyarginines are the main low amphipathic class of peptides.[51,52,53] A second major class of CPPs is characterized by pronounced amphipathicity, in which the contribution to overall charge is primarily due to lysine residues, where MAO and transportan are the main peptides. The third

class of CPPs is composed of peptides in which charged and hydrophobic residues are separated in the amino acid chain such as pVEC and Pep-1.[54,55]

The internalization of CPPs occurs through distinct mechanisms that are primarily influenced by their physicochemical characteristics and the nature of the associated cargo. A exhaustive understanding of these uptake pathways is critical for the practical application of CPPs in therapeutic delivery.[56,57] Two types of intercellular uptake coexist: direct translocation across the plasma membrane, which occurs in an energy-independent manner, and endocytosis, which involves energy-dependent processes such as clathrin-mediated, caveolin-mediated, and macropinocytic pathways.

To support the systematic study and rational design of cell-penetrating peptides, several dedicated databases have been established to curate experimentally validated CPPs and their properties. Among these, CPPsite 2.0 (http://crdd.osdd.net/raghava/cppsite/) is a comprehensive resource that provides detailed information on CPP sequences, origin, length, cargo type, uptake efficiency, and biological activity, together with calculated physicochemical descriptors such as net charge, hydrophobicity, molecular weight, and isoelectric point. Complementarily, databases such as CellPPD (http://crdd.osdd.net/raghava/cellppd/) and MLCPP 2.0 (http://balalab-skku.org/mlcpp2/) integrate both experimentally validated and predicted CPPs, offering tools for sequence analysis, structure–function relationship studies, and in silico design of novel peptides. Collectively, these platforms enable correlation of sequence features with internalization efficiency and mechanism, thereby accelerating the development and optimization of CPP-based delivery systems.

1.2.1 Oligoarginines

Among the various subclasses of CPPs, oligoarginines, synthetic peptides composed of consecutive arginine residues i.e. (R_5 to R_{12}), have garnered extensive attention due to their high cationic charge density and efficient in cellular uptake. [58] These peptides demonstrate the ability to induce cancer cell death with differing degrees of efficacy through multiple underlying mechanisms.

The guanidinium moieties of arginine residues engage in bidentate electrostatic and hydrogen-bonding interactions with negatively charged cell-surface components such as glycosaminoglycans, thereby enhancing membrane binding and internalization [59], in fact arginine-rich peptides induce membrane manipulation/deformation that may activate ion channels, such as Ca^{2+} channel, signaling axis in tumor-targeted even if the specific delivery process remain unclear.[60] Crucially, length-dependent effects have been demonstrated: uptake is negligible for very short sequences (e.g., R_4), increases markedly for R_6 and R_8, but declines again for longer chains such as R_{10}, R_{12}, or R_{16}, potentially due to aggregation or altered interactions at the cell surface.[61,62]

A representative study by Jones in 2005 reports a comparative analysis of several CPPs, highlighting that polyarginines demonstrated one of the highest uptake efficiencies among them, though with increased cytotoxicity at higher concentrations.[63]

Structural modifications can further enhance polyarginine-mediated delivery: for example, fatty-acylation and cyclisation of short polyarginines (R_5, R_6) significantly boosted cellular uptake (up to ~13.7-fold for cyclic dodecanoyl-R_5) via energy-dependent endocytosis. Additionally, increasing rigidity through

cyclic backbones improves non-endocytic translocation efficiency by facilitating a more favorable spatial presentation of guanidinium groups.

2. Aim of the PhD research work

This PhD project was developed within an industrial–academic collaboration between Fischer Analytics GmbH (Bingen am Rhein, Germany) under the supervision of Dr. Hendrik Rusche, the Laboratory of Radiopharmaceutical Chemistry headed by Prof. Dr. Walter Mier (University clinic of Heidelberg, Germany), under the scientific supervision of Prof. Dr. Anna Maria Papini of the Interdepartmental Research Unit of Peptide & Protein Chemistry & Biology (University of Florence, Italy).

Fischer Analytics GmbH is a company specialized in advanced analytical technologies for biomolecules, with a strong focus on the development and application of innovative chromatographic and mass spectrometry platforms. Their expertise in multiple analytical modalities, including liquid chromatography and mass spectrometry, supported by bioinformatic tools for data integration and molecular characterization was relevant to develop this research work. The company mission is to translate advanced analytical strategies into practical solutions for biopharmaceutical and biotechnological applications, enabling precise characterization of complex biological molecules and conjugates.

The PhD work was positioned at the intersection of biotechnology, biopharmaceutical sciences, and analytical chemistry.

The partnership with Fischer Analytics provided access to technical expertise, and an environment focused on method innovation and industrial applicability, ensuring that the outcomes of this work could have direct translational potential in molecular characterization workflows for therapeutic biomolecules and quality control

This project also benefits from the scientific collaboration with Prof. Dr. Walter Mier's laboratory at the University of Heidelberg. The Heidelberg team provided expertise in therapeutic antibody research and clinical translation, in particular in biological and pharmacological evaluation of antibody-based constructs and oligoarginine peptides, supporting data interpretation from a biomedical and clinical perspective.

This synergy between the analytical strength of Fischer Analytics and the clinical focus of the Heidelberg group, together with the expertise in peptide chemistry of the Florence team, established an ideal platform for developing and validating new technologies at the interface between therapeutic innovation and analytical science.

The main objective of this PhD research was to develop a robust technology to prepare pure synthetic therapeutic monoclonal antibody conjugates for intracellular delivery.

A series of model therapeutic monoclonal antibodies constructs was synthesized using a non-specific lysine conjugation strategy. In particular the well-characterized monoclonal antibodies Rituximab, Matuzumab, and Trastuzumab that are commonly used in oncology and autoimmune diseases, were selected for this study. The conjugation employed a bifunctional linker enabling attachment of cell-penetrating arginine-rich peptides of varying length (R3C, R6C, R9C).

These constructs served as representative and reproducible test systems for assessing the performance of a new and efficient multi-dimensional liquid chromatography (2D-LC) system that I developed, particularly resolving

conjugation heterogeneity, determining drug-to-antibody ratio (DAR), and characterizing peptide attachment sites.

The 2D-LC system that I developed was conceived to enhance resolution, sensitivity, and structural insights. In this approach, a screening study of non-denaturing chromatographic techniques has been conducted to evaluate the possible integration of two, or more techniques, in a continuous system. This continuous flow configuration allowed to reduce manual sample handling preparation, selective collection of chromatographic fractions of interest, minimize material loss, and scale-up purification of larger volumes while maintaining the integrity of sensitive biomolecules.

Furthermore, a high-resolution mass spectrometry study was performed to resolve conjugation heterogeneity, determine drug-to-antibody ratio (DAR), and characterizing peptide attachment sites.

In summary, the target of this PhD work was to establish a novel methodology for industrial application at Fischer Analytics, capable of achieving high-resolution purification and characterization of therapeutic antibodies and related bioconjugates under native-like conditions. The integration of the industrial analytical expertise from Fischer Analytics with the biomedical focus of the University of Heidelberg created a unique research environment aimed at bridging the gap between instrumental innovation and therapeutic application. The outcomes of this work is expected in the medium term to provide a versatile analytical platform applicable not only to therapeutic antibody–peptide conjugates but also to a broader range of complex biologics including binding of cytotoxic drugs, contributing to the future development of precise and efficient

tools for biopharmaceutical research and quality assessment aimed to innovative personalized treatments for clinical applications.

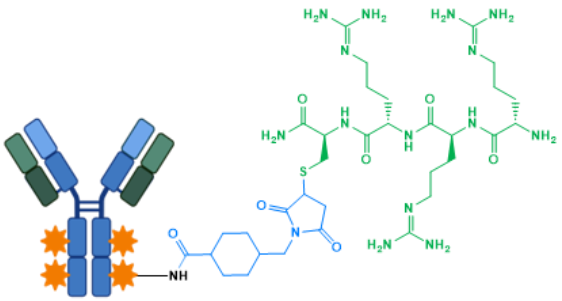

Fig.5: Model mAbs-CPP, bearing sulfoSMCC-R3C units.

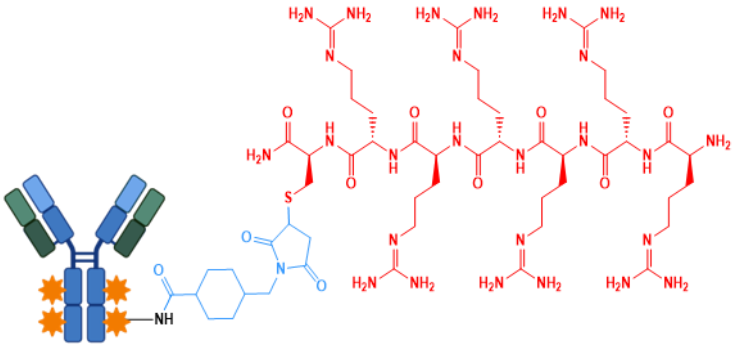

Fig.6: Model mAbs-CPP, bearing sulfoSMCC-R6C units.

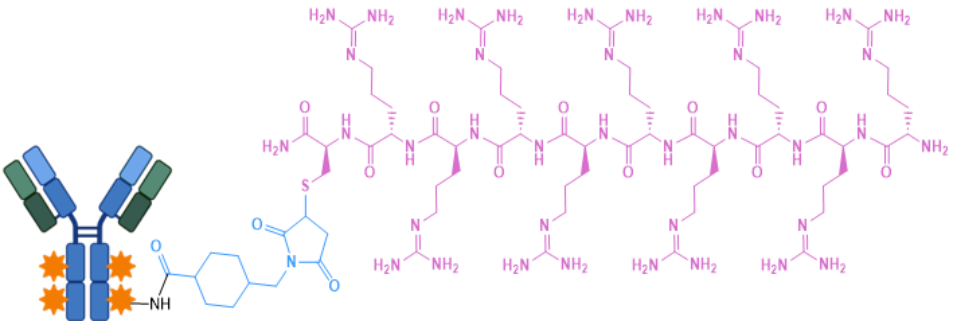

Fig.7: Model mAbs-CPP, bearing sulfoSMCC-R9C units.

3. Results and Discussion

The work presented in this section was conducted with the primary aim of establishing reliable purification and characterization methodologies for heterogeneous antibody conjugates, rather than optimizing the biological performance of the constructs themselves. Within the framework of this industrial PhD, the central scientific challenge lay in managing the analytical complexity associated with modified monoclonal antibodies, whose heterogeneity, arising from stochastic lysine conjugation, variable linker installation, and differences in peptide loading, imposes significant limitations on both purification efficiency and structural interpretation. For this reason, the antibody–linker–CPP constructs prepared in this study should be regarded as controlled model systems specifically designed to probe chromatographic behaviour, evaluate the resolving power of complementary non-denaturing and denaturing separation methods, and benchmark the performance of multidimensional LC workflows. This analytical focus aligns with the industrial objectives of the project, where the long-term goal is to create a scalable platform capable of supporting post-production processing of modified antibodies through rapid, non-destructive, and cost-efficient workflows. In this context, the following sections detail the production of model constructs and the subsequent optimization of chromatographic techniques required to dissect their heterogeneity and inform future platform development.

3.1 Production of constructs of three therapeutic antibodies for intracellular delivery

3.1.1 Design of selected oligoarginines

Oligoarginines are widely investigated cationic cell-penetrating peptides due to their easy synthesis, tunable chain length, and remarkable capacity in crossing

cellular membranes through electrostatic interactions with negatively charged surface moieties. These features make them a valuable tool for producing model antibody-CPP constructs.

For the case study of this project, three oligoarginines differing in chain length were selected to assess how peptide size and charge density influence conjugation behavior and chromatographic resolution to optimize the purification step. Their design was conceived to provide well-defined and chemically tractable model cargos for antibody–peptide conjugation.

The oligoarginines were not directly linked to the monoclonal antibody but coupled via a chemical spacer. The spacer selected was the sulfoSMCC (sulfosuccinimidyl 4-(N-maleimidomethyl)cyclohexane-1-carboxylate), a heterobifunctional reagent containing an NHS-ester reactive (N-hydroxysuccinimide) toward lysine ε-amino groups present in the antibody and a maleimido moiety able to react with thiol side-chain (see section 3.1.4) of a cysteine residue incorporated at the C-terminus of each oligoarginine peptide. Therefore, the selected peptides were a tetra-, hepta-, and decapeptide (H-RRRC-NH_2 (R3C), H-RRRRRRC-NH_2 (R6C), H-RRRRRRRRRC-NH_2 (R9C) (Figures 8, 9,10) consisting of three, six, and nine arginine residues, respectively.

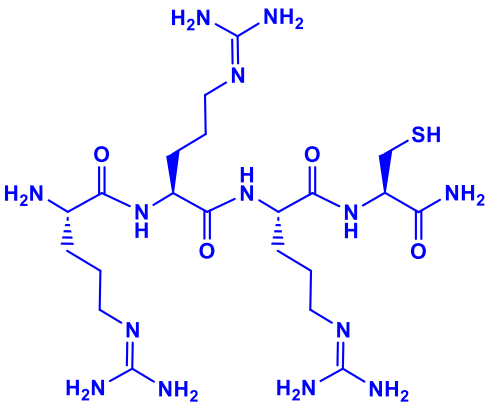

Fig.8: Tetrapeptide H-RRRC-NH_2 (R3C).

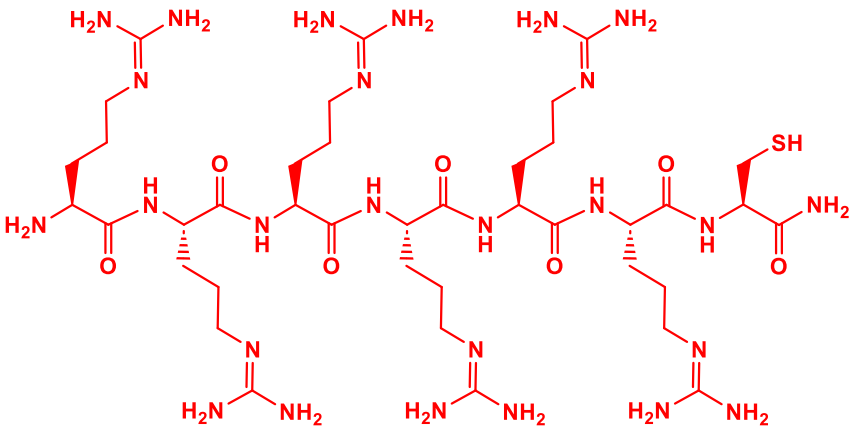

Fig. 9: Heptapeptide H-RRRRRRC-NH_2 (R6C).

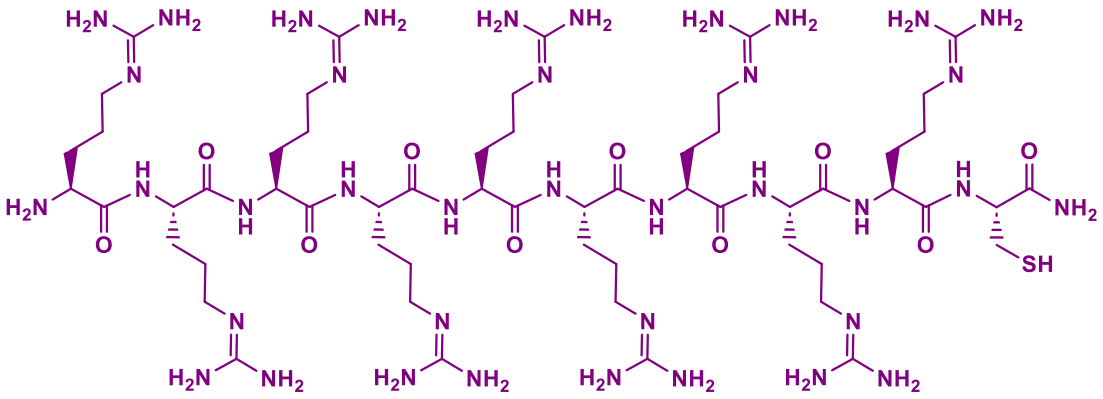

Fig.10: Decapeptide H-RRRRRRRRRC-NH_2 (R9C).

3.1.2 Solid-phase synthesis of oligoarginine peptides

The peptides were synthesized by microwave-assisted solid-phase peptide synthesis (MW-SPPS), employing Fmoc/tBu orthogonal protecting strategy and DIC/Oxyma Pure as coupling system on the automated microwave-assisted synthesizer Liberty Blue™ (CEM, USA).

Since the desired peptides should be C-terminal amides, the resin selected was a Rink Amide resin with a 0.336 mmol/g loading. (Fig. 11)

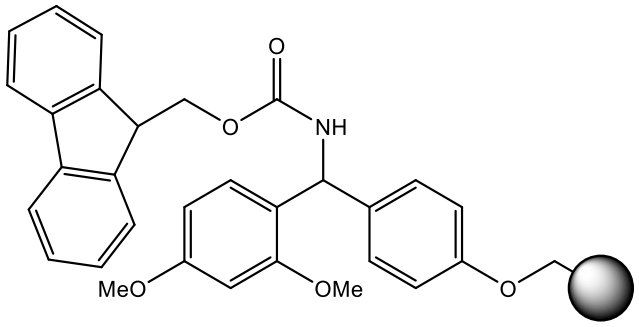

Fig.11: Fmoc-Rink Amide resin.

The resin was first swollen in dimethylformamide (DMF), to allow it to expand and expose all the active sites to the solvent, and then the MW-SPPS protocol was performed (see 5.2.1).

Considering the sequences, double and triple-coupling cycles were applied under MW-SPPS conditions to ensure complete amino acid incorporation and to minimize chain truncation, since arginine residues are known to exhibit slower coupling kinetics and aggregation propensity.

For each amino acid in the sequence, the subsequent steps were performed, and repeated iteratively for each amino acid:

- Standard deprotection conditions: 20% (v/v) piperidine/DMF
- Washings in DMF
- Couplings: DIC and Oxyma pure as coupling system and protected amino acid building blocks dissolved in DMF
- Washings in DMF

(Coupling and washing steps were repeated twice or three times if the first coupling was incomplete).

At the end of the synthesis the peptide-resin was Fmoc-deprotected on the N-terminus, washed with DMF and Dichloromethane (DCM) and then treated with a cleavage cocktail composed of 92.5:2.5:2.5:2.5 TFA:TIS:H_2O:EDT (Trifluoroacetic Acid:Triisopropylsilane:water:1,2-Ethanedithiol) (*v:v:v:v*) to cleave the peptide from the resin and remove all the protecting groups on the side chains. Then the peptide was precipitated with diethyl ether and washed multiples times to eliminate the reactive protecting groups that were once on the amino acids side chains (which are soluble in ether). After centrifugation the crude product was collected and purified.

Reversed-phase liquid chromatography (RPLC) is widely employed to purify peptides, enabling the removal of salts as well as potential side-products generated during the synthesis. This technique relies on a silica-based column, where alkyl chains of different lengths are covalently linked to the silica particles to which peptides interact primarily through hydrophobic forces. Usually, short alkyl chains are more suitable for purification of long sequences with high steric hindrance, while short peptides are mainly treated with longer alkyl chains. In most of the routine peptide analysis, columns based on n-octadecyl alkyl chains (C18) are employed. The mobile phases usually consist of binary mixtures of H_2O and CH_3CN (ACN), both acidified with 0.1% TFA. The addition of TFA, through its acidic ion-pairing properties, minimizes ionic interactions between the peptide and the stationary phase, thereby enhancing chromatographic resolution and peak shape.

Before purification, the analytical chromatograms of the crude oligoarginine peptides displayed a profile with multiple peaks of varying intensities, clearly indicating the presence of several synthesis by-products, corresponding to both arginine deletions and over coupling species. The presence of side products arised from difficult coupling in solid-phase synthesis of arginine-rich peptides. Arginine residues possess a bulky guanidinium side chain, typically protected by 2,2,4,6,7-pentamethyldihydrobenzofuran-5-sulfonyl groups (Pbf), which can cause steric hindrance during the coupling process. As a result, incomplete coupling reactions may occur, yielding deletion sequences lacking one or more Arg residues; these truncated analogues tend to elute slightly earlier than the desired peptide due to their reduced hydrophilicity. Oppositely over coupled analogues, can occur when residual activated species remain on the resin,

these products present as later-eluting peaks because of their increased polarity and molecular weight.

Because of side products in the crude peptide, a protocol of purification based on two steps had been set up:

1) Flash chromatography on Biotage® IsoleraOne, column: Biotage® SnapUltra Cartridge C18 12g
2) Semi-preparative chromatography on a Waters 600 HPLC coupled with Waters UV DAD 2487, column: Phenomenex ® Aqua 5u C18 (250x10,00 mm)

The collected fractions were analyzed using RP-HPLC coupled to ESI-MS, and the homogenous ones with a purity rate of over 95% were pulled together then lyophilized to obtain the final pure products.
By following this procedure, the peptides were obtained with a purity rate higher than 98 %.

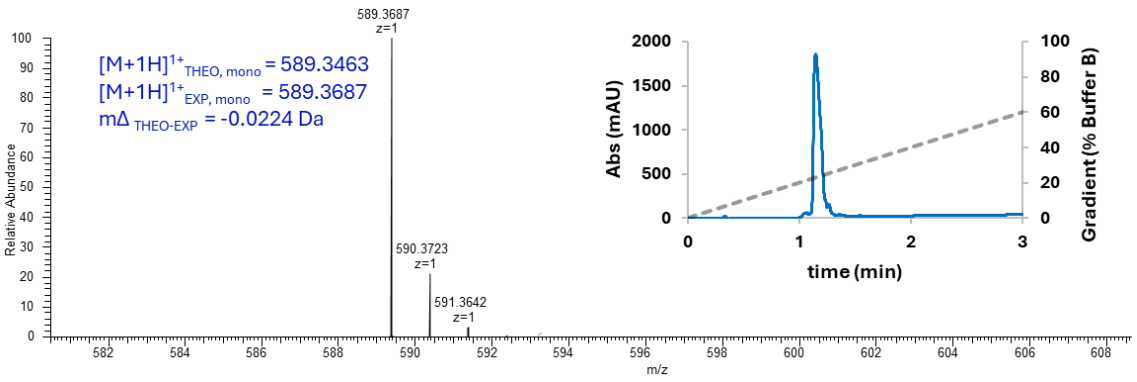

Fig.12: RP-HPLC (RP-HPLC Alliance Chromatography system (Waters, Milford Massachusetts, USA)) profile of R3C, C18 column Waters Acquity BEH (130 Å, 1.7 µm, 2.1 50 mm); temperature 35°C; flow, 0.6 ml/min; eluent, 0.1% (v/v) TFA in H_2O (A) and 0.1% (v/v) TFA in CH_3CN (B); λ 215 nm, gradient, 10-90% B in

10min. rt = 1.25min: 98%; ESI-MS (ESI-MS Micromass ZQ (Waters, Milford Massachusetts, USA)) spectrum of R3C-NH_2. ESI-MS (m/z): $[M+H]^{1+}$ 589.3463.

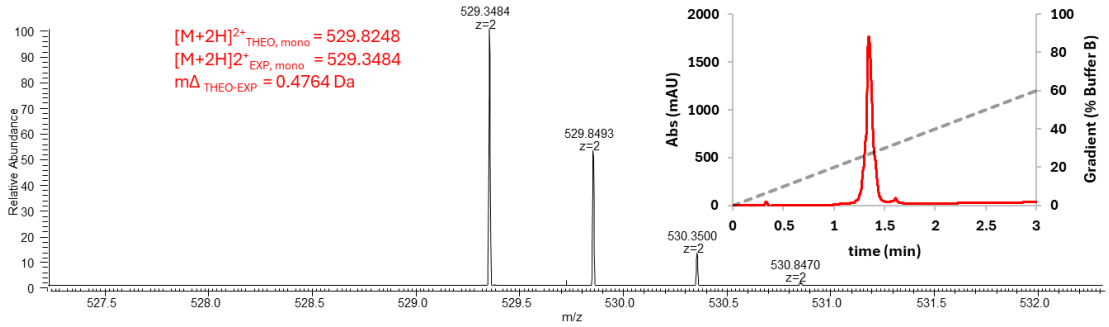

Fig.13: RP-HPLC (RP-HPLC Alliance Chromatography system (Waters, Milford Massachusetts, USA)) profile of R3C, C18 column Waters Acquity BEH (130 Å, 1.7 µm, 2.1 50 mm); temperature 35°C; flow, 0.6 ml/min; eluent, 0.1% (v/v) TFA in H_2O (A) and 0.1% (v/v) TFA in CH_3CN (B); λ, 215 nm, gradient, 10-90% B in 10min. rt = 1.25 min: 98%; ESI-MS (ESI-MS Micromass ZQ (Waters, Milford Massachusetts, USA)) spectrum of R6C-NH_2 ESI-MS (m/z): $[M+2H]^{2+}$ 529.8248.

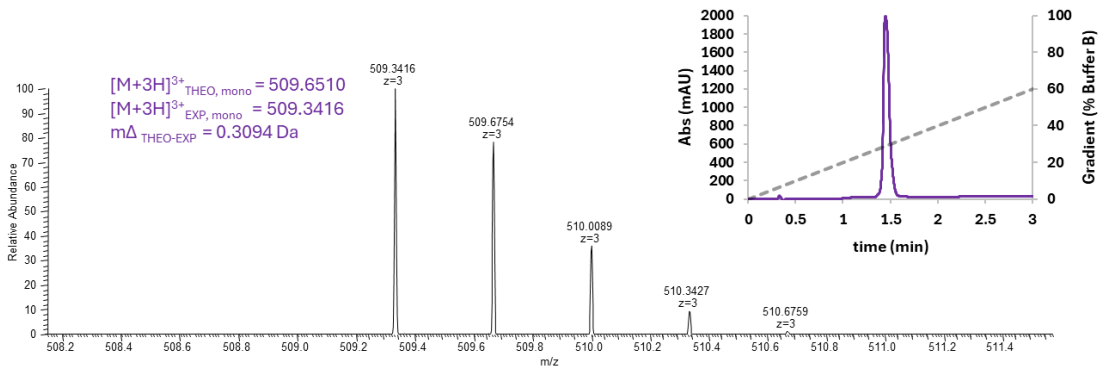

Fig.14: RP-HPLC (RP-HPLC Alliance Chromatography system (Waters, Milford Massachusetts, USA)) profile of R3C, C18 column Waters Acquity BEH (130 Å, 1.7 µm, 2.1 50 mm); temperature 35°C; flow, 0.6 ml/min; eluent, 0.1% (v/v) TFA in H_2O (A) and 0.1% (v/v) TFA in CH_3CN (B); λ, 215 nm, gradient, 10-90% B in 10min. rt = 1.25 min: 98%; ESI-MS (ESI-MS Micromass ZQ (Waters, Milford Massachusetts, USA)) spectrum of R9C-NH_2 ESI-MS (m/z): $[M+3H]^{3+}$ 509.6510.

3.1.3 In situ modification and activation of the therapeutic antibody to form the Antibody-sulfoSMCC-Rn conjugates

In the development of antibody–peptide conjugates, the conjugation step is crucial, as it governs the chemical stability, pharmacokinetics, and overall biological performance of the final construct. The success of an antibody conjugate depends not only on the selection of the antibody, linker, and payload, but also on how these components are covalently linked. [64,65]

Among the various conjugation approaches that have been established, including cysteine-based and enzymatic methodologies, random lysine side chain conjugation remains one of the most widely employed and experimentally robust techniques. Its simplicity, compatibility with native antibody structures, and well-established chemistry have supported the development of several clinically approved antibody–drug conjugates.[66]

Lysine conjugation exploits the natural abundance and high nucleophilicity of solvent-exposed ε-amino side chains in lysine residues, of which approximately forty are accessible in a typical IgG molecule under neutral aqueous conditions.[66] These residues react with electrophilic reagents such as N-hydroxysuccinimide (NHS) esters, isothiocyanates, benzoyl fluorides, or squarate derivatives, forming stable amide bonds without altering the antibody backbone.[67,68,69]

Although historically described as a random modification, lysine conjugation has been shown to yield consistent and reproducible site distributions under stable manufacturing parameters. Liu et al.[70] demonstrated that, despite the large number of potential reactive sites, the distribution of conjugation locations remains statistically constant when process parameters are rigorously controlled, supporting the scalability of lysine-based manufacturing.[71] Nevertheless, variations in reaction conditions can still lead to heterogeneous

drug-to-antibody ratios (DARs), which influence clearance rate, stability, and systemic toxicity. Excessive modification may disturb tertiary structure or antigen binding, whereas insufficient modification results in lower payload loading and reduced potency. [72]

Several physicochemical factors govern the efficiency and selectivity of lysine conjugation. The buffer composition and pH modulate the ionization of lysine ε-amines, thereby controlling their nucleophilicity. Mildly basic conditions (pH 7.5–8.5) typically maximize reactivity while minimizing the hydrolysis of the NHS ester. [73,74] Reaction stoichiometry, also, critically affects conjugation outcome: higher linker-to-antibody ratios promote higher drug-to-antibody ratios. Still, they may induce aggregation or structural perturbation, whereas lower ratios yield more homogeneous but less potent conjugates. [75,76,77] The temperature and reaction time determine the balance between coupling efficiency and degradation of reactive intermediates, and thus must be carefully optimized for each antibody and linker system.

The intrinsic hydrophobicity and charge state of the attached payloads can further influence conjugation performance. In the present project, the arginine-rich CPPs (R_3C, R_6C, R_9C) carry multiple positive charges, which can promote electrostatic interactions with negatively charged antibody regions and lead to aggregation during the coupling process.

To mitigate these effects, conjugations were carried out in non-denaturing aqueous buffers (such as phosphate or HEPES) containing appropriate ionic strength or stabilizing additives, which help maintain antibody solubility and native conformation.

3.1.4 Chemistry of the maleimido crosslinker

In this work, the random lysine conjugation approach was applied to generate monoclonal antibody–cell-penetrating peptide conjugates (mAbs-CPP) through a two-step reaction mediated by the heterobifunctional crosslinker sulfoSMCC.

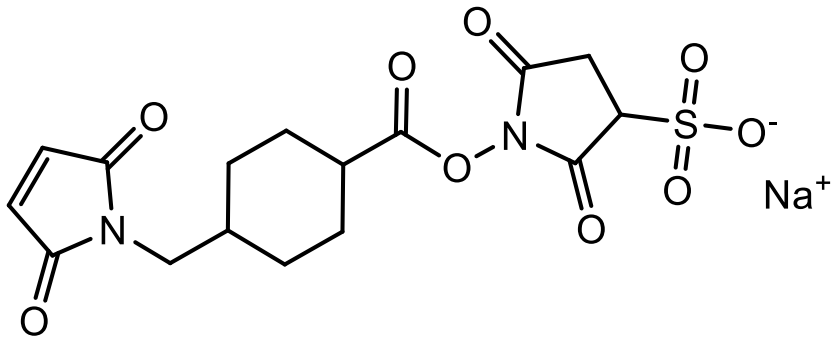

Fig.15: Sulfosuccinimidyl-4-(N-maleimidomethyl)cyclohexan-1-carboxylate (SULFOSMCC).

The NHS ester moiety of SULFOSMCC reacts first with accessible ε-amino groups of lysine residues located on the antibody surface. This reaction proceeds through nucleophilic acyl substitution, where the deprotonated amine attacks the carbonyl carbon of the NHS ester, releasing N-hydroxysuccinimide and forming a stable amide bond between the antibody and the cyclohexyl spacer of the linker.[78]

The second functional group, i.e., the maleimido one, remains intact during this step and is later used to couple the peptide. Subsequently, the maleimido undergoes a Michael addition with the thiol group of the C-terminal cysteine residue. The sulfur nucleophile attacks the electron-deficient double bond of the maleimido ring, generating a stable thioether bond that covalently links the peptide to the antibody through the crosslinker.

This two-step mechanism ensures orthogonal reactivity, minimizing cross-interference between functional groups, and allows conjugation under mild, near-physiological conditions that preserve antibody conformation and activity.

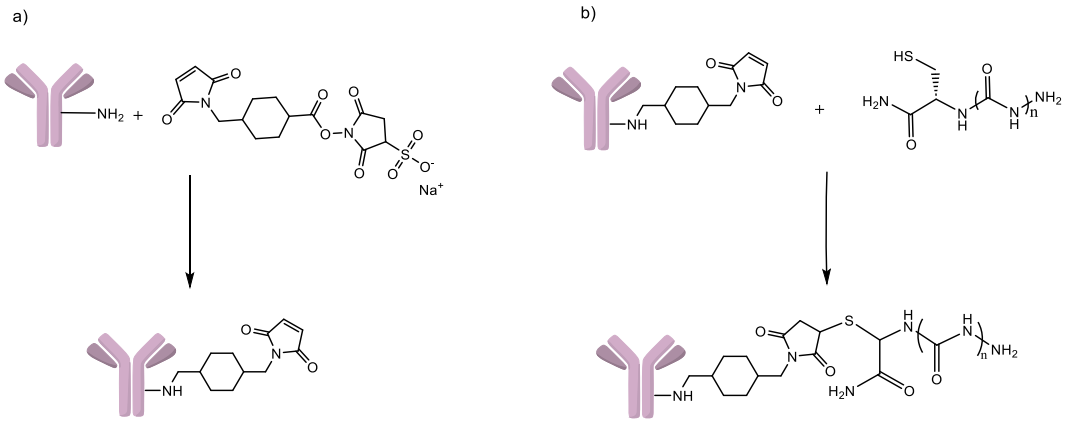

Scheme 1: Synthetic scheme of an antibody-SULFOSMCC-CPP conjugates; a) the SULFO-SMCC crosslinker adds to free lysine side chains of the antibody, b) via formation of a thioether with the maleimide-reactive group the CPP is linked to the antibody.

3.1.5 Optimization of the conjugation reactions

For both reactions, different reaction times (1-2 h), buffers (PBS vs. HEPES buffer), and distinct stoichiometric ratios of the reagents were tested to achieve optimal yield. The ideal reaction conditions are outlined below.

We demonstrated that the reactivity of the selected monoclonal antibodies (Rituximab, Trastuzumab, and Matuzumab) was similar overall, with Rituximab being primarily used to optimize the process.

Before conjugation, the monoclonal antibodies were transferred into HEPES or PBS buffer (pH 7) to remove formulation residues that could interfere with the coupling reaction. Antibody concentrations were determined spectrophotometrically.

Conjugation was assessed by varying the molar excess of the crosslinker, and complete removal of unreacted sulfoSMCC was verified following ultrafiltration. Activated mAbs were subsequently reacted with oligoarginine peptides through the maleimido moiety to enable covalent attachment. Peptide-to-antibody ratios of 1 and 3 equivalents were evaluated to determine the influence of stoichiometry on conjugation efficiency. All reactions proceeded under mild aqueous conditions without detectable antibody precipitation or degradation. These results demonstrate that surface modification of antibodies with oligoarginine via sulfoSMCC is achievable and that modulation of reactant stoichiometry provides a way to control peptide loading.

Furthermore, the amount of antibody used in each reaction ranged from 0.06 to 0.08 mol, with the corresponding sulfoSMCC quantity adjusted to 0.16, 0.32, 0.41 mol, depending on the targeted linker-to-antibody ratio. Considering that approximately 30–40 lysine ε-amine groups per IgG1 molecule are solvent-exposed and therefore available for modification, these conditions effectively target only a small fraction of the accessible amines. At the highest linker loadings tested, the stoichiometry corresponds to the theoretical modification of roughly 1 in 40, 2 in 40, or 3 in 40 lysine residues per antibody, confirming that the reactions were conducted well within the sub-stoichiometric regime.

Such low degrees of modification are essential to minimize structural perturbation and preserve biological activity, as IgG1 antibodies contain 80–90 lysine residues but only a subset contributes to antigen recognition or structural stability. Leveraging this intrinsic stoichiometric excess enables controlled, low-occupancy modification while reducing the risk of disrupting functionally important regions. Consistent with this rationale, the literature on lysine-based conjugation shows that high molar excesses of NHS-activated reagents yield

heterogeneous products with broad DAR distributions, reduced stability, and impaired pharmacological performance due to the stochastic nature of lysine reactivity.[76] Conversely, Pometti et al.[77] demonstrated that limiting the amount of NHS ester and applying kinetic control restricts the number of lysines undergoing modification, yielding less heterogeneous conjugates and better preserving antigen-binding capacity.

Overall, reducing the pool of reactive amines through sub-stoichiometric linker and peptide ratios markedly lowers the likelihood of modifying residues near the antigen-binding interface and decreases aggregation propensity—an especially important consideration when conjugating arginine-rich peptides whose pronounced positive charge promotes nonspecific interactions. Taken together, these findings support the use of sub-stoichiometric linker–peptide-to-antibody ratios as an effective strategy to preserve native structural integrity and maintain the biological activity of monoclonal antibodies.

We generated a panel of conjugates with all three mAbs, Rituximab, Trastuzumab, and Matuzumab bearing sulfoSMCC in combination with the cysteine-terminated CPPs R3C, R6C, and R9C. Conjugation reactions were performed using linker-to-CPP molar ratios of 1:1, 1:2, and 1:3, thereby yielding construct series with distinct levels of linker installation and peptide loading. The resulting species are designated as mAb-(sulfoSMCC)-R3C, mAb-(sulfoSMCC)-R6C, and mAb-(sulfoSMCC)-R9C. This structured variation in stoichiometry enabled us to systematically evaluate how modulation of linker and CPP equivalents shapes the distribution, composition, and loading profiles of the resulting antibody–CPP conjugates across all three mAbs.

3.1.6 Impact of TFA salts on the conjugation performance

To further investigate the conjugation process and assess potential interference from TFA counterions,[79] a proof-of-concept conjugation was performed using 6-maleimidohexanoic acid as reactive maleimido unit. Increasing amounts of CPP (R3C and R6C) were added to the reaction, maintaining the same reaction conditions optimized in section 3.1.5, to determine if the theoretical peptide amounts input corresponded to the concentration effectively available for the conjugation.

At time zero, the chromatographic profile revealed distinct, well-resolved peaks corresponding to the unreacted maleimido and the CPPs.

Upon incremental addition of R3C from 0.5 to 3.5 excess fold, the RPLC profiles showed a progressive decrease in intensity of maleimido and peptide peak intensities, corresponding to the emergence of a new product-associated peak, consistent with efficient consumption of the reagents units. A similar trend was observed with R6C peptide: increasing the equivalents of peptide reduced the maleimido signal and correspond to the comparison of a new peak to a different retention time, indicating successful conjugation.

In both experiments, residual TFA salts did not generate additional interfering peaks of good intensity, indicating that their presence did not compromise the reactivity of the maleimido group under the reaction conditions. It is important to note that the ratio of maleimido:CPP observed was 1:2, demonstrating that TFA did not interfere with the conjugation mechanism itself, but it could interfere with effective stoichiometry.

Collectively, these results demonstrated that the conjugation strategy remained robust in the presence of TFA salts, and that a systematic titration of CPP

equivalents was a reliable approach for calibrating peptide input and evaluating conjugation efficiency before its application to antibody-CPP system.

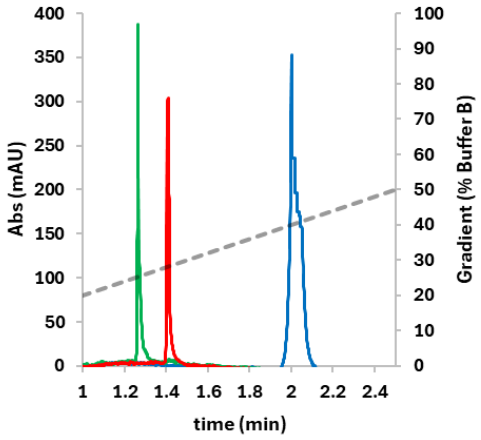

Fig. 16: RP-HPLC (Agilent 1100 series) traces of 6-maleimidohexaconic acid (blue),R3C pure (green),R6C pure (red) at time zero; Chromolith® Performance RP-18 (100 mm x 4.6 mm, Supelco); temperature 25°C; flow, 0.6 ml/min; eluent, 0.1% (v/v) TFA in H_2O (A) and 0.1% (v/v) TFA in CH_3CN (B); λ, 215 nm, gradient, 10–90% B in 5 min.

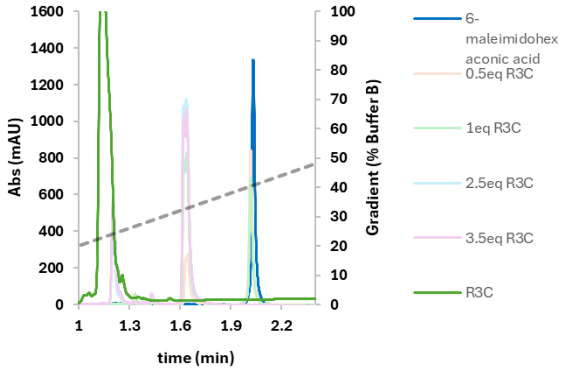

Fig. 17: RP-HPLC (Agilent 1100 series) traces of conjugation reaction among 6-maleimidohexaconic acid (blue),R3C pure (green) at different ratio; Chromolith® Performance RP-18 (100 mm x 4.6 mm, Supelco); temperature 25°C; flow, 0.6

ml/min; eluent, 0.1% (v/v) TFA in H_2O (A) and 0.1% (v/v) TFA in CH_3CN (B); λ, 215 nm, gradient, 10–90% B in 5 min.

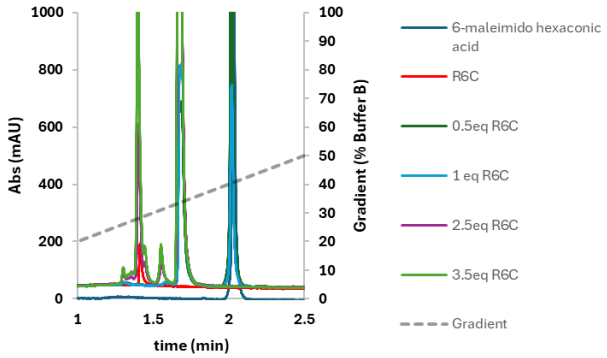

Fig. 18: RP-HPLC (Agilent 1100 series) traces of conjugation reaction among 6-maleimidohexaconic acid (blue),R6C pure (red) at different ratio; Chromolith® Performance RP-18 (100 mm x 4.6 mm, Supelco); temperature 25°C; flow, 0.6 ml/min; eluent, 0.1% (v/v) TFA in H_2O (A) and 0.1% (v/v) TFA in CH_3CN (B); λ, 215 nm, gradient, 10–90% B in 5 min.

3.1.7 Estimation of protein concentration

3.1.7.1 SDS-PAGE Gel Electrophoresis

Gel electrophoresis is a laboratory technique used to resolve complex protein mixtures, such as those derived from whole cells, subcellular fractions, chromatographic eluates or immune precipitates, according to their molecular weight and their m/z to analyze subunit composition, sample homogeneity, and isolate proteins.[80] The separation occurs because of the electric field applied, which pushes the protein through the gel. The separation also depends on the percentage of acrylamide used; a low percentage allows for a better separation of proteins with low molecular weights, whereas a higher percentage of acrylamide is better for proteins with high molecular weights.

For the separation of the produced mAb conjugates, a 12% acrylamide gel was employed under an electric field of 150V. Protein mixtures were denatured by treatment with sodium dodecyl sulfate (SDS) and heating at 100 °C, ensuring that the separation was based solely on molecular weight. This technique is called SDS-PAGE. With that said, the SDS-PAGE gel was performed on the complex mixtures produced by the two-step conjugation protocol used before (see 3.1.5).

SDS-PAGE was used to analyze the antibody–drug conjugates (ADCs) produced using the two-step conjugation protocol. Proteins were separated based on molecular weight by running a 12% acrylamide gel under denaturing conditions, allowing evaluation of heavy- and light-chain modifications. The focus was on the presence of two bands: around 50 kDa and 25 kDa, corresponding to the heavy chain and light chain, respectively.The light chain (≈25 kDa) was the most informative region, as the appearance of higher-molecular-weight bands indicated conjugation of CPP peptides to the antibody.

Across the three monoclonal antibodies, Rituximab, Matuzumab and Trastuzumab, distinct differences in conjugation efficiency and heterogeneity were observed. Rituximab generally showed the most pronounced and progressive modification, with stepwise increases in light-chain band intensity as peptide excess increased. Trastuzumab followed a similar trend but with a broader distribution of modified species, indicating a greater degree of heterogeneity. Matuzumab consistently exhibited weaker and more diffuse band shifts, demonstrating lower reactivity and reduced incorporation of CPPs under identical conditions.

A crucial variable influencing these outcomes was the buffer used during conjugation. In HEPES buffer, rituximab–CPP conjugates displayed discrete and well-resolved higher-molecular-weight species in the light-chain region, consistent with efficient and relatively homogeneous conjugation, reflected in a clearer Drug-Antibody ratio distribution. In contrast, reactions performed in PBS produced markedly less defined patterns, characterized by diffuse or smeared bands, especially in R6C samples, indicating increased heterogeneity and lower control over conjugation. Trastuzumab conjugates in PBS showed a similar loss of resolution, with broader and poorly separated modified species. These effects suggest that phosphate ions and higher ionic strength in PBS may interfere with maleimide linker reactivity and peptide accessibility. Matuzumab again showed poor performance in both buffers, but heterogeneity was noticeably more pronounced in PBS.

Overall, these findings demonstrated that HEPES buffer is significantly more favorable than PBS for mAb–(sulfoSMCC)-CPP conjugation, yielding sharper, more reproducible, and more homogeneous banding patterns across all antibodies tested. The differences are likely attributed to buffer-dependent variations in pH, ionic strength, and compatibility with maleimide chemistry. This comparison highlights the critical importance of buffer selection when optimizing conjugation conditions, as it strongly influences both the yield and the structural homogeneity of the resulting conjugates.

3.2 Purification of therapeutic antibodies screening of non-denaturing liquid chromatography techniques

Chromatography is one of the most versatile and indispensable techniques for both analytical and preparative applications, enabling compounds to be separated, purified, and characterized based on their interactions with the stationary and mobile phases. At the core of modern chromatographic science is high-performance liquid chromatography (HPLC), which has evolved into the leading technique for chemical analysis, separation, and purification.[81,82]

HPLC can be seen as a systematic and adaptable methodology capable of addressing both routine and complex analytical problems. Over the past few decades, advances in *column technology*, *stationary-phase design*, *gradient elution strategies*, and *detection systems* have greatly enhanced the performance, reproducibility, and selectivity of HPLC.[83]

Modern instrumentation allows the efficient separation of analytes ranging from small molecules to large biomacromolecules, including proteins, peptides, and conjugated biotherapeutics such as ADCs. In addition, developments in computer-assisted method optimization, multidimensional separations, and rigorous method validation have positioned HPLC as the cornerstone of analytical quality control in biopharmaceutical development.[84]

A fundamental distinction within chromatographic workflows lies between *non-denaturing* and *denaturing* separation modes.

Non-denaturing chromatographic techniques, such as size exclusion chromatography (SEC), ion exchange chromatography (IEX), hydrophobic interaction chromatography (HIC), and mixed-mode chromatography (MMC), operate under mild aqueous conditions that preserve the native conformation and biological activity of proteins, enabling the accurate assessment of size distribution, charge variants, and conformational stability.[85]

On the other hand, denaturing techniques, such as reverse-phase liquid chromatography (RPLC), employ high concentrations of organic modifiers or elevated temperatures to intentionally disrupt tertiary structure, exposing hydrophobic residues and enhancing resolution of chemically distinct variants. The complementary use of both categories provides a multidimensional understanding of structural integrity and modification patterns, which is particularly necessary for the separation and analysis of biotherapeutics.

Biotherapeutics are well known for their structural complexity, which depends on size heterogeneity, charge variation, hydrophobicity, and conjugation-induced modifications. Their purification and characterization necessitate the use of multiple, complementary chromatographic approaches to achieve a comprehensive analytical profile, leading to multidimensional liquid chromatography techniques. Operational parameters, including mobile-phase composition, buffer pH, ionic strength, temperature, and gradient slope strongly influence chromatographic performance. Variations in these chromatographic operating conditions affect the balance of solute–stationary phase interactions, thus modulating selectivity, retention, and resolution.

Generally speaking, separation and purification can be performed in three principal chromatographic modes: analytical, semi-preparative, and preparative. They operate with distinct operational characteristics and scales, driven by different forces, advantages/disadvantages, with their own specific applications.

The analytical mode is usually employed with high-performance liquid chromatography (HPLC). It is primarily used for high-resolution, high-sensitivity sample analysis. It employs columns packed with small particles and narrow pores, operated at high pressure, to deliver superior separation efficiency and

resolution required for the detailed evaluation of charge variants, isoforms, or aggregation states. Low sample capacity injection and the flow rate limit are the drawbacks of this modality.

Semi-preparative mode typically utilizes systems such as ÄKTA chromatography platforms, which are configured for intermediate-scale purification. It operates at a lower pressure, but it can process a higher number of samples with a nice resolution. This chromatographic mode is suitable for process development and optimization of purification conditions. It is often used as bridge between analytical characterization and large-scale production.

Finally, preparative chromatography is applied in large-scale purification. It handles large sample volumes at high flow rates, using columns packed with larger particles and wider pores to reduce backpressure. It sacrifices separation resolution for scalability to maximize yield and purity within shorter times rather than detailed characterization.

In this project, the analysis of and mAbs-sulfoSMCC-RnC has been conducted in both analytical and semi-preparative modes. The high resolution and sensitivity of the first modality have been used as a control and to study the heterogeneity of the produced conjugates, while the semi-preparative mode has been adopted for bulk purification, maintaining resolving power.

Both mAbs, Rituximab, Matuzumab, and Trastuzumab, as well as the corresponding conjugates produced, were analyzed using a collection of complementary chromatographic techniques: SEC, HIC, IEX, MMC, and RP-LC.

Each technique exploits distinct physicochemical properties of biomolecules, providing a comprehensive characterization and purification profile that is crucial for ensuring product quality and efficacy.

3.2.1 Size exclusion chromatography

Among the non-denaturing chromatographic techniques applied in biopharmaceutical analysis, size-exclusion chromatography (SEC), also known as gel filtration or gel permeation chromatography, represents one of the most widely used and reliable tools for the purification and characterization of protein therapeutics. In SEC, molecular separation is governed purely by hydrodynamic volume rather than chemical interactions, allowing macromolecules to be fractionated according to their effective size in solution. Larger species are excluded from the internal pores of the stationary phase and thus elute earlier, while smaller molecules penetrate deeper into the porous network and elute later. Because the mechanism is entropically driven and does not rely on binding equilibria, SEC can be performed under mild, fully aqueous conditions, preserving the native conformation and biological activity of the analyte.

In the context of therapeutic monoclonal antibodies (mAbs), SEC is considered a gold-standard analytical technique for detecting and quantifying size variants, such as monomers, dimers, and higher-order aggregates. Regulatory authorities, including the EMA and FDA, classify aggregation profiling by SEC as a critical quality attribute (CQA) for antibody-based therapeutics, given that protein aggregation can severely affect efficacy, pharmacokinetics, and immunogenicity. Beyond aggregation monitoring, SEC can also detect fragmentation phenomena (Fab or Fc cleavage) and evaluate product stability during manufacturing and storage. Its ability to provide direct information on molecular integrity makes SEC indispensable in both process development and quality control.

3.2.1.1 High-pressure size exclusion chromatography

The study was conducted using *TSKgel G4000SWXL* SEC column from *Tosoh Bioscience* to analyze mAbs-sulfoSMCC-RnC.

TSKgel G4000SWXL column is a hydrophilic silica-based stationary phase composed of spherical particles with a uniform 5 µm particle size. The controlled pore size distribution is expressly optimized for large biomolecule separation, such as antibodies and their conjugates, providing high-resolution separation of monomers, aggregates, and fragments under native-like conditions. Its high mechanical strength and chemical stability allow operation under a wide range of aqueous mobile phase conditions and pH values (pH 2–8), ensuring minimal non-specific interactions and maintaining protein integrity throughout analysis. The combination of these material properties facilitates accurate characterization of mAb-sulfoSMCC-RnC heterogeneity, aggregation state, and purity, making this column a widely accepted tool in biopharmaceutical research and quality control.[86]

It was decided to proceed performing isocratic run, in which the mobile phase composition remains constant throughout the entire separation process. In fact, a single aqueous solvent was pumped through the column without any change in pH or salt concentration. Isocratic elution is commonly used in HPLC and other chromatographic methods when the samples to be separated have similar chemical properties; it is a simple, reproducible, and easy to implement. Since the mobile phase composition is kept, method development and operational parameters are easy to modify.

For this study, two aqueous buffers have been tested:

- 20 mM MES, pH 7

- 50 mM Phosphate buffer + 0.1M NaCl pH 6.5

MES buffer is a zwitterionic buffering agent commonly used in biological and biochemical studies. It has a low ionic strength and, at low concentration, minimizes effects on protein solubility and conformation.

Phosphate Buffer, on the other hand, offers greater buffering capacity and is widely used in protein purification and characterization. The addition of NaCl increases the ionic strength, enhancing the protein solubility and stabilizing electrostatic interactions.

Phosphate buffer was chosen for this chromatography due to its better performance.

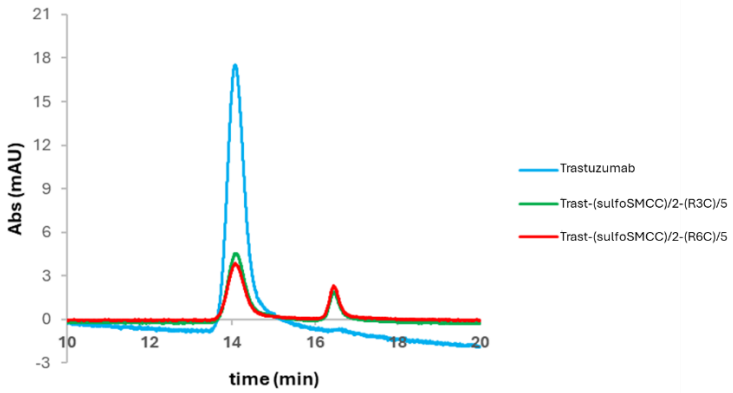

Fig. 19: SEC-HPLC (Agilent 1200 series) traces of mAb non modified (blue),Trast-(sulfoSMCC)-R3C (green),Trast-(sulfoSMCC)-R6C (red); *TSKgel G4000SWXL* SEC (300 mm x 7.8 mm, *Tosoh Bioscience*); temperature 25°C; flow, 0.8 ml/min; eluent, 50 mM Phosphate buffer + 0.1M NaCl pH 6.5 (A); λ, 215 nm, gradient, 100%A in 20 min.

3.2.1.2 Semi-preparative size exclusion chromatography

As already mentioned, the analysis of model mAbs-sulfoSMCC-RnC has also been performed in a semi-preparative mode.

The ÄKTA Purifier (GE Healthcare) was used to perform this type of chromatographic analysis. The ÄKTA Purifier system is a modular, automated chromatography platform designed for efficient purification and analysis of proteins at scales from micrograms to grams. The flow rate ranges from 0.001 to 10 mL/min or up to 100 mL/min (based on the model), with operating pressures up to 25 MPa, enabling high-resolution chromatographic separations. The system is equipped with three monitoring capabilities: multi-wavelength UV absorbance detection (up to 3 wavelengths, typically 190–700 nm), a pH meter, and conductivity measurements, facilitating comprehensive process control and chromatographic method development. The ÄKTA Purifier integrates seamlessly with the UNICORN™ control software, simplifying method development, automation, and scale-up. The system is characterized by its reliability, precision, and versatility, making it a widely adopted choice in biochemical and biopharmaceutical research settings.

For this specific analysis, the chosen chromatographic column was a HiTrap Desalting 5 mL (1.6 x 2.5 cm, Cyvita).

The HiTrap Desalting 5 mL column is a prepacked chromatography column filled with Sephadex G-25 Superfine resin, specifically engineered for rapid, efficient desalting and buffer exchange of biological samples. Separation is achieved based on molecular size, effectively removing low-molecular-weight substances such as salts and small contaminants from larger molecules like proteins and peptides. Its exclusion limit is approximately 5000 Da, hereby allowing differentiation between molecules above and below this molecular weight threshold. This makes it ideal for buffer exchange before or after chromatographic steps and reagent removal in protein purification workflows. The column comes ready to use with a convenient 5 mL bed volume and is

compatible with syringes, peristaltic pumps, and chromatography systems such as ÄKTA. It achieves fast separations, with typically over 95% sample recovery, and replaces longer methods as dialysis.

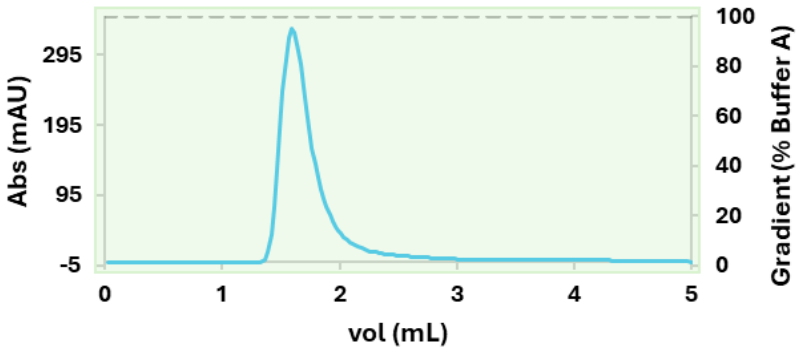

Fig. 20: SEC-Semipreparative (ÄKTA Purifier, GE Healthcare) chromatographic profile of Rituximab; HiTrap Desalting 5 mL (1.6 x 2.5 cm, Cyvita); temperature 25°C; flow, 1 ml/min; eluent, 50 mM Phosphate buffer + 0.1M NaCl pH 6.5 (A); λ, 215 nm, gradient, 100%A in 20 min.

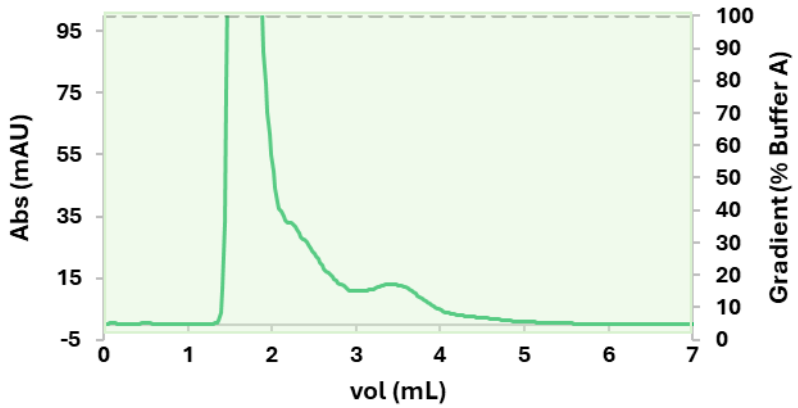

Fig. 21: SEC-Semipreparative (ÄKTA Purifier, GE Healthcare) chromatographic profile of Rit-sulfoSMCC-R3C; HiTrap Desalting 5 mL (1.6 x 2.5 cm, Cyvita); temperature 25°C; flow, 1 ml/min; eluent, 50 mM Phosphate buffer + 0.1M NaCl pH 6.5 (A); λ, 215 nm, gradient, 100%A in 20 min.

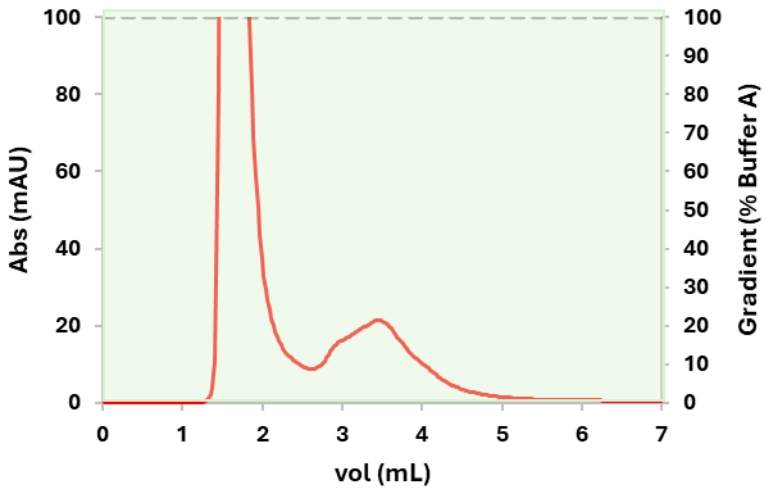

Fig. 22: SEC-Semipreparative (ÄKTA Purifier, GE Healthcare) chromatographic profile of Rit-sulfoSMCC-R6C; HiTrap Desalting 5 mL (1.6 x 2.5 cm, Cyvita); temperature 25°C; flow, 1 ml/min; eluent, 50 mM Phosphate buffer + 0.1M NaCl pH 6.5 (A); λ, 215 nm, gradient, 100%A in 20 min.

As shown in the presented chromatograms, the reference materials (RM), Rituximab, and its corresponding conjugates, bearing R3C and R6C peptides, exhibited no valid difference in molecular weight relative to the overall antibody mass. Consequently, this observation indicated that, within the resolution limits of the available instrumentation and the separation efficiency of the analytical and semi-preparative columns employed, it was not feasible to resolve the individual antibodies constructs species present in the mixture.

However, a clear distinction in retention behavior is observed between the antibody components and the excess unreacted peptides. When operating in semi-preparative mode on the ÄKTA system, a good peak resolution and recovery are achieved. This capability is anticipated to be highly valuable for developing and implementing two-dimensional liquid chromatography (2D-LC) experiments. In such configurations, the *HiTrap Desalting 5 mL* column is

expected to serve as an effective intermediate purification step for desalting step and salt removal from the elution buffer of the first dimension, to prevent interference with the subsequent chromatographic separation.

3.2.2 Hydrophobic interaction chromatography

Hydrophobic Interaction Chromatography (HIC) is a key non-denaturing chromatographic technique extensively employed in the biopharmaceutical field for the purification and characterization of protein therapeutics, including monoclonal antibodies and antibody constructs.

Its underlying mechanism exploits variations in surface hydrophobicity among biomolecules, allowing their separation under mild aqueous conditions that preserve tertiary and quaternary structures.

The separation in HIC is governed by the hydrophobic effect, an entropically driven process associated with the ordering of water molecules around non-polar solute surfaces. Under high concentrations of kosmotropic salts, such as ammonium sulfate, sodium citrate, or potassium phosphate, the solubility of hydrophobic regions decreases, promoting their interaction with hydrophobic ligands e.g., butyl, phenyl, or octyl groups, immobilized on the stationary phase. Proteins bind to the resin under these high-salt conditions and are subsequently eluted by gradually decreasing the ionic strength of the mobile phase, weakening hydrophobic interactions and releasing molecules in order of increasing hydrophobicity.

For therapeutic antibodies, HIC provides valuable information on surface hydrophobicity, conformational stability, aggregation tendency, and post-translational modifications such as oxidation or deamidation.

3.2.2.1 High-pressure hydrophobic interaction chromatography

Hydrophobic interaction chromatography (HIC) was employed as a strategic non-denaturing chromatography to evaluate and optimize the separation of the prepared antibodies conjugates.

A Tosoh Bioscience TSKgel HIC-ADC Butyl column (5 µm particle size, 4.6 × 100 mm dimensions) was selected for this purpose. This column is specifically engineered for the characterization of antibodies conjugates, featuring butyl-functionalized silica particles that provide a moderate hydrophobic environment suitable for resolving differences in hydrophobicity while preserving protein structural integrity, which is necessary to protect the activity.[87] The column's optimized pore structure and surface coverage enable high recovery and reproducible separations under mild, non-denaturing conditions, crucial for maintaining antibody conformations and ensuring accurate comparative analysis between reference mAbs and their conjugates.

To establish the most suitable chromatographic conditions, a systematic buffer screening was performed to assess the effects of salt concentration and pH on retention behavior and resolution (Table 1).

	Phase A	**Phase B**
1	1,1 M $(NH_4)_2SO_4$, 100 mM PP Buffer, pH 7	100 mM PP Buffer, 25% (v/v) IPA, pH 7
2	1,5 M $(NH_4)_2SO_4$, 100 mM PP Buffer, pH 7	100 mM PP Buffer, 25% (v/v) IPA, pH 7
3	1,2 M $(NH_4)_2SO_4$, 25 mM PP Buffer, pH 6	25 mM PP Buffer, 25% (v/v) IPA, pH 6

4	1,5 M $(NH_4)_2SO_4$, 25 mM PP Buffer, pH 6	25 mM PP Buffer, 25% (v/v) IPA, pH 6
5	1,2 M $(NH_4)_2SO_4$, 25 mM PP Buffer, pH 8	25 mM PP Buffer, 25% (v/v) IPA, pH 8
6	1,5 M $(NH_4)_2SO_4$, 25 mM PP Buffer, pH 8	25 mM PP Buffer, 25% (v/v) IPA, pH 8

Table1: HIC mobile phases tested, different in salt concentrations and pH.

The stationary phase in HIC retains proteins via reversible hydrophobic interactions, which are strongly modulated by ionic strength and the nature of the dissolved salt. High concentrations of kosmotropic salts such as ammonium sulfate enhance hydrophobic interactions by reducing the solvation of hydrophobic regions on both the protein and the stationary phase. Low salt concentration, hydrophobic interactions weaken, leading to protein elution. Therefore, it was imperative to optimize salt concentration to balance resolution and column performance, as high ionic strengths can increase backpressure, reduce flow stability, and increase the risk of protein precipitation.

In this study, buffer systems containing 1.1–1.5 M ammonium sulfate were tested at three pH levels (pH 6, pH 7 and pH 8), each combined with phosphate buffer and 25% (*v/v*) isopropanol (IPA) in the elution buffer to maximize gradient linearity and minimize nonspecific interactions. Among the tested conditions, the system using 1.2 M $(NH_4)_2SO_4$ in 25 mM phosphate buffer at pH 8 (option 5) demonstrated the most favorable performance. This composition provided sufficient retention of the antibody and conjugate species while maintaining manageable system pressure and flow rate, and reducing viscosity.

Each optimized method (mobile phases and chromatographic method) was first validated using the reference monoclonal antibody (Rituximab, Trastuzumab, and Matuzumab) to establish baseline retention characteristics, followed by the analysis of corresponding conjugate samples bearing R3C and R6C peptide conjugates.

In the resulting chromatograms (Fig.23, Fig.24, Fig.25), both reference antibodies and conjugates exhibited similar overall elution profiles, indicating no significant alterations in molecular weight or gross hydrophobicity attributable to conjugation. However, the mAbs constructs samples showed broader, less symmetric peaks, particularly at higher peptide equivalents. Among the different chromatographic methods investigated, a step-wise gradient from 0% buffer B to 12% B in 5 min, followed by a linear gradient from 12 to 50% B in 15 min at a flow rate of 1 mL/min, provided better results.

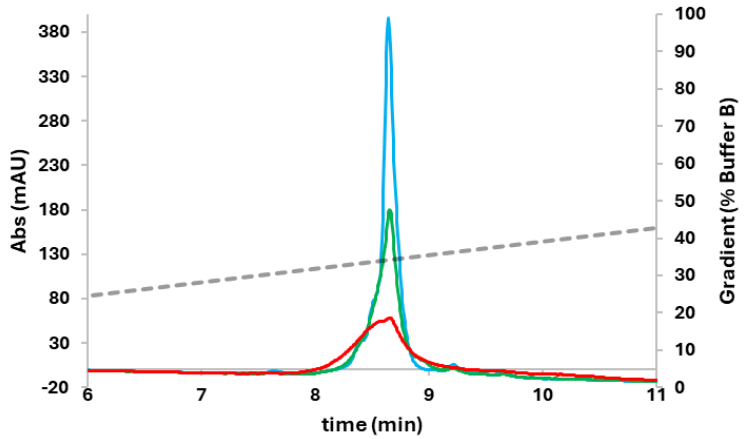

Fig.23: HIC-HPLC (Agilent 1200 series) traces of mAb non modified (blue),Rit-(sulfoSMCC)-R3C (green), Rit-(sulfoSMCC)-R6C (red); TSKgel HIC-ADC Butyl column (5 µm particle size, 100 mm × 4.6, Tosoh Bioscience); temperature 25°C; flow, 1 ml/min; eluent, 1,2 M $(NH_4)_2SO_4$, 25 mM PP Buffer, pH 8 (A) and 25 mM PP

Buffer, 25% (v/v) IPA, pH 8 (B); λ, 215 nm, step-wise gradient, 0%-12% B in 5 min, 12-50% B in 15 min.

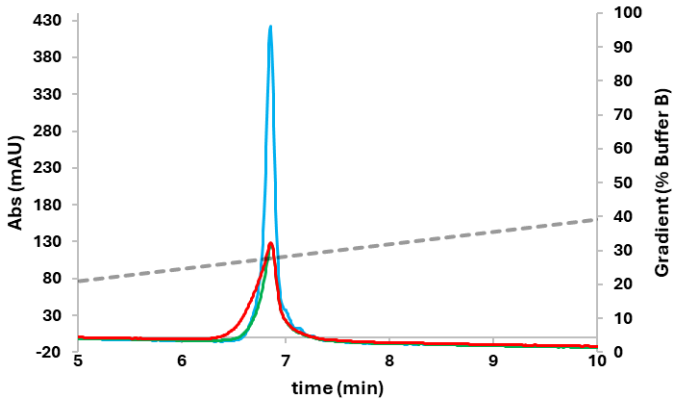

Fig. 24: HIC-HPLC (Agilent 1200 series) traces of Trastuzumab non modified (blue),Trast-(sulfoSMCC)-R3C (green),Trast-(sulfoSMCC)-R6C (red); TSKgel HIC-ADC Butyl column (5 µm particle size, 100 mm × 4.6, Tosoh Bioscience); temperature 25°C; flow, 1 ml/min; eluent, 1,2 M $(NH_4)_2SO_4$, 25 mM PP Buffer, pH 8 (A) and 25 mM PP Buffer, 25% (v/v) IPA, pH 8 (B); λ, 215 nm, step-wise gradient, 0%-12% B in 5 min, 12-50% B in 15 min.

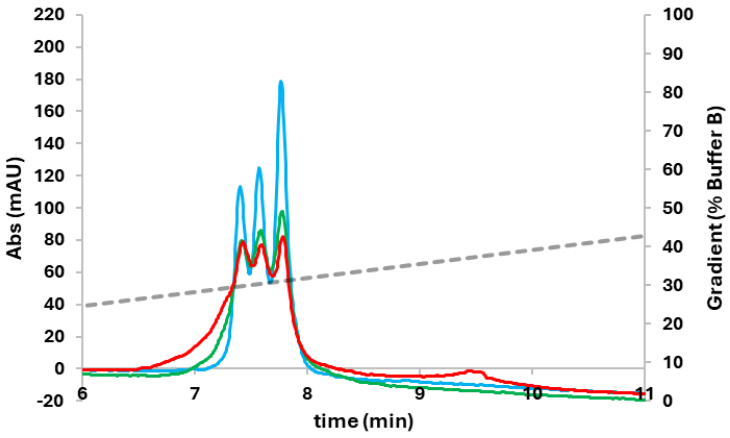

Fig. 25: HIC-HPLC (Agilent 1200 series) traces of Matuzumab non modified (blue),Mat-(sulfoSMCC)-R3C (green),Mat-(sulfoSMCC)-R6C (red); TSKgel HIC-

ADC Butyl column (5 µm particle size, 100 mm × 4.6, Tosoh Bioscience); temperature 25°C; flow, 1 ml/min; eluent, 1,2 M $(NH_4)_2SO_4$, 25 mM PP Buffer, pH 8 (A) and 25 mM PP Buffer, 25% (v/v) IPA, pH 8 (B); λ, 215 nm, step-wise gradient, 0%-12% B in 5 min, 12-50% B in 15 min.

The broadened peak shape suggested the coexistence of multiple conjugate populations differing in hydrophobic surface properties, which was in line with the heterogeneity expected from the chosen conjugation strategy, random lysine conjugation. The variety of conjugation sites across the antibody surface, where the number and location of attached linkers-peptides influence the distribution of exposed hydrophobic regions and since HIC separations depend primarily on surface hydrophobicity rather than total payload content, conjugates carrying the same number of linker–peptide units still elute at similar retention times if the conjugation occurs in hydrophilic instead of hydrophobic domains of the antibody, manifesting in peak broadening or co-elution.

Even the use of high-pressure chromatographic conditions on the HPLC system did not yield any significant improvement in resolving the separation of complex conjugates mixture. The co-elution and broad peak profiles indicated that the hydrophobic differences among the conjugate species were too small to be resolved under the tested gradient and column conditions, highlighting a limitation of this chromatographic technique in analyzing oligoarginine-conjugated antibodies.

3.2.2.2 Semi-preparative hydrophobic interaction chromatography

When analysing the mAbs constructs mixture on ÄKTA chromatography system under semi-preparative conditions, satisfactory peak resolution and recovery were achieved.

The column used was *SkillPak™ 5 mL TOYOPEARL® Phenyl-650-M* (8 mm ID x 100 mm L, Tosoh Bioscience). Its stationary phase is composed of hydroxylated methacrylic polymer beads, 65 µm in size and 100 nm in pore size, functionalized with phenyl ligands. This resin exhibits high chemical and mechanical stability, allowing cleaning-in-place (CIP) procedures and operation at elevated flow rates while maintaining structural integrity. The Phenyl-650M column provides efficient separation of proteins, isoforms, and aggregates. It demonstrates a dynamic binding capacity operating under back pressures up to 0.3 MPa. The column delivers excellent asymmetry factors, typically 0.8-1.4, indicative of high peak symmetry and chromatographic efficiency. Its resolving power depends by the phenyl ligand's balanced hydrophobic interaction strength, which facilitates discrimination among protein variants based on surface hydrophobicity while preserving native conformations, suitable for mAbs separation. Compared to smaller-particle resins like TOYOPEARL Phenyl-650S, it offers moderate resolution and improved pressure-flow characteristics, ideal for preparative and scale-up workflows.[88]

Based on the website literature and the previous screening of buffers, it was decided to proceed with 1,5 M (NH4)2SO4 + 100 mM PP Buffer, pH 7, as phase A, and 100 mM PP Buffer + 25% (v/v) IPA pH 7, as buffer B. And with a broader gradient range, 10-90 % B in 30 min with a slower flow rate of 0.5 mL/min.

As shown in the chromatograms (Fig.26), the peaks exhibited satisfactory recovery, indicating efficient sample elution and minimal loss. The retention time of the unmodified mAbs and the conjugate antibody mixture (Rit-(sulfoSMCC)-R3C) was relatively consistent, but the symmetry and shape of the peaks were almost the same. However, effective separation of distinct species in the complex mixture was not achieved.

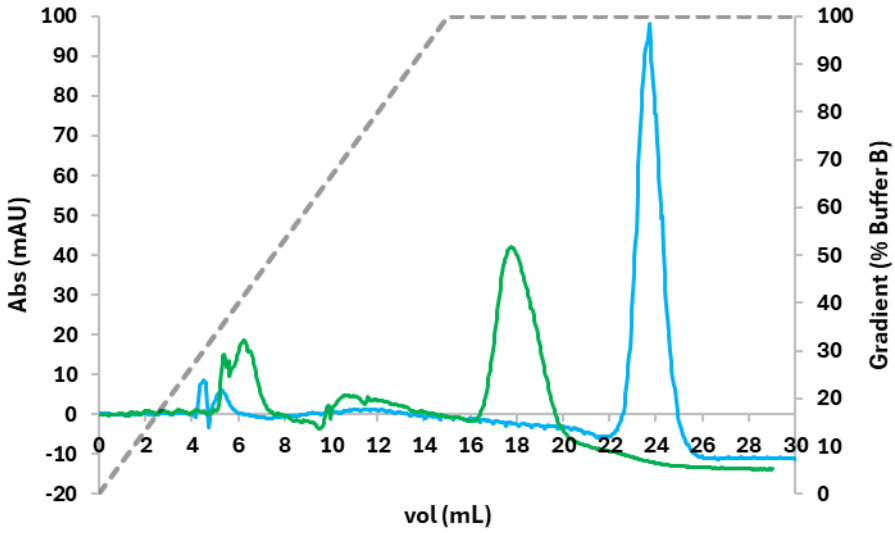

Fig.26: SEC-Semipreparative (ÄKTA Purifier (GE Healthcare) traces of Rituximab non modified (blue),Rit-(sulfoSMCC)-R3C (green); *SkillPak™ 5 mL TOYOPEARL® Phenyl-650-M* (8 mm ID x 100 mm L, Tosoh Bioscience); temperature 25°C; flow, 0.5 ml/min; eluent, eluent, 1,5 M $(NH_4)_2SO_4$ + 100 mM PP Buffer, pH 7 (A), 100 mM PP Buffer + 25% (v/v) IPA pH 7 (B), λ, 215 nm, gradient, 10%-90% B in 30 min.

3.2.3 Ion exchange chromatography

Ion-exchange chromatography (IEX) is one of the most established and versatile chromatographic techniques employed for the purification and analytical characterization of therapeutic monoclonal antibodies (mAbs) and other protein-based biopharmaceuticals. The method separates biomolecules based on differences in net surface charge under defined buffer conditions, exploiting reversible electrostatic interactions between oppositely charged functional groups on the protein and the stationary phase. The retention mechanism is governed primarily by the relationship between the isoelectric point (pI) of the protein and the pH of the mobile phase. When the pH is below the pI, the protein bears a net positive charge and binds to cation exchangers; above its pI, it

becomes negatively charged and interacts with anion exchangers. This behavior can be finely tuned by controlling buffer composition, ionic strength, and gradient profile.

Depending on the sign of the surface charge, separations are performed either in cation-exchange (CEX) or anion-exchange (AEX) mode.

Cation-exchange chromatography (CEX), in particular, is widely employed because most antibodies carry a net positive charge at physiological pH, allowing an easy and effective binding to negatively charged resins. In CEX two modalities are possible:

- strong cation exchangers, bearing sulfonic acid groups, that maintain consistent charge across a broad pH range, providing robust and reproducible separations ideal for large-scale purification
- weak cation exchangers, functionalized with carboxylic acid groups, which exhibit pH-dependent charge behavior, offering finer selectivity and milder elution conditions for analytical applications.

In this study, weak cation exchange (WCX) was selected as the CEX chromatographic technique because it allows the separation based on the post-translational modifications and, in the case of mAbs constructs, the number, attachment sites, and positional orientation on the antibody surface of conjugated payloads, even minor alterations in charge or local environment can therefore result in distinct retention behaviors, providing valuable insights into the heterogeneity of mAbs-sulfoSMCC-RnC preparations.

3.2.3.1 High-pressure ion exchange chromatography

To identify the most suitable chromatographic conditions in HPLC analysis, several weak cation exchange (WCX) columns from different manufacturers

were evaluated under both salt-gradient and pH-gradient elution modes. The tested columns included:

- Phenomenex® Biozen (6 µm particle size, 150 × 4.6 mm)
- Bischoff Chromatography Polyencap (150 × 4.0 mm)
- Thermo Scientific™ ProPac™ WCX-10 (250 × 4.0 mm)
- Tosoh Bioscience TSKgel CMX-STAT (7 µm particle size, 100 × 4.6 mm)

Among these, the Tosoh Bioscience TSKgel CMX-STAT column exhibited superior performance in terms of resolution, reproducibility, and peak symmetry. The Tosoh CMX-STAT column is specifically engineered for the charge profiling of antibodies and constructs. The stationary phase consists of nonporous hydrophilic polymer beads functionalized with carboxymethyl (CMX) groups, which impart weak cation-exchange properties, ensuring high binding capacity and sharp peak profiles even for large biomolecules. The column's low hydrophobicity minimizes nonspecific adsorption, while its surface chemistry provides a uniform and reproducible charge distribution, enabling excellent resolution of minor isoforms and charge variants.[89]

This column was particularly effective in distinguishing between the native antibodies and their conjugated forms. The chromatograms revealed distinct elution profiles for each antibody, reflecting the intrinsic differences in their surface charge.

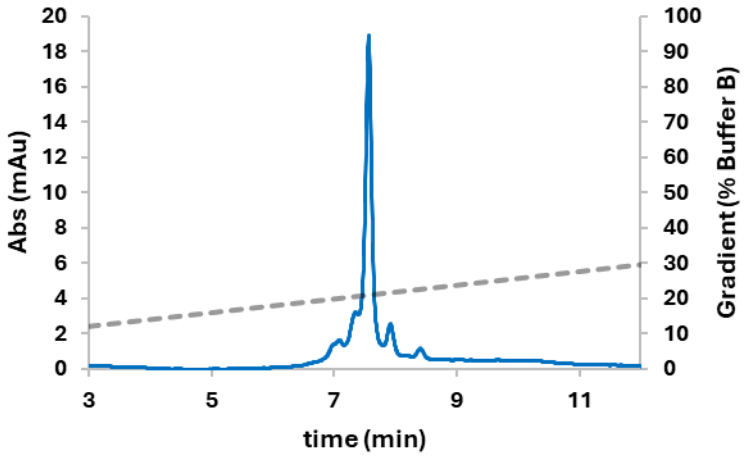

Fig.27: WCX-HPLC (Agilent 1100 series) chromatographic profile of Rituximab; TSKgel CMX-STAT (7 µm particle size, 100 × 4.6 mm, Tosoh Bioscience), temperature 25°C; flow, 1 ml/min; eluent, 10 mM PP buffer pH 7 (A), 10 mM PP buffer + 500 mM NaCl pH 7 (B); λ, 215 nm, gradient, 10-90% B in 20 min.

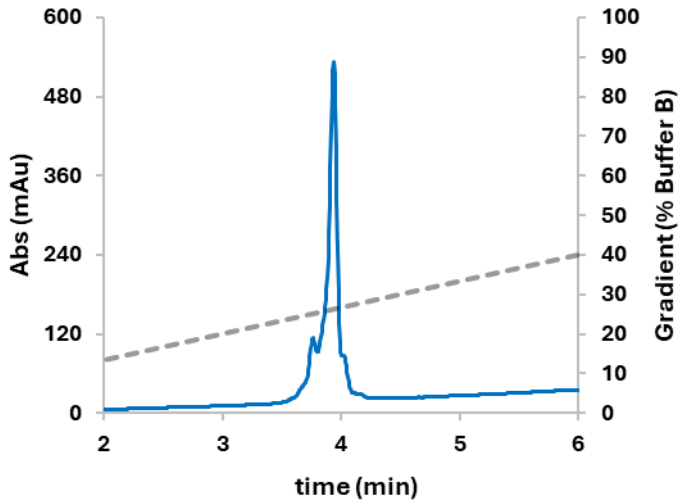

Fig.28: WCX-HPLC (Agilent 1100 series) chromatographic profile of Trastuzumab; TSKgel CMX-STAT (7 µm particle size, 100 × 4.6 mm, Tosoh Bioscience), temperature 25°C; flow, 1 ml/min; eluent, 10 mM PP buffer pH 7 (A),

10 mM PP buffer + 500 mM NaCl pH 7 (B); λ, 215 nm, gradient, 10-90% B in 20 min.

The column demonstrated the ability to differentiate among isomeric and positional variants, particularly for Matuzumab (where three isoforms are equally present). The resolution achieved for these charge variants provides valuable information on the conjugation process, reflecting the efficiency and selectivity of the coupling reactions.

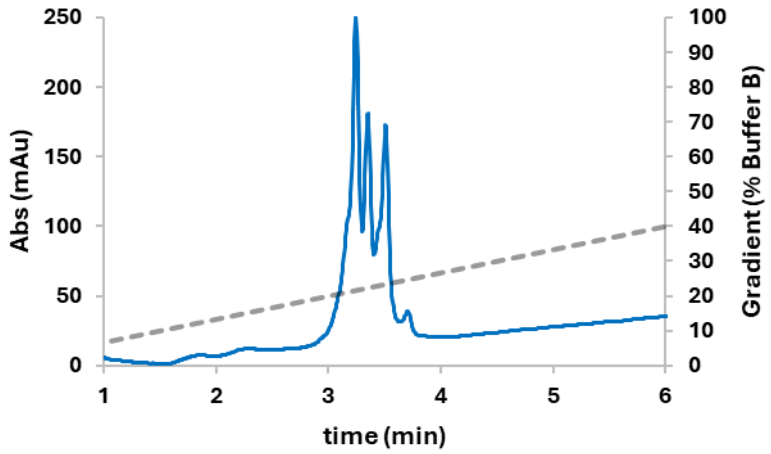

Fig. 29: WCX-HPLC (Agilent 1100 series) chromatographic profile of Matuzumab; TSKgel CMX-STAT (7 µm particle size, 100 × 4.6 mm, Tosoh Bioscience), temperature 25°C; flow, 1 ml/min; eluent, 10 mM PP buffer pH 7 (A), 10 mM PP buffer + 500 mM NaCl pH 7 (B); λ, 215 nm, gradient, 10-90% B in 20 min.

Moreover, within each antibodies-sulfoSMCC-RnC preparation, it was possible to discern multiple partially resolved peaks corresponding to species bearing different numbers of conjugated linker–peptide units , such as mono-, di-, or tri-substituted species, and as supposed based on their drug-antibody ratio they present a different behavior into the column which is confirm by the difference in the retention time. Moreover we can suppose that even the position where the

conjugation took place, so the lysine that had been modified, had impact on the retention, in fact even by working with low excess of peptide, the peaks corresponding to the modified antibodies were ragged.

Below are the chromatograms of modified antibodies (Rituximab, Trastuzumab, and Matuzumab) with varying ratios of linker-peptide units (Fig.30, Fig.31, Fig.32) where the chromatographic analysis revealed that the conjugation between the antibody and the linker–peptide moieties does not proceed to full conversion. The extent of conjugation was markedly influenced by the number of linker–peptide equivalents employed in the reaction. Specifically, the chromatographic profiles corresponding to the use of low excess of oliarginine peptides, Rit-(sulfoSMCC)-(R3C), Trast-(sulfoSMCC)-(R3C) and Mat-(sulfoSMCC)-(R3C) (yellow trace) exhibited fewer and less intense peaks, indicating an incomplete conjugation and a lower diversity of conjugated species. In contrast, the Rit-(sulfoSMCC)-(R3C), Trast-(sulfoSMCC)-(R3C) and Mat-(sulfoSMCC)-(R3C) (green trace) displayed a greater number of peaks with higher intensities, particularly at higher retention times.

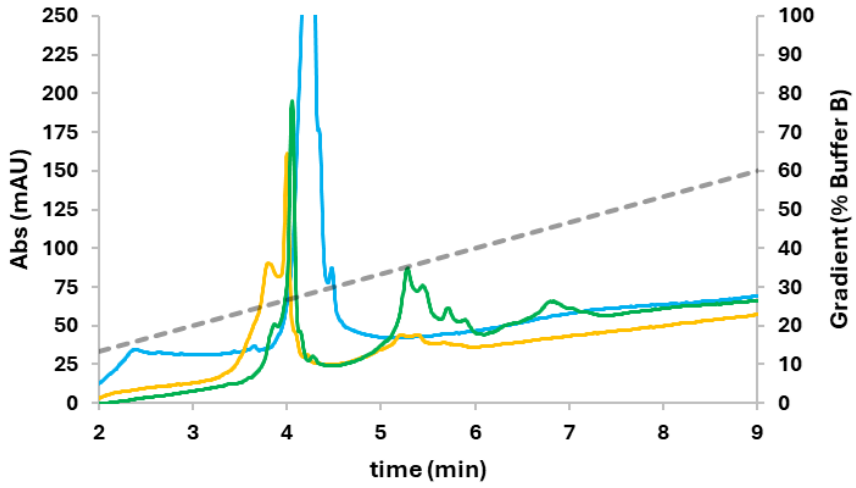

Fig.30: WCX-HPLC (Agilent 1100 series) traces comparison of coupling reaction among Rituximab (0.08 mol, blue trace) and the linker-CR3 (ratio of 1:1 (yellow trace) and 1:2 (green trace)); TSKgel CMX-STAT (7 µm particle size, 100 × 4.6 mm, Tosoh Bioscience), temperature 25°C; flow, 1 ml/min; eluent, A: 10 mM PP Buffer pH7, B: 10 mM PP Buffer, 500 mM NaCl pH7; λ, 215 nm, gradient, 10-80%B in 15 min.

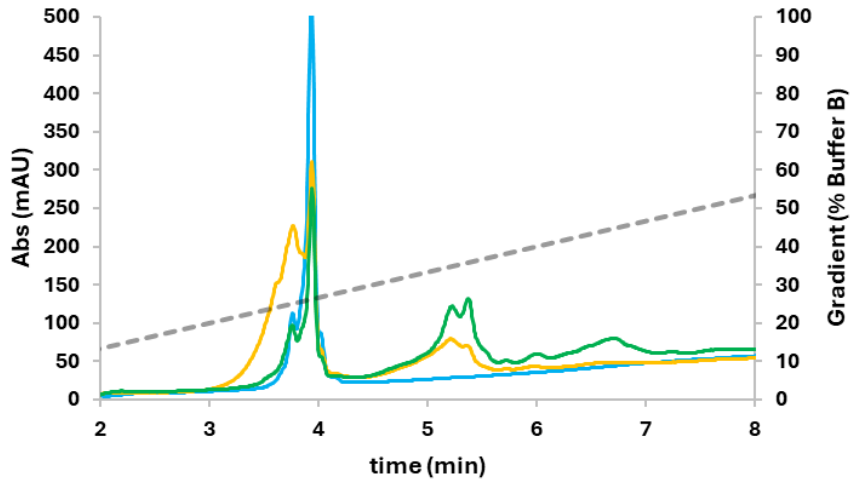

Fig.31: WCX-HPLC (Agilent 1100 series) traces comparison of coupling reaction among Trastuzumab (0.08 mol, blue trace) and the linker-CR3 (ratio of 1:1 (yellow trace) and 1:2 (green trace)). TSKgel CMX-STAT (7 µm particle size, 100 × 4.6 mm, Tosoh Bioscience), temperature 25°C; flow, 1 ml/min; eluent, A: 10 mM PP buffer

pH7, B: 10 mM PP buffer, 500 mM NaCl pH7; λ, 215 nm, gradient, 10-80%B in 15 min.

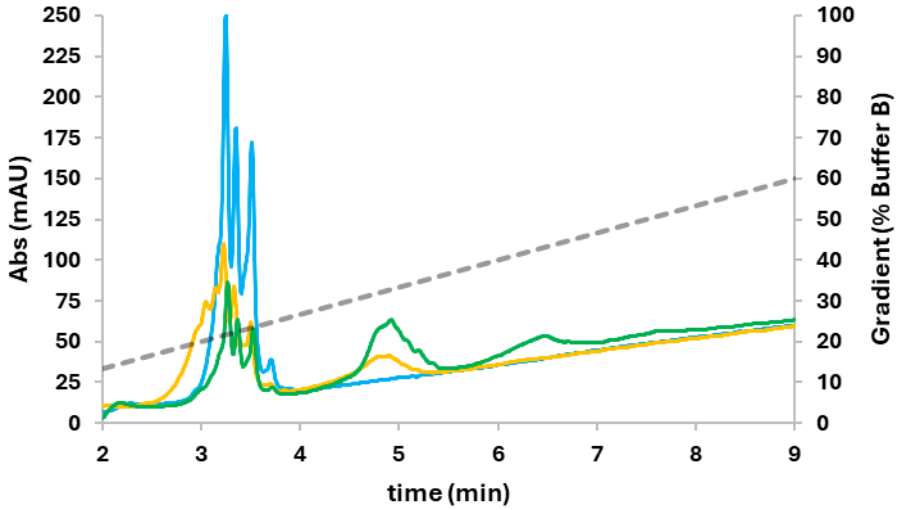

Fig.32: WCX-HPLC (Agilent 1100 series) traces comparison of coupling reaction among Matuzumab (0.08 mol, blue trace) and the linker-CR3 (ratio of 1:1 (yellow trace) and 1:2 (green trace)). TSKgel CMX-STAT (7 µm particle size, 100 × 4.6 mm, Tosoh Bioscience), temperature 25°C; flow, 1 ml/min; eluent, A: 10 mM PP Buffer pH7, B: 10 mM PP buffer, 500 mM NaCl pH7; λ, 215 nm, gradient, 10-80%B in 15 min.

Another crucial factor was determining whether the length of the oligoarginine peptides used for conjugation could affect the retention of the modified antibodies. And as shown in Fig.33, Fig.34 and Fig.35. The chromatographic profiles revealed a clear influence of CPP length on the retention behavior of the conjugates.

The modifiers bearing R3C moieties (green trace) eluted earlier than the one bearing R6C (red trace), indicating reduced interaction with the stationary phase. This demonstrated that the CPP length significantly altered the

physicochemical properties of the antibodies modified, leading to a distinct shift in retention time.

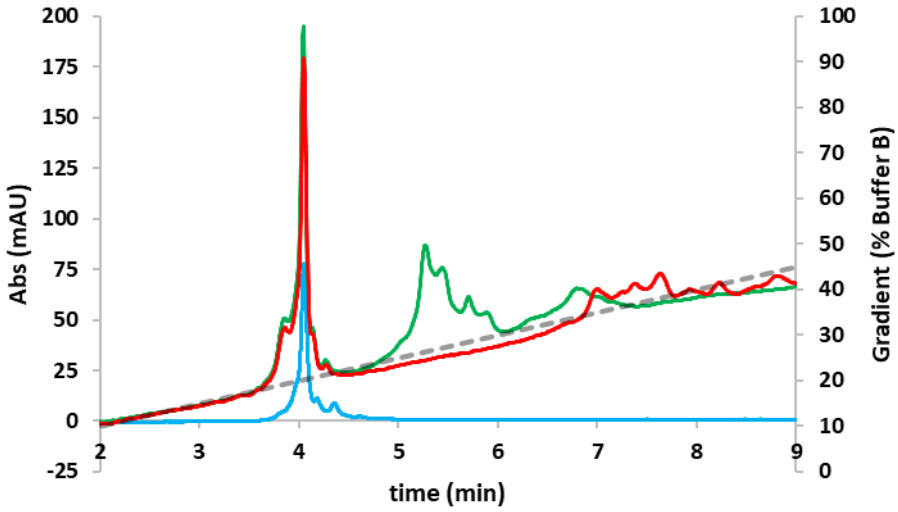

Fig.33: WCX-HPLC (Agilent 1100 series) traces of Rituximab non modified (blue),Rit-(sulfoSMCC)-R3C (green),Rit-(sulfoSMCC)-R6C (red); TSKgel CMX-STAT (7 µm particle size, 100 × 4.6 mm, Tosoh Bioscience), temperature 25°C; flow, 1 ml/min; eluent, 10 mM PP buffer pH 7 (A), 10 mM PP buffer + 500 mM NaCl pH 7 (B); λ, 215 nm, gradient, 10-90% B in 20 min.

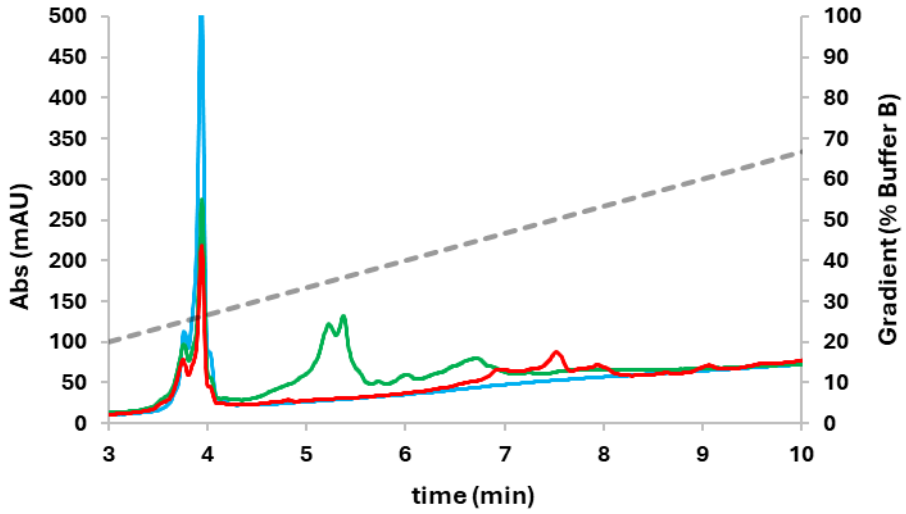

Fig.34: WCX-HPLC (Agilent 1100 series) traces of Trastuzumab non modified (blue), Trast-(sulfoSMCC)-R3C (green), Trast-(sulfoSMCC)-R6C (red); TSKgel CMX-STAT (7 µm particle size, 100 × 4.6 mm, Tosoh Bioscience), temperature 25°C; flow, 1 ml/min; eluent, 10 mM PP buffer pH 7 (A), 10 mM PP buffer + 500 mM NaCl pH 7 (B); λ, 215 nm, gradient, 10-90% B in 20 min.

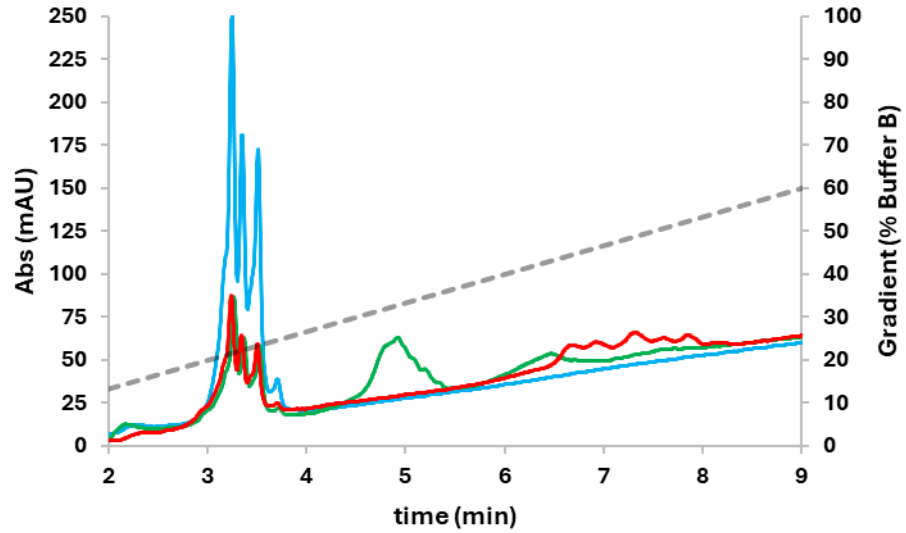

Fig.35: WCX-HPLC (Agilent 1100 series) traces of Matuzumab non modified (blue),Mat-(sulfoSMCC)-R3C (green),Mat-(sulfoSMCC)-R6C (red); TSKgel CMX-

STAT (7 µm particle size, 100 × 4.6 mm, Tosoh Bioscience), temperature 25°C; flow, 1 ml/min; eluent, 10 mM PP buffer pH 7 (A), 10 mM PP Buffer + 500 mM NaCl pH 7 (B); λ, 215 nm, gradient, 10-90% B in 20 min.

These findings indicate that the TSKgel CMX-STAT column possessed sufficient selectivity and resolving power to separate charge variants arising from stepwise conjugation, allowing visualization of subtle compositional heterogeneity within the modified antibodies mixture.

The optimized separation was achieved under salt-gradient conditions, employing Phase A (10 mM phosphate buffer, pH 7) and Phase B (10 mM phosphate buffer, 500 mM NaCl, pH 7). Increasing salt concentration, from phase A to Phase B, continuously weakened electrostatic interactions between the positively charged antibody surfaces and the negatively charged CMX groups of the stationary phase, leading to elution based on increasing isoelectric point (pI) or net positive charge. Thus, unconjugated mAbs, linker-modified intermediates, and fully conjugated mAbs could be clearly distinguished based on their retention behavior.

Such analytical resolution was essential for monitoring conjugation reproducibility and ensuring batch consistency in mAbs-sulfoSMCC-RnC production, which is why it has been used in this research as control analysis.

3.2.3.2 Semi-preparative ion exchange chromatography

Following the analytical evaluation, the same separation principles were scaled up in semi-preparative mode using the SkillPak™ TOYOPEARL® CMX-650S (8 mm ID x 100 mm L, Tosoh Bioscience) in the ÄKTA chromatography system. The stationary phase has a hydrophilic, cross-linked polymethacrylate matrix functionalized with carboxymethyl groups, providing high mechanical stability

and excellent mass-transfer characteristics. The particle size of 65 µm and pore diameter of 100 nm enable efficient binding and elution of high-molecular-weight proteins, including intact antibodies and modified antibodies. This column offers several advantages for preparative applications:

- it maintains high dynamic binding capacity (typically >100 mg mAb/mL of resin) even at moderate flow rates,
- exhibits low backpressure,
- tolerates a wide range of salt and pH conditions.

These features make it particularly suitable for scaling analytical WCX methods into semi-preparative purifications, allowing the isolation of individual charge variants or enrichment of specific conjugate populations.

When operated under the same optimized buffer system (10 mM phosphate buffer, pH 7; gradient to 500 mM NaCl), the resin showed good reproducibility, but the best resolution, and recovery of the protein species with clear separation between unmodified antibodies, linker-intermediate species, and polyarginine-conjugated mAbs was obtained working with mobile phases composed by 15 mM Tris, 15 mM sodium acetate pH9 as loading buffer (A) and by operating a salt gradient to elute by using as mobile phase B the loading buffer with an addition of 500 mM NaCl.

The semi-preparative WCX workflow on the ÄKTA system further demonstrated the robustness of the method. The combination of high resolution, scalability, and gentle separation conditions, with no denaturing agents, made this approach particularly advantageous for downstream analytical applications and for preparative recovery of conjugates intended for functional studies.

As shown in chromatograms in Fig.36 and Fig.37 analyzing in semipreparative mode the antibodies and their modified mixtures cost, as expect, in sensitivity and resolving power. It maintained a nice and prominent separation between the non-modified antibodies and the modified with short oligoarginines peptides, while the conjugates bearing R6C presented a poor resolution.

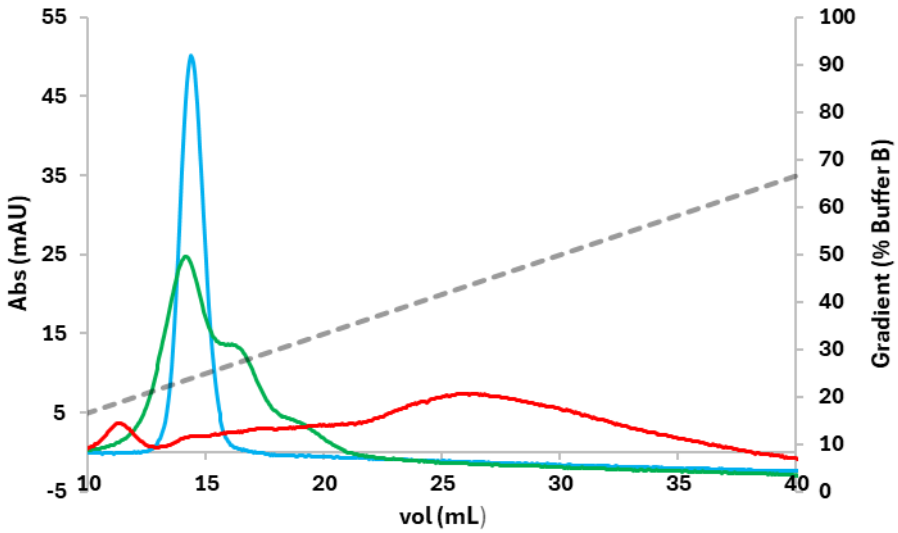

Fig.36: CMX-Semipreparative (ÄKTA Purifier (GE Healthcare) traces of Rituximab non modified (blue),Rit-(sulfoSMCC)-R3C (green), Rit-(sulfoSMCC)-R6C (red); SkillPak™ TOYOPEARL® CMX-650S (8 mm ID x 100 mm L, Tosoh Bioscience); temperature 25°C; flow, 0.5 ml/min; eluent, eluent, 15 mM Tris, 15 mM sodium acetate pH9 (A), 15 mM Tris, 15 mM sodium acetate, 500 mM NaCl pH9 (B), λ, 215 nm, gradient, 10%-90% B in 30 min.

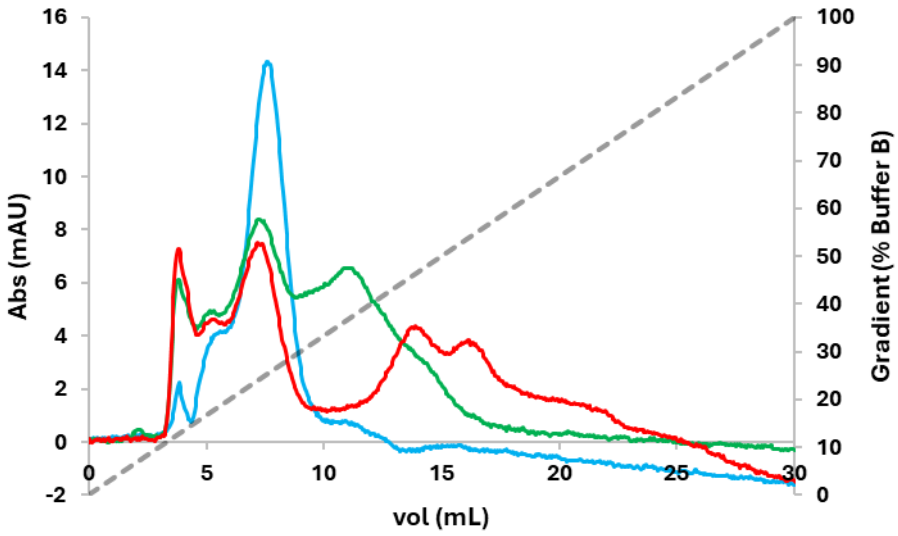

Fig.37: CMX-Semipreparative (ÄKTA Purifier (GE Healthcare) traces of Trastuzumab non modified (blue),Trast-(sulfoSMCC)-R3C (green), Trast-(sulfoSMCC)-R6C (red); SkillPak™ TOYOPEARL® CMX-650S (8 mm ID x 100 mm L, Tosoh Bioscience); temperature 25°C; flow, 0.5 ml/min; eluent, eluent, 15 mM Tris, 15 mM sodium acetate pH9 (A), 15 mM Tris, 15 mM sodium acetate, 500 mM NaCl pH9 (B), λ, 215 nm, gradient, 10%-90% B in 30 min.

As shown in Fig.38, Matuzumab was the antibody that exhibited the poorest resolution in this chromatographic method. In fact, when analyzing its R3C- and R6C-bearing conjugates, no dominant species could be distinguished. The resulting peaks were broad and low in intensity, preventing clear discrimination between the different conjugated forms.

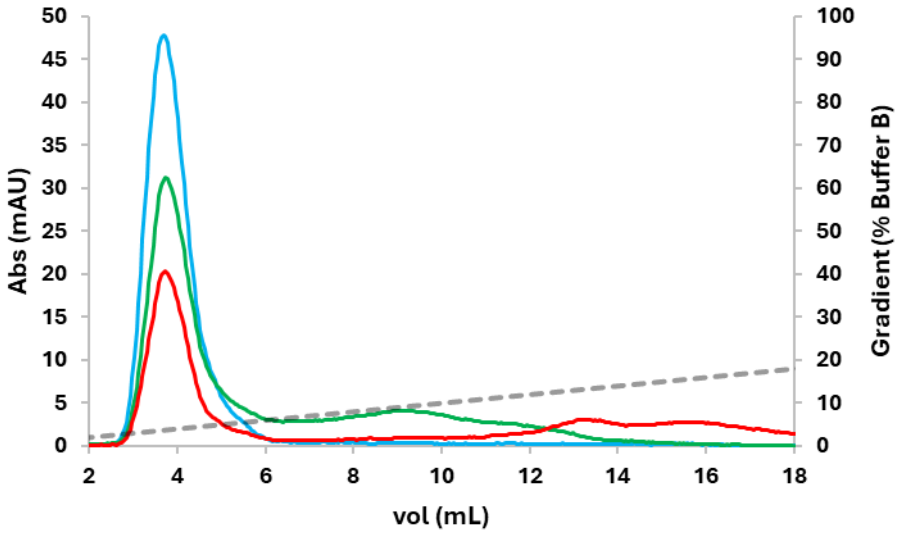

Fig.38: CMX-Semipreparative (ÄKTA Purifier (GE Healthcare) traces of Matuzumab non modified (blue),Mat-(sulfoSMCC)-R3C (green), Mat-(sulfoSMCC)-R6C (red); SkillPak™ TOYOPEARL® CMX-650S (8 mm ID x 100 mm L, Tosoh Bioscience); temperature 25°C; flow, 0.5 ml/min; eluent, eluent, 15 mM Tris, 15 mM sodium acetate pH9 (A), 15 mM Tris, 15 mM sodium acetate, 500 mM NaCl pH9 (B), λ, 215 nm, gradient, 10%-90% B in 30 min.

The successful resolution of mAbs constructs mixtures via WCX chromatography underscored the critical role of surface charge alterations introduced through the conjugation of positively charged oligoarginine peptides. Each additional peptide chain increased the antibody's local and global positive charge, thereby amplifying electrostatic interactions with the negatively charged stationary phase.

This property was effectively exploited to achieve charge-based discrimination among otherwise structurally similar species. Fundamentally, the ability to separate mAbs-sulfoSMCC-RnC variants differing by only one or two attached peptides highlights the exceptional performance of the TSKgel CMX-STAT and

CMX-650S stationary phases, with minimal band broadening and high reproducibility.

While the technique did not directly provide information on DAR, it offered an indispensable qualitative and semi-quantitative assessment of charge heterogeneity, which correlated with conjugation stoichiometry and site distribution.

Furthermore, the use of WCX as both an analytical and semi-preparative tool established a robust platform for monitoring conjugation outcomes, optimizing reaction conditions, and isolating defined antibodies conjugates subpopulations for further biophysical or biological evaluation.

3.2.4 Mixed-mode chromatography (MMC)

Mixed-mode chromatography (MMC), also known as multimodal or dual-mode chromatography, is an advanced chromatographic approach that integrates two or more separation mechanisms, typically ionic, hydrophobic, and hydrogen-bonding interactions, within a single stationary phase. Unlike traditional chromatographic techniques that rely on a single dominant interaction, MMC resins enable simultaneous and tunable binding behaviors, thereby enhancing selectivity, resolution, and loading capacity. Early investigations demonstrated that combining ion-exchange and hydrophobic functionalities within the same stationary phase allows the effective separation of proteins differing in both charge and hydrophobicity, even under mild aqueous conditions.

In this study, the *Eshmuno® CMX resin* (by Merck Life Science) was evaluated as a mixed-mode stationary phase for protein conjugates purification. It integrates the functional properties of both HIC and IEX into a single matrix, offering dual-mode selectivity that is particularly advantageous for separating species

differing in both surface charge and hydrophobicity. The stationary phase is composed of rigid polymethacrylate beads functionalized with tentacle ligands containing 2-amino-4-methylpentanoic acid moieties. The resin's structure enables moderate hydrophobic interactions that enhance selectivity toward hydrophobic or partially modified species, while the weak cationic exchange groups confer a controllable electrostatic contribution adjustable via pH. The ligand's branched aliphatic chain introduces a hydrophobic domain that expands the operational window of the resin, permitting efficient elution by either pH or salt gradients while maintaining high recovery. As reported in Merck's documentation[90], the resin is supplied as a 70% slurry in 20% ethanol with 150 mM NaCl, exhibits a compression factor of approximately 11–15%, and achieves > 3000 theoretical plates per meter with asymmetry between 0.7 and 1.6 under standard testing conditions. These physical parameters indicate a highly efficient and homogeneously packed stationary phase suitable for both analytical and preparative separations.[91,90] (Fig.39)

Fig.39: Stationary phase of Eshmuno® CMX Chromatography resin.

Eshmuno® CMX was initially developed for the purification of monoclonal antibodies (mAbs), ADCs, and fusion proteins, particularly those that are difficult to purify by conventional means. The dual-mode retention mechanism of Eshmuno® CMX is governed by the interplay between pH and ionic strength. At lower pH values (around 5), cationic interactions dominate, favouring protein binding, whereas at higher pH or elevated salt concentrations, hydrophobic interactions become more significant and modulate the elution behaviour. Its driving forces are:

- excellent dynamic binding capacity,
- tolerance to high flow rates and pressures (up to 8 bar),
- compatibility with both laboratory-scale and industrial chromatographic systems.

3.2.4.1 Semi-preparative mixed-mode chromatography

The initial evaluation of Eshmuno® CMX involved testing its resolving power through a step-wise elution protocol adapted from literature methods.[92 93]

The procedure consisted of sequential elution with buffers of varying ionic strength and pH:

- Equilibration buffer: 50 mM sodium acetate, 25 mM sodium sulfate, pH 5 (5 Column Volume(CV))
- Wash buffer 1: 100 mM MES, pH 5.5 (3.5 CV)
- Wash buffer 2: 15 mM TRIS, 15 mM sodium acetate, pH 9 (5 CV)
- Wash buffer 3: 50 mM sodium citrate, 100 mM sodium sulfate, pH 6.1 (6 CV)
- Elution buffer: 100 mM sodium succinate, 300 mM sodium sulfate, pH 6.0 (10 CV)

With the specified buffer compositions, the target protein eluted already during the washing step 3 instead of the designated elution buffer, as commonly described in published studies. The observed co-elution of species indicated that the ionic strength and pH steps were insufficient to exploit the full potential of the resin's mixed-mode functionality.

To address this, the salt concentration and pH were systematically tuned, but these modifications alone did not significantly improve resolution. Ergo, a new strategy employing a combined salt and pH gradient was developed to modulate the balance between electrostatic and hydrophobic interactions during elution.

The optimized mobile phases were:

- *Phase A*: 15 mM TRIS, 15 mM sodium acetate, pH 9
- *Phase B*: 50 mM phosphate buffer (PP buffer), 1 M NaCl, pH 10.2

A general chromatographic method 0–100% B gradient over 30 minutes at a flow rate of 2 mL/min was applied.

Two columns packed with Eshmuno® CMX resin by Isera GmbH with a maximum operation pressure of 8 bar and different bed volumes were tested:

- 8 mm ID × 300 mm length (CV = 15 mL)
- 8 mm ID × 30 mm length (CV = 1.5 mL)

From a theoretical statement, the column length (L) directly affects the resolving power by increasing the number of equilibrium stages or theoretical plates (N). According to the plate theory and gradient elution models, peak capacity in gradient chromatography scales with the square root of column length ($N \propto L$,

peak capacity $\propto \sqrt{L}$). Therefore, doubling or tripling the column length can markedly enhance resolution while preserving chromatographic selectivity, at the cost of increased back pressure and analysis time. Longer columns permit finer spatial distribution of analyte bands and better discrimination between closely related molecular species, such as antibodies constructs subpopulations differing by a single conjugation event.

These principles were confirmed by comparing chromatograms obtained with the two columns. The longer 300 mm column showed sharper, better-resolved peaks and a higher number of theoretical plates compared to the 30 mm column. This difference was particularly evident in the separation of complex antibodies-modified mixtures, where partially modified species and unmodified antibodies exhibited overlapping peaks on the short-column chromatogram but were well differentiated on the long-column chromatogram.

Using optimized composition buffer (Phase A: 15 mM TRIS, 15 mM sodium acetate, pH 9; Phase B: 50 mM phosphate buffer (PP buffer), 1 M NaCl, pH 10.2), both the unmodified antibodies and their ADC eluted as well-defined peaks with high recovery and reproducibility. As illustrated in Fig.40, Fig.41, and Fig. 42, the method yielded sharp, symmetrical peaks, confirming that the gradient approach effectively engaged both the ionic and hydrophobic retention mechanisms of the Eshmuno® CMX resin.

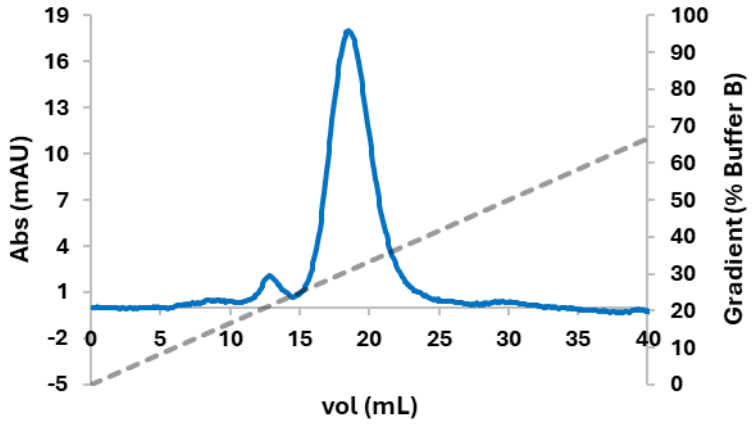

Fig. 40: MMC-Semipreparative (ÄKTA Purifier (GE Healthcare) chromatographic profile of Rituximab; Eshmuno® CMX (8 x 300 mm, Merck); temperature 25°C; flow, 2 ml/min; eluent, 15 mM TRIS, 15 mM Sodium Acetate pH9 (A), 50 mM Phosphate buffer, 1M NaCl pH 10.2 (B); λ, 215 nm, gradient, 0-100%B in 30 min.

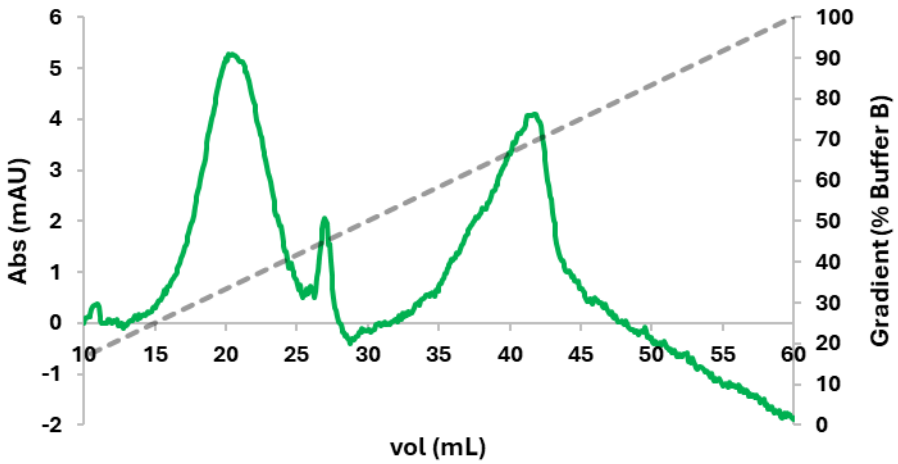

Fig. 41: MMC-Semipreparative (ÄKTA Purifier (GE Healthcare) chromatographic profile of Rit-(sulfoSMCC)-R3C; Eshmuno® CMX (8 x 300 mm, Merck); temperature 25°C; flow, 2 ml/min; eluent, 15 mM TRIS, 15 mM Sodium Acetate

pH9 (A), 50 mM Phosphate buffer, 1M NaCl pH 10.2 (B); λ, 215 nm, gradient, 0-100%B in 30 min.

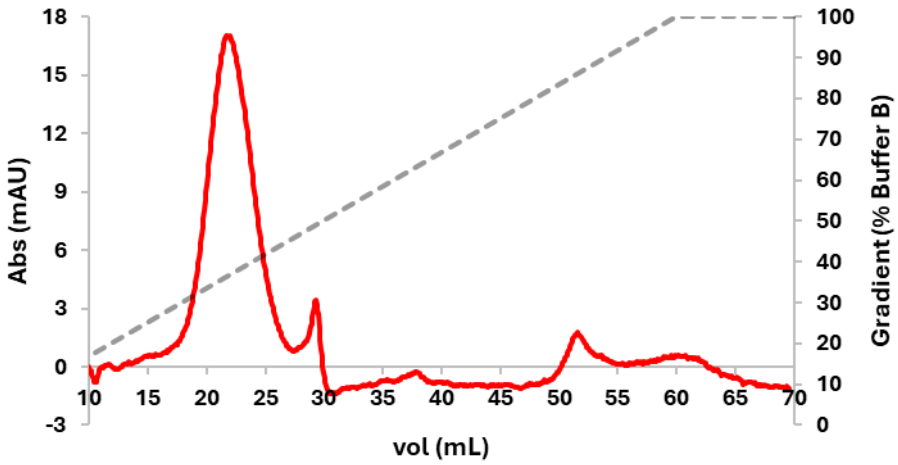

Fig. 42: MMC-Semipreparative (ÄKTA Purifier (GE Healthcare) chromatographic profile of Rit-(sulfoSMCC)-R6C; Eshmuno® CMX (8 x 300 mm, Merck); temperature 25°C; flow, 2 ml/min; eluent, 15 mM TRIS, 15 mM Sodium Acetate pH9 (A), 50 mM Phosphate buffer, 1M NaCl pH 10.2 (B); λ, 215 nm, gradient, 0-100%B in 30 min.

The chromatographic profiles revealed distinct differences between native rituximab and the antibodies conjugates. While the unmodified antibody exhibits a single, symmetrical peak corresponding to the monomeric form, both mAbs-sulfoSMCC-R3C and mAbs-sulfoSMCC-R6C samples displaied multiple additional peaks eluting at later retention times. These new signals reflected heterogeneous conjugation products, including species with different DARs, partially modified intermediates, or minor aggregates. The altered retention behavior indicated that conjugation modified the antibody's surface charge and hydrophobicity, producing variants with distinct physicochemical properties.

Such peak multiplicity was consistent with the formation of a distribution of conjugated isoforms and highlights the intrinsic heterogeneity introduced during the bioconjugation process.

Moreover, the longer column (8 × 300 mm) exhibited superior resolution and peak capacity compared to the shorter version (8 × 30 mm), attributable to its larger bed volume and higher theoretical plate number. For the shorter column, the elution profile showed a single broad peak, with no discernible separation between native and modified antibody species, indicating limited resolution. In contrast, the longer column provided better discrimination, suggesting the presence of multiple species differing in the degree of conjugation. (Fig.43, Fig.44) The extended column length enabled more efficient exploitation of mixed-mode interactions, thereby enhancing selectivity toward species with different net charges and hydrophobicity profiles.

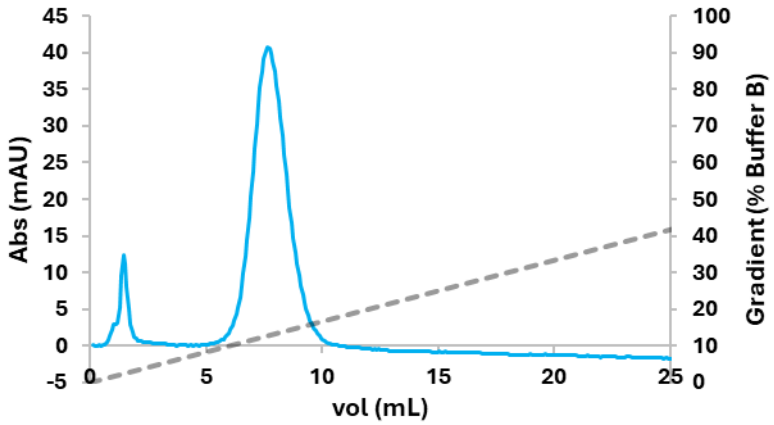

Fig.43: MMC-Semipreparative (ÄKTA Purifier (GE Healthcare) chromatographic profile of Rituximab; Eshmuno® CMX (8 x 30 mm, Merck); temperature 25°C; flow, 2 ml/min; eluent, 15 mM TRIS, 15 mM Sodium Acetate pH9 (A), 50 mM Phosphate buffer, 1M NaCl pH 10.2 (B); λ, 215 nm, gradient, 0-100%B in 30 min.

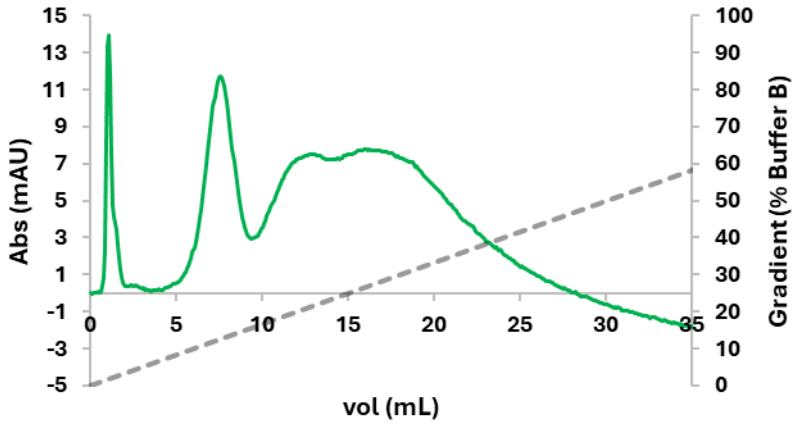

Fig.44: MMC-Semipreparative (ÄKTA Purifier (GE Healthcare) chromatographic profile of Rit-(sulfoSMCC)-R3C; Eshmuno® CMX (8 x 30 mm, Merck); temperature 25°C; flow, 2 ml/min; eluent, 15 mM TRIS, 15 mM Sodium Acetate pH9 (A), 50 mM Phosphate buffer, 1M NaCl pH 10.2 (B); λ, 215 nm, gradient, 0-100%B in 30 min.

The observed performance underscores the central role of MMC in exploiting the physicochemical diversity introduced by RnC conjugation. Adding oligoarginine peptides moieties, increases the net positive charge and slightly altered the hydrophobic surface distribution of the antibody that can be exploited by the dual-mode mechanism of Eshmuno® CMX. The resin's balanced interaction strength allows retention modulation without protein denaturation, preserving the native structure of the conjugates.

In conclusion, this chromatographic strategy provides a powerful analytical tool for characterizing heterogeneity and verifying conjugation efficiency, while also being adaptable to process-scale purification. The combination of high plate number, tunable selectivity, and operational robustness made Eshmuno® CMXX a versatile choice for both method development and manufacturing applications.

3.2.5 Reversed-phase chromatography

In this section of screening different chromatographic techniques to analyze intact mAbs and antibodies constructs under non-denaturing or mild conditions, reverse-phase liquid chromatography was evaluated as a complementary separation technique. This technique offers high reproducibility and sensitivity, especially in resolving minor hydrophobic differences between protein species. Separation occurs by partitioning the analytes between a hydrophobic stationary phase and an aqueous–organic mobile phase.

However, antibodies are large, slightly hydrophobic molecules with complex tertiary structures, and optimizing RPLC for intact separation requires careful selection of the stationary phase and column geometry, as well as fine-tuning of temperature and mobile-phase composition.

3.2.5.1 High-pressure reversed phase chromatography

In the present study, two columns with different stationary-phase chemistries were compared to assess their suitability for intact antibody and modified antibodies separations. The first was an *AdvanceBio RP-mAb Diphenyl column* (Agilent Technologies, 2.1 × 150 mm, 3.5 µm), designed to enhance π–π and hydrophobic interactions via a diphenyl ligand bonded to a silica support and it is more suitable for small peptide fragments or moderately hydrophobic proteins.

The second was a *Phenomenex® BioZen Intact XB-C8 column* (4.6 × 100 mm, 3.6 µm), which features a core–shell particles with a C8 bonded ligand morphology and a moderately hydrophobic C8 alkyl-bonded stationary phase. This column is designed explicitly for intact protein separations, including antibodies and fragments. The features of this column include:

- large pore size that allows antibodies and conjugates to access internal surfaces without excessive excluded volume effects,
- Core-shell architecture, which improves peak sharpness,
- Moderate hydrophobicity (C8 ligand), which mitigates overly strong binding and excessive tailing commonly seen in C18 phases with large proteins,
- Stable operation under elevated temperature conditions.

To further explore separation selectivity, two of the most chromatographic operating conditions, such as column temperature and mobile-phase composition, were tuned. Large biomolecules like antibodies have complex three-dimensional structures and flexible surface regiones, varying temperature can influence conformational dynamics, solvation shells, and the exposure of hydrophobic pockets.

The conventional water–acetonitrile–TFA mobile phases were compared with a modified eluent system inspired by recent literature on modified antibodies analysis. The alternative mobile phases were formulated as follows:

- MPA: H_2O + 0.1% TFA + IPA (98:2, v/v)
- MPB: IPA:ACN:MPA (70:20:10, v/v/v)

These mixed-organic systems introduced isopropanol as a secondary organic modifier, increasing elution strength and altering the selectivity profile. Isopropanol interacts differently with protein surfaces than acetonitrile, due to its higher viscosity and reduced polarity, resulting in gentler desorption of hydrophobic domains and often leading to improved peak recovery for hydrophobic conjugates or denatured fragments. (Fig. 45)

Increasing temperature typically accelerates diffusion, reduces mobile-phase viscosity, and may partially relax conformations, thereby enhancing mass transfer and sharpening peaks. In practice, running the BioZen column at 80 °C rather than a lower temperature (60 °C) often yields better peak shape. (Fig.46)

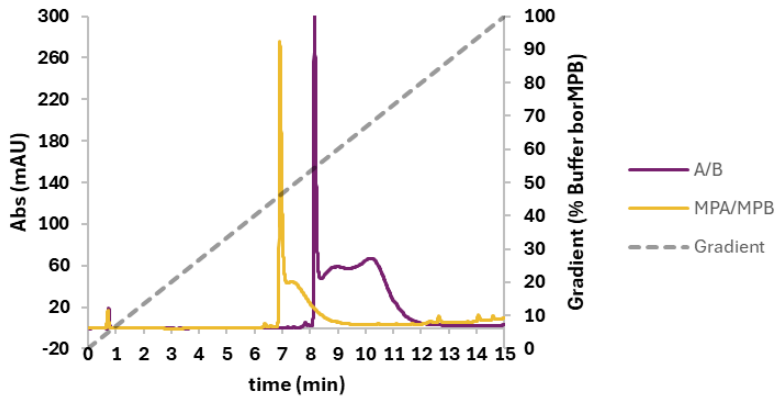

Fig. 45: RP-HPLC (Agilent 1100 series) traces of Rituximab in different eluent system (A and B trace purple; MPA and MPB, trace yellow); *BioZen Intact XB-C8 column* (4.6 × 100 mm, 3.6 µm, *Phenomenex®*), temperature 70°C; flow, 0.6 ml/min; eluent, 0.1% (v/v) TFA in H_2O (A) and 0.1% (v/v) TFA in CH_3CN (B),H_2O + 0.1% TFA + IPA (98:2, v/v) (MPA), IPA:ACN:MPA (70:20:10, v/v/v) (MPB); λ, 215 nm, gradient, 0-100% B in 15 min.

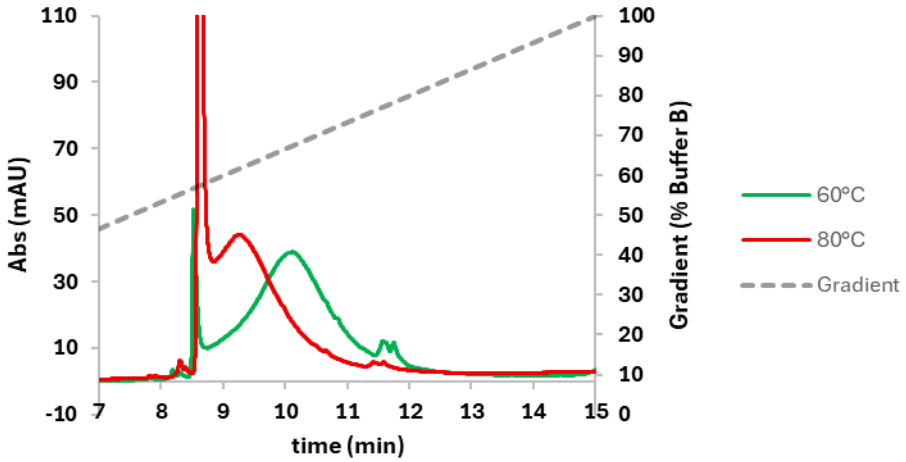

Fig.46: RP-HPLC (Agilent 1100 series) traces of Rituximab in chromatographic conditions; B*ioZen Intact XB-C8 column* (4.6 × 100 mm, 3.6 µm, *Phenomenex®*), temperature 60°C(green trace), 80°C (red trace); flow, 0.6 ml/min; eluent H_2O + 0.1% TFA + IPA (98:2, v/v) (MPA), IPA:ACN:MPA (70:20:10, v/v/v) (MPB); λ, 215 nm, gradient, 0-100% B in 15 min.

3.2.6 Final remarks

The comparative study of non-denaturing and denaturing chromatographic methodologies confirmed that the inherent complexity of not-site specific lysine conjugates cannot be fully elucidated through a single analytical approach.

The chromatographic behavior observed reflects the physicochemical changes introduced upon conjugation, including shifts in surface charge, hydrophobicity, and molecular size. These modifications lead to distinct retention profiles and, in some cases, the appearance of additional peaks corresponding to intermediate or over-conjugated forms. Each technique contributed unique and complementary insights: SEC enabled quantitative evaluation of monomer content, fragments, and aggregates; IEX resolved charge variants and provided information on conjugation-induced modifications providing a first indication of

DAR; MMC connected these mechanisms to offer tunable selectivity through simultaneous hydrophobic and ionic interactions.

Optimization of experimental conditions, such as buffer composition, pH, ionic strength, and gradient, proved fundamental for achieving adequate resolution and minimizing nonspecific adsorption, particularly for hydrophobic or highly charged conjugates.

3.3 Multi-dimensional Liquid Chromatography (mD-LC)

The development of therapeutic antibodies conjugated with oligoarginine moieties presents a unique analytical challenge, owing to their structural complexity, heterogeneous conjugation profiles, and the coexistence of closely related variants. Traditional one-dimensional liquid chromatography (LC) methods often lack the resolving power required to discriminate between such multifaceted species, particularly when analytes differ subtly in charge, hydrophobicity, or conjugation degree. To overcome these limitations, multidimensional liquid chromatography (mD-LC) has emerged as a powerful approach capable of significantly enhancing selectivity and resolution by coupling orthogonal separation mechanisms.

In the present work, mD-LC was employed to characterize and evaluate the conjugation profiles of therapeutic antibody–oligoarginine constructs. The methodology was explored in both fully comprehensive and single heart-cutting configurations to assess their relative efficiency and applicability to complex bioconjugate analysis. In the comprehensive mode, the entire first-dimension effluent was transferred to the second dimension, enabling exhaustive mapping of all eluting species and providing a global view of the antibody heterogeneity landscape. Conversely, the heart-cutting mode was strategically applied to isolate and further resolve specific chromatographic regions containing critical or partially overlapping components, thus allowing a focused examination of key conjugate species with improved analytical throughput.

3.3.1 Construction and validation of two-dimensional chromatography system

A part of this project aimed to develop a robust multidimensional liquid chromatography system capable of purify synthetic therapeutic monoclonal

antibody conjugates integrating different chromatographic techniques, such as SEC, IEX, HIC, MMC or RP.

Based on the results obtained from the screening of different one-dimensional chromatographic techniques, discussed in paragraph 3.2, it was decided to exploit the resolving power of the chromatographic modes which provided the best separation between the unmodified antibody and the mixture of various modified antibody species, species that differ in the number of attached linker–peptide units and in their conjugation sites.

For this reason, a chromatographic setup comprising two semi-orthogonal, chromatographic dimensions in series was designed, allowing analysis in both full comprehensive and single heart-cut modes.

The selected chromatographic techniques were:

- Ion-exchange chromatography (cation exchange mode)
- Mixed-mode chromatography (Eshmuno® CMX)

The ÄKTA Purifier system was selected to perform these analyses. To adapt this semi-preparative system for 2D-LC, several instrumental modifications were required, including the installation of additional electronic valves and manual switch flow valves, as well as method adjustments to integrate information on flow path and switching timing.

Furthermore, when designing a mD-LC experiment involving different chromatographic modes in series, several factors must be carefully considered in advance.

The first and most critical aspect was the compatibility of the mobile phases used in each dimension. It was essential to ensure that the eluents were

mutually miscible and did not compromise the solubility of the analytes transferred between dimensions, while maintaining the integrity of the stationary phase in the second dimension. Another crucial factor was the elution strength of the mobile phases, specifically whether the solvent composition from the first dimension was too strong to affect retention and resolution in the second dimension.

The second key parameter to consider was the overall system's peak capacity, which depended on the efficiency of compound transfer from the first to the second dimension, the dilution factor during this transfer, and the secondary column's sensitivity and resolving power.

The first step in building the mD-LC system focused on verifying the compatibility of the chromatographic techniques selected for series separation: cation exchange chromatography and mixed-mode chromatography.

In particular, the primary focus was on the compatibility of the mobile phases. For both chromatographic methods, aqueous mobile phases with different saline compositions and pH values were used. It was necessary to assess whether the mixtures from both chromatographies were miscible and whether the elution strength of the first chromatography's mobile phase mixture was sufficient to achieve elution in the second dimension.

But first, as a proof-of-concept, it was decided to confirm that both separations maintained the physicochemical integrity of mAbs and their modified throughout the process. For this reason, peaks collected from mixed-mode chromatography (Eshmuno® CMX column (8 mm ID x 300 mm L)) and cation exchange chromatography (SkillPak® 5 mL TOYOPEARL™ CMX-650S) were isolated, concentrated using Amicon Ultra centrifugal filters (0.5 mL, 10 kDa cut-

off), and subsequently reinjected into weak cation exchange (WCX) chromatography in analytical conditions.

For both the unmodified and the modified antibodies, it was possible to maintain the same retention behavior, confirming that these chromatographic techniques did not compromise the integrity or retention. These tests had been performed for Rituximab and Trastuzumab, and for the case study, only a few of the produced antibodies species produced had been analyzed.

As shown in Fig.47-50, Rit-(sulfoSMCC)-R3C had been checked first by performing an analytical run using TSKGel CMX-STAT (Tosoh Bioscience) to have an understanding of the chromatographic profile, and the same complex mixture had been loaded on Eshmuno® CMXX, where the two main peaks retention time (r.t.) of 9 min and the one at r.t. 17 min had been collected and analyzed through HPLC IEX chromatography. From the behavior and shape of the peaks, it was confirmed that the integrity of the proteins did not have been compromised.

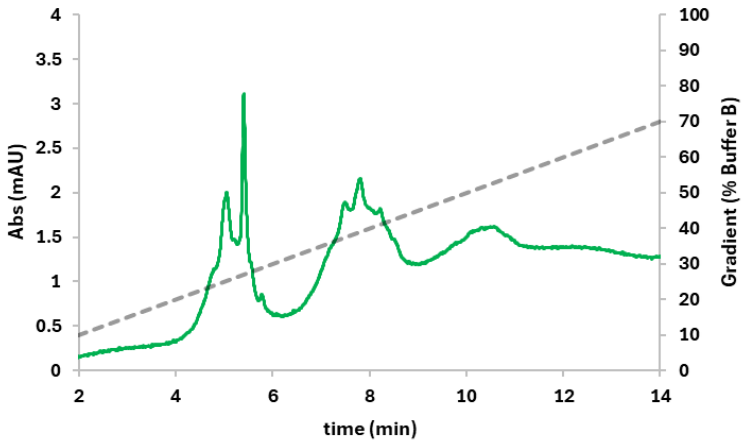

Fig.47: WCX-HPLC (Agilent 1100 series) chromatographic profile of Rit-(sulfoSMCC)-(R3C); TSKgel CMX-STAT (7 µm particle size, 100 × 4.6 mm, Tosoh Bioscience), temperature 25°C; flow, 1 ml/min; eluent, 10 mM PP buffer pH 7 (A),

10 mM PP buffer + 500 mM NaCl pH 7 (B); λ, 215 nm, gradient, 10-90% B in 20 min.

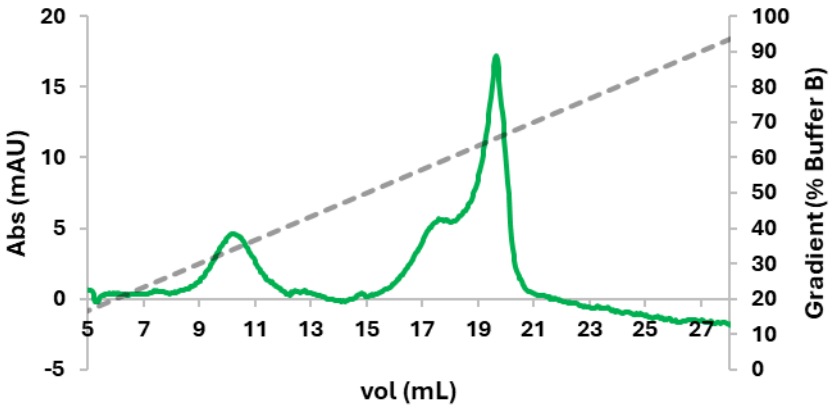

Fig.48: MMC-Semipreparative (ÄKTA Purifier (GE Healthcare) chromatographic profile of Rit-(sulfoSMCC)-R3C; Eshmuno® CMX (8 x 300 mm, Merck); temperature 25°C; flow, 2 ml/min; eluent, 15 mM TRIS, 15 mM Sodium Acetate pH9 (A), 50 mM Phosphate buffer, 1M NaCl pH 10.2 (B); λ, 215 nm, gradient, 0-100%B in 30 min

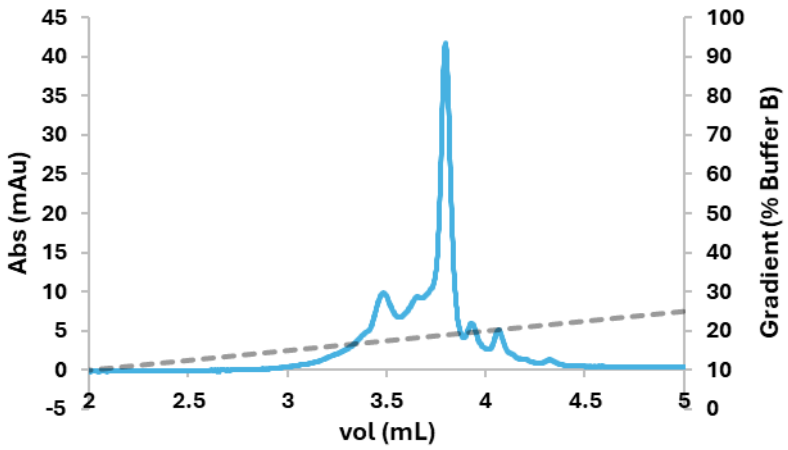

Fig.49: WCX-HPLC (Agilent 1100 series) chromatographic profile of Rituximab peak collected from MMC semipreprative run; TSKgel CMX-STAT (7 µm particle size, 100 × 4.6 mm, Tosoh Bioscience), temperature 25°C; flow, 1 ml/min; eluent,

10 mM PP buffer pH 7 (A), 10 mM PP buffer + 500 mM NaCl pH 7 (B); λ, 215 nm, gradient, 10-90% B in 20 min.

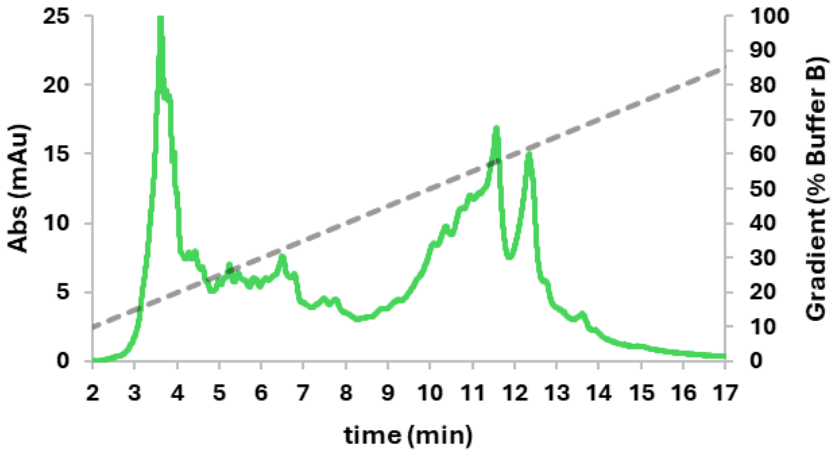

Fig.50: WCX-HPLC (Agilent 1100 series) chromatographic profile of Rit-(sulfoSMCC)-R3C peak collected from MMC semipreprative run; TSKgel CMX-STAT (7 µm particle size, 100 × 4.6 mm, Tosoh Bioscience), temperature 25°C; flow, 1 ml/min; eluent, 10 mM PP buffer pH 7 (A), 10 mM PP buffer + 500 mM NaCl pH 7 (B); λ, 215 nm, gradient, 10-90% B in 20 min.

As said before, the same work plan has been applied to SkillPak™ TOYOPEARL® CMX 650-S. In Fig.51-54 the chromatograms Trast-(sulfoSMCC)-R3C are shown. In order the preliminary analytical chromatogram for the complex mixture, the semi-preparative run where the peaks of reference material and their conjugates have been collected separately and, after concentration, loaded back on the analytical system to verify the state of the proteins. And, again, it was safe to say that both chromatography techniques do not degrade the protein and there is a good recovery.

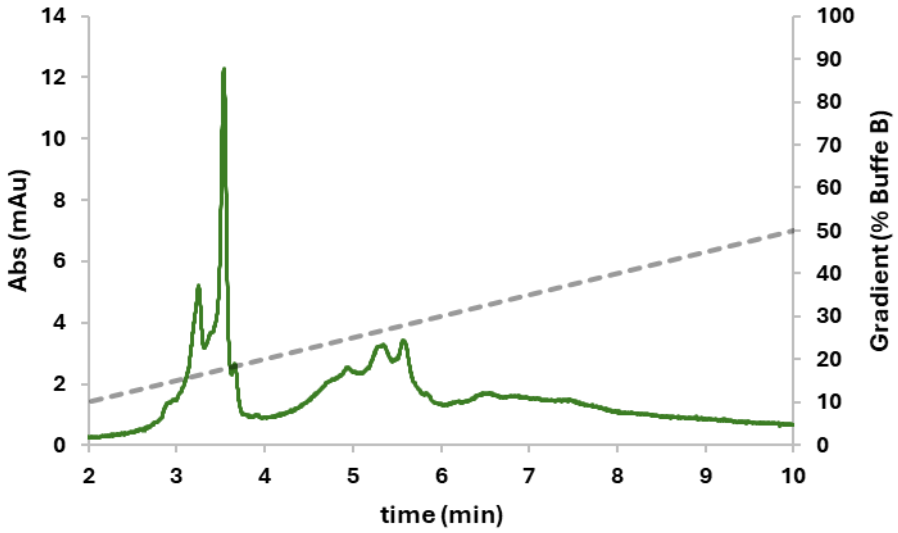

Fig.51: WCX-HPLC (Agilent 1100 series) chromatographic profile of Trast-(sulfoSMCC)-(R3C); TSKgel CMX-STAT (7 µm particle size, 100 × 4.6 mm, Tosoh Bioscience), temperature 25°C; flow, 1 ml/min; eluent, 10 mM PP buffer pH 7 (A), 10 mM PP buffer + 500 mM NaCl pH 7 (B); λ, 215 nm, gradient, 10-90% B in 20 min.

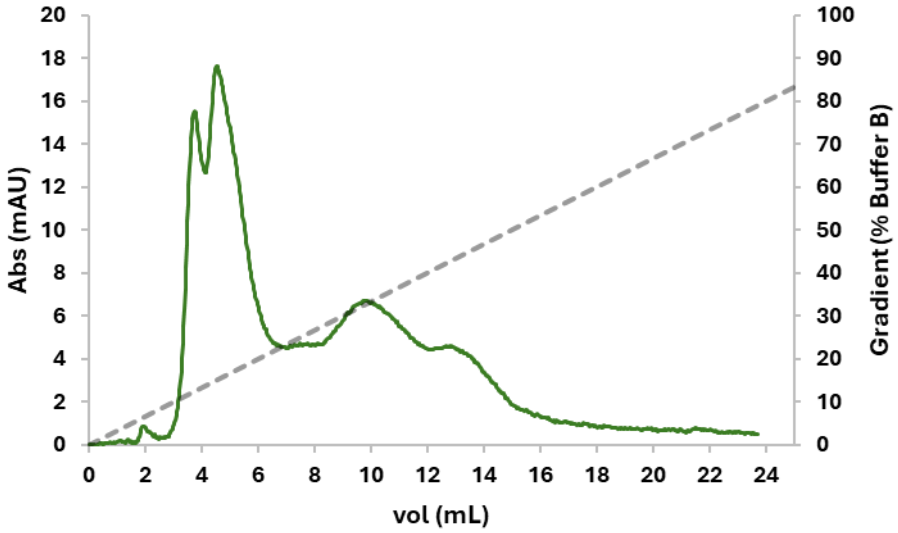

Fig.52: CMX-Semipreparative (ÄKTA Purifier (GE Healthcare) chromatographic profile of Trast-(sulfoSMCC)-R3C; SkillPak™ TOYOPEARL® CMX-650S (8 mm ID x

100 mm L, Tosoh Bioscience); temperature 25°C; flow, 0.5 ml/min; eluent, eluent, 1,5 M (NH4)2SO4 + 100 mM PP Buffer, pH 7 (A), 100 mM PP buffer + 25% (v/v) IPA pH 7 (B), λ, 215 nm, gradient, 10%-90% B in 30 min.

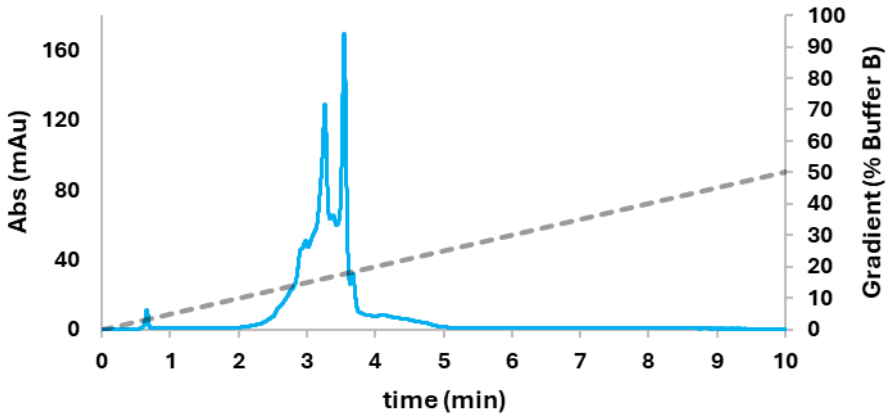

Fig.53: WCX-HPLC (Agilent 1100 series) chromatographic profile of Trastuzumab peak collected from MMC semipreprative run; TSKgel CMX-STAT (7 µm particle size, 100 × 4.6 mm, Tosoh Bioscience), temperature 25°C; flow, 1 ml/min; eluent, 10 mM PP buffer pH 7 (A), 10 mM PP buffer + 500 mM NaCl pH 7 (B); λ, 215 nm, gradient, 10-90% B in 20 min.

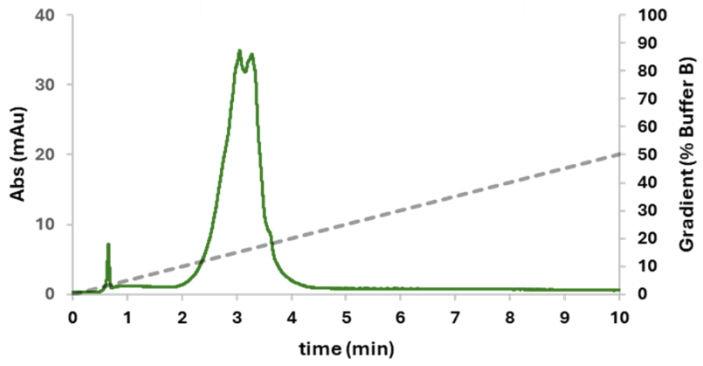

Fig.54: WCX-HPLC (Agilent 1100 series) chromatographic profile of Trast-(sulfoSMCC)-R3C peak collected from MMC semipreprative run; TSKgel CMX-STAT (7 µm particle size, 100 × 4.6 mm, Tosoh Bioscience), temperature 25°C;

flow, 1 ml/min; eluent, 10 mM PP buffer pH 7 (A), 10 mM PP buffer + 500 mM NaCl pH 7 (B); λ, 215 nm, gradient, 10-90% B in 20 min.

Once established that neither mixed-mode nor IEX chromatography compromised the physicochemical integrity of antibodies constructs, maintaining their retention behavior, the next step was to assess their sequential compatibility, verifying whether fractions collected from Eshmuno® CMX runs were concentrated and injected onto the IEX column.

The chromatographic profiles indicated that both techniques were compatible and that sample transfer between them was feasible without peak distortion or sample degradation. In Fig.55-57, it was possible to follow the analytical chromatographic profile of Rit-(sulfoSMCC)-R3C, the Eshmuno® CMX chromatograms, from which the peak eluted at 40 mL had been collected, exchanged buffer, concentrated, and injected into the IEX column.

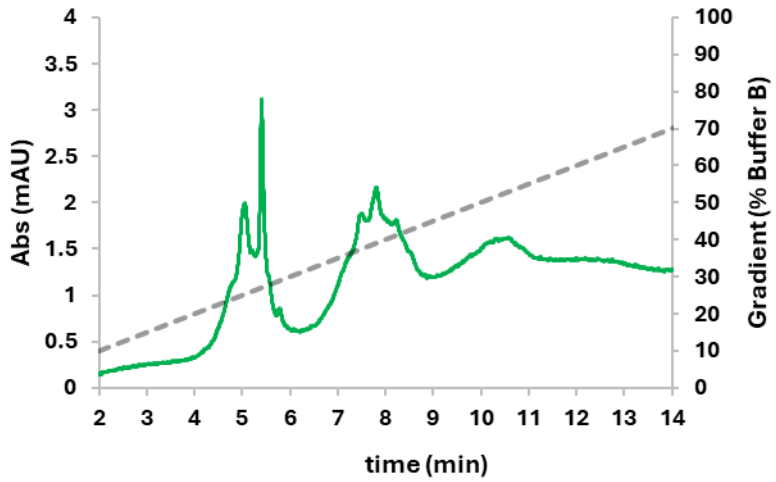

Fig.55: WCX-HPLC (Agilent 1100 series) chromatographic profile of Rit-(sulfoSMCC)-(R3C); TSKgel CMX-STAT (7 µm particle size, 100 × 4.6 mm, Tosoh Bioscience), temperature 25°C; flow, 1 ml/min; eluent, 10 mM PP buffer pH 7 (A),

10 mM PP buffer + 500 mM NaCl pH 7 (B); λ, 215 nm, gradient, 10-90% B in 20 min.

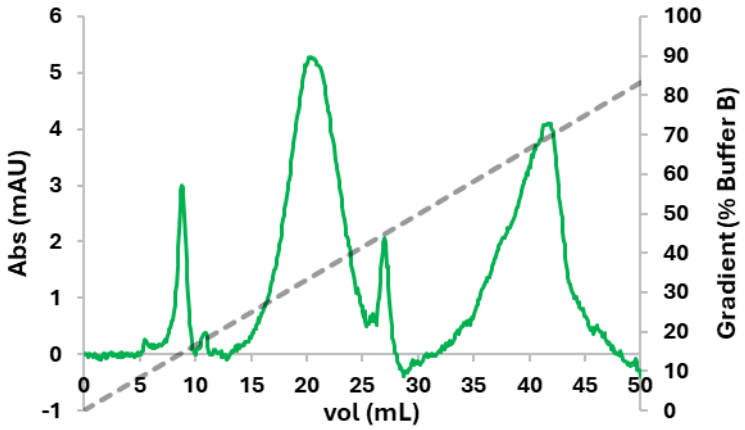

Fig.56: MMC-Semipreparative (ÄKTA Purifier (GE Healthcare) chromatographic profile of Rituximab; Eshmuno® CMX (8 x 300 mm, Merck); temperature 25°C; flow, 2 ml/min; eluent, 15 mM TRIS, 15 mM Sodium Acetate pH9 (A), 50 mM Phosphate buffer, 1M NaCl pH 10.2 (B); λ, 215 nm, gradient, 0-100%B in 30 min.

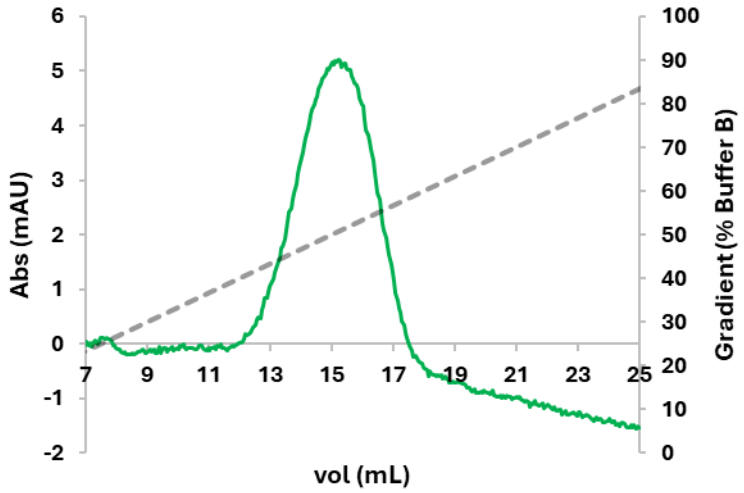

Fig.57: CMX-Semipreparative (ÄKTA Purifier (GE Healthcare) chromatographic profile of Rit-(sulfoSMCC)-R3C peak collected from MMC run; SkillPak™ TOYOPEARL® CMX-650S (8 mm ID x 100 mm L, Tosoh Bioscience); temperature 25°C; flow, 0.5 ml/min; eluent, eluent, MPA: 15 mM TRIS, 15 mM Acetate, pH 9, MB1: 15 mM Tris, 15 mM Acetate, 500 mM NaCl, pH 9, λ, 215 nm, gradient, 10%-90% B in 30 min.

The next logical step was to explore whether these two methods could be directly connected within a single chromatographic system.

To evaluate this, it was necessary to address the composition of the mobile phases for each chromatography. Both IEX and MMC used the same buffer as mobile phase A (MPA: 15 mM TRIS, 15 mM Acetate, pH 9), while the mobile phase B had a complete different composition: different salt, different salt concentration and different pH. The eluent buffer for IEX was the mobile phase A with addition of 500 mM NaCl (MB1: 15 mM Tris, 15 mM Acetate, 500 mM NaCl, pH 9) instead the mobile phase B for MMC was a low concentration of PP buffer

and high amount of NaCl at more basic pH (MPB2: 50 mM PP Buffer, 1 M NaCl, pH 10.2).

Based on the composition of the buffers, it was safe to say that they were perfectly miscible. It was also safe to say that the elution strength of MPB2 was much stronger than the one of MPB1, since the concentration of NaCl was doubled, 1 M instead of 500 mM.

For this reason, it was decided to test Eshmuno® CMX with MPB1 to verify whether a milder salt gradient, while maintaining the pH gradient, was already sufficient to elute the protein from the stationary phase. As shown in Fig.58 this buffer composition exhibited sufficient elution strength to recover the antibody; however, it led to a reduction in resolution.

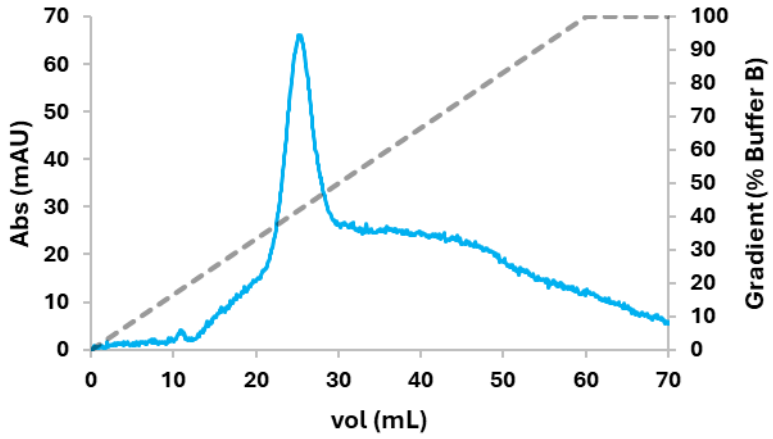

Fig.58: MMC-Semipreparative (ÄKTA Purifier (GE Healthcare) chromatographic profile of Rituximab; Eshmuno® CMX (8 x 300 mm, Merck); temperature 25°C; flow, 2 ml/min; eluent, MPA:15 mM TRIS, 15 mM Sodium Acetate pH9, MBP1:15 mM Tris, 15 mM Acetate, 500 mM NaCl, pH 9; λ, 215 nm, gradient, 0-100%MPB in 30 min.

Based on these performances, it was decided to keep using the MPB1 for IEX and the MPB2 for MMC to elute antibodies from the stationary phase.

But this study uncovered the need of an intermediate desalting step between the two chromatographies to preserve the resolving power of both dimensions.

The next phase of the work was focused on understanding how to handle a 2D-LC system. A conventional ÄKTA Purifier setup is composed of a set of pumps, an injection valve, a UV detector, and an outlet valve, see Fig.59, and it serves as single dimension purification.

The extension to two dimensions required reconfiguring flow paths and introducing additional valve control to enable smooth transitions between mobile phases and between chromatographic dimensions, while preserving overall pressure stability and detector integration.

Having two separations online required an additional valve for dimension switching: an added valve acts as a dedicated flow-path selector, routing eluate from D1 into D2 or bypassing it as needed. This valve ensures pressure balance during transitions and maintains detector stability.

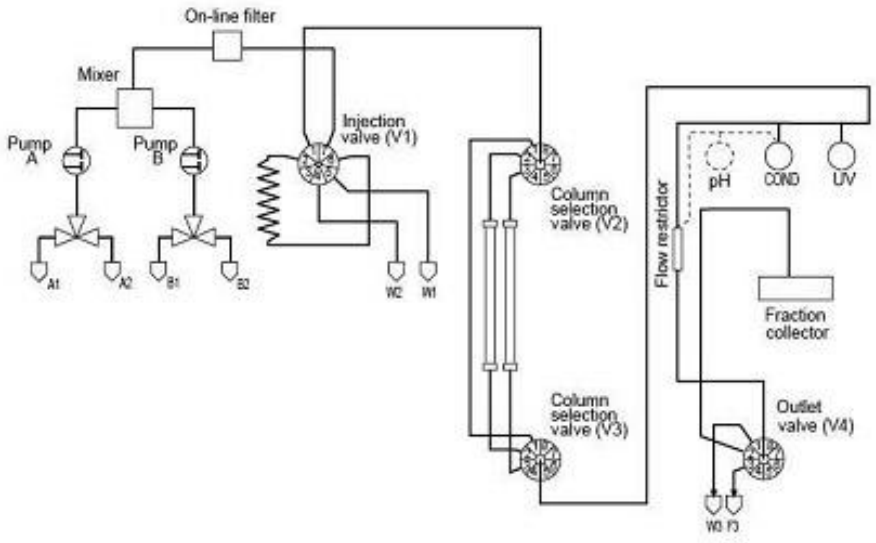

Fig.59: General scheme of mD-LC, highlighting the presence of two multiport valves (column selection valve V2, column selection valve V3)

First validation experiments were carried out using SEC as the first dimension, coupled with either MMC or IEX as the second dimension.

The experimental workflow for these preliminary trials used a full comprehensive 2D-LC approach. The flow originated from the solvent delivery pumps and proceeded to the injection valve, where mAbs or mAbs conjugates were manually introduced into the system. After the injection, the protein sample was loaded onto the first-dimension chromatographic column (SEC), where the entire elution profile was transferred through a valve-switching mechanism, directing the effluent to the second-dimension column (Eshmuno® CMX or SkillPak™ 5 mL TOYOPEARL® CMX 650S) for subsequent separation. The final eluate was monitored by a UV detector, with chromatographic signals recorded continuously throughout the analysis. The working diagram for this set-up is show below in Fig.60.

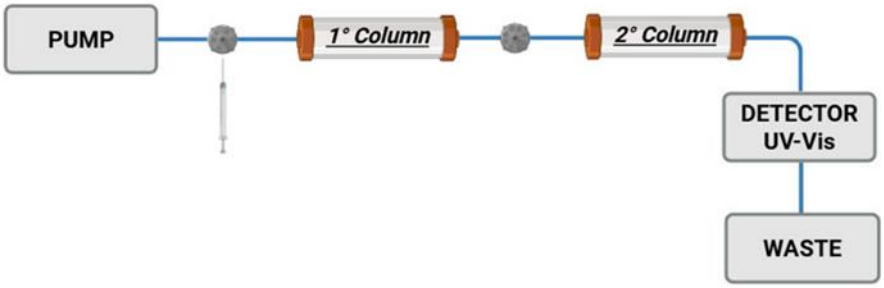

Fig.60: Schematic diagram of a linear two-column liquid chromatography setup.

The SEC chromatography was selected as 1D because it exhibits a mild, non-interacting mechanism that minimized sample perturbation and thus served as a suitable preliminary check of system integrity.

Using a HiTrap™ 5 mL Desalting column in isocratic gradient (MPA: 15 mM TRIS, 15 mM Acetate, pH 9), the effluent was directed into Eshmuno® CMXX as second dimension (MPB2: 50 mM PP buffer, 1 M NaCl, pH 10.2) using a 0–100% salt gradient over 30 minutes at 2 mL/min, yielding coherent peak patterns with a slight decrease in UV signal intensity, traceable to dilution during SEC elution phase, and most importantly managing pressure regulation, as reported in chromatograms, Fig.61 and Fig.62.

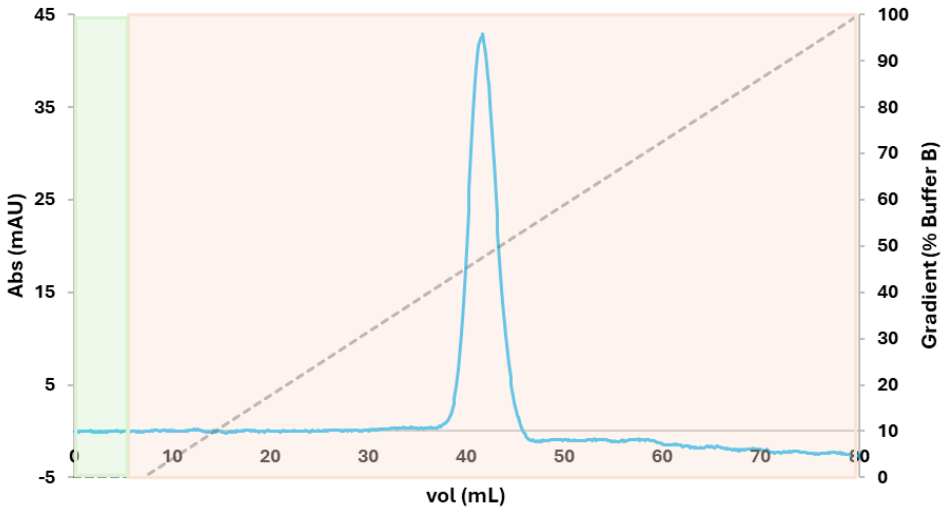

Fig. 61: Two-dimensional chromatographic profile of Rituximab; [1]D: SEC (HiTrap Desalting 5 mL 1.6 x 2.5 cm, Cyvita), [2]D: MMC (Eshmuno® CMX, 8 x 300 mm, Merck),ÄKTA Purifier (GE Healthcare); temperature 25°C; flow, 2 ml/min; eluent, 15 mM TRIS, 15 mM sodium acetate pH9 (A), 50 mM PP buffer, 1 M NaCl, pH 10.2λ, 215 nm, gradient, 100%A in 7 min and 0-100%B in 30min.

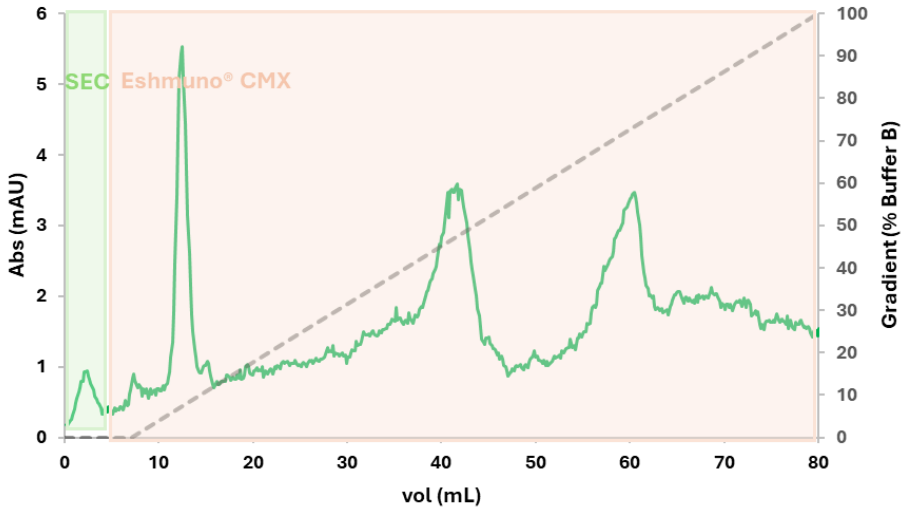

Fig.62: Two-dimensional chromatographic profile of Rit-(sulfoSMCC)-R3C; [1]D: SEC (HiTrap Desalting 5 mL 1.6 x 2.5 cm, Cyvita), [2]D: MMC (Eshmuno® CMX, 8 x 300 mm, Merck),ÄKTA Purifier (GE Healthcare); temperature 25°C; flow, 2

ml/min; eluent, 15 mM TRIS, 15 mM sodium acetate pH9 (A), 50 mM PP buffer, 1 M NaCl, pH 10.2λ, 215 nm, gradient, 100%A in 7 min and 0-100%B in 30min.

Later, the same design of experiment (DoE) was used with the SkillPak™ 5 mL TOYOPEARL® CMX 650S (IEX column) as 2D, using a 0–100% salt gradient over 30 minutes at 1 mL/min (MPB1: 15 mM TRIS, 15 mM Acetate, pH9). And, in this setting, a good coherence in peak patterns was maintained with an effective fraction transfer.

The results demonstrated reproducible chromatographic profiles for Rituximab and its modified variants (Rit-(sulfoSMCC)-R3C and Rit-(sulfoSMCC)-R6C), as shown in Fig.63-65.

Nevertheless, the preservation of peak shape and retention order confirmed the functionality and robustness of the 2D-LC configuration for both chromatographic combinations.

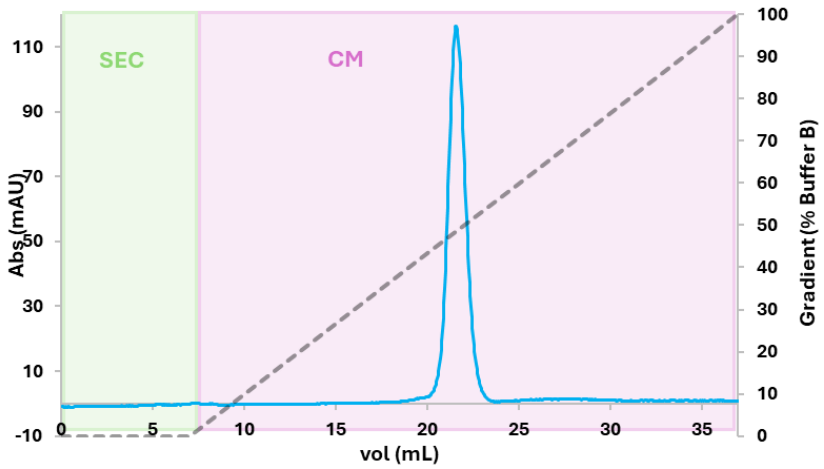

Fig.63: Two-dimensional chromatographic profile of Rituximab; [1]D: SEC (HiTrap Desalting 5 mL 1.6 x 2.5 cm, Cyvita), [2]D: MC (SkillPak™ TOYOPEARL® CMX-650S

(8 mm ID x 100 mm L, Tosoh Bioscience),ÄKTA Purifier (GE Healthcare); temperature 25°C; flow, 2 ml/min; eluent, 15 mM TRIS, 15 mM sodium acetate pH9 (A), 15 mM TRIS, 15 mM sodium acetate, 500 mM NaCl, pH 9; λ, 215 nm, gradient, 100%A in 7 min and 0-100%B in 30min.

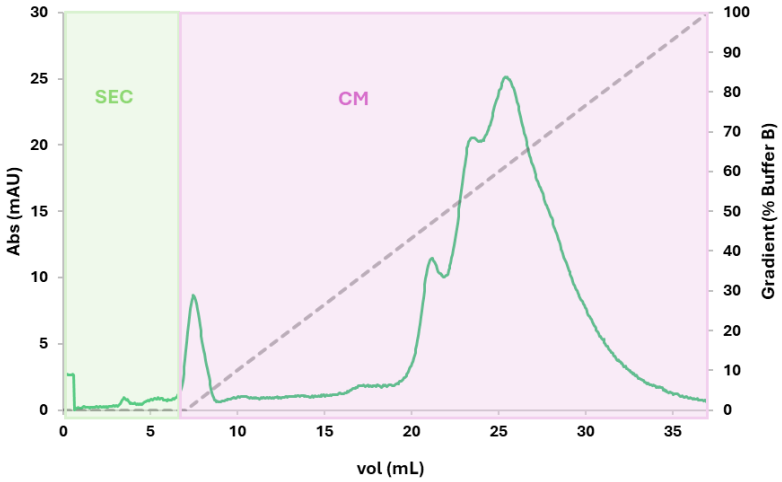

Fig.64: Two-dimensional chromatographic profile of Rit-(sulfoSMCC)-R3C; [1]D: SEC (HiTrap Desalting 5 mL 1.6 x 2.5 cm, Cyvita), [2]D: MC (SkillPak™ TOYOPEARL® CMX-650S (8 mm ID x 100 mm L, Tosoh Bioscience),ÄKTA Purifier (GE Healthcare); temperature 25°C; flow, 2 ml/min; eluent, 15 mM TRIS, 15 mM sodium acetate pH9 (A), 15 mM TRIS, 15 mM sodium acetate, 500 mM NaCl, pH 9; λ, 215 nm, gradient, 100%A in 7 min and 0-100%B in 30min.

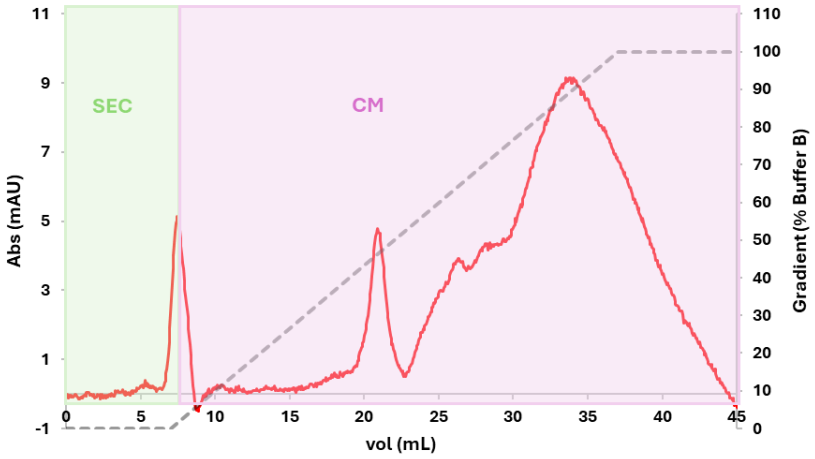

Fig.65: Two-dimensional chromatographic profile of Rit-(sulfoSMCC)-R6C; [1]D: SEC (HiTrap Desalting 5 mL 1.6 x 2.5 cm, Cyvita), [2]D: MC (SkillPak™ TOYOPEARL® CMX-650S (8 mm ID x 100 mm L, Tosoh Bioscience),ÄKTA Purifier (GE Healthcare); temperature 25°C; flow, 2 ml/min; eluent, 15 mM TRIS, 15 mM sodium acetate pH9 (A), 15 mM TRIS, 15 mM sodium acetate, 500 mM NaCl, pH 9; λ, 215 nm, gradient, 100%A in 7 min and 0-100%B in 30min.

An important technical challenge encountered was the inability to simultaneously record chromatograms from both dimensions due to hardware limitations, specifically, the presence of a single UV detector. To resolve this, the flow path was redesigned to allow the effluent to pass twice through the detector, enabling sequential monitoring of both chromatographic dimensions.

This modification, though mechanically simple, proved essential for reliable data acquisition and comprehensive system evaluation. The sample was introduced through an injection port and initially separated on the first-dimension column. The eluate passed through a UV-Vis detector for real-time chromatographic monitoring. A valve was used to divert fractions either to waste or towards the second-dimension column for further orthogonal separation.

After the second-dimension column, the flow returns UV-Vis detector and, to the waste.

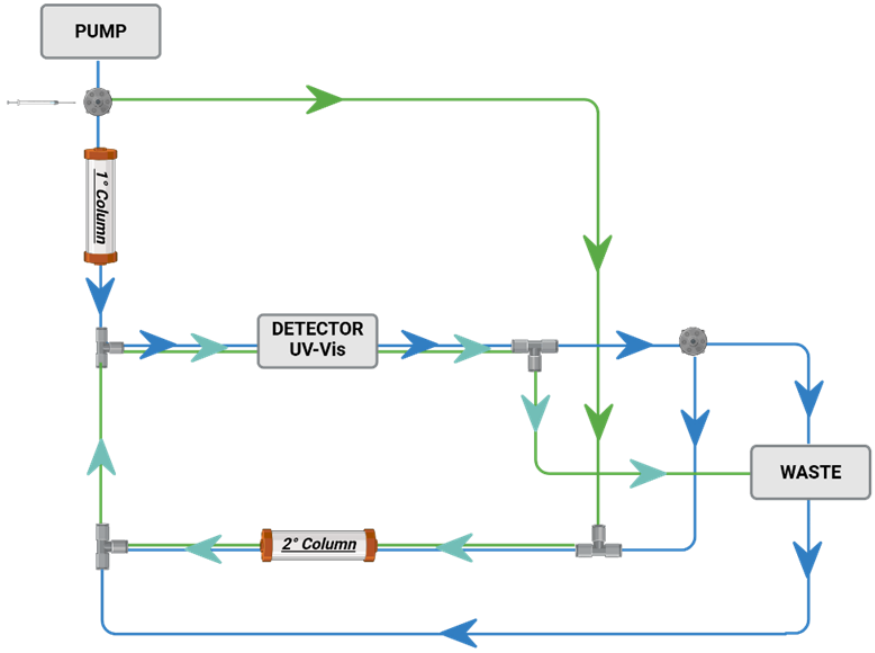

Fig.66: Schematic diagram of 2D-LC system with column switching and UV–Vis detection, allowing sequential separation, on-line monitoring, and selective fraction collection direction.

To test the robustness and performance of the newly constructed ÄKTA Purifier setting, validation analyses of a rituximab and an Rit-(sulfoSMCC)-R3C were performed while conserving the chromatographic operation conditions described above.

In Fig. 67-68, the runs performed with SEC as 1D and Eshmuno® CMX as the 2D separation are shown. While Fig.69-70 is shown the analogue workplan, but with IEX as the second dimension in chromatography. The chromatographic data

obtained demonstrate that the 2D-LC system operated reliably under the experimental conditions used.

The separation profiles revealed satisfactory recovery of all major peaks, indicating that sample transfer between dimensions was efficient and that the system performance met the expected analytical standards. These results confirmed that the developed setup was suitable for the comprehensive characterization of monoclonal antibodies and related conjugates, providing reproducible and good-quality separations across both chromatographic dimensions.

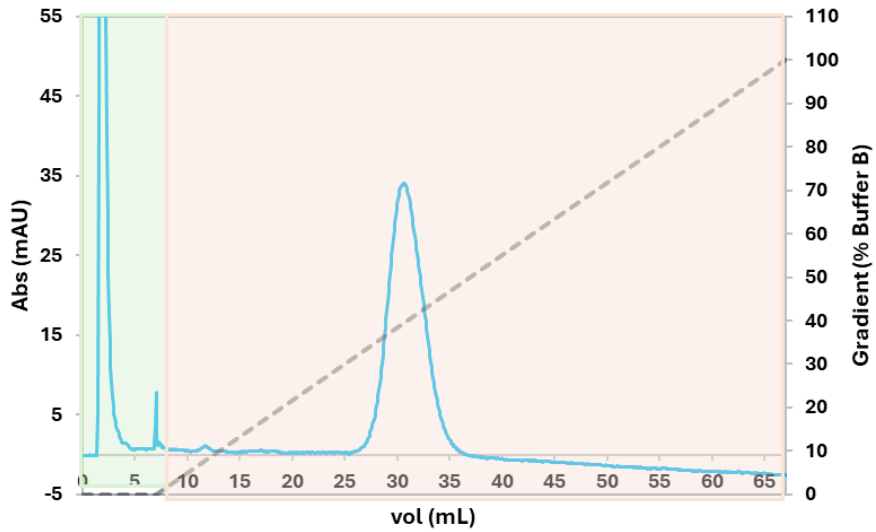

Fig.67: Two-dimensional chromatographic profile (LC x LC) of Rituximab; [1]D: SEC (HiTrap Desalting 5 mL 1.6 x 2.5 cm, Cyvita), [2]D: MMC (Eshmuno® CMX, 8 x 300 mm, Merck),ÄKTA Purifier (GE Healthcare); temperature 25°C; flow, 2 ml/min; eluent, 15 mM TRIS, 15 mM sodium acetate pH9 (A), 50 mM PP buffer, 1 M NaCl, pH 10.2 (B); λ, 215 nm, gradient, 100%A in 7 min and 0-100%B in 30min.

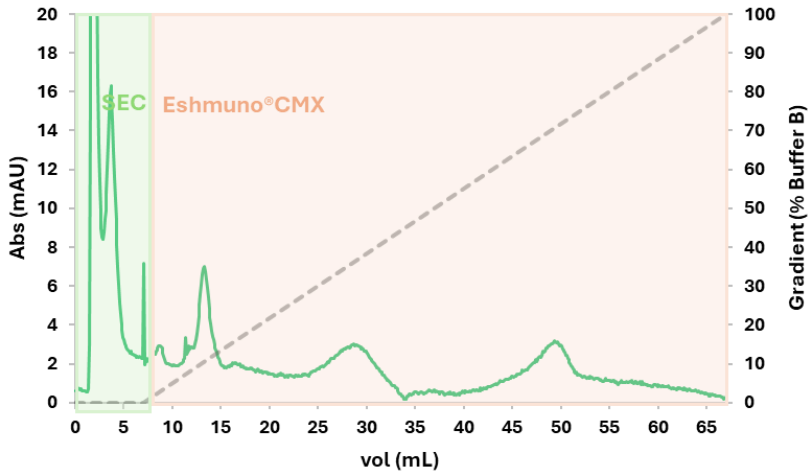

Fig.68: Two-dimensional chromatographic profile (LC x LC) of Rit-(sulfoSMCC)-R3C; [1]D: SEC (HiTrap Desalting 5 mL 1.6 x 2.5 cm, Cyvita), [2]D: MMC (Eshmuno® CMX, 8 x 300 mm, Merck),ÄKTA Purifier (GE Healthcare); temperature 25°C; flow, 2 ml/min; eluent, 15 mM TRIS, 15 mM sodium acetate pH9 (A), 50 mM PP buffer, 1 M NaCl, pH 10.2 (B); λ, 215 nm, gradient, 100%A in 7 min and 0-100%B in 30min.

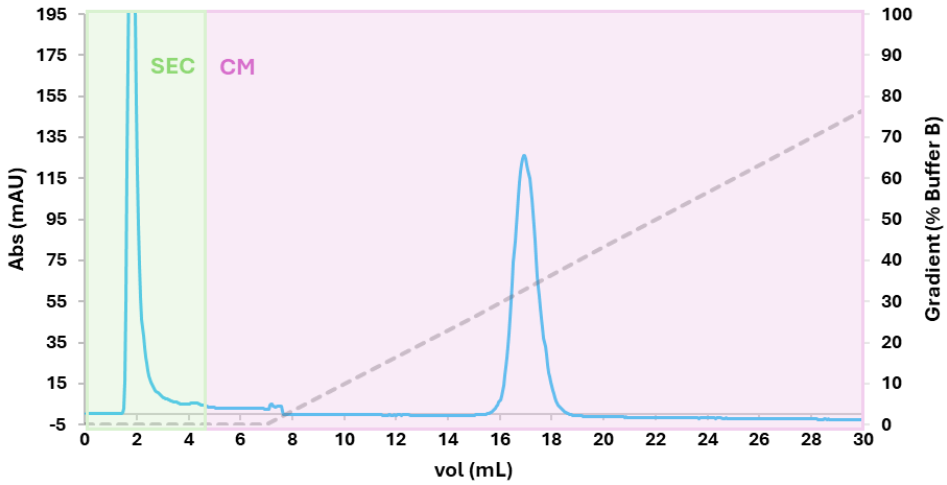

Fig.69: Two-dimensional chromatographic profile (LC x LC) of Rituximab; [1]D: SEC (HiTrap Desalting 5 mL 1.6 x 2.5 cm, Cyvita), [2]D: CMX (SkillPak™ TOYOPEARL® CM-650S (8 mm ID x 100 mm L, Tosoh Bioscience),ÄKTA Purifier (GE Healthcare); temperature 25°C; flow, 1 ml/min; eluent, 15 mM TRIS, 15 mM

sodium acetate pH9 (A), 15 mM TRIS, 15 mM sodium acetate 500mM NaCl, pH9 (B);λ, 215 nm, gradient, 100%A in 5 min and 0-100%B in 30min.

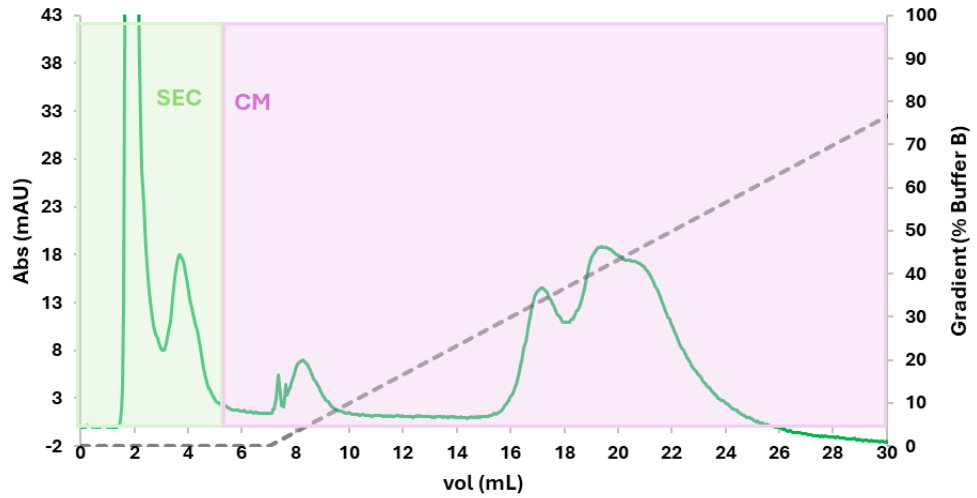

Fig.70: Two-dimensional chromatographic profile (LC x LC) of Rit-(sulfoSMCC)-R3C, [1]D: SEC (HiTrap Desalting 5 mL 1.6 x 2.5 cm, Cyvita), [2]D: CMX (SkillPak™ TOYOPEARL® CM-650S (8 mm ID x 100 mm L, Tosoh Bioscience),ÄKTA Purifier (GE Healthcare); temperature 25°C; flow, 1 ml/min; eluent, 15 mM TRIS, 15 mM sodium acetate pH9 (A), 15 mM TRIS, 15 mM sodium acetate 500mM NaCl, pH 9 (b); λ, 215 nm, gradient, 100%A in 5 min and 0-100%B in 30min.

3.3.2 Two-dimensional liquid chromatography system with an online desalting step

With the two-dimensional system fully operational, the final development stage focused on coupling the two chromatographies techniques that offered the highest resolving power for the samples: MMC and IEX.

Previous tests (see section 3.3.1) had indicated that the elution strength of one dimension could interfere with separation in the subsequent dimension. Therefore, a desalting step was incorporated between the two to prevent cross-

dimensional interference and to preserve resolution. The new schematic profile of the flow path for analysis is shown in Fig.71.

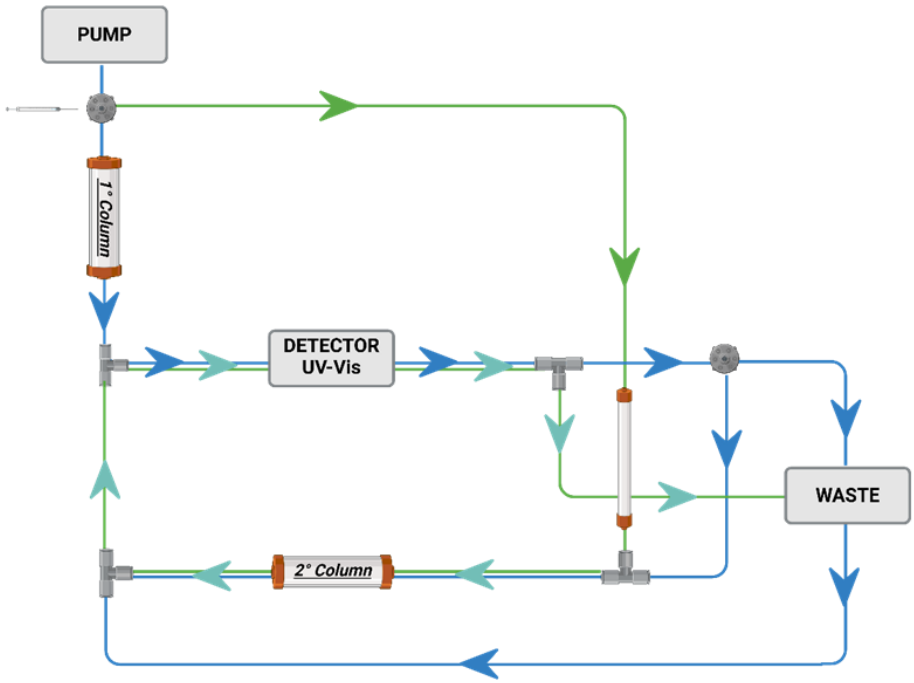

Fig.71: Two-dimensional chromatographic system with UV–Vis detection and an intermediate desalting step for sequential separation and purification.

Until this point, all analyses had been conducted in full comprehensive mode, the entire effluent from the first dimension was transferred continuously to the second. While this ensured complete sample coverage, it resulted in long analysis times and substantial data complexity.

To address these limitations, a heart-cutting approach was employed, targeting only specific fractions of species for transfer.

This strategy enhanced analytical efficiency, reduced run time, and allowed focused examination of defined molecular subpopulations.

The optimized workflow, consisting of IEX as the first dimension, a SEC-based desalting step, and Eshmuno® CMXX as the second, was successfully validated using both reference antibodies (Rituximab (Fig.72) and Trastuzumab (Fig.74)) and their modified mixtures (Rit-(sulfoSMCC)-R3C (Fig.73) and Trast-(sulfoSMCC)-R3C (Fig.75)).

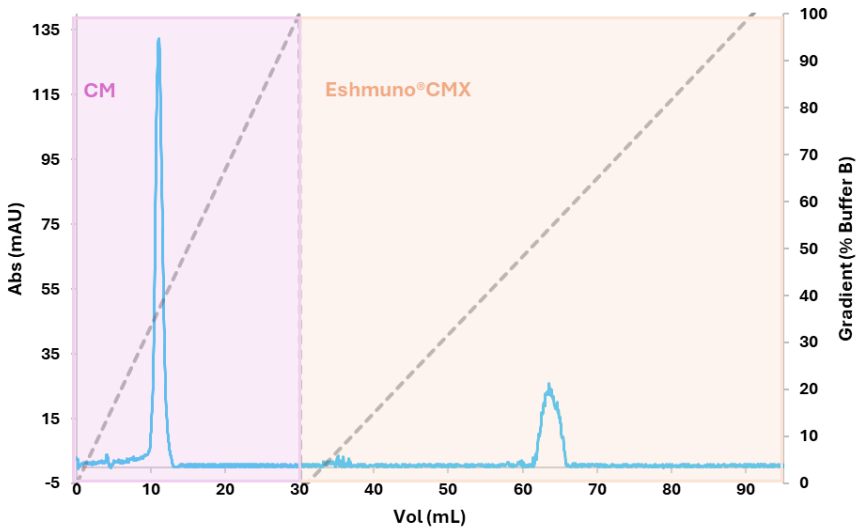

Fig.72: Two-dimensional chromatographic profile (LC-LC) of Rituximab, [1]D: CMX (SkillPak™ TOYOPEARL® CM-650S (8 mm ID x 100 mm L, Tosoh Bioscience), SEC (HiTrap Desalting 5 mL 1.6 x 2.5 cm, Cyvita), [2]D: MMC Eshmuno® CMX (8 x 300 mm, Merck),ÄKTA Purifier (GE Healthcare); temperature 25°C; 1D: flow 1 ml/min; eluent, 15 mM TRIS, 15 mM sodium acetate pH9 (MPA), 15 mM TRIS, 15 mM sodium acetate 500mM NaCl, pH 9 (MPB1); λ, 215 nm, gradient, 0-100% MPB1 in 30min; 2D: flow 2 ml/min; eluent, 15 mM TRIS, 15 mM sodium acetate pH9 (MPA), 50 mM Phosphate buffer, 1M NaCl pH 10.2 (MPB2); λ, 215 nm, gradient, 0-100% MPB2 in 30min.

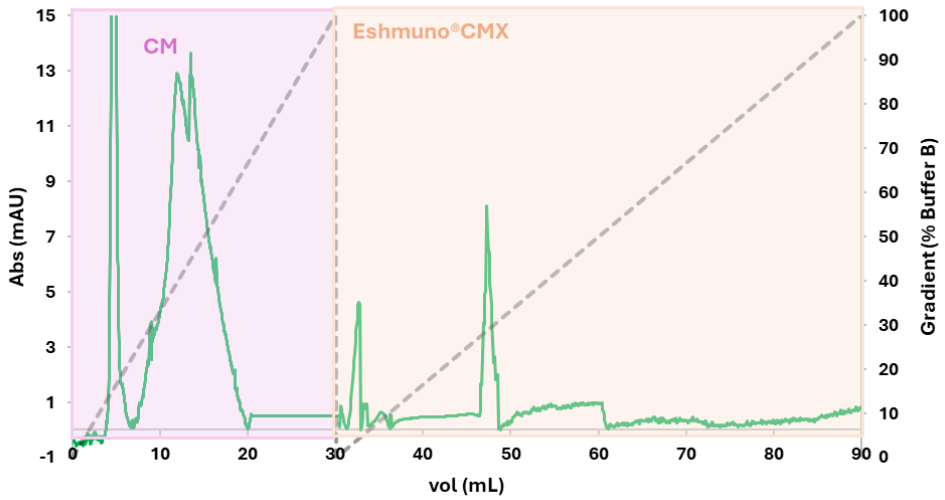

Fig.73: Two-dimensional chromatographic profile (LC-LC) of Rit-(sulfoSMCC)-R3C, [1]D: CMX (SkillPak™ TOYOPEARL® CM-650S (8 mm ID x 100 mm L, Tosoh Bioscience), SEC (HiTrap Desalting 5 mL 1.6 x 2.5 cm, Cyvita), [2]D: MMC Eshmuno® CMX (8 x 300 mm, Merck),ÄKTA Purifier (GE Healthcare); temperature 25°C; 1D: flow 1 ml/min; eluent, 15 mM TRIS, 15 mM sodium acetate pH9 (MPA), 15 mM TRIS, 15 mM sodium acetate 500mM NaCl, pH 9 (MPB1); λ, 215 nm, gradient, 0-100% MPB1 in 30min; 2D: flow 2 ml/min; eluent, 15 mM TRIS, 15 mM sodium acetate pH9 (MPA), 50 mM Phosphate buffer, 1M NaCl pH 10.2 (MPB2); λ, 215 nm, gradient, 0-100% MPB2 in 30min.

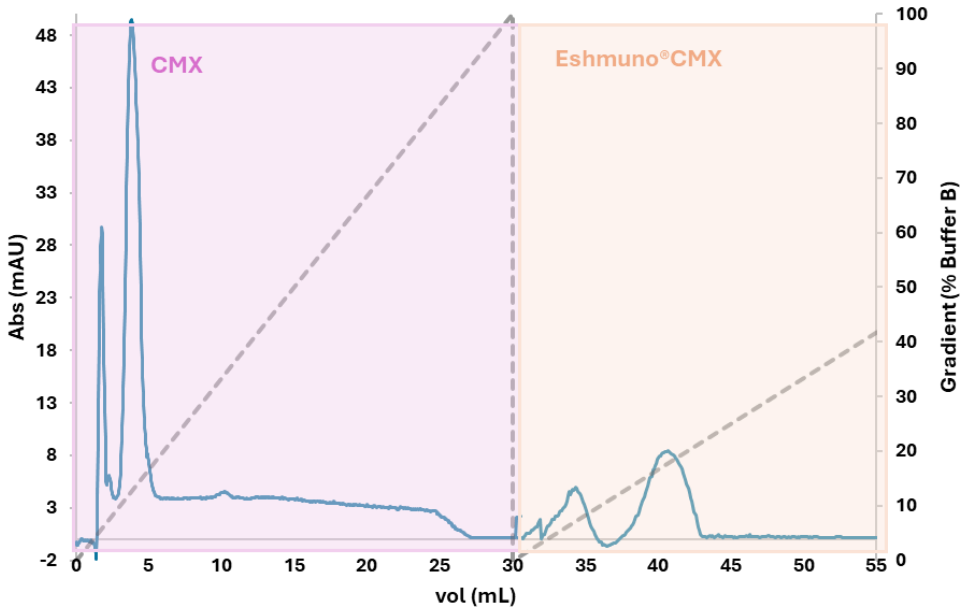

Fig.74: Two-dimensional chromatographic profile (LC x LC) of Trastuzumab, [1]D: CMX (SkillPak™ TOYOPEARL® CM-650S (8 mm ID x 100 mm L, Tosoh Bioscience), SEC (HiTrap Desalting 5 mL 1.6 x 2.5 cm, Cyvita), [2]D: MMC Eshmuno® CMX (8 x 300 mm, Merck),ÄKTA Purifier (GE Healthcare); temperature 25°C; 1D: flow, 1 ml/min; eluent, 15 mM TRIS, 15 mM sodium acetate pH9 (MPA), 15 mM TRIS, 15 mM sodium acetate 500mM NaCl, pH 9 (MPB1); λ, 215 nm, gradient, 0-100% MPB1 in 30min; 2D: flow,2 ml/min; eluent, 15 mM TRIS, 15 mM sodium acetate pH9 (MPA), 50 mM Phosphate buffer, 1M NaCl pH 10.2 (MPB2); λ, 215 nm, gradient, 0-100% MPB2 in 30min.

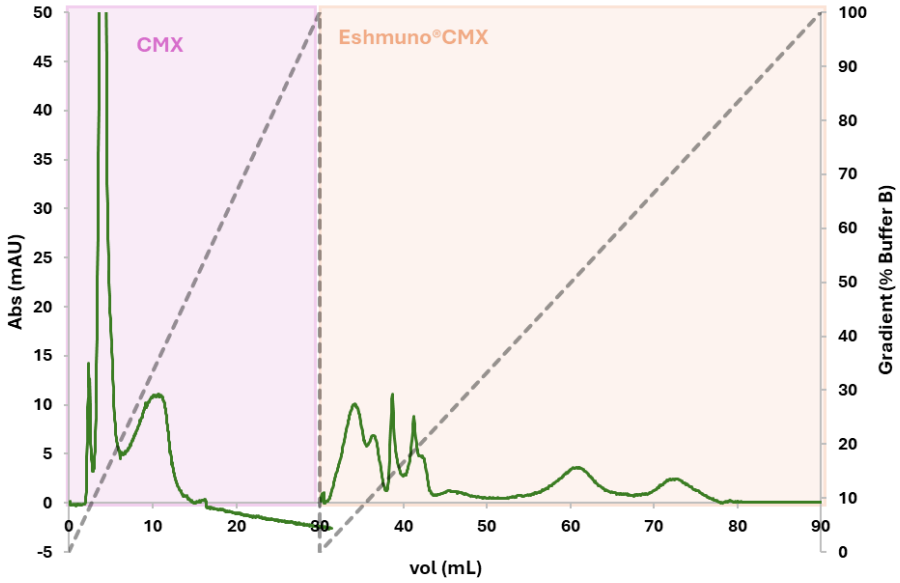

Fig.75: Two-dimensional chromatographic profile (LC x LC) of Trast-(sulfoSMCC)-R3C, [1]D: CMX (SkillPak™ TOYOPEARL® CM-650S (8 mm ID x 100 mm L, Tosoh Bioscience), SEC (HiTrap Desalting 5 mL 1.6 x 2.5 cm, Cyvita), [2]D: MMC Eshmuno® CMX (8 x 300 mm, Merck),ÄKTA Purifier (GE Healthcare); temperature 25°C; 1D: flow, 1 ml/min; eluent, 15 mM TRIS, 15 mM sodium acetate pH9 (MPA), 15 mM TRIS, 15 mM sodium acetate 500mM NaCl, pH 9 (MPB1); λ, 215 nm, gradient, 0-100% MPB1 in 30min; 2D: flow,2 ml/min; eluent, 15 mM TRIS, 15 mM sodium acetate pH9 (MPA), 50 mM Phosphate buffer, 1M NaCl pH 10.2 (MPB2); λ, 215 nm, gradient, 0-100% MPB2 in 30min.

3.4 Mass Spectrometry

The advent of recombinant protein therapeutics has transformed modern medicine, providing highly specific and potent agents for oncology, autoimmune, and inflammatory diseases. As the molecular complexity of these biologics increased, especially with the introduction of conjugates antibodies, where a monoclonal antibody is covalently linked to cytotoxic or bioactive payloads, the analytical requirements for their comprehensive characterization expanded dramatically. Among all analytical tools developed to meet these demands, mass spectrometry (MS) has emerged as an indispensable technology, offering unmatched sensitivity, accuracy, and molecular resolution for both research and quality control.

From early peptide fingerprinting to state-of-the-art high-resolution, multi-level strategies, MS now provides a complete structural picture of these complex molecules. The complementary use of top-, middle-, and bottom-level analyses delivers both macroscopic and site-specific insights, while LC–MS integration has brought these capabilities into the manufacturing realm.

The high mass accuracy, sensitivity, and dynamic range of modern MS instruments have therefore established this technology as the gold standard for mAb and ADC analysis throughout development, manufacturing, and clinical application.

In this section, MS was employed as a complementary and confirmatory technique to chromatography, serving a dual purpose:

- establishing a robust analytical baseline for the unmodified antibody
- monitoring molecular changes introduced with conjugation

This two-step approach ensures that analyses of mAbs constructs can be interpreted within a more structural framework.

Rituximab was selected as the model mAb. The protein was subjected to enzymatic digestion using a combined trypsin/chymotrypsin protocol, and the resulting peptide mixture was analyzed on the Q Exactive™ Plus Orbitrap mass spectrometer.

The results were exemplary: sequence coverage for the heavy chain (sp|P001|Rituximab) reached 92.46%, and for the light chain (sp|P002|Rituximab) it reached 100% (see Fig.76), providing nearly complete mapping of the antibody primary structure.

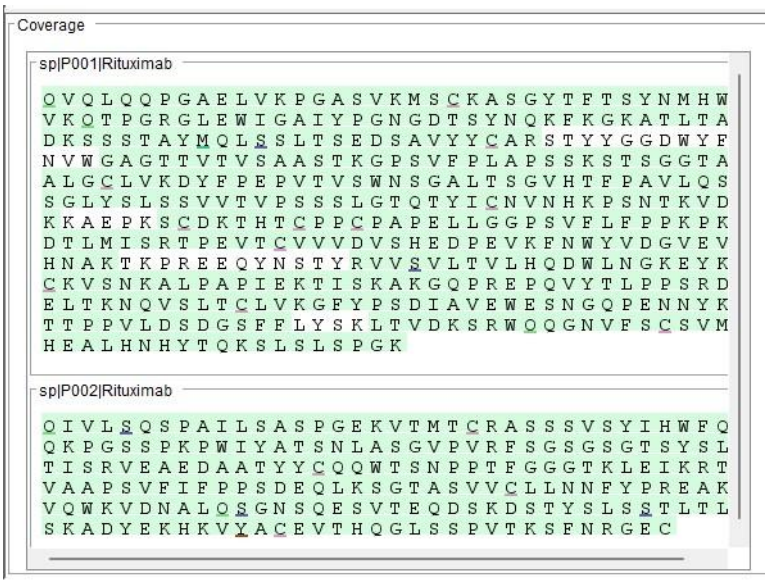

Fig.76: Sequence coverage of heavy and light chains of Rituximab.

Such extensive coverage was crucial, as it enabled unambiguous localization of post-translational modifications and provided a foundation for identifying potential lysine residues involved in conjugation.

With these results, the robustness of the analytical workflow had been confirmed, and the enzymatic digestion protocol validated as reproducible and efficient.

Analysis of the intact Rituximab mass spectrum further substantiated the robustness of the method. The mass spectrum revealed the major proteoforms corresponding to the light and heavy chains, as well as a main peak at 147.08 kDa, which precisely matched the theoretical molecular weight of Rituximab. The multiple adjacent peaks observed were consistent with the heterogeneity of IgG1 and the presence of glycoform microvariants (Fig.78-79).

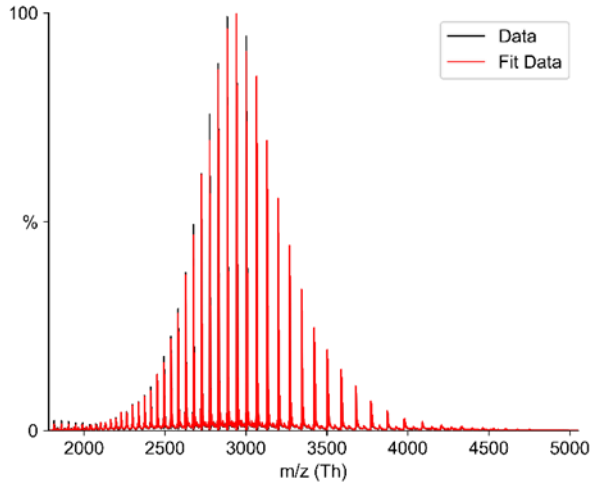

Fig.77: Mass spectrum with spectral fitting, illustrating the distribution and deconvolution of protein charge states of rituximab.

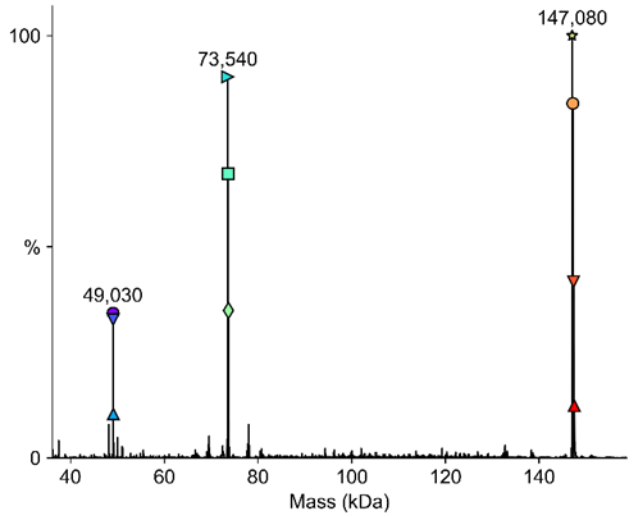

Fig. 78: Deconvoluted mass spectrum of rituximab highlighting major proteoforms. Light chain (49.030 kDa), heavy chain (73.540 kDa), and intact antibody (147.080 kDa).

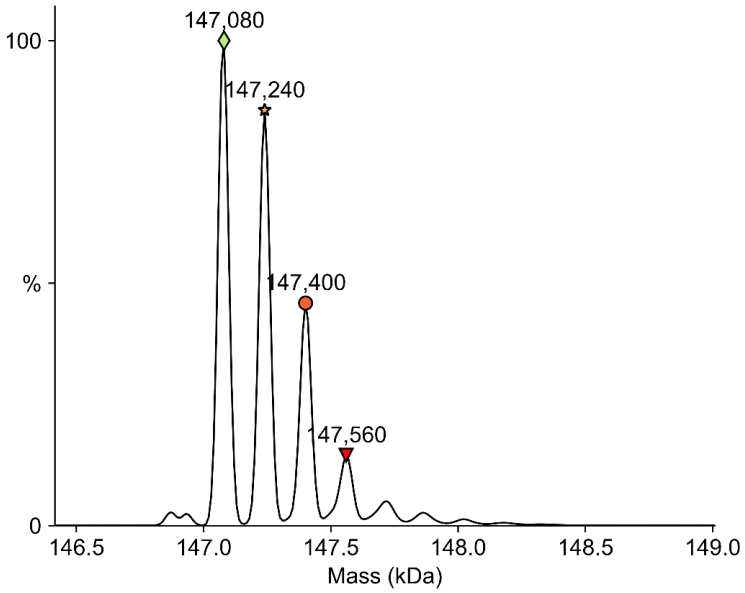

Fig.79: Zoom in of the intact antibody peak, where corresponding peaks of microvariants, such as glycoforms are shown.

Following the successful characterization of the native antibody, the same analytical workflow was applied to mAbs-sulfoSMCC-RnC mixtures generated by conjugating Rituximab R3C peptide (Rit-(sulfoSMCC)-R3C).

For R2S5R3C mixture, sequence coverage for the heavy chain (sp|P001|Rit-(sulfoSMCC)-R3C) reached 89.36%, and for the light chain (sp|P002|Rit-(sulfoSMCC)-R3C) it reached 97.16% (see Fig.80), providing a good, even if reduced, primary structure mapping of the antibody, in line with the conjugations that happened on the skeleton of the antibody.

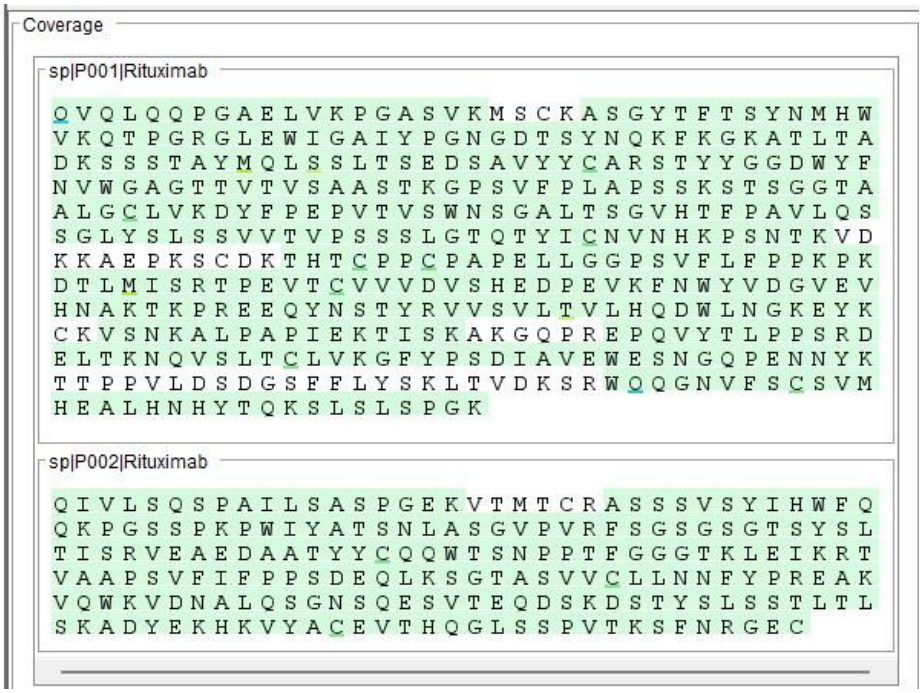

Fig.80: Sequence coverage of heavy and light chains of R2S5R3C mixture

The deconvoluted mass spectrum of this conjugate (see Fig. 82-83) displayed distinct mass increments relative to the unmodified antibody, each corresponding to additional linker and peptide moieties.

The resulting spectral complexity reflected the expected distribution of conjugation states and confirmed that multiple lysine residues were successfully modified, consistent with a non-site-specific conjugation mechanism.

From the comparison, it was possible to establish that the DAR for Rit-(sulfoSMCC)-R3C mixture was between 1 and 2, which means that one or two units of linker-peptide have been attached to random lysine available on the antibody's surface in the conditions of conjugation applied.

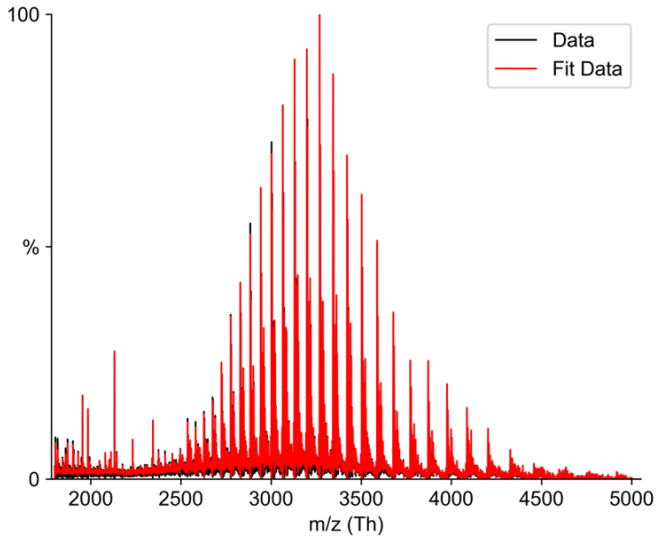

Fig.81: Representative mass spectrum with spectral fitting, illustrating the distribution and deconvolution of protein charge states of RIT-(sulfoSMCC)-R3C antibodies mixture

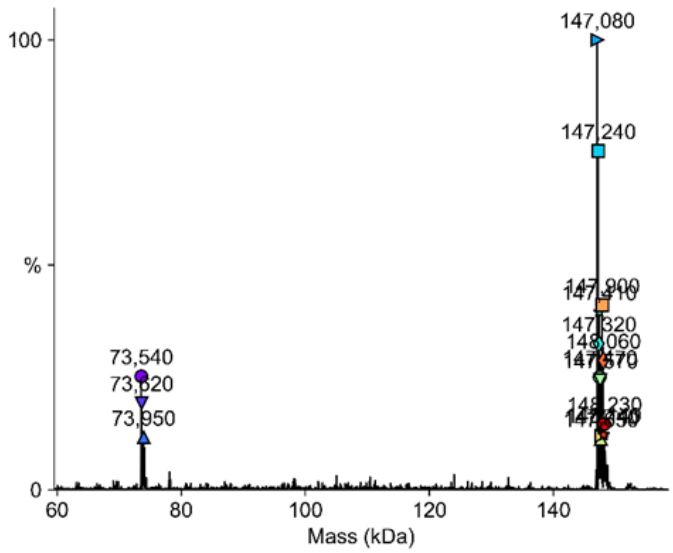

Fig.82: Deconvoluted mass spectrum of Rit-(sulfoSMCC)-R3C highlighting the intact antibody conjugate

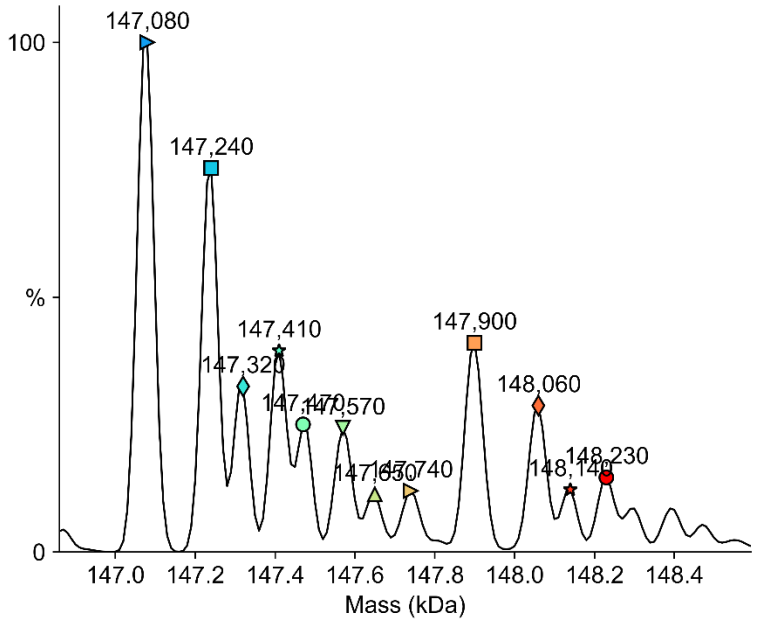

Fig.83: Zoom in of the intact antibody peak, where the complexity of the mixture composition is shown by the presence of these multiple peaks all near in mass.

When comparing the mass spectra of unmodified Rituximab and the Rit-(sulfoSMCC)-R3C mixture, several key observations arose. First, the clear mass shift provided direct molecular evidence of successful conjugation. Second, the broadening of the isotopic envelope and the presence of multiple overlapping peaks indicated an increase in molecular heterogeneity, fully consistent with the broadened chromatographic profiles observed in previous sections.

This parallel between MS and LC data underscores the complementarity of the two techniques: chromatography provides global separation, while MS offers precise molecular confirmation.

4. Conclusion and future perspectives

The research presented in this thesis addressed a key analytical challenge in the field of synthetic therapeutic bioconjugates: the development of a robust, high-resolution platform for the purification and characterization of monoclonal antibody–cell-penetrating peptide (mAb–CPP) conjugates under non-denaturing conditions.

The work was conceived at the intersection of biotechnology, analytical chemistry, and industrial innovation, leveraging the complementary expertise of Fischer Analytics GmbH in advanced chromatography and mass spectrometry, the peptide synthesis proficiency of the University of Florence, and the clinical insight of the University of Heidelberg. This multidisciplinary framework enabled the design, synthesis, and comprehensive analytical assessment of model antibody conjugates, paving the way for improved technologies in therapeutic antibody characterization and process development.

A central part of the project involved the design and synthesis of model conjugates using three clinically established monoclonal antibodies, Rituximab, Matuzumab, and Trastuzumab, coupled with oligoarginine peptides of increasing length (R3C, R6C, R9C). The heterobifunctional crosslinker sulfoSMCC was selected as a chemical spacer to achieve orthogonal reactivity between amine and thiol functional groups. Through systematic variation of reaction parameters such as pH, buffer composition, stoichiometry, and incubation time, optimal conjugation conditions were defined.

A major outcome of this work was the establishment of a systematic chromatographic screening for the evaluation of non-denaturing separation techniques applicable to therapeutic antibodies and their conjugates. Four

chromatographic modalities, Size-Exclusion Chromatography (SEC), Hydrophobic Interaction Chromatography (HIC), Ion-Exchange Chromatography (IEX), and Mixed-Mode Chromatography (MMC), were comparatively assessed for their ability to resolve molecular heterogeneity and monitor conjugation progress.

SEC confirmed the preservation of molecular integrity and the absence of aggregation during conjugation, validating the mildness of the synthetic conditions. Both analytical and semi-preparative SEC demonstrated effective separation between antibody species and unreacted peptides, establishing SEC as a valuable primary purification step within multidimensional workflows.

HIC showed limited resolution among conjugated species due to the overall hydrophilic nature of oligoarginines, HIC proved useful for detecting subtle conformational effects and process consistency.

IEX, particularly in weak cation-exchange mode, yielded the highest analytical resolution, revealing charge heterogeneity associated with conjugation extent and peptide length. The TSKgel CMX-STAT column successfully separated charge variants corresponding to mono-, di-, and tri-substituted species, confirming that IEX is a sensitive probe for conjugation heterogeneity and a reliable tool for batch consistency monitoring.

Finally, MMC demonstrated the capability to discriminate subtle differences arising from combined charge and hydrophobic effects, offering the most comprehensive and flexible selectivity among the techniques tested. Its dual retention mechanism suggests that MMC can effectively complement SEC and IEX in integrated purification schemes, particularly within multidimensional liquid chromatography systems.

Together, these studies established a solid foundation for the integration of chromatographic methods into a continuous 2D-LC platform, capable of performing sequential non-denaturing separations prior to online or offline mass spectrometric analysis. This architecture minimizes sample manipulation, enhances throughput, and enables the selective isolation of target fractions for subsequent structural characterization.

The mass spectrometry (MS) analyses conducted within this project further expanded the structural understanding of mAb–CPP conjugates. Using LC–MS platforms, mass profiles of both intact and subunit-level species were obtained under native-like conditions. The results confirmed that peptide conjugation produced predictable mass shifts consistent with the theoretical addition of oligoarginine units, with no detectable degradation or structural rearrangement of the antibody backbone. Importantly, MS analysis validated the chemical integrity of the thioether linkage formed via sulfoSMCC and provided complementary data to chromatographic findings on conjugation heterogeneity.

In a broader context, this study underscores the indispensable role of LC–MS in the structural elucidation and quality control of complex biotherapeutics. The integration of chromatographic selectivity with high-resolution MS detection allows a multidimensional description of molecular composition, heterogeneity, and modification site distribution, features that are increasingly critical in modern Quality by Design (QbD) approaches to biopharmaceutical manufacturing.

From a methodological standpoint, this work contributes to the optimization of analytical platforms for therapeutic antibody conjugates in three principal ways.

First, it demonstrates that multi-dimensional liquid chromatography can be systematically adapted to resolve physicochemical heterogeneity in large biomolecules without compromising their native conformation.

Second, it establishes a reproducible workflow for antibody–peptide conjugation using random lysine modification, validated through multiple orthogonal analytical methods.

Third, it introduces a conceptual and technological framework for 3D-LC–MS coupling, providing the basis for future automated systems that combine non-denaturing purification, fraction collection, and direct mass analysis in a single continuous process.

The outcomes of this research therefore extend beyond the immediate scope of antibody–CPP conjugates. The developed methodologies are readily transferable to a wide range of biotherapeutic formats, including ADCs, bispecific antibodies, and recombinant fusion proteins. By offering higher resolution, reduced sample handling, and improved analytical throughput, the proposed system can significantly enhance the efficiency of biopharmaceutical characterization and process control in both research and industrial settings.

Looking ahead, several avenues emerge from the results of this work. The successful integration of non-denaturing chromatographic modes into a multidimensional framework opens the path to the full realization of a continuous 3D-LC–MS platform for biomolecule analysis. Future developments will focus on optimizing the interface between chromatographic dimensions, minimizing dead volumes, and refining fraction transfer protocols to enable fully automated operation. Extending this approach to native mass spectrometry

would further enhance the capacity to correlate physicochemical properties with structural integrity and biological function.

5. Experimental part

5.1 Materials

Rixathon solution 500 mg/mL by Sandoz S.p.A. (Rituximab);

EMD 72000 hMAb425 powder by Merck KGaA (Matuzumab);

Herceptin® powder by Roche (Trastuzumab).

HEPES Buffer pH7: 25 mM HEPES, 150 mM NaCl , NaOH to adjust pH. Preparation: Dissolve the salts in ~800 mL of ultrapure water. Adjust pH to 7.0 Bring to final volume (1 L) with water. Sterile-filter (0.22 µm) and store at 4 °C.

PBS Buffer pH7: 137 mM NaCl, 2.7 mM KCl, 10 mM Na_2HPO_4, 1.8 mM KH_2PO_4. Preparation: Dissolve the salts in ~800 mL of ultrapure water. Adjust pH to 7.0 ± 0.05 using 1 M HCl or 1 M NaOH. Bring to final volume (1 L) with water. Sterile-filter (0.22 µm) and store at 4 °C.

Coomassie Blue: 0.025% (w/v) Coomassie Blue G-250, 45% (v/v) MeOH, 10% (v/v) Glacial acetic acid. Recipe for 1L:Add 450 mL methanol and 100 mL glacial acetic acid to a clean 1 L beaker or bottle. Add 0.25 g Coomassie Brilliant Blue R-250 powder. Stir at room temperature until fully dissolved (use a magnetic stirrer). Bring to 1 L with distilled water.

Silver Blue Coomassie: 0.12% (w/v) Coomassie Blue G-250, 10% H_3PO_4, 10% $(NH_4)_2SO_4$, 20% MeOH. Recipe for 1L: Add to 100 mL of H_2O milliQ + 100 mL of H_3PO_4 and 100 mg of $(NH_4)_2SO_4$ dissolve under magnetic stirring, add 1.2 g of Coomassie Blue G-250, + 600mL of H_2O milliQ, + 200 mL of MeOH.

Mobile Phases Composition:

MPA: 15 mM TRIS, 15 mM Sodium Acetate, pH9 ; MPB1: 15 mM TRIS, 15 mM sodium Acetate, 500 mM NaCl, pH9 ; MPB2: 50 mM PP Buffer, 1 M NaCl, pH 10.2;

A1: H_2O + 0.1 % TFA, B1: ACN+ 0.1 % TFA , A2: H_2O + 0.1 % TFA + 2 % IPA, B2: IPA:ACN:MPA (70:20:10)

Chromatographic analyses were performed using the following instrumentation:

- *Agilent 1100/12000 Series HPLC System* (Agilent Technologies, USA): Equipped with a quaternary pump, autosampler, column oven (temperature range 10–80 °C), and diode-array UV–Vis detector (190–600 nm). The system operates up to 400 bar pressure and was controlled using ChemStation software. Used primarily for analytical SEC, HIC, IEX, and RP-LC runs.
- *Waters ACQUITY UPLC System* (Waters, Milford, MA, USA): UHPLC platform equipped with binary solvent manager, sample manager, and photodiode array detector. The system allows operation up to 15,000 psi and supports sub-2 µm particle columns for high-resolution separations.
- *ÄKTA Purifier Chromatography System* (GE Healthcare / Cytiva, Sweden): Modular system for semi-preparative and preparative chromatography, featuring UV detection (up to 3 wavelengths), conductivity and pH monitoring, and controlled by UNICORN™ software. Flow rate range: 0.001–100 mL/min; pressure limit: 25 MPa.

Liquid chromatography-mass spectrometry instrumentation:

LC system: Agilent 1200 Series HPLC system (Agilent Technologies, Santa Clara, USA) ; Column: ReproSil-Pur 200 C18-AQ column (1.9 µm, 2 × 200 mm; Dr. Maisch GmbH)

Mass spectrometer: Q Exactive™ Plus Orbitrap (Thermo Fisher Scientific) equipped with ESI source; hybrid quadrupole-Orbitrap with C-trap and HCD cell. Waters MassPREP Micro Desalting column (2.1 × 5 mm, 20 µm, 1000 Å; Waters,Milford, USA).

MS Software:

Deconvolution of the raw MS data was performed using *UniDec* version 8.0.1 software.3.

FragPipe was employed for its comprehensive and rapid proteomics workflow, enabling efficient peptide identification, post-processing, and support for multiple quantification methods.

MZmine was used for its versatile capabilities in LC-MS data processing, including peak detection, alignment, and quantification, facilitating robust downstream analysis of metabolomic and peptide datasets.

5.2 Methodologies

5.2.1 Peptide synthesis

5.2.1.1 Procedure for Microwave-assisted automatic SPPS

The synthesis of H-R3C-NH_2, H-R6C-NH_2, and H-R9C-NH_2 was carried out on a Liberty Blue™ automatic synthesizer equipped with a Teflon reaction vessel. Fmoc/tBu orthogonal protection strategy was used while microwaves were applied both in coupling and deprotection steps. Nitrogen bubbling ensured thorough mixing during all the reactions.

The resin Fmoc-Rink amide resin (loading 0.36 mmol/g), was weighed and put in the reaction vessel for 15 min to allow swelling. In the meantime, amino acid

building blocks solution, coupling and deprotection solutions were prepared with the following concentrations, based on a 0.025 scale synthesis: amino acid building block 0.2 M, Piperidine 20% in DMF , Oxyma Pure 0.5 M, DIC 0.25 M. Chain elongation occurred through a single coupling procedure for each amino acid building block assisted by the use of microwave energy, following the protocol reported in Table2.

STEP	Temperature (°C)	Power (W)	Holding Time (sec)
Deprotection	75	155	15
	90	30	50
Coupling	75	170	15
	90	30	110

Table2: Temperature (°C), power (W) and time conditions (sec) applied during deprotection and coupling steps of MW-SPPS.

The steps followed during MW-SPPS are summarized as follows (Table3) and were done iteratively until complete elongation of the sequence was obtained.

Operation	Addition	Volume
Deprotection	20% piperidine in DMF	3 mL
Washing	DMF	2 mL x 3
Amino acid building blocks and coupling reagents	Amino acid building block solution, DIC 0.25 M, Oxyma Pure 0.5M	0.63 mL, 1 mL, 0.5 mL

Washing	DMF	3 mL x 3

Table3: Different steps of microwave-assisted solid phase peptide synthesis (MW-SPPS).

Following peptide synthesis, the final deprotection was carried out manually. The resin was initially swollen in fresh DMF for 10 minutes and subsequently filtered under vacuum. A 20% piperidine solution in DMF was then added for 5 minutes, after which the solution was removed by vacuum filtration. A second portion of 20% piperidine in DMF was applied for 10 minutes, followed by filtration. The resin was finally washed sequentially with fresh DMF and DCMX and subsequently dried under vacuum.

Cleavage was carried out with a mixture of 92,2% TFA, 2.5% TIS, 2.5% H_2O, 2.5% EDT. For each 100 mg of resin 1 mL cleavage solution was used, with an excess of 1 mL. The resin was mixed for 4h at room temperature due to the presence of the high number of arginines residues.

After the resin was filtered and the liquid collected, the addition of cold diethyl ether caused the peptide to precipitate. To enhance this process, the falcons were placed at -20°C for 20 minutes. Afterwards, centrifugation was performed at 4°C for 5 minutes at 4000 rpm. The cold diethyl ether was drained, and the process was repeated twice. Finally, the filtered product was lyophilised.

5.2.1.2 Procedure of purification and characterization of the synthetic peptides

Purifications were carried out on:

- Biotage® IsoleraOne , with a Biotage® SnapUltra Cartridge C18 12g column. Solvents used were: Solvent A H2O+0.1% (*v/v*) TFA and Solvent B ACN+0.1% (*v/v*) TFA. Samples were prepared by dissolving 100 mg of crude peptide in

max 5 mL of milliQ water. The flow was set at 10 mL/min and fractions were collected automatically by setting the value of Abs at 0.2 mAU.

- Waters 600 HPLC coupled with Waters UV DAD 2487 with a Sepax Bio-C18 reversedd-phase column. Solvents used were: Solvent A H2O+0.1% (v/v) TFA and Solvent B ACN+0.1% (v/v) TFA. Samples were prepared by dissolving up to 20 mg of each peptide in 2 mL of milliQ water. The flow rate was set at 4 mL/min. Fractions were collected manually by monitoring the absorbance at both 215 nm and 254 nm (peptide bond absorption wavelength and aromatic group absorption wavelength, respectively).

Characterization of the collected homogenous fractions was performed using RP-HPLC Alliance Chromatography system (Waters, Milford Massachusetts, USA) with a BEH C18 (1.7 µm 2.1× 50 mm) column coupled to a single quadrupole ESI-MS Micromass ZQ (Waters, Milford Massachusetts, USA).

5.2.2 Preparation of monoclonal Antibodies

Rituximab (solution, 10 mg) and Matuzumab (powder, 20 mg) preparation:

Equilibrate in HEPES Buffer pH7 (or PBS Buffer pH7) with NAP-25 column

1. Add 0.5 mL of buffer
2. Drain by gravity
3. Add 2 mL of protein solution
4. Drain by gravity
5. Add 3 mL of desired buffer to elute
6. Drain and collect

Trastuzumab Preparation:

1. Weight in 20 mg of antibody

2. Add 500 µL of desired buffer
3. Transfer to Amicon ultra 0.5 mL cut-off 10kDa
4. Centrifuge 14000 rcf foe 15 min
5. Repeat point 2 and 4 for trice
6. Invert filter in a fresh tube
7. Centrifuge 1000 rcf for 2 min
8. Adjust concentration with desired buffer

5.2.3 Conjugation procedure

For activation, 200 µL of antibody solution (3 mg/mL in HEPES buffer/PBS buffer) was mixed with 1.78 µL of freshly prepared sulfoSMCC (15 mg/mL in DMSO; 1/2/5/7 equiv). The reaction mixture was vortexed briefly and incubated for 2 h at room temperature with gentle mixing (600 rpm). After incubation, the mixture was diluted to 500 µL with HEPES buffer and purified by SEC (Illustra NAP-5 column) to remove excess crosslinker.

The concentration of the purified antibody–SMCC intermediate was determined, and 2/5/7/12 equiv of cysteine-containing CPP (20 mg/mL in HEPES buffer/PBS buffer) were added. The reaction mixture was vortexed and incubated for 2 h at room temperature (600 rpm). The conjugation mixture was then diluted with HEPES buffer and purified by ultrafiltration using Amicon Ultra centrifugal filters (100 kDa or 30 kDa cut-off) to remove unreacted CPP.

5.2.4 Electrophoresis on gel

The molecular weight of the mAbs, Rituximab, Matuzumab and Trastuzumab were roughly 150kDa, but it was decided to proceed with denaturing condition for this analysis and the gel performed was with 12% of polyacrillamide.

The gels were composed with two parts: the Running gel and Stacking gel; in Table 4 the amounts of components.

	Running Gel	**Stacking Gel**
H2O milliQ	*3.25 mL*	*2.65 mL*
Acrylammyde	*4 mL*	*1 mL*
1.5M TRIS-HCl pH 8.8	*2.5 mL*	*/*
0.5M TRIS-HCl pH6.8	*/*	*1.25 mL*
10% SDS	*100 µL*	*50 µL*
10% APS	*100 µL*	*50µL*
TEMED	*10 µL*	*5 µL*

The gel preparation started with adding together acrylamide, buffer and H2O milliQ for both running and stacking gel. Then adding APS and TEMED to the running gel gently invert four times and quickly fill the gels. Wait 30-40 minutes to stiffen and then ultimate the stacking gel adding APS and TEMED, again gently invert and quickly pour it and add the comb. Once they were completely solidified they were stocked with wet paper at +4°C.

The samples before been loaded in the gels were mixed with 5X SDS Loading buffer (300 mM Tris HCl, 10% w/v SDS, 25% v/v β-mercaptoethanol, 0.1% w/v Coomassie Blue, 50% glycerol), boil for 10 min at 100°C and spun down.

The buffer used during the gel run was TGS1X. To develop the gel, Coomassie Blue stain/Silver Coomassie Blue was used, and the destain was performed with the Coomassie Blue destain solution (10% AcOH, 50% MeOH, 40% H2O), followed by washing with Milli-Q H2O.

5.2.5 Chromatographic operating conditions

Below is the list of chromatographies that have been tested, the operating conditions used, and columns.

5.2.5.1 Size exclusion chromatography

-Tosoh TSKgel G4000SWXL (7.8 × 300 mm, 5 µm); 50 mM phosphate buffer + 0.1 M NaCl, pH 6.5; flow rate 0.5 mL/min, isocratic elution; detection at 280 nm.

-HiTrap Desalting 5 mL (2.5 x 4.6 CMX, Cyvita), 15 mM Tris/15 mM sodium acetate pH 9, flow rate 1 mL/min, isocratic elution, detection at 280 nm.

5.2.5.2 Hydrophobic interaction chromatography

-Tosoh TSKgel HIC-ADC Butyl (4.6 × 100 mm, 5 µm); gradient from 1.5 M $(NH_4)_2SO_4$ in 100 mM phosphate buffer (pH 7) to 100 mM phosphate buffer + 25 % IPA, flow rate 0.8 mL/min/1 mL/min, detection at 280 nm and 214 nm.

-SkillPak™ 5mL TOYOPEARL Phenyl 650-M (8 mm ID x 100 MM L, Tosoh Bioscience), gradient from 1.5 M $(NH_4)_2SO_4$ in 100 mM phosphate buffer (pH 7) to 100 mM phosphate buffer + 25 % IPA, flow rate 0.5 mL/min, detection at 280 nm.

5.2.5.3 Ion exchange chromatography

-Tosoh TSKgel CMX-STAT (4.6 × 100 mm, 7 µm); gradient from 10 mM phosphate buffer (pH 7) to 10 mM phosphate buffer + 500 mM NaCl; flow rate 0.8 mL/min; detection at 280 nm and 214 nm.

-SkillPak™ 5mL TOYOPEARL Phenyl 650-M (8 mm ID x 100 MM L, Tosoh Bioscience), gradient from 15 mM Tris/15 mM sodium acetate pH 9 to 15 mM Tris/15 mM sodium acetate + 500 mM NaCl pH 9, flow rate 1 mL/min; detection at 280 nm.

5.2.5.4 Mixed-mode chromatography

-Eshmuno® CMXX (Merck); A: 15 mM Tris/15 mM sodium acetate (pH 9), B: 50 mM phosphate + 1 M NaCl (pH 10.2); gradient 0–100 % B over 30 min; flow rate 2 mL/min; detection at 280 nm.

5.2.5.5 Reversed-phase liquid chromatography

-Phenomenex BioZen Intact XB-C8 (4.6 × 100 mm, 3.6 µm); A: H_2O + 0.1 % TFA + 2 % IPA, B: IPA:ACN:MPA (70:20:10); gradient 0–100 % B over 25 min; 80 °C; flow rate 0.4 mL/min; detection at 214 nm.

Each analytical run loads 5 µg of protein OC from a diluted stock at 1mg/mL. For each preparative analysis, the amount of protein ranged from 150 to 250 µg OC.

5.2.6 Multi-dimensional liquid chromatography

All chromatographic experiments were performed on an ÄKTA™ Purifier system (Ge Healthcare Life Sciences) configured and modified for multidimensional liquid chromatography operation.

The standard single-dimension setup was adapted by installing additional electronically controlled switching valves and manual flow-switch valves to enable smooth routing of the effluent between chromatographic dimensions. The system comprised dual solvent delivery pumps, an injection valve, a UV–Vis detector, and an outlet valve. A secondary flow-path selector valve was implemented to direct the eluate from the 1D column either to the 2D column or to waste, allowing operation in full comprehensive or heart-cutting modes. Because the system included a single UV–Vis detector, the flow path was redesigned to ensure that the eluate passed sequentially through the detector after both separations, thereby ensuring continuous and comparable signal

acquisition. The UNICORN™ software suite was employed for instrument control, gradient programming, and data acquisition.

5.2.6.1 Size-exclusion chromatography

Size-exclusion chromatography was employed as the first dimension during system validation and as an intermediate desalting step in selected workflows.

- Column: HiTrap™ 5 mL Desalting column (2.5 CMX ID x 4.6 CMX L, Cytiva)
- Mobile phase: 15 mM Tris, 15 mM acetate, pH 9
- Chrom. method: Isocratic
- Flow rate: 1 mL/min
- Detection: UV 280 nm
- Temperature: room temperature

5.2.6.2 Ion-Exchange Chromatography

Cation-exchange chromatography was used both as an individual separation mode and as first dimension of the 2D-LC system.

- Column: SkillPak™ 5 mL TOYOPEARL® CMX 650S (8 mm ID x 100 mm L, Tosoh Bioscience)
- Mobile phase A (MPA): 15 mM Tris, 15 mM acetate, pH 9
- Mobile phase B (MPB1): 15 mM Tris, 15 mM acetate, 500 mM NaCl, pH 9
- Gradient: 0–100 % B over 30 min
- Flow rate: 1 mL/min
- Detection: UV 280 nm
- Temperature: room temperature

5.2.6.3 Mixed-Mode Chromatography

Mixed-mode chromatography was carried out using the Eshmuno® CMX stationary phase, combining ionic and hydrophobic interaction mechanisms.

- Column: Eshmuno® CMXX (8 mm ID × 300 mm L)
- Mobile phase A (MPA): 15 mM Tris, 15 mM acetate, pH 9
- Mobile phase B (MPB2): 50 mM phosphate buffer, 1 M NaCl, pH 10.2
- Gradient: 0–100 % MPB2 over 30 min, hold at 100% MPB2 for 10 min
- Flow rate: 2 mL/min
- Detection: UV 280 nm
- Temperature: room temperature

5.2.6.4 Multidimensional chromatographic workflows

The 2d-LC system have been tested in different configurations depending on the experimental objective:

- Full Comprehensive 2D-LC (SEC × IEX or SEC × Eshmuno® CMX):

the entire effluent from the 1D column was transferred continuously to the 2D column via automated valve switching. This configuration enabled complete sample coverage and validation of the overall system operation.

- Heart-Cutting 2D-LC (IEX → SEC → MMC):

Selected chromatographic regions, so called heart cuts, containing analytes of interest were transferred from the first to the second dimension. This approach reduced total run time, minimized solvent consumption, and focused on targeted molecular subpopulations. The inclusion of an intermediate SEC desalting step improved inter-dimensional compatibility and overall chromatographic resolution.

5.2.7 Deglycosylation of monoclonal antibodies

Antibody mixtures of 20 µg were deglycosylated by using 1250 U PNGase F at 50°C for 90 min.

1. Prepare Mix A and Mix B (per 20 µg of antibody sample):

Mix A ***Mix B***

Substance	***V (µL)***	***Substance***	***V (µL)***
10X Buffer	4.0	mAb sample	x
PNGase F	0.5	Water	35.5 - x

2. Per sample, mix 35.5 of Mix B with 4.5 of Mix A
3. Incubate at 50 °C for 90 min
4. To remove interfering buffer components, use an ultra centrifuge 0.5 mL tube with a cut-off of 10 KDa. Centrifuge 7000 rpm, 5 min at room temperature.
5. To rebuffer in HEPES Buffer pH7, centrifuge as in 4. But adding 1:1 (*v:v*) of buffer:sample.

5.2.8 Trypsin/Chymiotrypsin Digestion Protocol

The monoclonal antibody sample was denatured and reduced in 50 mM ammonium bicarbonate buffer pH 7.8. Disulfide bonds were reduced using tris(2-carboxyethyl)phosphine (TCEP) and alkylated with iodoacetamide to prevent reformation. Digestion was performed by adding trypsin at a 1:25 enzyme-to-protein ratio (w/w), followed by incubation at 37°C for 12 hours. The reaction was terminated by lowering the pH to <4 with formic acid. For chymotrypsin digestion, analogous conditions were employed, with pH adjusted to 7.8 and the enzyme-to-protein ratio optimized accordingly.

5.2.9 LC-MS Analysis

The elution of unmodified antibody and modified antibodies followed a linear gradient from 0.05% trifluoroacetic acid (TFA) in water to 0.05% TFA in

acetonitrile over 25 minutes, at a flow rate of 0.2 mL/min and a column temperature of 60°C, with detection at 214 nm and injection of 5-7 µg of protein on the column. The desalting step was performed with a gradient starting with 100% 0.1% FA in H_2O for 2 minutes, then gradually shifting to 50% acetonitrile over 0.5 minutes. This was maintained isocratically for the next 2.5 minutes, followed by a final ramp to 100% ACN over the last 2 minutes. The flow rate was set to 0.5 mL/min, with injection volumes ranging from 1 to 5 µL.

For mass spectrometric detection, the Q Exactive Plus Orbitrap mass spectrometer was employed, running in positive ion mode. Full mass spectra were collected within an m/z range from 1800 to 5000, applying in-source collision-induced dissociation (CID) at 80 eV.

Appendix 1-Strategy of conjugation for therapeutic monoclonal antibodies and their conjugates

Antibody-drug conjugates (ADCs) represent a new type of biopharmaceutical consisting of a toxic agent covalently conjugated to monoclonal antibodies [1] via an engineered chemical linker.[2] [3]

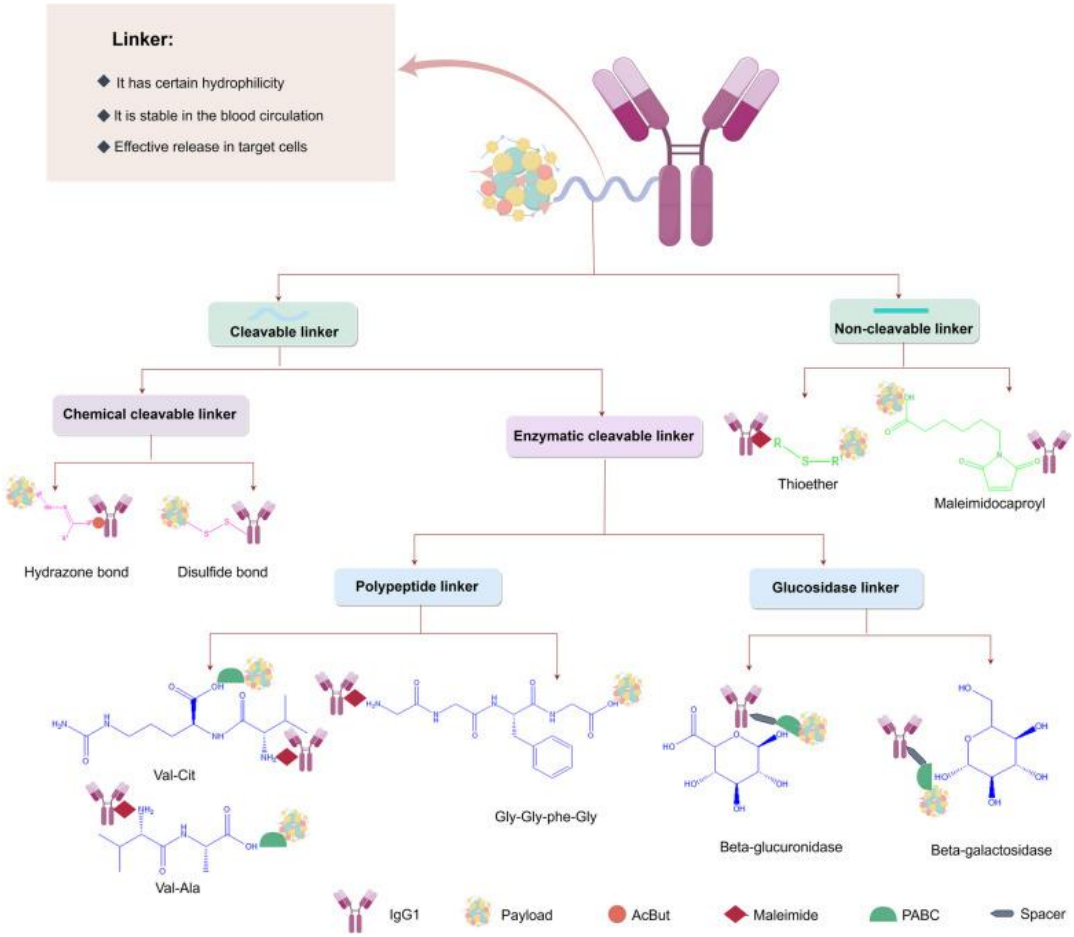

Fig. Scheme of type of conjugation strategy for antibody constructs [4]

Their clinical success in recent years in cancer treatment has been demonstrated with 15 ADCs approved globally 2024 [5], and currently over 400 ADCs are under evaluation in various stages of clinical trials. [4] [6]

The success of an ADC's performance, including its efficacy, safety, therapeutic index and pharmacokinetics, depends on the choice of payload, linker and antibody, but more importantly, on how these three individual components are linked.[7] [8]

Thus, recent studies have been directed toward the rational design of linkers, defining the optimal conjugation sites and fine-tuning reaction parameters such as buffer composition, conjugation chemistry, and stoichiometry; [9] to maximize homogeneity, enhance the stability [10] and improve cellular uptake. [11] [12]

Traditionally, conjugation methods are categorized into two main groups:

- random conjugation/non-site-conjugation
- site-specific conjugation

This classification highlights their main difference: homogeneity. [13] [14]

In the past studies, a new category called site-specific but non-site-selective has been used to engineer ADCs, in this category enzymatic-tag, glycan remodeling and affinity peptides are included.

The site-specific conjugation is also described as site-selective since used engineered cysteine or non-natural amino acids.[15]

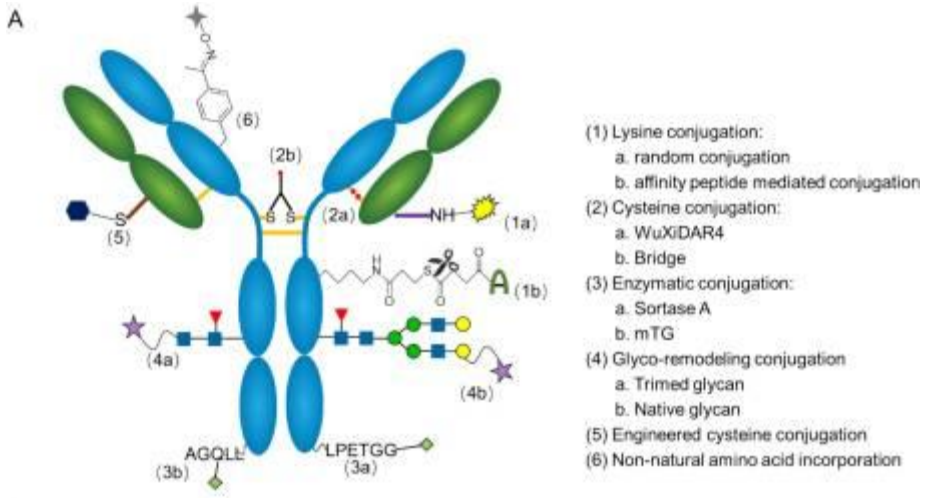

Fig. Scheme of conjugation techniques and interchain cysteine conjugation process.

Random Conjugation

Random conjugation is also known as random lysine conjugation. Lysine conjugation is a well-established strategy for ADCs production, exploiting the approximately 40 solvent-accessible Ɛ-amino groups on lysine side chains, which have high nucleophilicity in neutral conditions.[16] In fact, the electron-rich nucleophilic sites of lysine are targeted by electrophilic reagents [17] enabling the attachment of linker-payloads without a direct alteration of the antibody backbone.

To date, the FDA has approved five lysine-based conjugates in clinical trials.

Based on this success, a wide variety of linkers has been studied and produced to refine the bond forming, including N-hydroxysuccinimide (NHS) esters and their derivatives[16], benzoyl fluorides [18], isothiocyanates[19] and squaramate ester[20]. These linkers undergo hydrolysis in aqueous environments, and NHS ester instability represents a key factor that limits the effective linker-to-protein ratio during conjugation. Less reactive linkers may exhibit reactivity with -SH residues of cysteine under mild conditions, where the modification proceeds only slowly. For example, sulfonyl groups can be used as connector for cysteine [21], while sulfonyl acrylate can react with two cysteine residues to act as bridging linkers[22].

At first, the high reactivity of lysine-directed conjugation led to their classification as random modifications, but Liu et al.[23] demonstrated that the distribution of conjugation sites was found to be consistent under stable and controlled manufacturing conditions. This finding supports the reliability and scalability of the manufacturing process of lysine conjugationin current commercial ADC production. However, variations in reaction conditions may still produce heterogeneous drug-to-antibody ratios (DARs), which are associated with accelerated clearance and increased systemic toxicity.

Under mild conjugation conditions, random lysine conjugation can produce more homogeneous results for less reactive linkers with the most reactive lysine residues on the protein surface.[24]

Overall, despite its inherent heterogeneity, lysine conjugation remains a robust and widely applied approach for ADC production, yielding chemically stable and reproducible conjugates that have supported multiple regulatory approvals. At the same time, the

developments of site-specific lysine conjugate techniques expand their potential by improving conjugate homogeneity, broadening their therapeutic potential and safety profile.

Site-Specific, not site-selective conjugation

Interchain cysteine conjugation

Interchain cysteine conjugation exploits disulfide bonds in solvent-exposed regions of the antibody. The disulfide bonds can be easily reduced to generate eight free thiols by treatment with reducing reagents such as tris(2-carboxyethyl)phosphine (TCEP) and dithiothreitol (DTT).

Thiols, as nucleophiles, are softer and more amenable to Micheal addition compared to SN2 reactions at lysine residues, leading to less heterogeneous drug-antibody ratios (DARs).[25]

Maleimide chemistry has become the predominant approach in this category for its efficiency and almost quantitative thiol-succinimide bond formation under mild conditions.[26] Cysteine-mediated heterogeneity is considerably less than the lysine-based strategy due to the smaller number of thiol groups compared to amino residues [27], and this biorthogonal chemistry is ideal for producing engineered antibodies with 2,4,6,8 payloads.[28]

Maleimide conjugation stands out for simplicity, mild conditions, and high yields; and to date, the majority of currently approved ADCs, including ten of the fifteen marketed products, employ maleimide-thiol conjugation.

However, maleimide-thiol conjugates are susceptible to reverse Michael addition reactions, which could lead to premature payload release through serum protein interactions, altering the stability of the ADCs in plasma, reducing the effectiveness and safety.[29] [30]

Recent innovations have sought to address the residual heterogeneity of cysteine-mediated conjugation.

Platforms such as WuXiDAR4™ (https://www.wuxibiologics.com/wuxidar4/) use selective hinge shielding during reduction to favour DAR4 species, significantly increasing homogeneity and broadening the therapeutic window.[31] Disulfide re-bridging technologies represent another strategy, using bis-reactive linkers to reconnect reduced disulfides while

simultaneously introducing payloads. These approaches enable greater control over the DAR, preserve antibody morphology, and enhance serum stability.[32] Still, disulfide re-bridging can generate undesirable, so-called, “half-antibody” species, potentially impairing antibody-dependent cell-mediated cytotoxicity activity of ADCs compared to their parent antibodies.[33] Ongoing studies focus on refining linker chemistry and reaction conditions, to enhance yield and stability while mitigating the formation of these species. [34] [35]

Cysteine conjugation technologies continue to evolve, striking a balance between efficiency and controllability, while also addressing challenges in homogeneity and stability. Maleimide conjugation remains the gold standard, but emerging technologies, such as hinge shielding and disulfide re-bridging offer refined control over DAR and promising avenues for next-generation ADC design.

Enzymatic-tag conjugation

Enzymatic-mediated conjugation has emerged as a powerful tool for site-specific conjugation of payloads to antibodies, offering superior homogeneity compared to lysine conjugation and interchain cysteine conjugation.

This technology uses enzymes that recognize specific amino acid motifs, enabling precise coupling without extensive heterogeneity.

Sortase A (SrtA) is one example of a clinically used enzyme. It is a 30kDa transpeptidase which cleaves LPXTG motifs to form a thioester acyl-enzyme intermediate to enable N-terminal transfer of payloads. [36]

Another example is the formylglycine-generating enzyme, which modifies CXPXR motifs by oxidizing cysteine to formylglycine (https://onlinelibrary.wiley.com/doi/pdf/10.1097/01.HS9.0000847476.69621.cd).

Other clinically used enzymes are farnesyltransferase-based conjugation which modifies antibodies by adding isoprenoid groups to cysteine residues in a CaaX tag,[37] [38] and microbial transglutaminase which targets specific natural sites in antibodies, such as Q295, forming amide bonds between the γ-carboxy amide of glutamine and a free amine group of a payload.[39] [40]

Numerous additional enzymes, including tubulin-tyrosine ligase and SNAP-tag, remain under preclinical investigation.

Enzymatic-mediated conjugation methodology has a significant influence on both efficiency and overall product performance [41], but despite these advantages, this technology introduces technical challenges.

Efficient conjugation often requires genetic engineering of antibody sequences to provide recognition motifs that affect biological performance.

Some studies report superior conjugation yields with heavy-chain tags, whereas others highlight potential functional advantages with light-chain tagging.[42] [43] The introduction of heterologous tags may elevate immunogenicity risk, necessitating the use of low immunogenicity sequences or change of conjugation strategy.[44]

Efforts to improve enzymatic-mediated conjugation focus on enhancing catalytic efficiency, reducing material costs, and minimizing reaction reversibility. For example, wild-type SrtA has a poor catalytic activity, and a deep study in optimizing the process has shown that a two-step coupling instead of a longer single-step improves the catalytic activity, which helps the scalability and reduces the process waste.[45]

Enzymatic-mediated conjugation represents a promising and validated technique for ADC production. By offering high site-specificity and product homogeneity, it can enhance therapeutic safety and efficacy.

Ongoing advancements in enzyme engineering, tag design, and manufacturing processes will continue to push their clinical application. The research is also focused on reducing the risks associated with immunogenicity to ease the use.

Glycan remodelling conjugation

Over the past decade, glycol conjugation has gained popularity in both academia and industrial world for the ADCs production.

This conjugation method, unlike most enzyme-mediated techniques, does not require amino acid sequence engineering but exploits the conserved N-glycosylation site at Asp297 of IgG antibodies.[46]

Early approaches involved oxidation of cis-diols on glycans using sodium periodate ($NaIO_4$) to generate aldehyde groups for subsequent modification; more recent strategies, instead, rely on glycan remodeling, in which native glycans are enzymatically replaced/trimmed with modified structures that can be functionalized with linkers or payloads.

A promising example is Synaffix's GlycoConnect™ technology, which employs an endoglycosidase and a galactosyltransferase to trim natural glycans to incorporate an azido-modified galactose.[46]

Six programs using this strategy are currently in active clinical phase evaluation alongside several preclinical candidates. (https://synaffix.com/partnered-pipeline/) (ClinicalTrials.gov)

Despite its success, the approach requires multiple enzymes and conjugation steps, which can increase development complexity, reduce overall yield, and elevate manufacturing costs. To simplify the process, newer glycan remodeling methods based on endo S2 and its engineered variants have emerged. The enzymes enable deglycosylation and transfer of pre-functionalized glycans in a single step, eliminating the need for multiple enzymatic reactions.[47] [48]

From a process development standpoint, glycan remodeling methods vary in complexity and efficiency. Synaffix's GlycoConnect™ platform employs a two-enzyme, three-step protocol involving endoglycosidase and galactosyltransferase, which, while effective, increases development complexity, reduces yield, and elevates CMC costs. In contrast, endo S2-based technologies integrate deglycosylation and glycan transfer in a single step, offering a more streamlined, efficient, and cost-effective approach to producing homogeneous ADCs.[49]

Affinity peptide conjugation

Affinity-peptide conjugation exploits short peptides derived from protein A or protein G that selectively bind to the Fc region of antibodies. By positioning reactive linkers or linker-payloads near specific lysine residues (typically K248, K288 or K337). This methodology enhances efficiency at designated sites while minimizing random modifications.[50] However,

large non-native peptides may interfere with Fc function by hindering FcRn binding, potentially reducing ADC internalization.

Early implementations involved covalently attaching linkers to the affinity peptide itself, which subsequently formed stable covalent bonds with the antibody.[51]

To overcome these limitations, traceless affinity-directed approaches have been developed. Ajinomoto's AJICAP™ platform is an example, in which the first generation employed disulfide linkages removable under reductive conditions, and the second generation introduced thioesters that are directly displaced by lysine during conjugation.[52]

All things considered, affinity-peptide conjugation offers a versatile approach to site-biased ADC generation, balancing improved site-selectivity with efforts to reduce structural perturbation of the antibody and preserve critical Fc functions.

Site-specific and site-selective conjugation

Cysteine residues have long been central to protein and peptide modification strategies because of the high reactivity of their thiol groups. The concept of introducing a payload at defined positions by substituting native residues with cysteine has been introduced by Junutula et al[53] and leads to the development of cysteine-engineered antibodies, commonly referred to as ThioMabs.

Even if highly effective, cysteine engineering is not universally applicable, in fact, specific substitutions can disrupt protein folding. Structural and biophysical surrender matter: positions with limited solvent accessibility and positive local charge were shown to suppress malemide exchange and promote stability through rapid hydrolysis of the maleimide adduct.[42 54]

The pharmaceutical behaviour of these conjugates is closely related to site selection and drug loading. Siddharth et al.[55] developed a mechanistic PK/PD model for ThioMab™ drug conjugates (TDCs), demonstrating the existence of a correlation between high DAR values and drug deconjugation, total antibody clearance, and tumor cell killing rates, demonstrating, moreover, that deconjugation occurs more readily from heavy-chain sites.

To complete Ohri et al.[56] systematically screened 648 cysteine-substituted variants of trastuzumab, identifying 38 stable conjugation sites for both maleimide and disulfide linkers. Both studies confirmed that the *in vitro* plasma stability of site-specific ADCs closely correlates with their *in vivo* stability.

Site-specific ADCs exhibit superior preclinical profiles than not-site specific ADCs, nevertheless there have been limited data on their clinical advantages.[57]

Refinements to cysteine-engineering technologies have further improved the quality and reproducibility of ADCs. Engineered cysteines are typically exploited through reduction, re-oxidation, and conjugation steps, during which native hinge cysteines reform disulfides, while the engineered residues remain available for payload attachment. Current efforts are also directed at identifying optimal sites for generating uncapped monoclonal antibodies that maintain free cysteines during culture and purification, preserving antibody integrity.

Taken together, these advances establish cysteine engineering as a powerful and versatile platform for producing site-specific ADCs. By enabling rational placement of reactive thiols, controlling conjugation chemistry, and refining manufacturing conditions, this technology provides stable, homogeneous, and clinically viable ADCs, several of which have advanced into clinical development.

Influence of physiochemical parameters on antibody-drug conjugation

The efficiency, selectivity, and quality of antibody-linker-payload conjugation are profoundly affected by the physicochemical conditions under which the reactions occur. Among these, conjugation chemistry (see paragraph 4.1.1), buffer composition, and the stoichiometric ratio of reactants are particularly critical, as they determine not only the success of the conjugation step but also the long-term stability, pharmacological and therapeutic performance.[58]

Buffer composition and pH are decisive in modulating the ionization state of nucleophilic residues such as lysine Ɛ-amines and cysteine thiols, which are primary targets of conjugation.

Even a subtle shift in pH can markedly influence reactivity. For example, maleimide-thiol conjugation proceeds most efficiently under mild basic or neutral conditions, whereas in acidic solution, the conjugation efficiency is reduced and promotes the hydrolysis of malemides. Under excessively basic conditions, side reactions can be accelerated, leading to instability in both the linker and the antibody.

Moreover, the choice of buffer components and characteristics such as ionic strength or the presence of stabilizing additives that can mitigate or exacerbate antibody aggregation, unfolding or loss of binding activity, making buffer optimization an indispensable step in conjugation process development.[59] [60]

Finally, the stoichiometry of reactants (molar ratio of linker/payload to antibody) is a delicate parameter to tune to balance efficacy and stability. Employing higher linker/drug equivalents increases the possibility of achieving higher payload loading, thereby raising the DAR. However, excessive modification (high DAR) can induce structural perturbations, antibody unfolding, or aggregation and may interfere with antigen recognition.[61]

High DAR conjugates are also prone to faster systemic clearance and altered biodistribution[62], potentially increasing off-target toxicity. Simultaneously, low DAR conjugates can have a reduced therapeutic potency.[63]

Preclinical and clinical evidence suggest that an intermediate DAR, a range of 2-4 drugs per antibody, has the best compromise between potency and tolerability. For example, the AJICAP second-generation technology exemplifies how controlling stoichiometry through selective lysine modification enables reproducible DARs and improved therapeutic indices.[64]

Overall, buffer composition, pH variant, and stoichiometry highlight the inherently multivariable nature of antibody conjugation processes; and a careful optimization of these parameters is essential not only to maximize conjugation efficiency but also to ensure biostability, pharmacological effectiveness, and clinical safety.

(1) Hoffmann, R. M.; Coumbe, B. G. T.; Josephs, D. H.; Mele, S.; Ilieva, K. M.; Cheung, A.; Tutt, A. N.; Spicer, J. F.; Thurston, D. E.; Crescioli, S.; Karagiannis, S. N. Antibody Structure and Engineering Considerations for the Design and Function of Antibody Drug Conjugates (ADCs). OncoImmunology 2018, 7 (3), e1395127. https://doi.org/10.1080/2162402X.2017.1395127.

(2) Wang, R.; Hu, B.; Pan, Z.; Mo, C.; Zhao, X.; Liu, G.; Hou, P.; Cui, Q.; Xu, Z.; Wang, W.; Yu, Z.; Zhao, L.; He, M.; Wang, Y.; Fu, C.; Wei, M.; Yu, L. Antibo

dy–Drug Conjugates (ADCs): Current and Future Biopharmaceuticals. J. Hematol. Oncol.J Hematol Oncol 2025, 18 (1), 51. https://doi.org/10.1186/s13045-025-01704-3.

(3) Jain, N.; Smith, S. W.; Ghone, S.; Tomczuk, B. Current ADC Linker Chemistry. Pharm. Res. 2015, 32 (11), 3526–3540. https://doi.org/10.1007/s11095-015-1657-7.

(4) Wang, R.; Hu, B.; Pan, Z.; Mo, C.; Zhao, X.; Liu, G.; Hou, P.; Cui, Q.; Xu, Z.; Wang, W.; Yu, Z.; Zhao, L.; He, M.; Wang, Y.; Fu, C.; Wei, M.; Yu, L. Antibody–Drug Conjugates (ADCs): Current and Future Biopharmaceuticals. J. Hematol. Oncol.J Hematol Oncol 2025, 18 (1), 51. https://doi.org/10.1186/s13045-025-01704-3.

(5) Wei, Q.; Li, M.; Du, Q.; Liu, X. Association between Opioids Use and Risk of Multiple Cancers: A Two-Sample Mendelian Randomization Study. J. Anesth. Transl. Med. 2024, 3 (1), 1–9. https://doi.org/10.1016/j.jatmed.2024.02.004.

(6) Hong, Y.; Nam, S.-M.; Moon, A. Antibody–Drug Conjugates and Bispecific Antibodies Targeting Cancers: Applications of Click Chemistry. Arch. Pharm. Res. 2023, 46 (3), 131–148. https://doi.org/10.1007/s12272-023-01433-6.

(7) Akram, F.; Ali, A. M.; Akhtar, M. T.; Fatima, T.; Shabbir, I.; Ul Haq, I. The Journey of Antibody-Drug Conjugates for Revolutionizing Cancer Therapy: A Review. Bioorg. Med. Chem. 2025, 117, 118010. https://doi.org/10.1016/j.bmc.2024.118010.

(8) Thudium, K.; Bilic, S.; Leipold, D.; Mallet, W.; Kaur, S.; Meibohm, B.; Erickson, H.; Tibbitts, J.; Zhao, H.; Gupta, M. American Association of Pharmaceutical Scientists National Biotechnology Conference Short Course: Translational Challenges in Developing Antibody-Drug Conjugates: May 24, 2012, San Diego, CA. mAbs 2013, 5 (1), 5–12. https://doi.org/10.4161/mabs.22909.

(9) Ducry, L.; Stump, B. Antibody–Drug Conjugates: Linking Cytotoxic Payloads to Monoclonal Antibodies. Bioconjug. Chem. 2010, 21 (1), 5–13. https://doi.org/10.1021/bc9002019.

(10) Wakankar, A. A.; Feeney, M. B.; Rivera, J.; Chen, Y.; Kim, M.; Sharma, V. K.; Wang, Y. J. Physicochemical Stability of the Antibody–Drug Conjugate Trastuzumab-DM1: Changes Due to Modification and Conjugation Processes. Bioconjug. Chem. 2010, 21 (9), 1588–1595. https://doi.org/10.1021/bc900434c.

(11) Behrens, C. R.; Liu, B. Methods for Site-Specific Drug Conjugation to Antibodies. mAbs 2014, 6 (1), 46–53. https://doi.org/10.4161/mabs.26632.

(12) Moore, E. J.; Rice, M.; Roy, G.; Zhang, W.; Marelli, M. Emerging Conjugation Strategies and Protein Engineering Technologies Aim to Improve ADCs in the Fight against Cancer. Xenobiotica 2024, 54 (8), 469–491. https://doi.org/10.1080/00498254.2024.2339993.

(13) Stephan, J. P.; Kozak, K. R.; Wong, W. L. T. Challenges in Developing Bioanalytical Assays for Characterization of Antibody–Drug Conjugates. Bioanalysis 2011, 3 (6), 677–700. https://doi.org/10.4155/bio.11.30.

(14) Sadiki, A.; Vaidya, S. R.; Abdollahi, M.; Bhardwaj, G.; Dolan, M. E.; Turna, H.; Arora, V.; Sanjeev, A.; Robinson, T. D.; Koid, A.; Amin, A.; Zhou, Z. S. Site-Specific Conjugation of Native Antibody. Antib. Ther. 2020, 3 (4), 271–284. https://doi.org/10.1093/abt/tbaa027.

(15) Fan, Q.; Chen, H.; Wei, G.; Wei, D.; Wang, Z.; Zhang, L.; Wang, J.; Zhu, M. A Review of Conjugation Technologies for Antibody Drug Conjugates. Antib. Ther. 2025, 8 (2), 157–170. https://doi.org/10.1093/abt/tbaf010.

(16) Zhu, M.; Zhou, L.; Hu, S.; Miao, Q.; Gong, J.; Zhang, N.; Zhang, G.; Wang, M.; Wang, J.; He, H.; Wang, Y. Rational Design and Systemic Appraisal of an EGFR-Targeting Antibody–Drug Conjugate LR-DM1 for Pancreatic Cancer. J. Med. Chem. 2022, 65 (10), 7141–7153. https://doi.org/10.1021/acs.jmedchem.1c01920.

(17) Spicer, C. D.; Pashuck, E. T.; Stevens, M. M. Achieving Controlled Biomolecule–Biomaterial Conjugation. Chem. Rev. 2018, 118 (16), 7702–7743. https://doi.org/10.1021/acs.chemrev.8b00253.

(18) Lehot, V.; Kuhn, I.; Nothisen, M.; Erb, S.; Kolodych, S.; Cianférani, S.; Chaubet, G.; Wagner, A. Non-Specific Interactions of Antibody-Oligonucleotide

Conjugates with Living Cells. Sci. Rep. 2021, 11 (1), 5881. https://doi.org/10.1038/s41598-021-85352-w.

(19) Schlein, E.; Syvänen, S.; Rokka, J.; Gustavsson, T.; Rossin, R.; Robillard, M.; Eriksson, J.; Sehlin, D. Functionalization of Radiolabeled Antibodies to Enhance Peripheral Clearance for High Contrast Brain Imaging. Mol. Pharm. 2022, 19 (11), 4111–4122. https://doi.org/10.1021/acs.molpharmaceut.2c00536.

(20) Vizier, R.; Adumeau, P.; Moreau, M.; Goncalves, V.; Denat, F. Moving Beyond Isothiocyanates: A Look at the Stability of Conjugation Links Toward Radiolysis in89 Zr-Labeled Immunoconjugates. Bioconjug. Chem. 2024, 35 (5), 633–637. https://doi.org/10.1021/acs.bioconjchem.4c00105.

(21) Hwang, D.; Rader, C. Site-Specific Antibody–Drug Conjugates in Triple Variable Domain Fab Format. Biomolecules 2020, 10 (5), 764. https://doi.org/10.3390/biom10050764.

(22) Matos, M. J.; Oliveira, B. L.; Martínez-Sáez, N.; Guerreiro, A.; Cal, P. M. S. D.; Bertoldo, J.; Maneiro, M.; Perkins, E.; Howard, J.; Deery, M. J.; Chalker, J. M.; Corzana, F.; Jiménez-Osés, G.; Bernardes, G. J. L. Chemo- and Regioselective Lysine Modification on Native Proteins. J. Am. Chem. Soc. 2018, 140 (11), 4004–4017. https://doi.org/10.1021/jacs.7b12874.

(23) Wu, G.; Gao, Y.; Liu, D.; Tan, X.; Hu, L.; Qiu, Z.; Liu, J.; He, H.; Liu, Y. Study on the Heterogeneity of T-DM1 and the Analysis of the Unconjugated Linker Structure under a Stable Conjugation Process. ACS Omega 2019, 4 (5), 8834–8845. https://doi.org/10.1021/acsomega.9b00430.

(24) Hwang, D.; Tsuji, K.; Park, H.; Burke, T. R.; Rader, C. Site-Specific Lysine Arylation as an Alternative Bioconjugation Strategy for Chemically Programmed Antibodies and Antibody–Drug Conjugates. Bioconjug. Chem. 2019, 30 (11), 2889–2896. https://doi.org/10.1021/acs.bioconjchem.9b00609.

(25) Chalker, J. M.; Bernardes, G. J. L.; Lin, Y. A.; Davis, B. G. Chemical Modification of Proteins at Cysteine: Opportunities in Chemistry and Biology. Chem. – Asian J. 2009, 4 (5), 630–640. https://doi.org/10.1002/asia.200800427.

(26) Sun, M. M. C.; Beam, K. S.; Cerveny, C. G.; Hamblett, K. J.; Blackmore, R. S.; Torgov, M. Y.; Handley, F. G. M.; Ihle, N. C.; Senter, P. D.; Alley, S. C. Reduction−Alkylation Strategies for the Modification of Specific Monoclonal Antibody Disulfides. Bioconjug. Chem. 2005, 16 (5), 1282–1290. https://doi.org/10.1021/bc050201y.

(27) Valliere-Douglass, J. F.; Hengel, S. M.; Pan, L. Y. Approaches to Interchain Cysteine-Linked ADC Characterization by Mass Spectrometry. Mol. Pharm. 2015, 12 (6), 1774–1783. https://doi.org/10.1021/mp500614p.

(28) Ochtrop, P.; Hackenberger, C. P. R. Recent Advances of Thiol-Selective Bioconjugation Reactions. Curr. Opin. Chem. Biol. 2020, 58, 28–36. https://doi.org/10.1016/j.cbpa.2020.04.017.

(29) Szijj, P. A.; Bahou, C.; Chudasama, V. Minireview: Addressing the Retro-Michael Instability of Maleimide Bioconjugates. Drug Discov. Today Technol. 2018, 30, 27–34. https://doi.org/10.1016/j.ddtec.2018.07.002.

(30) Wang, Y.; Xie, F.; Liu, L.; Xu, X.; Fan, S.; Zhong, W.; Zhou, X. Development of Applicable Thiol-Linked Antibody–Drug Conjugates with Improved Stability and Therapeutic Index. Drug Deliv. 2022, 29 (1), 754–766. https://doi.org/10.1080/10717544.2022.2039807.

(31) You, J.; Zhang, J.; Wang, J.; Jin, M. Cysteine-Based Coupling: Challenges and Solutions. Bioconjug. Chem. 2021, 32 (8), 1525–1534. https://doi.org/10.1021/acs.bioconjchem.1c00213.

(32) Forte, N.; Chudasama, V.; Baker, J. R. Homogeneous Antibody-Drug Conjugates via Site-Selective Disulfide Bridging. Drug Discov. Today Technol. 2018, 30, 11–20. https://doi.org/10.1016/j.ddtec.2018.09.004.

(33) Bahou, C.; Love, E. A.; Leonard, S.; Spears, R. J.; Maruani, A.; Armour, K.; Baker, J. R.; Chudasama, V. Disulfide Modified IgG1: An Investigation of Biophysical Profile and Clinically Relevant Fc Interactions. Bioconjug. Chem. 2019, 30 (4), 1048–1054. https://doi.org/10.1021/acs.bioconjchem.9b00174.

(34) Lee, M. T. W.; Maruani, A.; Baker, J. R.; Caddick, S.; Chudasama, V. Next-Generation Disulfide Stapling: Reduction and Functional Re-Bridging All in One. Chem. Sci. 2016, 7 (1), 799–802. https://doi.org/10.1039/C5SC02666K.

(35) Bahou, C.; Richards, D. A.; Maruani, A.; Love, E. A.; Javaid, F.; Caddick, S.; Baker, J. R.; Chudasama, V. Highly Homogeneous Antibody Modification through Optimisation of the Synthesis and Conjugation of Functionalised Dibromopyridazinediones. Org. Biomol. Chem. 2018, 16 (8), 1359–1366. https://doi.org/10.1039/C7OB03138F.

(36) Spirig, T.; Weiner, E. M.; Clubb, R. T. Sortase Enzymes in Gram-positive Bacteria. Mol. Microbiol. 2011, 82 (5), 1044–1059. https://doi.org/10.1111/j.1365-2958.2011.07887.x.

(37) Wang, M.; Casey, P. J. Protein Prenylation: Unique Fats Make Their Mark on Biology. Nat. Rev. Mol. Cell Biol. 2016, 17 (2), 110–122. https://doi.org/10.1038/nrm.2015.11.

(38) Li, Q.; Cheng, Y.; Tong, Z.; Liu, Y.; Wang, X.; Yan, M.; Chang, J.; Wang, S.; Du, C.; Li, L.; Wu, C.; Wang, M.; Wang, Z.; Wu, Z.; Wang, X.; Jin, Y.; Diao, L.; Sun, Y.; Zhang, Y.; Hui, A.-M.; Xu, B. HER2-Targeting Antibody Drug Conjugate FS-1502 in HER2-Expressing Metastatic Breast Cancer: A Phase 1a/1b Trial. Nat. Commun. 2024, 15 (1), 5158. https://doi.org/10.1038/s41467-024-48798-w.

(39) Dennler, P.; Chiotellis, A.; Fischer, E.; Brégeon, D.; Belmant, C.; Gauthier, L.; Lhospice, F.; Romagne, F.; Schibli, R. Transglutaminase-Based Chemo-Enzymatic Conjugation Approach Yields Homogeneous Antibody–Drug Conjugates. Bioconjug. Chem. 2014, 25 (3), 569–578. https://doi.org/10.1021/bc400574z.

(40) Hussain, A.; Grimm, A.; Sheng, W.; Zhang, C.; Al-Rawe, M.; Bräutigam, K.; Abu Mraheil, M.; Zeppernick, F.; Meinhold-Heerlein, I. Toward Homogenous Antibody Drug Conjugates Using Enzyme-Based Conjugation Approaches. Pharmaceuticals 2021, 14 (4), 343. https://doi.org/10.3390/ph14040343.

(41) Huang, B. C. B.; Kim, Y. C.; Bañas, S.; Barfield, R. M.; Drake, P. M.; Rupniewski, I.; Haskins, W. E.; Rabuka, D. Antibody-Drug Conjugate Library Prepared by Scanning Insertion of the Aldehyde Tag into IgG1 Constant Regions. mAbs 2018, 10 (8), 1182–1189. https://doi.org/10.1080/19420862.2018.1512327.

(42) Shen, B.-Q.; Xu, K.; Liu, L.; Raab, H.; Bhakta, S.; Kenrick, M.; Parsons-Reponte, K. L.; Tien, J.; Yu, S.-F.; Mai, E.; Li, D.; Tibbitts, J.; Baudys, J.; Saad, O. M.; Scales, S. J.; McDonald, P. J.; Hass, P. E.; Eigenbrot, C.; Nguyen, T.; Solis, W. A.; Fuji, R. N.; Flagella, K. M.; Patel, D.; Spencer, S. D.; Khawli, L. A.; Ebens, A.; Wong, W. L.; Vandlen, R.; Kaur, S.; Sliwkowski, M. X.; Scheller, R. H.; Polakis, P.; Junutula, J. R. Conjugation Site Modulates the in Vivo Stability and Therapeutic Activity of Antibody-Drug Conjugates. Nat. Biotechnol. 2012, 30 (2), 184–189. https://doi.org/10.1038/nbt.2108.

(43) Strop, P.; Liu, S.-H.; Dorywalska, M.; Delaria, K.; Dushin, R. G.; Tran, T.-T.; Ho, W.-H.; Farias, S.; Casas, M. G.; Abdiche, Y.; Zhou, D.; Chandrasekaran, R.; Samain, C.; Loo, C.; Rossi, A.; Rickert, M.; Krimm, S.; Wong, T.; Chin, S. M.; Yu, J.; Dilley, J.; Chaparro-Riggers, J.; Filzen, G. F.; O'Donnell, C. J.; Wang, F.; Myers, J. S.; Pons, J.; Shelton, D. L.; Rajpal, A. Location Matters: Site of Conjugation

Modulates Stability and Pharmacokinetics of Antibody Drug Conjugates. Chem. Biol. 2013, 20 (2), 161–167. https://doi.org/10.1016/j.chembiol.2013.01.010.

(44) Debon, A.; Siirola, E.; Snajdrova, R. Enzymatic Bioconjugation: A Perspective from the Pharmaceutical Industry. JACS Au 2023, 3 (5), 1267–1283. https://doi.org/10.1021/jacsau.2c00617.

(45) Chen, L.; Cohen, J.; Song, X.; Zhao, A.; Ye, Z.; Feulner, C. J.; Doonan, P.; Somers, W.; Lin, L.; Chen, P. R. Improved Variants of SrtA for Site-Specific Conjugation on Antibodies and Proteins with High Efficiency. Sci. Rep. 2016, 6 (1), 31899. https://doi.org/10.1038/srep31899.

(46) Shivatare, S. S.; Shivatare, V. S.; Wong, C.-H. Glycoconjugates: Synthesis, Functional Studies, and Therapeutic Developments. Chem. Rev. 2022, 122 (20), 15603–15671. https://doi.org/10.1021/acs.chemrev.1c01032.

(47) Shi, W.; Li, W.; Zhang, J.; Li, T.; Song, Y.; Zeng, Y.; Dong, Q.; Lin, Z.; Gong, L.; Fan, S.; Tang, F.; Huang, W. One-Step Synthesis of Site-Specific Antibody–Drug Conjugates by Reprograming IgG Glycoengineering with LacNAc-Based Substrates. Acta Pharm. Sin. B 2022, 12 (5), 2417–2428. https://doi.org/10.1016/j.apsb.2021.12.013.

(48)

(49) Kishimoto, S.; Nakashimada, Y.; Yokota, R.; Hatanaka, T.; Adachi, M.; Ito, Y. Site-Specific Chemical Conjugation of Antibodies by Using Affinity Peptide for the Development of Therapeutic Antibody Format. Bioconjug. Chem. 2019, 30 (3), 698–702. https://doi.org/10.1021/acs.bioconjchem.8b00865.

(50) Postupalenko, V.; Marx, L.; Pantin, M.; Viertl, D.; Gsponer, N.; Giudice, G.; Gasilova, N.; Schottelius, M.; Lévy, F.; Garrouste, P.; Segura, J.-M.; Nyanguile, O. Site-Selective Template-Directed Synthesis of Antibody Fc Conjugates with Concomitant Ligand Release. Chem. Sci. 2024, 15 (4), 1324–1337. https://doi.org/10.1039/D3SC04324J.

(51) Yu, C.; Tang, J.; Loredo, A.; Chen, Y.; Jung, S. Y.; Jain, A.; Gordon, A.; Xiao, H. Proximity-Induced Site-Specific Antibody Conjugation. Bioconjug. Chem. 2018, 29 (11), 3522–3526. https://doi.org/10.1021/acs.bioconjchem.8b00680.

(52) Matsuda, Y.; Robles, V.; Malinao, M.-C.; Song, J.; Mendelsohn, B. A. Comparison of Analytical Methods for Antibody–Drug Conjugates Produced by Chemical Site-Specific Conjugation: First-Generation AJICAP. Anal. Chem. 2019, 91 (20), 12724–12732. https://doi.org/10.1021/acs.analchem.9b02192.

(53) Junutula, J. R.; Raab, H.; Clark, S.; Bhakta, S.; Leipold, D. D.; Weir, S.; Chen, Y.; Simpson, M.; Tsai, S. P.; Dennis, M. S.; Lu, Y.; Meng, Y. G.; Ng, C.; Yang, J.; Lee, C. C.; Duenas, E.; Gorrell, J.; Katta, V.; Kim, A.; McDorman, K.; Flagella, K.; Venook, R.; Ross, S.; Spencer, S. D.; Lee Wong, W.; Lowman, H. B.; Vandlen, R.; Sliwkowski, M. X.; Scheller, R. H.; Polakis, P.; Mallet, W. Site-Specific Conjugation of a Cytotoxic Drug to an Antibody Improves the Therapeutic Index. Nat. Biotechnol. 2008, 26 (8), 925–932. https://doi.org/10.1038/nbt.1480.

(54) Sussman, D.; Westendorf, L.; Meyer, D. W.; Leiske, C. I.; Anderson, M.; Okeley, N. M.; Alley, S. C.; Lyon, R.; Sanderson, R. J.; Carter, P. J.; Benjamin, D. R. Engineered Cysteine Antibodies: An Improved Antibody-Drug Conjugate Platform with a Novel Mechanism of Drug-Linker Stability. Protein Eng. Des. Sel. 2018, 31 (2), 47–54. https://doi.org/10.1093/protein/gzx067.

(55) Sukumaran, S.; Gadkar, K.; Zhang, C.; Bhakta, S.; Liu, L.; Xu, K.; Raab, H.; Yu, S.-F.; Mai, E.; Fourie-O'Donohue, A.; Kozak, K. R.; Ramanujan, S.; Junutula, J. R.; Lin, K. Mechanism-Based Pharmacokinetic/Pharmacodynamic Model for THIOMABTM Drug Conjugates. Pharm. Res. 2015, 32 (6), 1884–1893. https://doi.org/10.1007/s11095-014-1582-1.

(56) Ohri, R.; Bhakta, S.; Fourie-O'Donohue, A.; Dela Cruz-Chuh, J.; Tsai, S. P.; Cook, R.; Wei, B.; Ng, C.; Wong, A. W.; Bos, A. B.; Farahi, F.; Bhakta, J.; Pillow, T. H.; Raab, H.; Vandlen, R.; Polakis, P.; Liu, Y.; Erickson, H.; Junutula, J. R.; Kozak, K. R. High-Throughput Cysteine Scanning To Identify Stable Antibody Conjugation Sites for Maleimide- and Disulfide-Based Linkers. Bioconjug. Chem. 2018, 29 (2), 473–485. https://doi.org/10.1021/acs.bioconjchem.7b00791.

(57) Herrera, A. F.; Patel, M. R.; Burke, J. M.; Advani, R.; Cheson, B. D.; Sharman, J. P.; Penuel, E.; Polson, A. G.; Liao, C. D.; Li, C.; Schuth, E.; Vaze, A.; Samineni, D.; Elstrom, R.; Cooper, J.; Diefenbach, C. Anti-CD79B Antibody–Drug Conjugate DCDS0780A in Patients with B-Cell Non-Hodgkin Lymphoma: Phase 1 Dose-Escalation Study. Clin. Cancer Res. 2022, 28 (7), 1294–1301. https://doi.org/10.1158/1078-0432.CCR-21-3261.

(58) Fu, Z.; Li, S.; Han, S.; Shi, C.; Zhang, Y. Antibody Drug Conjugate: The "Biological Missile" for Targeted Cancer Therapy. Signal Transduct. Target. Ther. 2022, 7 (1), 93. https://doi.org/10.1038/s41392-022-00947-7.

(59) Wagh, A.; Song, H.; Zeng, M.; Tao, L.; Das, T. K. Challenges and New Frontiers in Analytical Characterization of Antibody-Drug Conjugates. mAbs 2018, 10 (2), 222–243. https://doi.org/10.1080/19420862.2017.1412025.

(60) Gordon, M. R.; Canakci, M.; Li, L.; Zhuang, J.; Osborne, B.; Thayumanavan, S. Field Guide to Challenges and Opportunities in Antibody–Drug Conjugates for Chemists. Bioconjug. Chem. 2015, 26 (11), 2198–2215. https://doi.org/10.1021/acs.bioconjchem.5b00399.

(61) Rahban, M.; Ahmad, F.; Piatyszek, M. A.; Haertlé, T.; Saso, L.; Saboury, A. A. Stabilization Challenges and Aggregation in Protein-Based Therapeutics in the Pharmaceutical Industry. RSC Adv. 2023, 13 (51), 35947–35963. https://doi.org/10.1039/D3RA06476J.

(62) Díaz-Tejeiro, C.; López De Sá, A.; Poyatos-Racionero, E.; Ballestín, P.; Bartolomé, J.; Calvo, E.; Moreno, V.; Moris, F.; Pérez-Segura, P.; Gyorffy, B.; Pandiella, A.; Ocaña, A. Understanding the Preclinical Efficacy of Antibody–Drug Conjugates. Int. J. Mol. Sci. 2024, 25 (23), 12875. https://doi.org/10.3390/ijms252312875.

(63) Nguyen, T. D.; Bordeau, B. M.; Balthasar, J. P. Mechanisms of ADC Toxicity and Strategies to Increase ADC Tolerability. Cancers 2023, 15 (3), 713. https://doi.org/10.3390/cancers15030713.

(64) Fujii, T.; Matsuda, Y.; Seki, T.; Shikida, N.; Iwai, Y.; Ooba, Y.; Takahashi, K.; Isokawa, M.; Kawaguchi, S.; Hatada, N.; Watanabe, T.; Takasugi, R.; Nakayama, A.; Shimbo, K.; Mendelsohn, B. A.; Okuzumi, T.; Yamada, K. AJICAP Second Generation: Improved Chemical Site-Specific Conjugation Technology for Antibody–Drug Conjugate Production. Bioconjug. Chem. 2023, acs.bioconjchem.3c00040. https://doi.org/10.1021/acs.bioconjchem.3c00040.

Appendix 2- Multi dimensional liquid chromatography (mD-LC)

Liquid chromatography (LC), has long been an indispensable tool in analytical chemistry, owing to its versatility, broad applicability to nonvolatile or thermally labile compounds, and its capacity for high-resolution separations.[1] [2]

The development of high-performance liquid chromatography (HPLC), back in the 1960-70s,[3] with tightly packed columns and high-pressure pumping systems, revolutionized analysis by delivering rapid, reproducible separations with quantitative precision.[4] And its evolution into ultra-high-pressure liquid chromatography (UHPLC) further advanced resolution and analysis speed.[4] [5] [6]

When analyzing increasingly complex mixtures, protein digests, metabolomic samples, synthetic oligonucleotides, or botanical extracts, the LC and HPLC quickly reach their limits in terms of separation mechanisms.

Peaks began to overlap,[7] and near-isomers are co-eluted,[8] while small impurities remained buried under dominant components. Longer gradients, alternative mobile phases, and column chemistries could only partially improve resolution, at the cost of longer analysis times[9] and reduced sensitivity due to band broadening.[10]

With the rapid advances and the increasing need for biologically active molecules and biotherapeutics in the pharmaceutical world, LC alone cannot cope with the combinatorial complexity of modern samples.[11] It became clear that there was a need to improve the separation and purification technologies, and if one dimension of selectivity was insufficient, adding a second orthogonal or complementary dimension could multiply resolving power without impractically extending run time.[12] [11]

Theoretical foundations of multi-dimensional liquid chromatography

The conception and optimization of a multidimensional liquid chromatography (mD-LC) system relies fundamentally on three core concepts that together determine its resolving capacity, the degree of orthogonality between dimensions, and operational feasibility.[13] [14]

The *orthogonality* defines the degree to which the multiple separation dimensions differ in their selectivity.[15] When the retention mechanisms differ significantly, as in RP-LC and IEX, analytes are distributed more uniformly across the two-dimensional separation space.[16] [15] This uniformity reflects the system's ability to exploit independent physicochemical interactions, maximizing the number of distinct separation pathways.[17] [18] Quantitative assessment of orthogonality, using metrics such as correlation coefficients or information theory–based indices, provides a rational basis for selecting stationary-phase chemistries or mobile-phase conditions.[19]

In practice, achieving high orthogonality requires careful pairing of separation modes that minimize correlation between retention factors while maintaining chemical compatibility between dimensions.[20] Nevertheless, even with an optimal orthogonality, the performance of an mD-LC system can be severely limited by *undersampling*. It occurs when the modulation frequency of the second dimension is insufficient to capture the full temporal profile of first-dimension peaks. Suppose the second-dimension cycle time is too long compared to the first-dimension peak width.[21] In that case, portions of analyte bands are lost, along with the information they carry, leading to a reduction in effective resolution and an underestimation of the system's true peak capacity. [18]

Theoretical models often express multidimensional separation performance as the product of the peak capacities of each dimension; actually, it is typically lower due to incomplete orthogonality, undersampling, and inefficient use of the separation space.[22] [23]

The *effective peak capacity* depends not only on the theoretical multiplication of individual dimensions but also on how uniformly and completely the two-dimensional separation space is populated with resolved analyte peaks.[24] Improving space utilization involves balancing analysis time, modulation period, gradient steepness, and phase compatibility to achieve the most efficient distribution of peaks within the available separation window.[25]

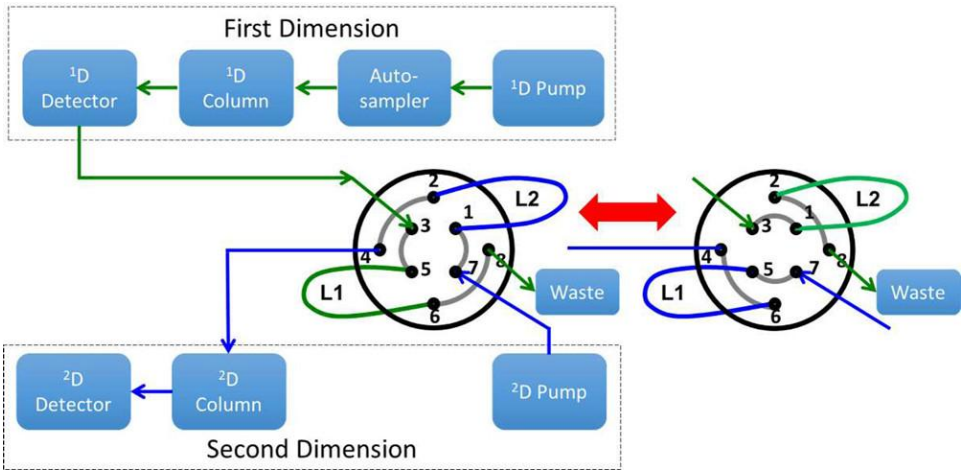

Fig.1: Diagram of a typical 2D-LC instrument highlighting the centrality of the valve[26]

Classification of Multidimensional LC Modes

When discussing mD-LC, several distinct modes of coupling and sampling can be employed, each offering different balances between resolution, selectivity, and analysis time.[27] [28] Basically, the way the first dimension is transferred to the second

determines the operational mode and the system's performance and applicability.[29] [30]

It is possible to recognize three major categories:

- *Full comprehensive* (LC×LC)
- *Selective comprehensive* (sLC×LC)
- *Heart-cutting* (LC–LC, or multiple heart-cutting, mLC–LC)

Each approach represents a compromise between information content, instrumental complexity, and analysis elaboration.[31] Full comprehensive LC×LC maximizes the exploitation of orthogonality and total peak capacity, but at the cost of higher data density. Heart-cutting methods, in contrast, offer greater flexibility, shorter total analysis times, and simplified data interpretation, though at the expense of global sample coverage.[32]

Full Comprehensive (LC×LC)

In a fully comprehensive, multidimensional liquid chromatography system, the entire effluent from the first dimension is systematically transferred to the second dimension for subsequent separation.[27] [33] And it means that every fraction of the first-dimension eluate undergoes further separation in the second dimension, ensuring that no chemical information from the original chromatographic process is lost.[1] [34] Providing a truly comprehensive representation of sample complexity by exploiting the complete orthogonality between two distinct separation mechanisms.[23]

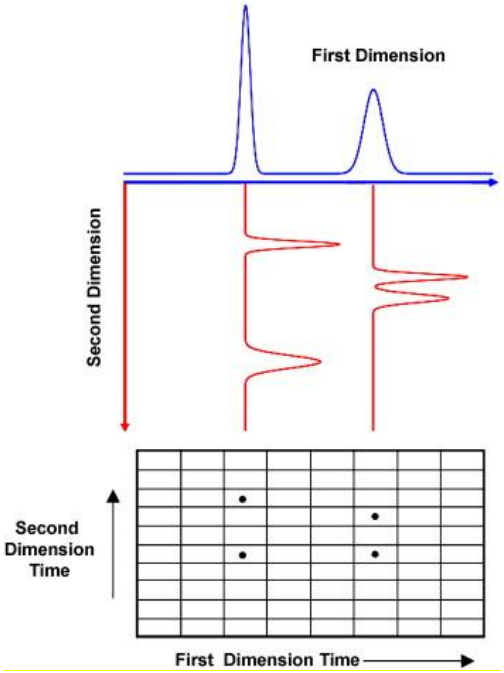

Fig.2: Schematic illustration of a comprehensive two-dimensional liquid chromatography (LC×LC) separation.

In LC×LC, the first-dimension separation generally occurs under mild conditions, using lower flow rates and longer analysis times to exploit the resolving power of this first separation.[35] At fixed time intervals, called modulation periods ranging from a few seconds to tens of seconds, discrete fractions of the first dimension are collected into storage loops or trapping devices.

During each modulation cycle, the second-dimension separation proceeds faster to ensure that each chromatogram finishes before the next fraction arrives.[36] The result is a continuous sequence of rapid second-dimension runs synchronized with the slower first-dimension elution.

This approach presents numerous advantages. The first and most crucial one lies in its comprehensive nature: every compound entering the system is subjected to both separation mechanisms, maximizing the analytical information obtained.[37]

However, this approach imposes several practical and instrumental constraints. The second-dimension separations must be extremely rapid, placing stringent demands on column efficiency, kinetic performance, and instrumental timing precision.[38] It also entails increased solvent consumption, more complex valving and synchronization requirements, and the generation of large data volumes that necessitate advanced computational handling.[39]

That said, advances in micro- and nano-flow technology, high-efficiency column design, and fast-gradient operation have made LC×LC more accessible, establishing this methodology as a powerful and mature technique for high-resolution analysis of complex mixtures.[39]

Selective comprehensive (sLC×LC)

Selective comprehensive multi-dimensional liquid chromatography, also referred to as restricted, targeted, or zone-comprehensive 2D-LC, represents an intermediate configuration between full comprehensive LC×LC and classical heart-cutting LC–LC.[40]

Unlike full comprehensive, only a subset of the first-dimension effluent, typically a chromatographic region or band containing analytes of interest, is directed to second-dimension analysis, while the rest may be discarded.[41]

That is the one, but significant difference compared to LC×LC: the second dimension operates in a comprehensive fashion within selected zones, but the whole system does not sample the entire first-dimension profile.

This approach is practical when prior knowledge indicates that only certain regions of the first-dimension chromatogram contain compounds relevant to the study of interest. It provides a practical balance between depth of information and operational simplicity.[37]

In selective comprehensive mode the first-dimension separation proceeds continuously under conventional conditions. A switching valve or flow redirector identifies specific retention time windows corresponding to regions of analytical interest and transfers only these windows for second-dimension separation, while the remaining effluent is directed to the waste or another detector.[1] [42] In sLC×LC modulation occurs at regular intervals, and each collected fraction is rapidly analyzed in the second dimension. The result is a fully comprehensive analysis, but restricted to the selected portion of the chromatogram, minimizing unnecessary analysis of background or uninformative regions. [42]

Recent implementations employ multiple sampling loops, parallel modulation channels, or adaptive gating schemes to target multiple chromatographic zones with different resolution requirements or compound classes.[43]

What has been described offers several advantages, making it an appealing alternative for targeted or semi-targeted applications.[1]

It reduces solvent consumption, acquisition time, and computational load, enhancing resolving power and efficiency for the chromatographic zones that matter most, improving separation depth and sensitivity where it is most needed, while simplifying data processing.[44] At the same time, however, sLC×LC sacrifices global coverage, since regions outside the targeted zones are excluded from second-dimension analysis, unknown or undesired compounds may remain undetected. Moreover, its system introduces additional instrumental and synchronization challenges, since a precise

coordination between first-dimension elution and second-dimension is required without perturbing the ongoing first-dimension separation.[25 45]

Overall, selective comprehensive LC offers a good balance between the detailed information provided by full comprehensive LC and the practical constraints.[46] It is a powerful mD-LC tool when the analytical investigation is conducted with prior knowledge of the sample composition, which minimizes solvent consumption while maintaining high chromatographic performance.[43]

Heart-cutting (LC–LC, or multiple heart-cutting, mLC–LC)

Heart-cutting multidimensional liquid chromatography (LC–LC, or mLC–LC when multiple heart cuts are performed) is the most selective and targeted LC approach among multidimensional chromatographic methods.[43 47]

In this mode, only predefined zones, called hearts, of the first-dimension separation, typically corresponding to chromatographic regions containing critical analytes or unresolved peak clusters, are redirected to the second-dimension column for the additional grade of separation.[48]

LC-LC offers an efficient strategy to enhance selectivity, where needed, avoiding the complexity and increased data load associated with LC×LC systems.[49] This approach is convenient for confirmatory analyses, impurity profiling, and targeted investigations of specific components within moderately complex sample matrices.[50]

In a heart-cutting configuration, the first-dimension chromatographic separation proceeds under normal conditions.[43] A switching valve or array of multi-port valves (Fig.53) is programmed to direct selected retention-time windows into storage loops or directly into the second-dimension column.[51]

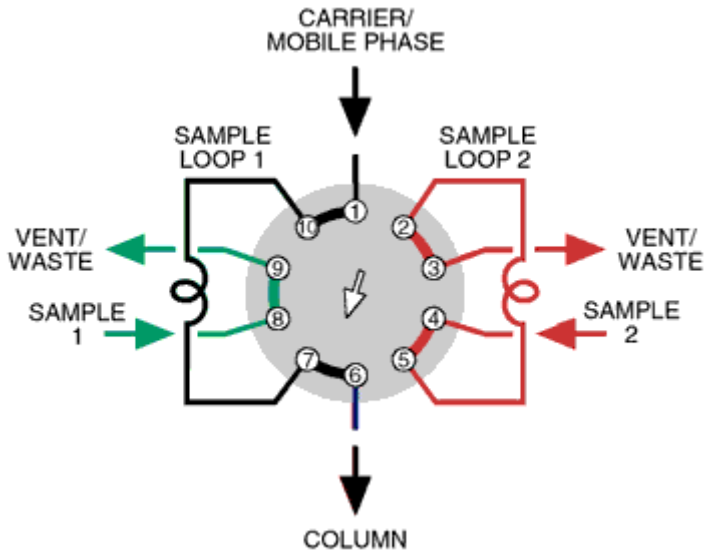

Fig.3: Example of a multi-port valve

The cuts are chosen based on prior knowledge or real-time detection and targeted zones where co-elution or analytical ambiguity is expected.[52] The second-dimension separation is then performed on each heart cut independently, with a good flexibility in run time. Each cut can thus be optimized individually, employing appropriate stationary-phase chemistry, gradient profile, or elution time to achieve maximal resolution for the target analytes.[52]

As demonstrated herein, the primary advantage of heart-cutting LC lies in its instrumental simplicity and operational flexibility. Moreover, since only selected regions of interest are subjected to secondary analysis, the approach conserves solvent, reduces analysis time, and minimizes data complexity.[53] As noted for sLC×LC, this advantage limits its comprehensiveness, and many portions of the chromatogram are not detected or evaluated. This method requires complex

accurate valve timing and synchronization to ensure that target peaks are precisely captured without sample loss or cross-contamination.[38] [52]

But despite these challenges, heart-cutting LC is a pragmatic strategy for targeted multidimensional separations, which balances the simplicity of one-dimensional LC and enhances the selectivity for the second dimension separation, making it suitable for analysis of complex samples where it is not essential to have the full chromatographic coverage.

Practical and Theoretical Considerations in Multidimensional Liquid Chromatography

In designing a functional and robust mD-LC system, it is important to note few challenges that can have an impact on the outcome and success of purification. Among these parameters second dimension kinetics (mass transfer, dispersion and peaks constraints), Inter-Dimensional Compatibility and instrument robustness, reproducibility, and calibration.

Second-Dimension Kinetics

As mentioned for LC×LC and sLC×LC, the second dimension must complete each separation in a few seconds to align with the modulation cycle of the first dimension. Thus, fast mass-transfer kinetics and minimal extra-column dispersion are essential.[54]

The column design and the stationary-phase morphology of the second-dimension separation become critical parameters for the system's peak capacity.[46] [43]

Since even microlitre-scale dispersion can severely broaden peaks at fast timescales, dead volumes in valves, loops, and tubing must be minimized. Temperature stability and precise flow control are also critical; both the composition of the mobile phase

and the steepness of the gradient are crucial to achieving rapid elution without compromising selectivity or reproducibility.[55] The achievable kinetic window is defined by balancing gradient steepness, flow rate, and particle morphology.

In practice, the kinetic performance of the second dimension serves as the bottleneck in mD-LC, and optimising it enhances both modulation feasibility and global resolution.

Inter-Dimensional Compatibility

Compatibility between the two chromatographic dimensions is essential for reproducible analyte transfer. Solvent mismatch, such as a strong 1D eluent entering a weaker 2D phase, can cause loss of retention or precipitation. [43] Active or passive modulation is often used to dilute or re-equilibrate fractions before injection into the 2D column.[56]

Differences in flow rate between dimensions are guided by switching-valve modulators or trapping interfaces, which temporarily store and then inject the sample cut at higher 2D flow rates.[46]

On-loop focusing or trapping columns are applied to re-concentrate analytes and enhance sensitivity.[57] The interface must minimize carryover, and synchronize precisely with the modulation cycle. Effective inter-dimensional design thus ensures that kinetic gains in 2D translate into real analytical resolution.

(1) Snyder, L. R.; Dolan, J. W. Milestones in the Development of Liquid Chromatography. In *Liquid Chromatography*; Elsevier, 2017; pp 1–15. https://doi.org/10.1016/B978-0-12-805393-5.00001-4.
(2) Gordon, A. H.; Martin, A. J. P.; Synge, R. L. M. A Study of the Partial Acid Hydrolysis of Some Proteins, with Special Reference to the Mode of Linkage of the Basic Amino-Acids. *Biochem. J.* **1941**, *35* (12), 1369–1387. https://doi.org/10.1042/bj0351369.
(3) Marchetto, A.; Tirapelle, M.; Mazzei, L.; Sorensen, E.; Besenhard, M. O. In Silico High-Performance Liquid Chromatography Method Development via Machine Learning. *Anal. Chem.* **2025**, *97* (13), 6991–7001. https://doi.org/10.1021/acs.analchem.4c03466.
(4) Celia Henry Arnaud,. 50 Years of HPLC. *CEN Glob. Enterp.* **2016**, *94* (24), 28–33. https://doi.org/10.1021/cen-09424-cover1.
(5) Ettre, L. S. Key Moments in the Evolution of Liquid Chromatography. *J. Chromatogr. A* **1990**, *535*, 3–12. https://doi.org/10.1016/S0021-9673(01)88931-7.
(6) Michael W. Dong. The Essence of Modern HPLC: Advantages, Limitations, Fundamentals, and Opportunities, 2013.
(7) Chatzitzika, C.; Gatt, R.; Valdramidis, V.; Mizzi, L. HPLC Analysis of Phenolic Compounds and Flavonoids with Overlapping Peaks. *Food Technol. Biotechnol.* **2020**, *58* (1), 12–19. https://doi.org/10.17113/ftb.58.01.20.6395.
(8) Sojo, L. E.; Lum, G.; Chee, P. Internal Standard Signal Suppression by Co-Eluting Analyte in Isotope Dilution LC-ESI-MS. *The Analyst* **2003**, *128* (1), 51–54. https://doi.org/10.1039/b209521c.
(9) Jandera, P.; Halama, M.; Novotná, K.; Bunčeková, S. Characterization and Comparison of HPLC Columns for Gradient Elution. *Chromatographia* **2003**, *57* (S1), S153–S161. https://doi.org/10.1007/BF02492098.
(10) R. J. Lynch, T. Blaffert, P. J. N. A Study of the Practical Limitations of Principal Components Analysis and the Labelling of Unresolved HPLC Peaks.
(11) Ira S. Krull, Anurag S. Rathore, R. K. Multidimensional Separation Techniques for Characterization of Biotherapeutics, 2020.
(12) Guiochon, G. The Limits of the Separation Power of Unidimensional Column Liquid Chromatography. *J. Chromatogr. A* **2006**, *1126* (1–2), 6–49. https://doi.org/10.1016/j.chroma.2006.07.032.
(13) Dwight R Stoll. Recent Advances in 2D-LC for Bioanalysis, 2015.
(14) Van Den Hurk, R. S.; Pursch, M.; Stoll, D. R.; Pirok, B. W. J. Recent Trends in Two-Dimensional Liquid Chromatography. *TrAC Trends Anal. Chem.* **2023**, *166*, 117166. https://doi.org/10.1016/j.trac.2023.117166.

(15) Gilar, M.; Olivova, P.; Daly, A. E.; Gebler, J. C. Orthogonality of Separation in Two-Dimensional Liquid Chromatography. *Anal. Chem.* **2005**, *77* (19), 6426–6434. https://doi.org/10.1021/ac050923i.
(16) Malerod, H.; Lundanes, E.; Greibrokk, T. Recent Advances in On-Line Multidimensional Liquid Chromatography. *Anal Methods* **2010**, *2* (2), 110–122. https://doi.org/10.1039/B9AY00194H.
(17) Michelle Camenzuli. The Role of Surface Coverage and Orthogonality Metrics in Two-Dimensional Chromatography, 2017.
(18) Epshtein, N. A. System Suitability Requirements for Liquid Chromatography Methods: Controlled Parameters and Their Recommended Values (Review). *Pharm. Chem. J.* **2020**, *54* (5), 518–525. https://doi.org/10.1007/s11094-020-02231-w.
(19) Camenzuli, M.; Schoenmakers, P. J. A New Measure of Orthogonality for Multi-Dimensional Chromatography. *Anal. Chim. Acta* **2014**, *838*, 93–101. https://doi.org/10.1016/j.aca.2014.05.048.
(20) Gilar, M.; Fridrich, J.; Schure, M. R.; Jaworski, A. Comparison of Orthogonality Estimation Methods for the Two-Dimensional Separations of Peptides. *Anal. Chem.* **2012**, *84* (20), 8722–8732. https://doi.org/10.1021/ac3020214.
(21) Davis, J. M.; Stoll, D. R.; Carr, P. W. Effect of First-Dimension Undersampling on Effective Peak Capacity in Comprehensive Two-Dimensional Separations. *Anal. Chem.* **2008**, *80* (2), 461–473. https://doi.org/10.1021/ac071504j.
(22) Petersson, P.; Frank, A.; Heaton, J.; Euerby, M. R. Maximizing Peak Capacity and Separation Speed in Liquid Chromatography. *J. Sep. Sci.* **2008**, *31* (13), 2346–2357. https://doi.org/10.1002/jssc.200800064.
(23) Stoll, D. R.; Li, X.; Wang, X.; Carr, P. W.; Porter, S. E. G.; Rutan, S. C. Fast, Comprehensive Two-Dimensional Liquid Chromatography. *J. Chromatogr. A* **2007**, *1168* (1–2), 3–43. https://doi.org/10.1016/j.chroma.2007.08.054.
(24) Li, X.; Stoll, D. R.; Carr, P. W. Equation for Peak Capacity Estimation in Two-Dimensional Liquid Chromatography. *Anal. Chem.* **2009**, *81* (2), 845–850. https://doi.org/10.1021/ac801772u.
(25) Pirok, B. W. J.; Gargano, A. F. G.; Schoenmakers, P. J. Optimizing Separations in Online Comprehensive Two-dimensional Liquid Chromatography. *J. Sep. Sci.* **2018**, *41* (1), 68–98. https://doi.org/10.1002/jssc.201700863.
(26) Stoll, D. R.; Carr, P. W. Two-Dimensional Liquid Chromatography: A State of the Art Tutorial. *Anal. Chem.* **2017**, *89* (1), 519–531. https://doi.org/10.1021/acs.analchem.6b03506.
(27) Ronald E. Majors. Multidimensional and Comprehensive Liquid Chromatography, 2005.

(28) Stoll, D. R.; Li, X.; Wang, X.; Carr, P. W.; Porter, S. E. G.; Rutan, S. C. Fast, Comprehensive Two-Dimensional Liquid Chromatography. *J. Chromatogr. A* **2007**, *1168* (1–2), 3–43. https://doi.org/10.1016/j.chroma.2007.08.054.
(29) Patrik Petersson, S. B. Dealing with Wandering First-Dimension Peaks in 2D-LC Separations, 2022.
(30) Arena, K.; Cacciola, F.; Laganà Vinci, R.; Dugo, P.; Mondello, L. Exploration of Comprehensive Two-Dimensional Liquid Chromatography: Theoretical Aspects and Practical Considerations - A Tutorial. *J. Chromatogr. Open* **2025**, *7*, 100222. https://doi.org/10.1016/j.jcoa.2025.100222.
(31) Peter Schoenmakers, B. W. J. P. Practical Approaches to Overcome the Challenges of Comprehensive Two-Dimensional Liquid Chromatography, 2018.
(32) Dsouza, B. R.; Joseph, A.; Das, S.; Alex, A. T. Multiple Heart-Cutting Two-Dimensional Liquid Chromatography: Recent Developments and Applications. *Curr. Anal. Chem.* **2021**, *17* (3), 339–354. https://doi.org/10.2174/1573411016666200630114826.
(33) Shimazu Web-site. What Is Comprehensive Two-Dimensional LC?
(34) Mondello, L.; Dugo, P.; Donato, P.; Herrero, M.; Montero, L.; Schmitz, O. J. Comprehensive Two-Dimensional Liquid Chromatography. *Nat. Rev. Methods Primer* **2023**, *3* (1), 86. https://doi.org/10.1038/s43586-023-00269-0.
(35) Dugo, P.; Cacciola, F.; Kumm, T.; Dugo, G.; Mondello, L. Comprehensive Multidimensional Liquid Chromatography: Theory and Applications. *J. Chromatogr. A* **2008**, *1184* (1–2), 353–368. https://doi.org/10.1016/j.chroma.2007.06.074.
(36) Nell, E. H. J.; Muller, M.; De Villiers, A. Advances in Online Comprehensive Two-Dimensional Liquid Chromatography Method Development. *Annu. Rev. Anal. Chem.* **2025**, *18* (1), 359–381. https://doi.org/10.1146/annurev-anchem-071524-090321.
(37) *Multidimensional Liquid Chromatography: Theory and Applications in Industrial Chemistry and the Life Sciences*, 1st ed.; Cohen, S. A., Schure, M. R., Eds.; Wiley, 2008. https://doi.org/10.1002/9780470276266.
(38) Papatheocharidou, C.; Samanidou, V. Two-Dimensional High-Performance Liquid Chromatography as a Powerful Tool for Bioanalysis: The Paradigm of Antibiotics. *Mol. Basel Switz.* **2023**, *28* (13), 5056. https://doi.org/10.3390/molecules28135056.
(39) Anthony Ehkirch, A. C. The Current Status and Future of Two- and Multidimensional Liquid Chromatography in Pharmaceutical R&D and QC, 2020.
(40) Groskreutz, S. R.; Swenson, M. M.; Secor, L. B.; Stoll, D. R. Selective Comprehensive Multi-Dimensional Separation for Resolution Enhancement in High Performance Liquid Chromatography. Part I: Principles and

Instrumentation. *J. Chromatogr. A* **2012**, *1228*, 31–40. https://doi.org/10.1016/j.chroma.2011.06.035.
(41) Lv, W.; Shi, X.; Wang, S.; Xu, G. Multidimensional Liquid Chromatography-Mass Spectrometry for Metabolomic and Lipidomic Analyses. *TrAC Trends Anal. Chem.* **2019**, *120*, 115302. https://doi.org/10.1016/j.trac.2018.11.001.
(42) Davis, J. M.; Stoll, D. R. Likelihood of Total Resolution in Liquid Chromatography: Evaluation of One-Dimensional, Comprehensive Two-Dimensional, and Selective Comprehensive Two-Dimensional Liquid Chromatography. *J. Chromatogr. A* **2014**, *1360*, 128–142. https://doi.org/10.1016/j.chroma.2014.07.066.
(43) Peter W. Carr, D. R. S. *Multi-Dimensional Liquid Chromatography: Principles, Practice, and Applications (Chromatographic Science Series)*; 2022.
(44) Groskreutz, S. R.; Swenson, M. M.; Secor, L. B.; Stoll, D. R. Selective Comprehensive Multi-Dimensional Separation for Resolution Enhancement in High Performance Liquid Chromatography. Part I: Principles and Instrumentation. *J. Chromatogr. A* **2012**, *1228*, 31–40. https://doi.org/10.1016/j.chroma.2011.06.035.
(45) Tome, T.; Žigart, N.; Časar, Z.; Obreza, A. Development and Optimization of Liquid Chromatography Analytical Methods by Using AQbD Principles: Overview and Recent Advances. *Org. Process Res. Dev.* **2019**, *23* (9), 1784–1802. https://doi.org/10.1021/acs.oprd.9b00238.
(46) Pirok, B. W. J.; Stoll, D. R.; Schoenmakers, P. J. Recent Developments in Two-Dimensional Liquid Chromatography: Fundamental Improvements for Practical Applications. *Anal. Chem.* **2019**, *91* (1), 240–263. https://doi.org/10.1021/acs.analchem.8b04841.
(47) Lv, W.; Shi, X.; Wang, S.; Xu, G. Multidimensional Liquid Chromatography-Mass Spectrometry for Metabolomic and Lipidomic Analyses. *TrAC Trends Anal. Chem.* **2019**, *120*, 115302. https://doi.org/10.1016/j.trac.2018.11.001.
(48) Naja Wessel Jacobsen, L. D. N. Two-Dimensional Liquid Chromatography (2D-LC) with Multiple Heart-Cutting, 2018.
(49) Gu, X.; Yang, L.; Tao, Q.; Ai, J.; Yan, C.; Zheng, J.; Hong, L. Application of Heart-Cutting Two-Dimensional Liquid Chromatography-Mass Spectrometry to the Characterization of Highly Polar Impurities in Calcium Gluconate Injection. *J. Chromatogr. A* **2022**, *1685*, 463632. https://doi.org/10.1016/j.chroma.2022.463632.
(50) Agilent. Confirmation of Peptide-Related Impurity Intact Mass Using Agilent 1290 Infinity II Bio 2D-LC and InfinityLab LC/MSD XT.
(51) Körmöczi, T.; Szabó, Í.; Farkas, E.; Penke, B.; Janáky, T.; Ilisz, I.; Berkecz, R. Heart-Cutting Two-Dimensional Liquid Chromatography Coupled to Quadrupole-

Orbitrap High Resolution Mass Spectrometry for Determination of N,N-Dimethyltryptamine in Rat Plasma and Brain; Method Development and Application. *J. Pharm. Biomed. Anal.* **2020**, *191*, 113615. https://doi.org/10.1016/j.jpba.2020.113615.

(52) Angsuwattana, P.; Wichitnithad, W.; Punpreuk, Y.; Halim, H.; Sritularak, B.; Thitikornpong, W.; Rojsitthisak, P. Development of a Simplified Heart-Cutting Two-Dimensional Liquid Chromatography Method for Green Analysis of Four Polyphenols in *Aerides* Plants. *ACS Sustain. Chem. Eng.* **2025**, *13* (11), 4489–4498. https://doi.org/10.1021/acssuschemeng.4c10145.

(53) Caño-Carrillo, I.; Gilbert-López, B.; Montero, L.; Martínez-Piernas, A. B.; García-Reyes, J. F.; Molina-Díaz, A. Comprehensive and Heart-cutting Multidimensional Liquid Chromatography–Mass Spectrometry and Its Applications in Food Analysis. *Mass Spectrom. Rev.* **2024**, *43* (5), 936–976. https://doi.org/10.1002/mas.21845.

(54) Comprehensive Two-Dimensional Liquid Chromatography (LCxLC): A Review, 2011.

(55) Moussa, A.; Lauer, T.; Huygens, B.; Stoll, D.; Desmet, G.; Broeckhoven, K. Modelling of Analyte Profiles and Band Broadening Generated by Interface Loops Used in Two-Dimensional Liquid Chromatography Operated in the First-In-First-Out Mode. *J. Chromatogr. A* **2025**, *1763*, 466425. https://doi.org/10.1016/j.chroma.2025.466425.

(56) Chen, Y.; Montero, L.; Luo, J.; Li, J.; Schmitz, O. J. Application of the New At-Column Dilution (ACD) Modulator for the Two-Dimensional RP×HILIC Analysis of Buddleja Davidii. *Anal. Bioanal. Chem.* **2020**, *412* (7), 1483–1495. https://doi.org/10.1007/s00216-020-02392-3.

(57) Wicht, K.; Baert, M.; Schipperges, S.; Von Doehren, N.; Desmet, G.; Van Geem, K. M.; De Villiers, A.; Lynen, F. Enhanced Sensitivity in Comprehensive Liquid Chromatography: Overcoming the Dilution Problem in LC × LC via Temperature-Responsive Liquid Chromatography. *Anal. Chem.* **2022**, *94* (48), 16728–16737. https://doi.org/10.1021/acs.analchem.2c03300.

Appendix 3 - Mass spectrometry

The advent of recombinant protein therapeutics has revolutionized medicine over the past few decades, offering highly-specific agents in oncology, autoimmune diseases, and beyond.[1] As the complexity of these biomolecules increased, particularly with the development of ADCs, in which a mAb scaffold is covalently linked to one or more small-molecule cytotoxic payloads, so too did the analytical demands for characterizing them.[2 3]

Mass spectrometry (MS) has emerged as a pivotal technology in the characterization and quality control of mAbs and ADCs.[4] The past few decades have also been fundamental for advances in mass spectrometer technology, such as ionization techniques, analyzer resolving power, mass accuracy and dynamic range.[5 6] Furthermore, because of its sensitivity, accuracy, and ability to resolve molecular heterogeneity, MS provides unparalleled insight into molecular composition, post-translational modifications (PTMs), such as glycosylation, higher-order structures, and DAR determination.[7 2]

Historical Background

Early protein characterization relied primarily on electrophoresis, isoelectric focusing, and UV-based chromatographic methods, which offered limited structural resolution.[8] The integration of MS technology into biotherapeutic analysis parallels advances in mass spectrometers' components. [9]

The introduction in the late 1980s, for example, of soft ionization techniques, such as electrospray ionization (ESI) and matrix-assisted laser desorption (MALDI), revolutionized protein analysis by enabling the transfer of large, fragile biomolecules into the gas phase without fragmentation.[10 11]

The first applications of MS to recombinant antibodies emerged in the 1990s,[12] focusing on molecular-weight confirmation and limited peptide mapping.[13] However, the true analytical revolution came with the rise of high-resolution analysers, quadrupole time-of-flight (Q-TOF),[14] Fourier transform ion cyclotron resonance (FT-ICR),[15] and Orbitrap instruments,[16] which provided the resolving power necessary to separate glycoforms, isotopic patterns, and drug-loaded species within complex biopharmaceuticals.[17] [18]

Modern MS instruments now routinely achieve mass accuracies of a few parts per million (ppm) and resolving powers exceeding 100,000.[6] Such capabilities, coupled with advanced ionisation and fragmentation techniques, have positioned MS as the central analytical tool for assessing critical quality attributes (CQAs) of mAbs and ADCs, including sequence integrity, PTMs, aggregation, and conjugation heterogeneity.[19] [20]

Structural complexity of mAbs and ADCs in mass spectrometry

Therapeutic antibodies are large glycoproteins of a molecular weight of approximately 150 kDa, composed of two identical heavy (~50 kDa) and two identical light (~25 kDa) chains stabilized by disulfide bonds.[21] These chains form a flexible Y-shaped structure where the arms contain the antigen-binding sites formed by variable regions at the amino termini of heavy and light chains. The heavy chains each contain multiple immunoglobulin domains, including constant and variable regions, while the light chains consist of two such domains. This molecular architecture allows antibodies to bind antigens with high specificity and affinity.[22]

And a key feature of therapeutic antibodies is the presence of numerous PTMs, most notably N-linked glycosylation at asparagine residues on the Fc domain (Asn297 is the most notable one). Glycosylation is critical for proper folding, enhancing stability, and modulating effector functions, such as antibody-dependent cellular cytotoxicity (ADCC) and complement activation.[23] The glycan structures attached to the antibody influence its interaction with Fc receptors and thus impact its therapeutic efficacy and safety profile.[24 25]

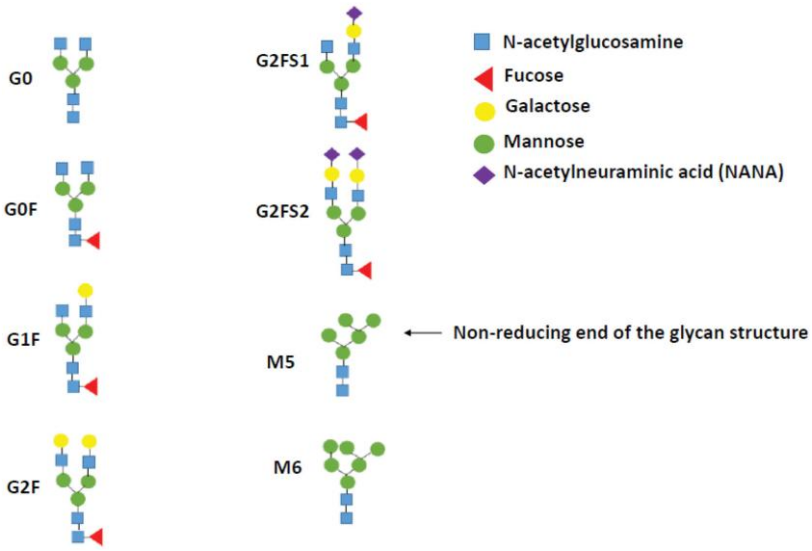

Fig.1: Chemical structure of N-glycan forms commonly found in monoclonal antibodies[26]

ADCs add another layer of complexity. Since they consist of a mAb scaffold covalently attached, via a synthetic linker, to several highly cytotoxic payloads, depending on the conjugation chemistry (lysine or cysteine linkage), each antibody may carry a variable number of drugs, producing a heterogeneous population of conjugates.[2]

For instance, cysteine-linked ADCs often display discrete DAR values of 0, 2, 4, 6, or 8,[27] whereas lysine conjugates yield broader, quasi-continuous distributions due to the presence of numerous reactive amine sites and, as a consequence, a vast number of positional isomers.

The analytical challenge is therefore twofold. Precisely quantifying the molecular heterogeneity present and accurately pinpointing or verifying the specific sites of conjugation and other modifications. To address these demands, a hierarchical mass spectrometry strategy has been developed, incorporating analyses at the top-, middle-, and bottom-levels to provide comprehensive structural and site-specific information.

Top-, Middle-, and Bottom-Level Mass Spectrometric Strategies

The true strength of modern MS lies in integrating data across the three analytical levels.

- Top-level analysis (see 7.3.1) provides rapid global assessment of mass confirmation, DAR estimation, and lot comparability.
- Middle-level analysis (see 7.3.2) dissects the molecule into manageable domains, enabling domain-specific DAR and PTM profiling.
- Bottom-level peptide mapping (see 7.3.3) provides site-specific structural confirmation.

The *multi-level structural characterization* paradigm demonstrates how integrating intact, subunit, and peptide data affords a complete view of ADC heterogeneity and structural integrity.

Such integration is now embedded in industry workflows for release testing, stability monitoring, and comparability exercises.

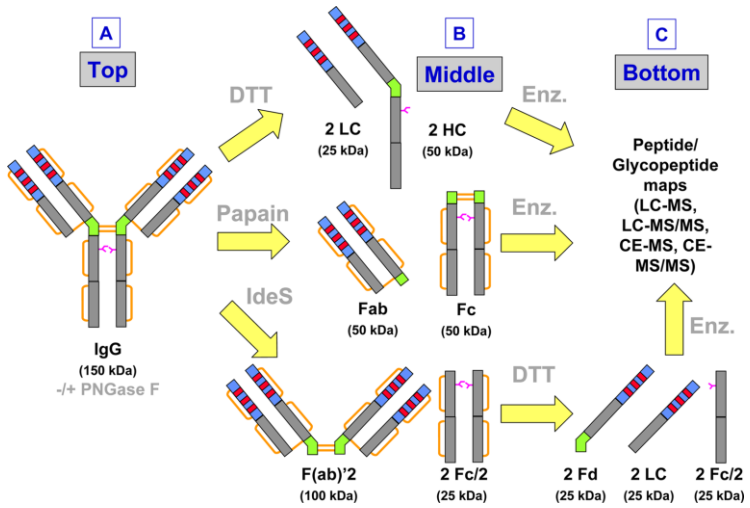

Fig.2: Antibody MS characterization flowchart: top-down, middle-down and -up, bottom-up.[28]

Top-Level Analysis

Top-down, also known as *intact-mass*, analysis involves measuring the intact mAb or ADC without prior digestion. When performed under denaturing ESI conditions, it provides fast, global information on molecular weight, glycoform composition, and overall drug loading. The deconvoluted spectrum reveals the distribution of DAR species, enabling the calculation of the average DAR and the drug distribution profile.[29] [28]

The so-called *native mass spectrometry*, is a significant refinement to this approach. The analyte is kept in near-physiological, non-denaturing buffers such as ammonium acetate. Native conditions preserve tertiary and quaternary structures, yielding lower charge states and simplified spectra.[30]

Top-level MS offers minimal sample preparation, high throughput, and accurate mass determination, making it ideal for rapid identity confirmation and batch

comparability testing.[31] Its main limitation is the lack of detailed sequence or site-specific information, due to the challenges of efficiently fragmenting such large ions. [32]

Middle-Level Analysis

Middle-level MS has become a cornerstone in the structural analysis of mAbs and ADCs.[33]

It involves enzymatic or chemical cleavage of antibodies into large, well-defined subunits, most commonly using the IdeS enzyme, which cleaves below the hinge region. Following reduction, these fragments are further separated into light chain (LC), Fd, and variable subunits, each approximately 25 kDa.[34]

This subdivision simplifies the complex antibody structure into manageable pieces, enabling detailed characterization of drug conjugation sites, micro-heterogeneity, and post-translational modifications.[35]

The *middle-down MS* approach has been demonstrated in both cysteine- and lysine-conjugated ADCs, enabling precise DAR determination, localization of conjugation sites, and monitoring of variants and glycoforms, providing a robust and complementary analytical tool widely applied in biopharmaceutical development.[33] [34]

It has been demonstrated by Botzanowski et al. in 2017, that native middle-level MS can characterize site-specific ADCs in a single run, offering a clear snapshot of molecular heterogeneity and higher-order structure.[36] While more recent studies, conducted by Wei et al. in 2024,[18] enhanced middle-down workflows by

assigning internal fragments, achieving near-complete sequence coverage and improved identification of glycosylation and conjugation sites.

The power of this approach lies in bridging the gap between native MS and peptide-level analysis, providing a balanced view of both global and local structure.

Bottom-Level Analysis

Bottom-up MS, also called peptide-mapping, remains the ultimate approach for sequence verification and site-specific PTM or conjugation identification.[37] [38] Proteolytic digestion, typically with trypsin or Lys-C, followed by LC–MS/MS enables amino-acid-level resolution.[39]

This method has long been the regulatory benchmark for confirming the identity of therapeutic antibodies and mapping conjugation sites in ADCs.[40]

Bottom-up analysis achieves the highest structural detail, but it introduces additional sample preparation steps that can generate artefactual modifications or peptide losses.[41] Furthermore, it sacrifices information on the intact molecular context, which can be critical for assessing overall product heterogeneity.[42] [43]

Consequently, bottom-up workflows are increasingly complemented by intact and subunit analyses to form comprehensive multi-level MS strategies.

LC–MS Coupling and Impact on Manufacturing Control

The coupling of liquid chromatography with mass spectrometry (LC–MS) has profoundly transformed biopharmaceutical analytics, marking one of the crucial technological advances that has enabled MS to transition from the research laboratory to routine industrial use.[44] [45]

LC pre-separation overcomes many of the practical limitations of direct infusion, such as sample salt concentration, ion suppression, and sample complexity, thereby enhancing MS performance.[46]

In particular, in biotherapeutics analysis, chromatographic purification helps separate major proteoforms that differ in glycosylation, charge variants, or payload number, thereby simplifying mass spectra and improving deconvolution accuracy.[47] Moreover, LC-MS workflows offer superior reproducibility and automation, two key features for regulated environments that require consistency and traceability.[48]

The robustness and informational depth of LC–MS data have led to its increasing acceptance by regulatory agencies, including the FDA and EMA, increasingly endorse analytical strategies aligned with Quality by Design (QbD) and Process Analytical Technology (PAT) principles, as primary characterization method for biotherapeutics. In this context, LC–MS has become a powerful in-process monitoring tool, providing near-real-time feedback during manufacturing. For example, LC–MS can detect shifts in glycosylation patterns, aggregation levels, or drug-loading distributions immediately after purification or conjugation steps.[49] When integrated with manufacturing control systems, LC–MS data help establish process fingerprints that ensure product consistency across batches. In the case of ADCs, continuous monitoring of DAR and payload distribution can

reveal subtle drifts in conjugation efficiency or linker stability, allowing for rapid corrective action.[50]

(1) Sharma, P.; Joshi, R. V.; Pritchard, R.; Xu, K.; Eicher, M. A. Therapeutic Antibodies in Medicine. *Molecules* **2023**, *28* (18), 6438. https://doi.org/10.3390/molecules28186438.
(2) Huang, R. Y.-C.; Chen, G. Characterization of Antibody–Drug Conjugates by Mass Spectrometry: Advances and Future Trends. *Drug Discov. Today* **2016**, *21* (5), 850–855. https://doi.org/10.1016/j.drudis.2016.04.004.
(3) Wagh, A.; Song, H.; Zeng, M.; Tao, L.; Das, T. K. Challenges and New Frontiers in Analytical Characterization of Antibody-Drug Conjugates. *mAbs* **2018**, *10* (2), 222–243. https://doi.org/10.1080/19420862.2017.1412025.
(4) Aaron O. Bailey; Kyle D'Silva; Rowan E. Moore; Eric Niederkofler; Michael W. Dong; Ken Cook, Jonathan Bones, Kelly Broster. Perspectives and Characterization on Antibody–Drug Conjugates, 2018.
(5) Jerome Workman Jr. Advancements and Emerging Techniques in Mass Spectrometry: A Comprehensive Review, 2024.
(6) Deschamps, E.; Calabrese, V.; Schmitz, I.; Hubert-Roux, M.; Castagnos, D.; Afonso, C. Advances in Ultra-High-Resolution Mass Spectrometry for Pharmaceutical Analysis. *Molecules* **2023**, *28* (5), 2061. https://doi.org/10.3390/molecules28052061.
(7) Debaene, F.; Bœuf, A.; Wagner-Rousset, E.; Colas, O.; Ayoub, D.; Corvaïa, N.; Van Dorsselaer, A.; Beck, A.; Cianférani, S. Innovative Native MS Methodologies for Antibody Drug Conjugate Characterization: High Resolution Native MS and IM-MS for Average DAR and DAR Distribution Assessment. *Anal. Chem.* **2014**, *86* (21), 10674–10683. https://doi.org/10.1021/ac502593n.
(8) Creamer, J. S.; Oborny, N. J.; Lunte, S. M. Recent Advances in the Analysis of Therapeutic Proteins by Capillary and Microchip Electrophoresis. *Anal Methods* **2014**, *6* (15), 5427–5449. https://doi.org/10.1039/C4AY00447G.
(9) Tank, P.; Vora, S.; D'Souza, F.; Kamble, S. S.; Rameshkumar, N. Advanced Mass Spectrometry Techniques for Monitoring Biopharmaceutical Host Cell Proteins. *Trends Biotechnol.* **2025**, S0167779925003117. https://doi.org/10.1016/j.tibtech.2025.07.026.
(10) Zaikin, V. G.; Borisov, R. S. Options of the Main Derivatization Approaches for Analytical ESI and MALDI Mass Spectrometry. *Crit. Rev. Anal. Chem.* **2022**, *52* (6), 1287–1342. https://doi.org/10.1080/10408347.2021.1873100.
(11) *Advances in MALDI and Laser-Induced Soft Ionization Mass Spectrometry*; Cramer, R., Ed.; Springer International Publishing: Cham, 2016. https://doi.org/10.1007/978-3-319-04819-2.

(12) James H. Bourell, Karl P. Clauser, Robert Kelley, Paul Carter, John T. Sturts. Electrospray Ionization Mass Spectrometry of Recombinantly Engineered Antibody Fragments, 1994.
(13) Shevchenko, A.; Wilm, M.; Vorm, O.; Mann, M. Mass Spectrometric Sequencing of Proteins from Silver-Stained Polyacrylamide Gels. *Anal. Chem.* **1996**, *68* (5), 850–858. https://doi.org/10.1021/ac950914h.
(14) Van Den Heuvel, R. H. H.; Van Duijn, E.; Mazon, H.; Synowsky, S. A.; Lorenzen, K.; Versluis, C.; Brouns, S. J. J.; Langridge, D.; Van Der Oost, J.; Hoyes, J.; Heck, A. J. R. Improving the Performance of a Quadrupole Time-of-Flight Instrument for Macromolecular Mass Spectrometry. *Anal. Chem.* **2006**, *78* (21), 7473–7483. https://doi.org/10.1021/ac061039a.
(15) Nikolaev, E. N.; Kostyukevich, Y. I.; Vladimirov, G. N. Fourier Transform Ion Cyclotron Resonance (FT ICR) Mass Spectrometry: Theory and Simulations. *Mass Spectrom. Rev.* **2016**, *35* (2), 219–258. https://doi.org/10.1002/mas.21422.
(16) Perry, R. H.; Cooks, R. G.; Noll, R. J. Orbitrap Mass Spectrometry: Instrumentation, Ion Motion and Applications. *Mass Spectrom. Rev.* **2008**, *27* (6), 661–699. https://doi.org/10.1002/mas.20186.
(17) Campuzano, I. D. G.; Netirojjanakul, C.; Nshanian, M.; Lippens, J. L.; Kilgour, D. P. A.; Van Orden, S.; Loo, J. A. Native-MS Analysis of Monoclonal Antibody Conjugates by Fourier Transform Ion Cyclotron Resonance Mass Spectrometry. *Anal. Chem.* **2018**, *90* (1), 745–751. https://doi.org/10.1021/acs.analchem.7b03021.
(18) Wei, B.; Lantz, C.; Ogorzalek Loo, R. R.; Campuzano, I. D. G.; Loo, J. A. Internal Fragments Enhance Middle-Down Mass Spectrometry Structural Characterization of Monoclonal Antibodies and Antibody-Drug Conjugates. *Anal. Chem.* **2024**, *96* (6), 2491–2499. https://doi.org/10.1021/acs.analchem.3c04526.
(19) Beck, A.; Terral, G.; Debaene, F.; Wagner-Rousset, E.; Marcoux, J.; Janin-Bussat, M.-C.; Colas, O.; Dorsselaer, A. V.; Cianférani, S. Cutting-Edge Mass Spectrometry Methods for the Multi-Level Structural Characterization of Antibody-Drug Conjugates. *Expert Rev. Proteomics* **2016**, *13* (2), 157–183. https://doi.org/10.1586/14789450.2016.1132167.
(20) Botzanowski, T.; Erb, S.; Hernandez-Alba, O.; Ehkirch, A.; Colas, O.; Wagner-Rousset, E.; Rabuka, D.; Beck, A.; Drake, P. M.; Cianférani, S. Insights from Native Mass Spectrometry Approaches for Top- and Middle-Level Characterization of Site-Specific Antibody-Drug Conjugates. *mAbs* **2017**, *9* (5), 801–811. https://doi.org/10.1080/19420862.2017.1316914.

(21) Davis, J. D.; Deng, R.; Boswell, C. A.; Zhang, Y.; Li, J.; Fielder, P.; Joshi, A.; Kenkare-Mitra, S. Monoclonal Antibodies: From Structure to Therapeutic Application. In *Pharmaceutical Biotechnology*; Crommelin, D. J. A., Sindelar, R. D., Meibohm, B., Eds.; Springer New York: New York, NY, 2013; pp 143–178. https://doi.org/10.1007/978-1-4614-6486-0_7.
(22) Chiu, M. L.; Goulet, D. R.; Teplyakov, A.; Gilliland, G. L. Antibody Structure and Function: The Basis for Engineering Therapeutics. *Antibodies Basel Switz.* **2019**, *8* (4), 55. https://doi.org/10.3390/antib8040055.
(23) *Immunobiology 5: The Immune System in Health and Disease*, 5th ed.; Janeway, C., Ed.; Garland Pub: New York, 2001.
(24) Jefferis, R. Isotype and Glycoform Selection for Antibody Therapeutics. *Arch. Biochem. Biophys.* **2012**, *526* (2), 159–166. https://doi.org/10.1016/j.abb.2012.03.021.
(25) Sha, S.; Agarabi, C.; Brorson, K.; Lee, D.-Y.; Yoon, S. N-Glycosylation Design and Control of Therapeutic Monoclonal Antibodies. *Trends Biotechnol.* **2016**, *34* (10), 835–846. https://doi.org/10.1016/j.tibtech.2016.02.013.
(26) Kaur, H. Characterization of Glycosylation in Monoclonal Antibodies and Its Importance in Therapeutic Antibody Development. *Crit. Rev. Biotechnol.* **2021**, *41* (2), 300–315. https://doi.org/10.1080/07388551.2020.1869684.
(27) Birdsall, R. E.; Shion, H.; Kotch, F. W.; Xu, A.; Porter, T. J.; Chen, W. A Rapid On-Line Method for Mass Spectrometric Confirmation of a Cysteine-Conjugated Antibody-Drug-Conjugate Structure Using Multidimensional Chromatography. *mAbs* **2015**, *7* (6), 1036–1044. https://doi.org/10.1080/19420862.2015.1083665.
(28) Beck, A.; Wagner-Rousset, E.; Ayoub, D.; Van Dorsselaer, A.; Sanglier-Cianférani, S. Characterization of Therapeutic Antibodies and Related Products. *Anal. Chem.* **2013**, *85* (2), 715–736. https://doi.org/10.1021/ac3032355.
(29) Anurag S. Rathore, J. A. Intact Mass Analysis of Biopharmaceuticals as Its Own Unique Application, 2021.
(30) Tamara, S.; Den Boer, M. A.; Heck, A. J. R. High-Resolution Native Mass Spectrometry. *Chem. Rev.* **2022**, *122* (8), 7269–7326. https://doi.org/10.1021/acs.chemrev.1c00212.
(31) Donnelly, D. P.; Rawlins, C. M.; DeHart, C. J.; Fornelli, L.; Schachner, L. F.; Lin, Z.; Lippens, J. L.; Aluri, K. C.; Sarin, R.; Chen, B.; Lantz, C.; Jung, W.; Johnson, K. R.; Koller, A.; Wolff, J. J.; Campuzano, I. D. G.; Auclair, J. R.; Ivanov, A. R.; Whitelegge, J. P.; Paša-Tolić, L.; Chamot-Rooke, J.; Danis, P. O.; Smith, L. M.; Tsybin, Y. O.; Loo, J. A.; Ge, Y.; Kelleher, N. L.; Agar, J. N. Best Practices and Benchmarks for Intact Protein Analysis for Top-down Mass

Spectrometry. *Nat. Methods* **2019**, *16* (7), 587–594. https://doi.org/10.1038/s41592-019-0457-0.
(32) He, L.; Weisbrod, C. R.; Marshall, A. G. Protein de Novo Sequencing by Top-down and Middle-down MS/MS: Limitations Imposed by Mass Measurement Accuracy and Gaps in Sequence Coverage. *Int. J. Mass Spectrom.* **2018**, *427*, 107–113. https://doi.org/10.1016/j.ijms.2017.11.012.
(33) Chen, B.; Lin, Z.; Zhu, Y.; Jin, Y.; Larson, E.; Xu, Q.; Fu, C.; Zhang, Z.; Zhang, Q.; Pritts, W. A.; Ge, Y. Middle-Down Multi-Attribute Analysis of Antibody-Drug Conjugates with Electron Transfer Dissociation. *Anal. Chem.* **2019**, *91* (18), 11661–11669. https://doi.org/10.1021/acs.analchem.9b02194.
(34) Watts, E.; Williams, J. D.; Miesbauer, L. J.; Bruncko, M.; Brodbelt, J. S. Correction to Comprehensive Middle-Down Mass Spectrometry Characterization of an Antibody–Drug Conjugate by Combined Ion Activation Methods. *Anal. Chem.* **2020**, *92* (17), 12097–12097. https://doi.org/10.1021/acs.analchem.0c03265.
(35) Middle-down Mass Spectrometry: An Interview with Roxana McCloskey, 2023.
(36) Botzanowski, T.; Erb, S.; Hernandez-Alba, O.; Ehkirch, A.; Colas, O.; Wagner-Rousset, E.; Rabuka, D.; Beck, A.; Drake, P. M.; Cianférani, S. Insights from Native Mass Spectrometry Approaches for Top- and Middle-Level Characterization of Site-Specific Antibody-Drug Conjugates. *mAbs* **2017**, *9* (5), 801–811. https://doi.org/10.1080/19420862.2017.1316914.
(37) Introduction to Peptide Mapping.
(38) Moradian, A.; Kalli, A.; Sweredoski, M. J.; Hess, S. The Top-down, Middle-down, and Bottom-up Mass Spectrometry Approaches for Characterization of Histone Variants and Their Post-translational Modifications. *PROTEOMICS* **2014**, *14* (4–5), 489–497. https://doi.org/10.1002/pmic.201300256.
(39) Chait, B. T. Mass Spectrometry: Bottom-Up or Top-Down? *Science* **2006**, *314* (5796), 65–66. https://doi.org/10.1126/science.1133987.
(40) Kelleher, N. L.; Lin, H. Y.; Valaskovic, G. A.; Aaserud, D. J.; Fridriksson, E. K.; McLafferty, F. W. Top Down versus Bottom Up Protein Characterization by Tandem High-Resolution Mass Spectrometry. *J. Am. Chem. Soc.* **1999**, *121* (4), 806–812. https://doi.org/10.1021/ja973655h.
(41) Varnavides, G.; Madern, M.; Anrather, D.; Hartl, N.; Reiter, W.; Hartl, M. In Search of a Universal Method: A Comparative Survey of Bottom-Up Proteomics Sample Preparation Methods. *J. Proteome Res.* **2022**, *21* (10), 2397–2411. https://doi.org/10.1021/acs.jproteome.2c00265.

(42) Wither, M. J.; Hansen, K. C.; Reisz, J. A. Mass Spectrometry-Based Bottom-Up Proteomics: Sample Preparation, LC-MS/MS Analysis, and Database Query Strategies. *Curr. Protoc. Protein Sci.* **2016**, *86* (1). https://doi.org/10.1002/cpps.18.
(43) Jiang, Y.; Rex, D. A. B.; Schuster, D.; Neely, B. A.; Rosano, G. L.; Volkmar, N.; Momenzadeh, A.; Peters-Clarke, T. M.; Egbert, S. B.; Kreimer, S.; Doud, E. H.; Crook, O. M.; Yadav, A. K.; Vanuopadath, M.; Hegeman, A. D.; Mayta, M. L.; Duboff, A. G.; Riley, N. M.; Moritz, R. L.; Meyer, J. G. Comprehensive Overview of Bottom-Up Proteomics Using Mass Spectrometry. *ACS Meas. Sci. Au* **2024**, *4* (4), 338–417. https://doi.org/10.1021/acsmeasuresciau.3c00068.
(44) Van Dongen, W. D.; Niessen, W. M. Lc–Ms Systems For Quantitative Bioanalysis. *Bioanalysis* **2012**, *4* (19), 2391–2399. https://doi.org/10.4155/bio.12.221.
(45) *LC-MS in Drug Bioanalysis*; Xu, Q. A., Madden, T. L., Eds.; Springer US: Boston, MA, 2012. https://doi.org/10.1007/978-1-4614-3828-1.
(46) Metz, T. O.; Zhang, Q.; Page, J. S.; Shen, Y.; Callister, S. J.; Jacobs, J. M.; Smith, R. D. The Future of Liquid Chromatography-Mass Spectrometry (LC-MS) in Metabolic Profiling and Metabolomic Studies for Biomarker Discovery. *Biomark. Med.* **2007**, *1* (1), 159–185. https://doi.org/10.2217/17520363.1.1.159.
(47) Matthew Lauber, S. F., Mateusz Imiołek. Advantages of Sequential or Bracketed Injection Methods to Improve the Chromatographic Analysis of Biotherapeutics, 2024.
(48) Shen, X.; Yan, H.; Wang, C.; Gao, P.; Johnson, C. H.; Snyder, M. P. TidyMass an Object-Oriented Reproducible Analysis Framework for LC-MS Data. *Nat. Commun.* **2022**, *13* (1), 4365. https://doi.org/10.1038/s41467-022-32155-w.
(49) Optimizing ADC Bioassays: LC-MS/MS Blends Speed with Cost-Effectiveness, 2024.
(50) What Is Process Analytical Technology?-Featured PAT Categories and Resources.

Appendix 4 - Q Exactive™ Plus Orbitrap mass spectrometer

Given these advantages, MS-based analysis was initiated in this research as a complementary characterization method to chromatography.

As a first step, it was necessary to establish a robust reference method for the unmodified monoclonal antibody, serving as the analytical baseline for subsequent conjugate comparisons.

The instrument chosen for this type of investigation was the Q Exactive™ Plus Orbitrap mass spectrometer by Thermo Fisher Scientific. (Fig.1)

Fig.1: Q Exactive™ Plus Orbitrap mass spectrometer (Thermo Fisher Scientific)

This MS spectrometer is a a hybrid high-resolution, accurate-mass instrument combining a quadrupole mass filter, a C-trap, a higher-energy collisional dissociation (HCD) cell, and an Orbitrap electrostatic mass analyzer. A scheme of the instrument layout and ion path is shown in Fig.2.

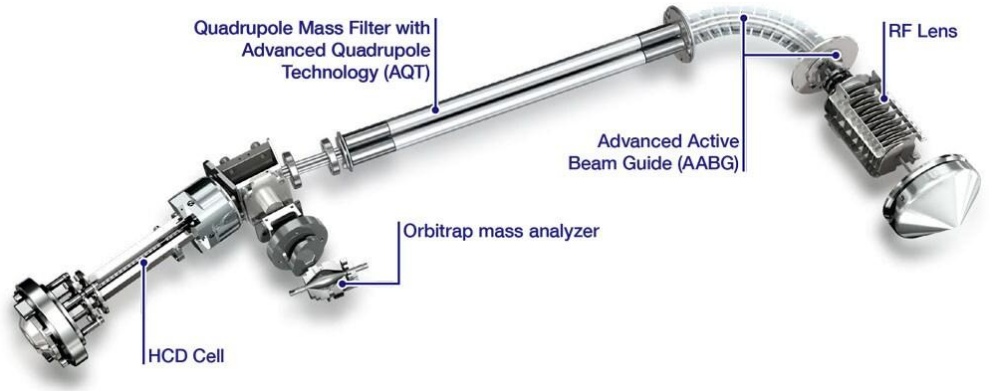

Fig.2: Schematic representation of ion generation and transmission in the Q Exactive™ Plus Orbitrap mass spectrometer, showing the ESI source, RF Lens, Advanced active beam guide, quadrupole, C-trap, HCD cell, and Orbitrap analyzer.

- 7.2.1.1 Ion Generation

In this system, ions are produced by electrospray ionization (ESI), which gently transfers molecules from solution into the gas phase. A high potential (typically 3–5 kV) applied between the emitter and the inlet forms a Taylor cone at the capillary tip, from which charged microdroplets are emitted. Assisted by a heated gas, the solvent evaporates, and the droplets undergo Coulomb fission, producing smaller droplets until gas-phase ions are released.[1 2]

ESI generates multiply charged ions, reducing the m/z of large biomolecules such as mAbs and ADCs, thereby bringing them within the Orbitrap's detection range.[2]

- 7.2.1.2 Ion Transfer and Focusing

The desolvated ions enter the instrument through a heated transfer capillary and pass into a series of RF ion guides. It improves transmission efficiency, particularly for high-m/z species, while maintaining a pressure gradient between

the atmospheric interface and high-vacuum regions. These ion-optical elements ensure optimal beam collimation and minimize ion losses.[3]

- 7.2.1.3 Quadrupole Mass Filter

After focusing, ions enter the quadrupole mass filter, composed of four parallel rods carrying oscillating RF and DC voltages. Only ions of specific m/z values experience stable trajectories and pass through the quadrupole; all others are filtered out. In full-scan mode, the quadrupole sequentially transmits a broad m/z range, whereas in MS/MS mode, it isolates precursor ions for fragmentation.[4]

- 7.2.1.4 C-Trap and HCD Cell

Selected ions are accumulated in the C-trap, which momentarily stores and focuses them before injection into the Orbitrap analyzer.[5] For fragmentation experiments, ions are directed into the adjacent HCD cell, where they collide with nitrogen gas under controlled energy to produce product ions. These fragments are then re-collected in the C-trap for analysis, enabling structural elucidation and peptide or subunit sequencing.

- 7.2.1.5 Orbitrap Analyzer

Ions are injected tangentially into the Orbitrap. This analyzer is a coaxial electrostatic trap consisting of a spindle-shaped central electrode and a surrounding outer electrode. They orbit around the central electrode while oscillating axially along its length. The frequency of these axial oscillations depends solely on the ions' m/z ratio. The Orbitrap provides sub-ppm mass accuracy and resolving power exceeding 100 000 FWHM at m/z 200, enabling high-confidence identification of glycoforms, conjugation states, and post-translational modifications in complex biotherapeutics.

(1) Oss, M.; Kruve, A.; Herodes, K.; Leito, I. Electrospray Ionization Efficiency Scale of Organic Compounds. *Anal. Chem.* **2010**, *82* (7), 2865–2872. https://doi.org/10.1021/ac902856t.
(2) Awad, H.; Khamis, M. M.; El-Aneed, A. Mass Spectrometry, Review of the Basics: Ionization. *Appl. Spectrosc. Rev.* **2015**, *50* (2), 158–175. https://doi.org/10.1080/05704928.2014.954046.
(3) Tolmachev, A. V.; Vilkov, A. N.; Bogdanov, B.; PĂsa-Tolić, L.; Masselon, C. D.; Smith, R. D. Collisional Activation of Ions in RF Ion Traps and Ion Guides: The Effective Ion Temperature Treatment. *J. Am. Soc. Mass Spectrom.* **2004**, *15* (11), 1616–1628. https://doi.org/10.1016/j.jasms.2004.07.014.
(4) M. Bonner Denton, P. E. M. The Quadrupole Mass Filter: Basic Operating Concepts, 1986.
(5) Olsen, J. V.; De Godoy, L. M. F.; Li, G.; Macek, B.; Mortensen, P.; Pesch, R.; Makarov, A.; Lange, O.; Horning, S.; Mann, M. Parts per Million Mass Accuracy on an Orbitrap Mass Spectrometer via Lock Mass Injection into a C-Trap. *Mol. Cell. Proteomics* **2005**, *4* (12), 2010–2021. https://doi.org/10.1074/mcp.T500030-MCP200.
(6) Singh, C.; Zampronio, C. G.; Creese, A. J.; Cooper, H. J. Higher Energy Collision Dissociation (HCD) Product Ion-Triggered Electron Transfer Dissociation (ETD) Mass Spectrometry for the Analysis of *N* -Linked Glycoproteins. *J. Proteome Res.* **2012**, *11* (9), 4517–4525. https://doi.org/10.1021/pr300257c.

Part 2

1. Introduction

1.1 Background

Type 2 Diabetes Mellitus (T2DM) represents one of the major global health burdens, characterized by a combination of peripheral insulin resistance, progressive pancreatic β-cell dysfunction, and chronic hyperglycemia.[95,96,97]

T2DM develops through complex interactions between genetic predisposition, lifestyle factors, and metabolic stress, leading to impaired glucose homeostasis[98] and it is closely associated with obesity and cardiovascular risk, representing one of the leading causes of morbidity and mortality worldwide.[99] [100]

According to *The Lancet Global Burden of Disease (GBD)* analysis in 2023, [101] more than 529 million adults were living with diabetes in 2021, corresponding to approximately 10.5 % of the world's adult population. The International Diabetes Federation (IDF) projects this figure to rise to 853 million by 2050, driven primarily by aging populations, urbanization, dietary transitions, and sedentary lifestyles. [102]

These data underscore the urgent need for early biomarkers and preventive interventions for this metabolic dysregulation that could lead to vascular damage and organ failure.

Therefore, understanding and detecting the molecular signatures of these processes are essential for both early diagnosis and the development of precision therapies.

1.2 Protein Glycation and Advanced Glycation End Products (AGEs) in diabetes

Glycation is a non-enzymatic post-translational modification in which reducing sugars, typically glucose, react with the amino groups of proteins, such as the side chains of lysine, arginine, or the N-terminal amino group. This reaction, known as the Maillard reaction, produces early glycation intermediates (Schiff bases and Amadori products), which further evolve into stable Advanced Glycation End Products (AGEs).(Scheme1)[103,104]

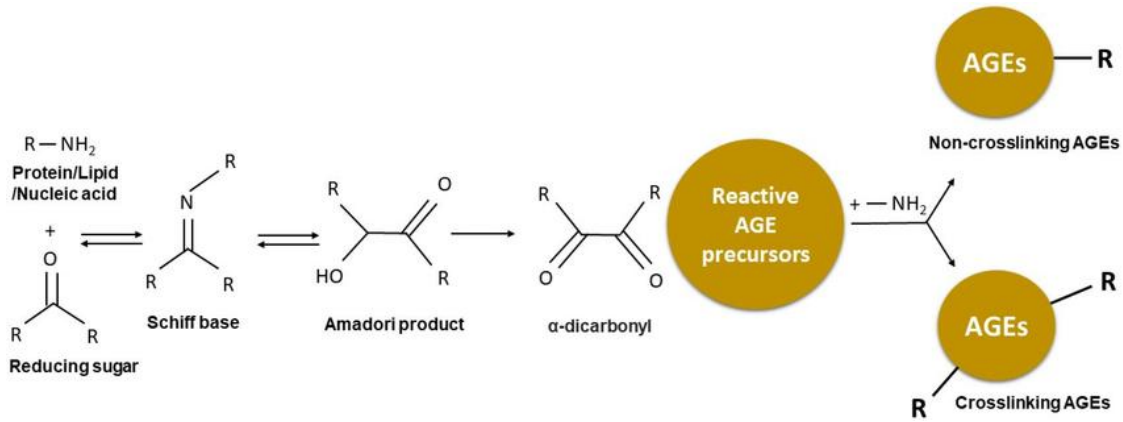

Scheme1: of Maillard reaction and Advanced Glycation Endproducts (AGEs) formation.[105]

AGEs accumulate naturally with age and are markedly increased under hyperglycemic conditions, leading to structural and functional changes in proteins.[106] [107] These alterations contribute to vascular stiffening, inflammation, and oxidative stress, all of which play central roles in diabetic complications, cardiovascular disease, and neurodegenerative disorders.[108]

From a molecular-recognition perspective, glycated peptides and AGEs introduce novel chemical epitopes, such as carboxymethyl-lysine, pentosidine,

and hydroimidazolone, which can be selectively recognized by specific antibodies or by AGE-binding receptors (RAGE).[109] [110] These recognition events are exploited both analytically, in the development of immunoassays and spectroscopic detection methods, and biologically, in the mediation of inflammation, oxidative stress, and endothelial dysfunction.[111]

The degree and pattern of protein glycation provide a molecular fingerprint of metabolic imbalance, serving as an integrative biomarker of diseases. Glycated peptides serve as biomarkers for metabolic, cardiovascular, renal, neurodegenerative, and inflammatory diseases in which chronic hyperglycemia and oxidative stress drive pathological protein modification.[112,113,114]

The recognition of AGEs is pivotal for elucidating diabetic pathology and also for advancing precision medicine, where molecular recognition guides both diagnosis and treatment.

1.2.1 Glycated peptides as biomarkers for diabetes

The pathophysiological connection between glycated peptides, AGEs, and T2DM is easy to understand.[115] It arises from the persistent exposure of biomolecules to elevated glucose concentrations and the nature of reactions collectively known as glycation. [116,117]

Glycated peptides satisfy the definition of markers, as measurable molecular indicators of physiological or pathological processes.[100] Their presence reflects integrated glycemic exposure and oxidative stress.[103]

Unlike total protein glycation, which provides bulk averages, peptide-level glycation mapping reveals specific reaction hotspots and their structural

environments. These peptides can therefore serve as molecular reporters of hyperglycemic states and disease progression.[118]

Among plasma proteins, human serum albumin (HSA) is a major target for non-enzymatic glycation due to its abundance and circulatory long half-life (~ 20 days). Furthermore, HSA represents an appealing early biomarker of glycemic status, since both the degree and site-specific pattern of its glycation undergo rapid alterations in response to short-term fluctuations in blood glucose levels, thereby providing a kinetic window of approximately 1–3 weeks that is distinct from that of HbA1c. [119,120,121]

Hemoglobin A1c (HbA1c) is formed by non-enzymatic glycation of the N-terminal valine of the hemoglobin β-chain and reflects mean glycemic exposure over the preceding 8–12 weeks, corresponding to the lifespan of erythrocytes, and is the standard biomarker for diabetes diagnosis and long-term monitoring, measured using highly standardized chromatographic, immunochemical, or enzymatic assays. However, its erythrocyte-dependent and time-averaged nature limits sensitivity to short-term glycemic fluctuations and renders it susceptible to red-cell turnover, motivating the exploration of albumin- and peptide-based glycation markers with shorter kinetic windows.[122, 123, 124]

Systematic reviews and meta-analyses conclude that glycated albumin shows good diagnostic accuracy for diabetes and prediabetes, with proposed decision thresholds in the ~15–18% range and performance complementary to HbA1c, particularly when red-cell turnover or renal disease confound HbA1c.[125,126,127]

At the molecular level, proteomic surveys and targeted LC–MS/MS assays have identified signature glycated HSA peptides whose abundances differ in early T2DM and correlate with glycemic indices, supporting their value as early-stage

biomarkers and as analytically robust readouts for short-term glycemic dynamics.[128,129]

Collectively, these data position glycated albumin, both as a bulk parameter and at the site-specific peptide level, as a sensitive reporter of recent hyperglycemia and an informative complement to HbA1c for early detection, risk stratification, and monitoring in T2DM.

1.3 Analytical techniques to identify and characterize glycation

The structural heterogeneity of glycation as a post-translational modification, combined with the wide variability in the physicochemical properties of the resulting adducts, poses a major analytical challenge for their detection and quantification. The products of non-enzymatic glycation encompass a chemically diverse ensemble, from early Schiff bases and Amadori compounds to AGEs, that differ in molecular weight, polarity, stability, and fluorescence. Consequently, no single analytical approach can comprehensively capture the full spectrum of these species.[130,118]

Over the past decades, a broad array of analytical methodologies has been developed to investigate glycation, spanning classical spectroscopic assays, chromatographic separations, and mass-spectrometric techniques, each offering distinct advantages and limitations.[131] Spectrophotometric and fluorimetric assays, while rapid and inexpensive, provide only bulk estimates of total glycation and lack molecular specificity. [132]

Chromatographic methods, particularly high-performance liquid chromatography (HPLC) and boronate-affinity chromatography (BAC), allow partial resolution of glycated from non-glycated proteins or peptides by

exploiting changes in polarity or the reversible covalent interaction between boronic acids and cis-diols. [133,134]

1.3.1 Fluorescence Spectroscopy

One of the earliest and most widely applied techniques exploits the intrinsic fluorescence of certain AGEs. Many fluorogenic AGEs, such as pentosidine and cross-linked imidazolines, absorb at 370 nm and emit around 440–460 nm,[135] providing a convenient and non-destructive mode of estimation.[136,137]

Fluorescence spectroscopy is particularly suited for quantification of AGE in serum, plasma, or tissue extracts. Moreover, in the past few decades, a non-invasive optical technique, has been developed for *in vivo* quantification of tissue AGEs, showing strong correlations with long-term glycemic exposure and vascular risk in patients with T2DM.[138]

This method lacks chemical specificity therefore fluorescence measurements are most informative when complemented by structurally selective assays.

1.3.2 Boronate affinity chromatography

Boronate affinity chromatography employs the reversible covalent interaction between boronic acid functional groups and cis-diol compounds, including carbohydrates, nucleosides, and glycoproteins.[139]

The underlying chemical mechanism of boronic sugar-binding ability is fundamentally related to its structural properties and acid-base behavior. Boronic acid exhibits Lewis acid characteristics due to its unbound boron center, which possesses an sp^2 hybridization with a vacant p orbital oriented perpendicular to the molecular plane. This orbital can accept electron pairs from Lewis bases, forming coordinative covalent bonds.[140]

In aqueous solution, when the ambient pH is equal to or exceeds the boronic acid's pK_a (typically around 8–9), the molecule interacts with hydroxide ions, altering its hybridization from sp^2 to sp^3 and generating a tetragonal boronated anion. This shift from a trigonal planar to a tetrahedral geometry significantly impacts its reactivity. The boronated anion actively forms reversible ester linkages with cis-diols, resulting in either five- or six-membered cyclic boronated esters depending on the spatial arrangement of the diol's hydroxyl groups.[141]

This acid-base equilibrium underpins the functionality of boronic acid complexes (BAC). Under mildly alkaline conditions, boronate-diol complexation is thermodynamically favored, enabling selective adsorption processes. Conversely, decreasing the pH below the boronic acid's pK_a leads to dissociation of the boronic acid-cis-diol complex as the boronic acid reverts to its neutral, trigonal planar sp^2 configuration. This pH-dependent reversible binding provides an effective switch for controlled adsorption and desorption based on environmental pH changes.[142]

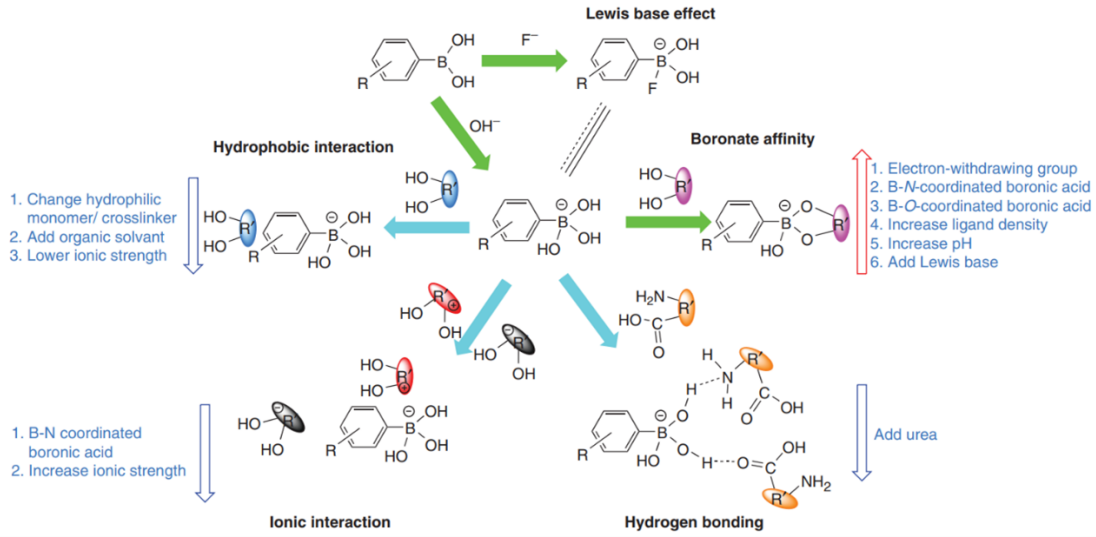

Scheme2: Selective control and factors influencing the performance of BAC are depicted. Green arrows indicate favorable interactions, whereas light blue arrows represent unfavorable ones. A red upward arrow signifies that the interaction can be enhanced by the specified factors, while blue arrows indicate that the interaction can be inhibited by the factors mentioned.[143]

A key aspect of the BAM-sugar interaction is the stereochemistry of the diol. Sugars with syn-periplanar hydroxyl pairs, such as those present in the furanose form of D-fructose, form stronger complexes than those with anti-periplanar arrangements, such as D-glucose.[144,145]

Consequently, boronic acids exhibit inherent selectivity for certain monosaccharides and glycoproteins; a property that has been exploited in glycan profiling, in the isolation of glycated peptides, and in glucose-sensing applications. [146]

1.3.2.1 Analytical and biomedical applications

Owing to their selective interaction with cis-diols, BAC have proven to be highly valuable in analytical biochemistry and clinical diagnostics.

In glyco-proteomics, it is widely used to isolate and enrich glycopeptides prior to LC–MS analysis.[147] In metabolomic studies, BAC enables preconcentration of nucleotides and, other hydroxylated metabolites. Its ability to form reversible complexes under mild aqueous conditions makes it suitable for biomarker detection, particularly in diabetes research, where it allows the selective trapping of glycated hemoglobin (HbA1c) and fructosamine peptides.[148]

Recent research has shifted the use of boronic acid-functionalized materials in biosensing and drug delivery.[149] Boronic acid-based fluorescent sensors have been developed for continuous glucose monitoring, exploiting the modulation of fluorescence intensity upon diol binding.[150]

Despite its simplicity, the practical application of BAC continues to face challenges. The limited binding strength at physiological pH hampers its performance with weakly interacting analytes, and the need for alkaline conditions can compromise biological stability, for this reason continuous innovation in boronic acid chemistry, ligand architecture, and support materials is steadily expanding the operational window of BAC toward physiological pH and enhancing its selectivity and reproducibility.

1.4 Analytical strategy for profiling glycated peptides in complex biological samples by LC-MS and MS tandem

Mass spectrometry (MS) has revolutionized the analysis of protein glycation by providing high-resolution, site-specific identification.

As already described in 1.2 paragraph, non-enzymatic glycation of serum proteins is an early and pervasive molecular consequence of chronic hyperglycemia.[151] In T2DM reducing sugars, such as glucose, react

spontaneously with amino groups, forming a spectrum of modifications that reflect a patient's glycemic exposure. The resulting Amadori products occur mainly on abundant plasma proteins like HSA, where they are created and degraded within the normal timeframe of protein turnover. Consequently, their quantification provides a sensitive and dynamic measure of short-term glycaemic control, complementing long-term markers such as HbA1c.[106]

Conventional immunochemical and chromatographic assays can estimate overall glycation but lack the site-specific detail needed to resolve individual modification sites or protein targets. In contrast, mass spectrometry enables precise detection and structural characterization of glycated peptides through accurate mass measurement and fragmentation analysis.[152,153]

Glycated peptides show a diagnostic mass increment of +162.0528 Da, corresponding to the addition of one hexose residue. Upon collision-induced dissociation (CID), they display reproducible and distinctive fragmentation patterns, characterized by stepwise neutral losses that confirm the presence of Amadori modifications.[154,155,156]

These diagnostic patterns are employed for confident identification of glycated sites on proteins such as HSA.[157] The reproducibility of these patterns across patient samples has enabled the establishment of signature panels of glycated HSA peptides, among them Lys199, Lys281, Lys525, and Lys549, that serve as molecular indicators of diabetic status.[158,159]

The analysis of glycated proteins in complex biological matrices, such as plasma, presents two key challenges:

1. low relative abundance in the complex peptides/proteins mixture,

2. high heterogeneity of glycation products.

To address these diametrically opposed aspects MS-based workflows employ selective enrichment steps combined with high-resolution separation prior to detection.

Generally speaking, a common MS-based workflow could be divided in four key strategic steps:

1. *Proteolytic digestion*: Serum or purified proteins are enzymatically digested, through trypsin, to generate peptides suitable for MS analysis,
2. *Selective enrichment*: Amadori peptides contain cis-diol structures, which can be captured by boronate-affinity media. This step enriches glycated peptides and reduces matrix interference.
3. *Liquid-chromatographic separation*: the enriched peptides are separated by reversedd-phase liquid chromatography (LC) under gradient elution.
4. *Electrospray ionization (ESI) and MS/MS analysis*: Peptides eluting from the LC column are ionized by ESI, generating multiply charged ions that are subsequently isolated and fragmented within the mass spectrometer, and MS tandem experiments.

In ESI, analyte ions are generated from solution under an electric field that produces charged microdroplets. For tryptic peptides, charge states of 2+ to 4+ are most common; these are readily transmitted and detected by ion-trap and Orbitrap instruments. Glycated peptides behave similarly to their unmodified counterparts but appear at higher m/z values due to the additional mass of the glucose adduct.[160] The presence of the carbohydrate adduct does not inhibit

ionization; however, it may slightly alter the charge-state distribution as a result of local polarity changes introduced at the glycation site.[161]

The characteristic series corresponds to a distinctive fragmentation pattern dominated by a cascade of neutral losses originating from the Amadori moiety.[162] The sequential elimination of water and formaldehyde molecules proceeds through the following characteristic mass losses:[163]

- −18 Da (H_2O loss)
- −36 Da (2 × H_2O)
- −54 Da (3 × H_2O; formation of a pyrylium-type structure)
- −84 Da (3 × H_2O + HCHO; formation of a furylium-type ion)

These losses appear as satellite peaks surrounding the precursor ion and, in certain cases, also around fragment ions retaining the glycation. Their regular spacing and relative intensity constitute a diagnostic ladder confirming the presence of Amadori modifications. Studies on glycated HSA peptides have demonstrated that this neutral-loss cascade is highly reproducible and largely independent of peptide sequence, making it a robust spectral fingerprint for glycation.[164,118]

1.4.1 Tandem Mass Spectrometry for Glycated Peptide Analysis

In collision-induced dissociation (CID), precursor ions are accelerated and allowed to collide with an inert gas, typically helium or nitrogen. Repeated low-energy collisions convert translational kinetic energy into internal vibrational energy, which induces cleavage of labile bonds.[165,166]

In peptides, the weakest bonds are usually the amide linkages, and when additional substituents such as glycation are present, these labile groups often

fragment preferentially, leading to the characteristic neutral losses before backbone cleavage occurs.

Since late 1980s and stats of 1990s, tandem mass spectrometry (MS/MS) has been applied to protein and peptide analysis. In a key work published in 1986 by Hunt et al.[167] tandem MS experiments have been used to identify peptide sequences directly from tryptic digestion of human apolipo-protein B (apoB), this study is, wordwide, considered the foundational paper of modern proteomics.

MS/MS spectrometry is a powerful tool to elucidate molecular structure by isolating a specific precursor ion (also called parent ion) and inducing its controlled fragmentation enabling precise identification of peptides, post-translational modifications, and other molecular features.[168]

The principle behind this technique has been expanded to MS^3 (MS/MS/MS) experiments, where a second round of fragmentation to selected ions is executed.[169] MS^3 can confirm modification sites, distinguish isomeric species, and resolve complex or overlapping spectra.[170]

2. Aim of PhD research work

The prevalence of Type 2 diabetes mellitus (T2DM) continues to rise globally, posing profound challenges to healthcare systems and to societies at large.

Early diagnosis and rigorous monitoring of disease progression are fundamental to limiting the onset of long-term micro- and macrovascular complications. In this regard, the non-enzymatic glycation of proteins and the subsequent formation of advanced glycation end-products (AGEs) have emerged as critical molecular events intimately linked to hyperglycemia, oxidative stress, and the pathophysiology of diabetic complications.

Despite extensive research over the past decades, translational markers derived from protein glycation remain insufficiently exploited in routine clinical practice, principally due to limitations in analytical sensitivity, specificity, and the lack of large-scale validation.

The present research aims to develop, optimize, and validate boronate-functionalised solid supports for the selective enrichment and characterization of glycated peptides as molecular indicators of early glycation events. The work builds on the unique affinity of boronic acids for cis-diol-containing compounds and explores how ligand structure, substitution pattern, and polymeric backbone influence the capture efficiency and selectivity of these materials toward Amadori-type adducts.

To achieve this, two distinct solid supports, ChemMatrix® Rink Resin (CMXRR) and ω-Aminohexyl–Agarose (AGRR), were functionalized with mono- and di-substituted phenylboronic acid moieties in para- and meta-orientations. The resulting materials were systematically characterized in terms of their chemical properties, stability, and binding performance. Controlled experiments with

synthetic model peptides representing unmodified, glycated, and glycosylated forms were first conducted to define the parameters governing affinity and specificity. After optimization with defined peptide standards, the best-performing boronate resins were evaluated on increasingly complex matrices, including mixtures of glycated peptides and protein hydrolysates, to assess their robustness, selectivity, and reproducibility under realistic analytical conditions.

Subsequently, the optimised workflow was applied to human serum samples to capture naturally occurring glycated peptides, particularly those derived from HSA, a major plasma protein known to undergo extensive glycation in diabetic conditions. The enriched fractions were analyzed by liquid chromatography coupled to mass spectrometry (LC–ESI-MS) to identify recurring glycated fragments and evaluate their potential as molecular biomarkers consistently present across different serum samples.

The expected outcome of this research is to establish a validated analytical platform integrating selective boronate-affinity enrichment and high-resolution mass spectrometry for the investigation of early-stage protein glycation.

Beyond its methodological innovation, this work aims to provide a proof of concept for the application of these synthetic boronate supports in the discovery of glycated peptide biomarkers directly from biological samples, bridging the gap between experimental chemistry and translational biomarker research in diabetes.

3. Results and discussion

3.1 Preparation of solid supports for the specific capture of deoxyfructosylated peptides

The analytical detection of glycated peptides in biological matrices remains challenging because of their low abundance and structural heterogeneity.

As described in paragraph 1.3.2, affinity-based enrichment strategies have been developed to selectively capture cis-diol–containing biomolecules. Among these, boronate affinity chromatography (BAC) has gained particular attention due to the ability of boronic acids to form reversible covalent complexes with 1,2- or 1,3-diols, such as those found in glucose and Amadori adducts.

The strength and reversibility of this interaction under mild pH conditions make boronic acid ligands ideal for isolating glycated species compatible with subsequent mass spectrometry (MS) analysis.

Over the past decades, various boronate-functionalized materials have been developed and commercialized. The best-known example is m-aminophenylboronic acid–agarose (Fig.1), available as an affinity gel for the selective capture of glycated and glycosylated biomolecules.

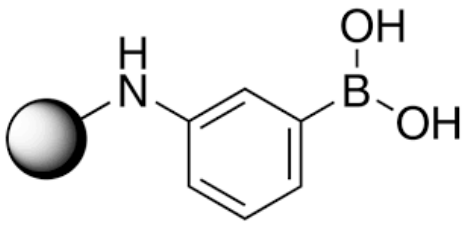

Fig.1: Structure of m-aminophenylboronic acid–agarose.

However, such materials often exhibit non-specific adsorption toward peptides containing hydroxyl-bearing amino acids, serine, threonine, or tyrosine, and limited loading capacity, motivating the search for new boronate supports with improved selectivity and performance.

To address these limitations, researchers have designed next-generation BAMs based on diverse polymeric or inorganic backbones, such as mesoporous silica, monolithic columns, magnetic nanoparticles, and synthetic resins like ChemMatrix®, which allow for higher ligand density and reduced non-specific binding.

3.1.1 Functionalization of resins varying the solid supports nature and units of phenylboronic acid

In a previous study published in 2020 in Molecules[171], ChemMatrix® Rink Resin (CMXRR) was selected to design a novel solid support. The resin was functionalized using a simple protocol, with lysine that acts as linker between the resin and two moieties of phenylboronate moieties, obtaining *p*-PhB-Lys(*p*-PhB)-CMXRR, to fish selectively glycopeptides.

Based on the results presented in that work, a set of boronate-functionalized solid supports was conceived to systematically explore how the chemical nature of the polymeric matrix and the spatial arrangement of phenylboronic acid moieties affect the affinity and selectivity toward glycated peptides.

For the present study different solid supports were designed. Based on two different solid supports, ChemMatrix® Rink Resin (CMXRR) and Agarose Resin (AG), functionalized with a spacer (a lysine) bearing one or two units of Boronate of *para*-phenyl boronic acid (*p*-PhB-OH) and meta-phenyl boronic acid (m-PhB-OH). Thus, the study aims to evaluate the influence of matrix composition, ligand

density, and electronic effects on the boronate–diol interaction. In particular, the distinction between para- and meta-substituted phenylboronic acids introduces subtle variations in electron distribution and steric accessibility at the boron center, which can significantly affect binding affinity and selectivity toward glycated peptides.

The solid supports of interest were:

- Resin 1: *p*-PhB-Lys(*p*-PhB)–ChemMatrix® Rink Resin
- Resin 2: m-PhB-Lys(m-PhB)–ChemMatrix® Rink Resin
- Resin 3: Ac-Lys(*p*-PhB)–ChemMatrix® Rink Resin
- Resin 4: Ac-Lys(m-PhB)–ChemMatrix® Rink Resin
- Resin 5: *p*-PhB-Lys(*p*-PhB)–Agarose Rink Resin
- Resin 6: m-PhB-Lys(m-PhB)–Agarose Rink Resin
- Resin 7: Ac-Lys(*p*-PhB)–Agarose Rink Resin
- Resin 8: Ac-Lys(*m*-PhB)–Agarose Rink Resin

3.1.1.1 Preparation of bi substituted phenylboronate resins

Both ChemMatrix® Rink Resin (CMXRR) (loading 0.60 mmol/g) and Agarose Rink Resin (AGRR) (loading 15 µmol/mL) were swollen in DMF for 30 min prior to functionalization. The Fmoc-Lys(Fmoc)-OH spacer (3 equiv.) was activated with HBTU/HATU (3 equiv.) and DIPEA (6 equiv.) in DMF and coupled to the resins for 40 min at 25 °C. After Fmoc deprotection with 20% piperidine in DMF, the resulting Lys–CMXRR and Lys–AGRR intermediates were washed with DMF and immediately reacted with 4-carboxyphenylboronic acid (*p*-PhB-OH, 6 equiv.) or 3-carboxyphenylboronic acid (*m*-PhB-OH, 6 equiv.) in the presence of

HBTU/HATU (6 equiv.) and DIPEA (12 equiv.) in DMF (10 mL). The coupling was allowed to proceed for 40 min at 25 °C with gentle stirring. The resins were washed sequentially with DMF (7 × 1 min) and DCMX (3 × 1 min) and monitored by the Kaiser test to confirm complete reaction.

The functionalized resins were dried under vacuum for 3 days. Small samples were cleaved with TFA/H_2O/TIS (95:2.5:2.5, v/v/v) for 3 h at room temperature to determine loading by UV analysis after lyophilization. The final products were obtained as follows:

- Resin 1 (p-PhB-Lys(p-PhB)–CMXRR): 3.00 g, loading 0.462 mmol/g
- Resin 2 (m-PhB-Lys(m-PhB)–CMXRR): 0.53 g, loading 0.289 mmol/g
- Resin 5 (p-PhB-Lys(p-PhB)–AGRR): loading 6.5 µmol/mL
- Resin 6 (m-PhB-Lys(m-PhB)–AGRR): loading 7.4 µmol/mL

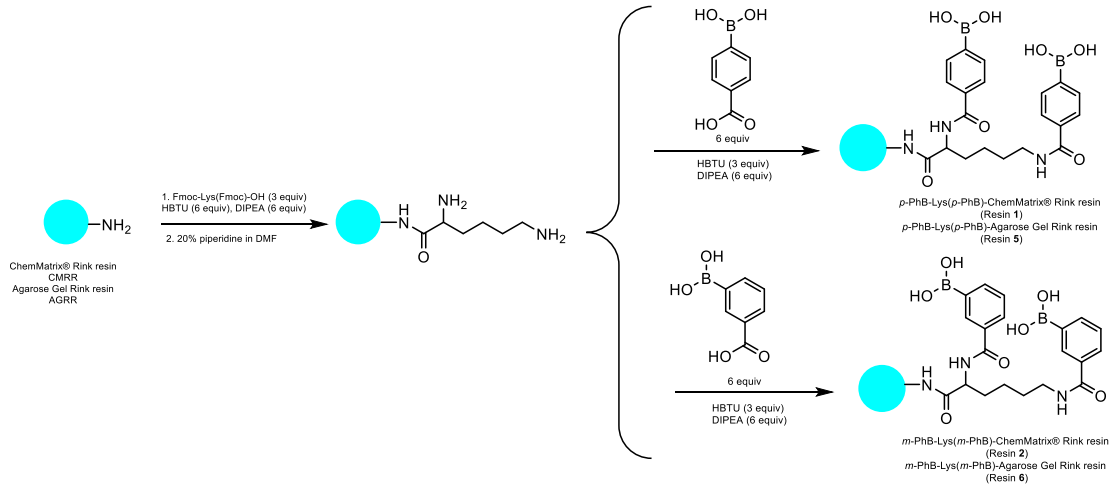

Scheme3: Synthetic pathway to obtain p-PhB-Lys(p-PhB)-ChemMatrix® Rink resin (Resin **1**), m-PhB-Lys(m-PhB)-ChemMatrix® Rink resin (Resin **2**), p-PhB-Lys(p-PhB)-Agarose Gel Rink resin (Resin **5**) and m-PhB-Lys(m-PhB)-Agarose Gel Rink resin (Resin **6**).

3.1.1.2 Preparation of mono substituted phenylboronate resins

ChemMatrix® Rink Resin (loading 0.60 mmol/g) and Agarose Rink Resin (loading 15 µmol/mL) were swollen in DMF for 30 min. The coupling of Fmoc-Lys(Mtt)-OH (3 equiv.) was performed under the same activation conditions as described in 3.1.1.1. After washing, the Mtt protecting group was selectively removed with TFA/TIS/DCMX (1:5:94, v/v/v), refreshed four times.

The exposed ε-amino group of lysine was then coupled to either 4-carboxyphenylboronic acid (*p*-PhB-OH, 3 equiv.) or 3-carboxyphenylboronic acid (*m*-PhB-OH, 3 equiv.) in the presence of HBTU (3 equiv.) and DIPEA (6 equiv.) in DMF. The mixture was stirred for 40 min at 25 °C, followed by washing with DMF (7 × 1 min) and DCMX (3 × 1 min).

Finally, the Nα-amino functions of the supported lysine residues were acetylated with acetic anhydride (10 equiv.) and DIPEA (10 equiv.) in DMF for 1 h. The resins were filtered, washed with DMF and DCMX, and dried under vacuum for 3 days. Cleavage tests using TFA/H_2O/TIS (95:2.5:2.5, v/v/v) confirmed successful derivatization and the following loadings:

- Resin 3 (Ac-Lys(p-PhB)–CMXRR): 0.55 g, 0.354 mmol/g
- Resin 4 (Ac-Lys(m-PhB)–CMXRR): 0.49 g, 0.151 mmol/g
- Resin 7 (Ac-Lys(p-PhB)–AGRR): loading 4.3 µmol/mL
- Resin 8 (Ac-Lys(m-PhB)–AGRR): loading 3.2 µmol/mL

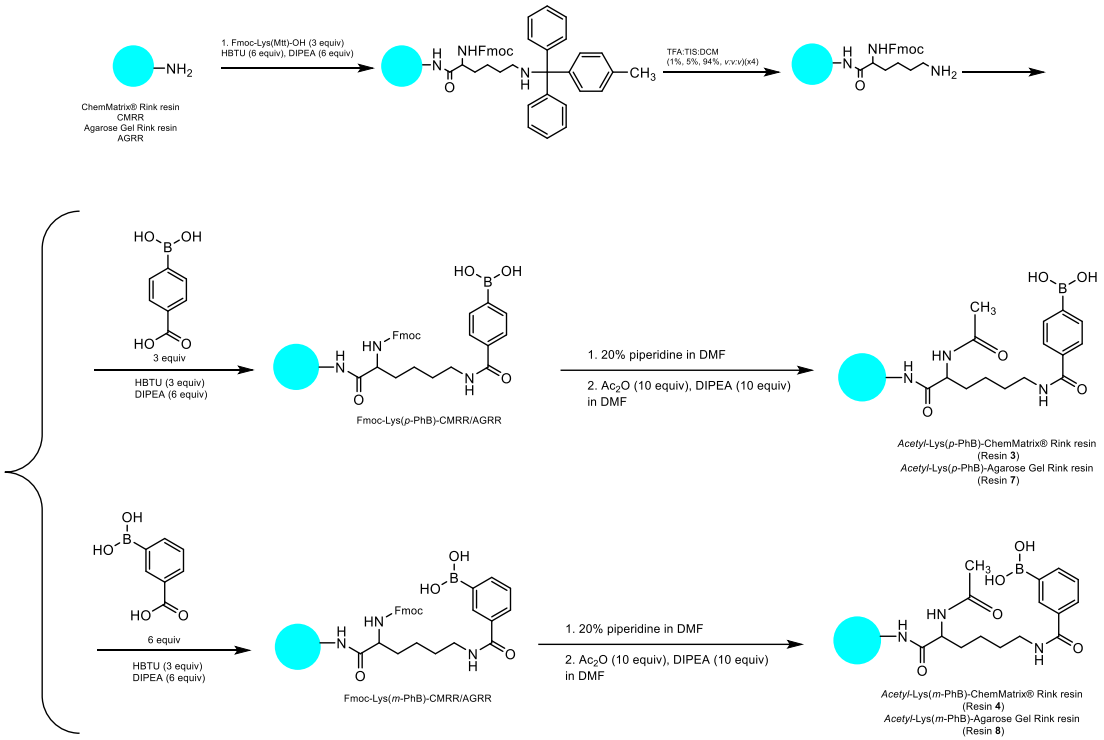

Scheme4: Synthetic pathway to obtain Ac-Lys(p-PhB)-ChemMatrix® Rink resin (Resin **3**), Ac-Lys(m-PhB)-ChemMatrix® Rink resin (Resin **4**), Ac-Lys(p-PhB)-Agarose Gel Rink resin (Resin **7**) and Ac-Lys(m-PhB)-Agarose Gel Rink resin (Resin **8**).

		No.	Resin	Loading (mmol/g)	Quantity (g)
CMXRR	di-modified	**R1**	*p*-PhB-Lys(*p*-PhB)-CMXRR	0.462	0.961
		R2	*m*-PhB-Lys(*m*-PhB)-CMXRR	0.354	0.533
	mono-modified	**R3**	Ac-Lys(*p*-PhB)-CMXRR	0.298	0.549
		R4	Ac-Lys(*m*-PhB)-CMXRR	0.151	0.487
AGRR	di-modified	**R5**	*p*-PhB-Lys(*p*-PhB)-AGRR	0.524	0.0284
		R6	*m*-PhB-Lys(*m*-PhB)-AGRR	0.406	0.0698
	mono-modified	**R7**	Ac-Lys(*p*-PhB)-AGRR	0.317	0.0252
		R8	Ac-Lys(m-PhB)-AGRR	0.203	0.0702

Table1: Functionalized resins to capture glycated peptides. CMXRR - ChemMatrix® Rink resin; AGRR - Agarose Rink resin.

3.2 Synthesis of specific deoxyfructosylated peptide fragments

Controlled glycation experiments on HSA and its peptide fragments constitute a practical approach to characterizing both the chemical formation of Amadori products and their analytical behavior under mass spectrometric conditions.[172,173]

To elucidate which amino acid residues are most susceptible to glycation, a study of La Polla et all of 2004 [174] combined enzymatic digestion, tandem mass spectrometric analysis, and molecular modeling enabling the recognition of the most putative sites.

Computational evaluation of solvent-accessible surface areas identified several lysine residues, Lys233, Lys276, Lys378, Lys525, and Lys545, as the most exposed and, therefore, the most reactive toward reducing sugars.

To achieve this, synthetic fragment peptides were designed as minimal sequence models encompassing the most reactive lysine residues, ERQIK**K**QTALVELVK and SSAKQRL**K**CASLQ.

To understand the impact of glycation on serum proteins, two HSA peptide fragments were designed as minimal sequence models: HSA1 (ERQIKKQTALVELVK, Fig. 2) and HSA2 (SSAKQRLKCASLQ, Fig. 3), which contain the most reactive lysine residues (K525, K545).

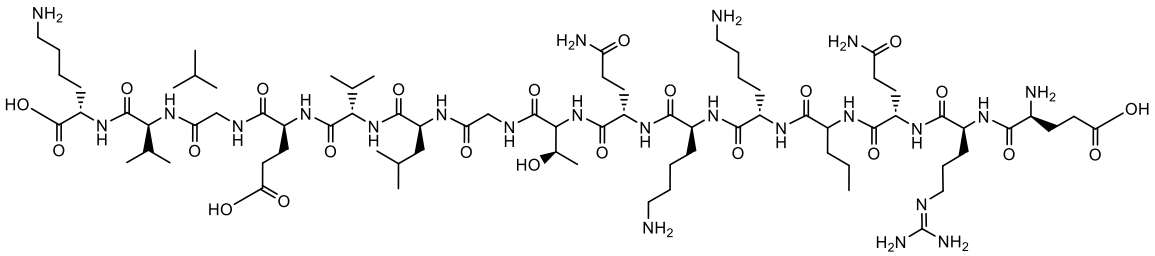

Fig.2: HSA1 peptide fragments, sequence: ERQIK**K**QTALVELVK.

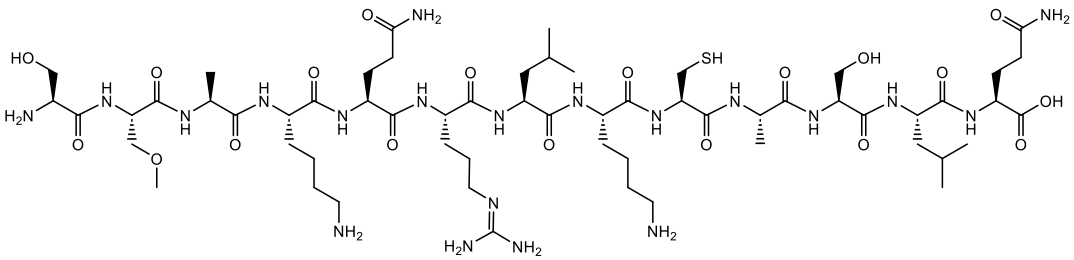

Fig.3 : HSA2 peptide fragments, sequence: SSAKQRL**K**CASLQ.

These peptides were synthesized using a MW-SPPS employing Fmoc/tBu orthogonal protecting strategy and DIC/Oxyma Pure as the coupling system on the automated MW-assisted synthesiser Liberty BlueTM (CEM, USA). And later

were glycated according to the Boratynski strategy, enabling the stepwise generation of early Amadori intermediates under controlled conditions.

Both peptides were designed to have n-terminal and c-terminal function free, the choice of the resins was settled on Wang resins. Fmoc-L-Lys(BOC)-Wang resin (Fig.4) for HSA1, and Fmoc-L-Gln-(Trt)-Wang resin (Fig.5) both with a loading of 0,6 mmol.

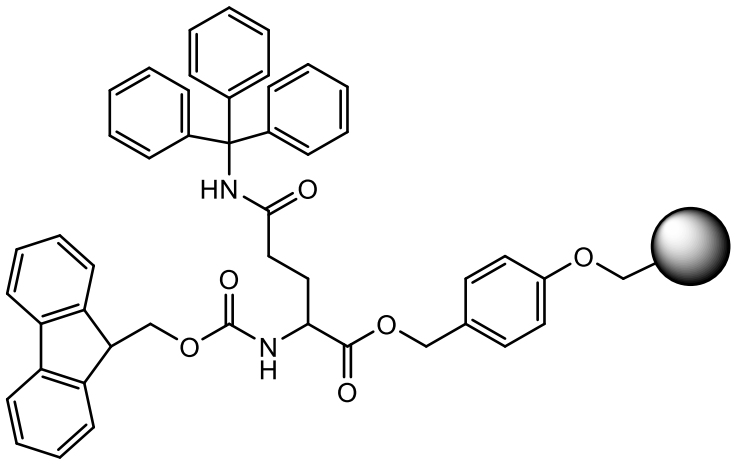

Fig.4: Fmoc-L-Lys(BOC)-Wang resin.

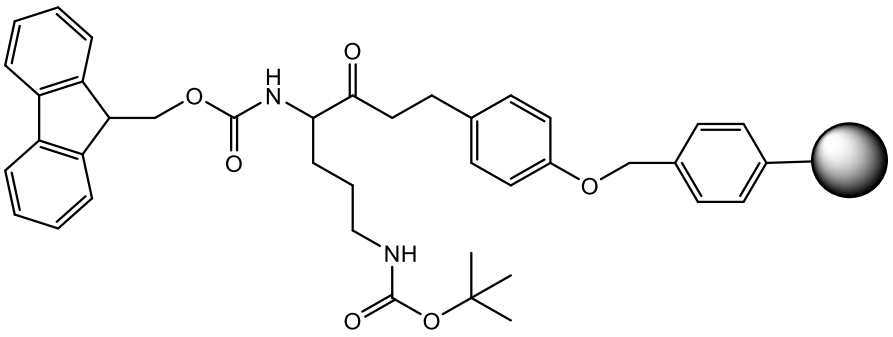

Fig.5: Fmoc-L-Gln-(Trt)-Wang resin.

The resin was first swollen in DMF, to allow it to expand and expose all the active sites to the solvent, and then the MW-SPPS was performed. Considering the sequences, double coupling cycles were applied under microwave-assisted SPPS conditions to ensure the complete incorporation of all amino acid into the growing sequence.

For each amino acid in the sequence, the subsequent steps were performed, and repeated iteratively for each amino acid:

- Standard deprotection conditions: 20% (v/v) piperidine/DMF.
- Washings in DMF
- Coupling: DIC and Oxyma pure as coupling system and protected amino acid building blocks dissolved in DMF
- Washings in DMF
- Coupling: DIC and Oxyma pure as coupling system and protected amino acid building blocks dissolved in DMF

After the resin with the peptide elongated was deprotected from the amino-terminal Fmoc protecting group, washed with DMF and DCMX and then treated with a cleavage mixture composed of 92.5:2.5:2.5:2.5 TFA:TIS:H_2O:EDT (*v:v:v:v*) to cleave the peptide from the resin and remove all the protecting groups on the side chains. The resin was then filtered and washed with diethyl ether to precipitate the peptide. After centrifugation the crude product was collected and glycated via Boratynsky strategy.

3.2.1 Glycation of peptides via Boratyński strategy

The peptides were selected as a representative substrate for controlled glycation. They were subjected to deoxyfructosylation following the Boratyński method [175], which enables covalent conjugation of reducing sugars to amino groups through a dry-thermal Maillard-type reaction. This procedure promotes condensation between the sugar carbonyl group and the ε-amino function of lysine, forming an unstable glycosylimine intermediate that rearranges to yield the corresponding 1-deoxy-D-fructosyl-lysine derivative.

The beauty of the Boratyński reaction lies in the fact that can be performed under various conditions, including aqueous or vacuum environments, mimicking glycation processes occurring in biological or industrial contexts. Under aqueous conditions at physiological pH, the reaction reflects early in vivo glycation steps.

For the present study, glycation was carried out by simply mixing peptides or proteins with sugars (D-Glucose) in a 1:2 ratio, then freeze-drying the mixture and heating it at 104°C for 40 minutes.

The success of the glycation reaction was followed by HPLC-ESI-MS analysis.

The chromatographic analysis of the glycated peptides revealed a clear shift in retention times compared to the non-glycated counterparts. This retention time shift provides direct evidence of successful sugar conjugation to the peptide fragments, confirming the formation of early Amadori products. Additionally, mass spectrometric analysis substantiated these findings by showing distinct mass increments corresponding not only to single but multiple sugar attachments on both peptide fragments. The presence of multiple glycated species demonstrates the heterogeneous nature of the glycation process and highlights the reactivity of multiple lysine residues within the synthetic sequences. Together, these chromatographic and mass spectrometric data

unequivocally confirm the controlled and specific glycation of the HSA-derived peptides, validating the effectiveness of the applied Boratyński strategy under the experimental conditions.

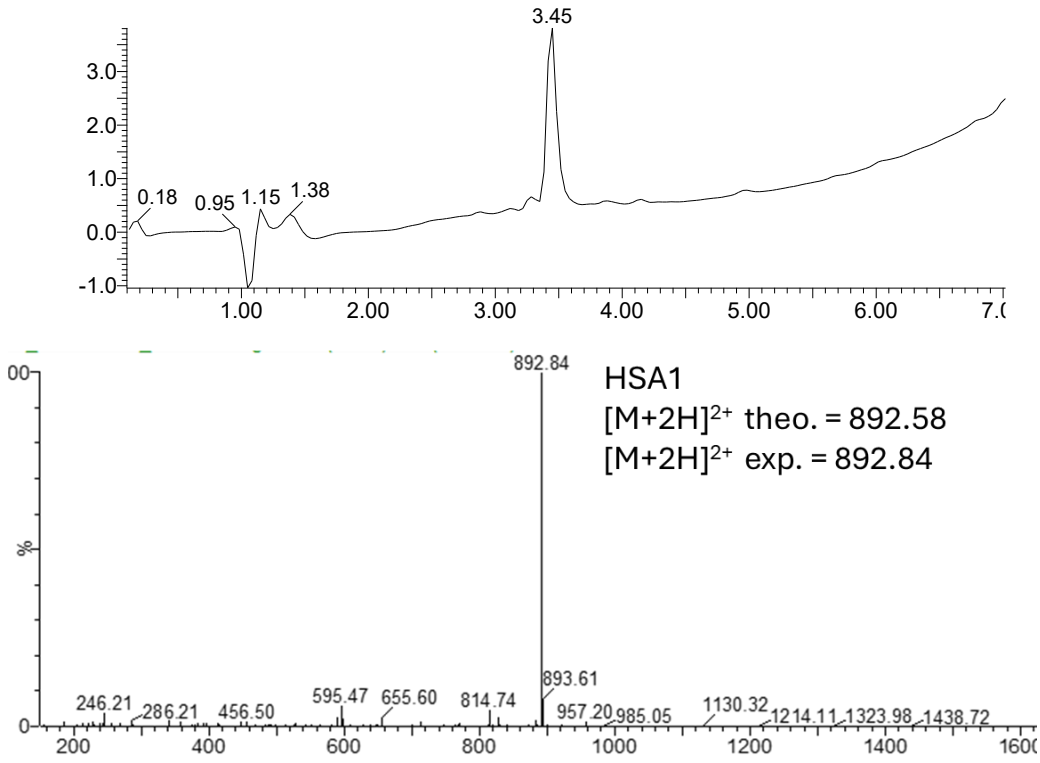

Fig.6: A) RP-HPLC (Alliance Chromatography system (Waters, Milford Massachusetts, USA)) of HSA1: C18 column Waters Acquity BEH (130 Å, 1.7 µm, 2.1 50 mm); temperature 35°C; flow, 0.6 ml/min; eluent, 0.1% (v/v) TFA in H2O (A) and 0.1% (v/v) TFA in CH3CN (B); λ, 215 nm, rt = 3.45 min; gradient, 20–80% B in 5 min. B) ESI-MS spectrum (ESI-MS Micromass ZQ (Waters, Milford Massachusetts, USA)) of HSA1, (m/z): $[M+H]^{2+}$ exp: 892.84.

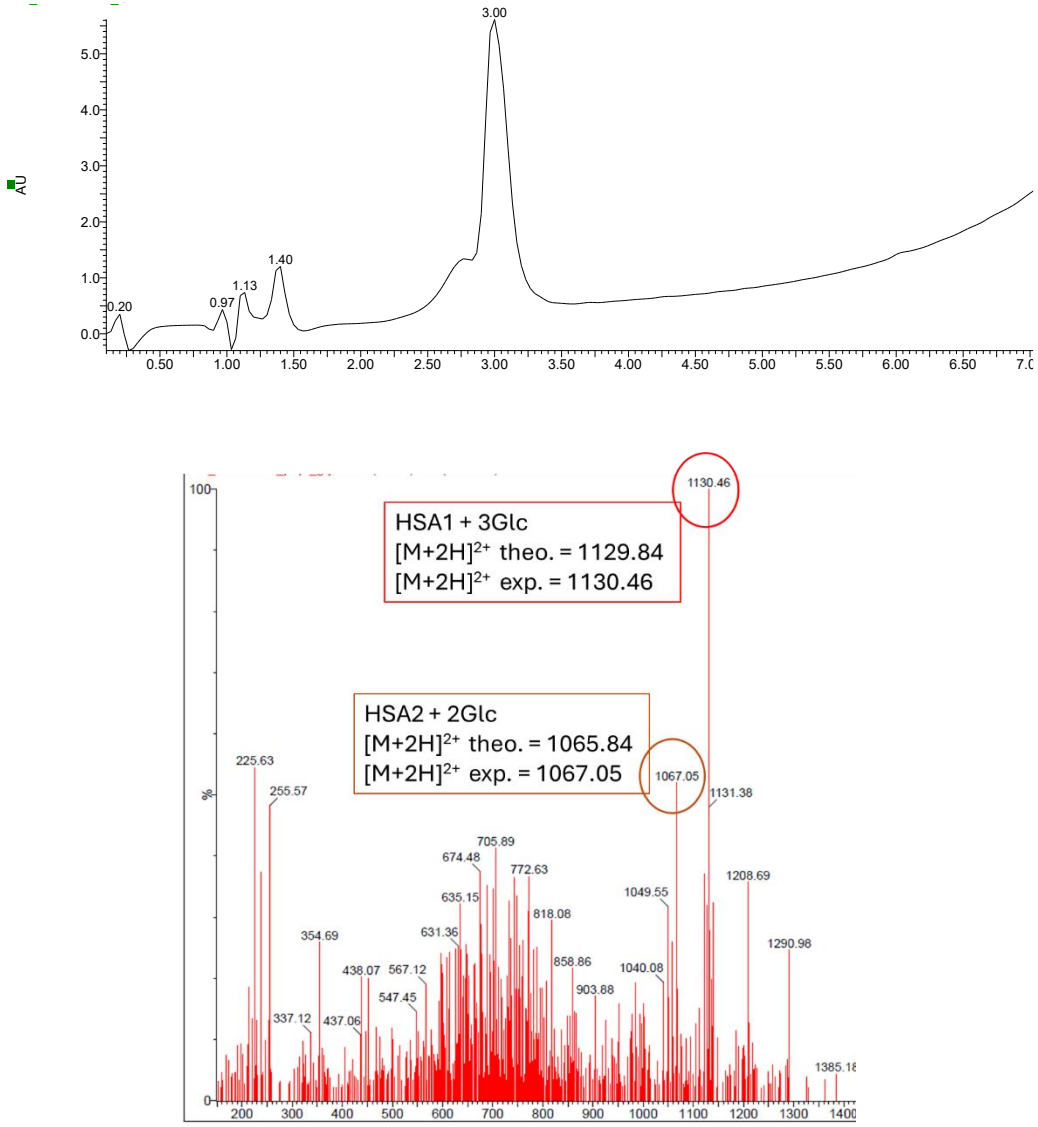

Fig.7: A) RP-HPLC (Alliance Chromatography system (Waters, Milford Massachusetts, USA)) of glycated HSA1: C18 column Waters Acquity BEH (130 Å, 1.7 µm, 2.1 50 mm); temperature 35°C; flow, 0.6 ml/min; eluent, 0.1% (v/v) TFA in H2O (A) and 0.1% (v/v) TFA in CH3CN (B); λ, 215 nm, rt = 3.00 min, gradient, 30–80% B in 5 min. B) ESI-MS spectrum (ESI-MS Micromass ZQ (Waters, Milford Massachusetts, USA)) of glycated HSA1, (m/z) of HSA1+2Glc: $[M+H]^{2+}$ exp: 1067.05, (m/z) HSA1+3Glc: $[M+H]^{2+}$ exp: 1130.46.

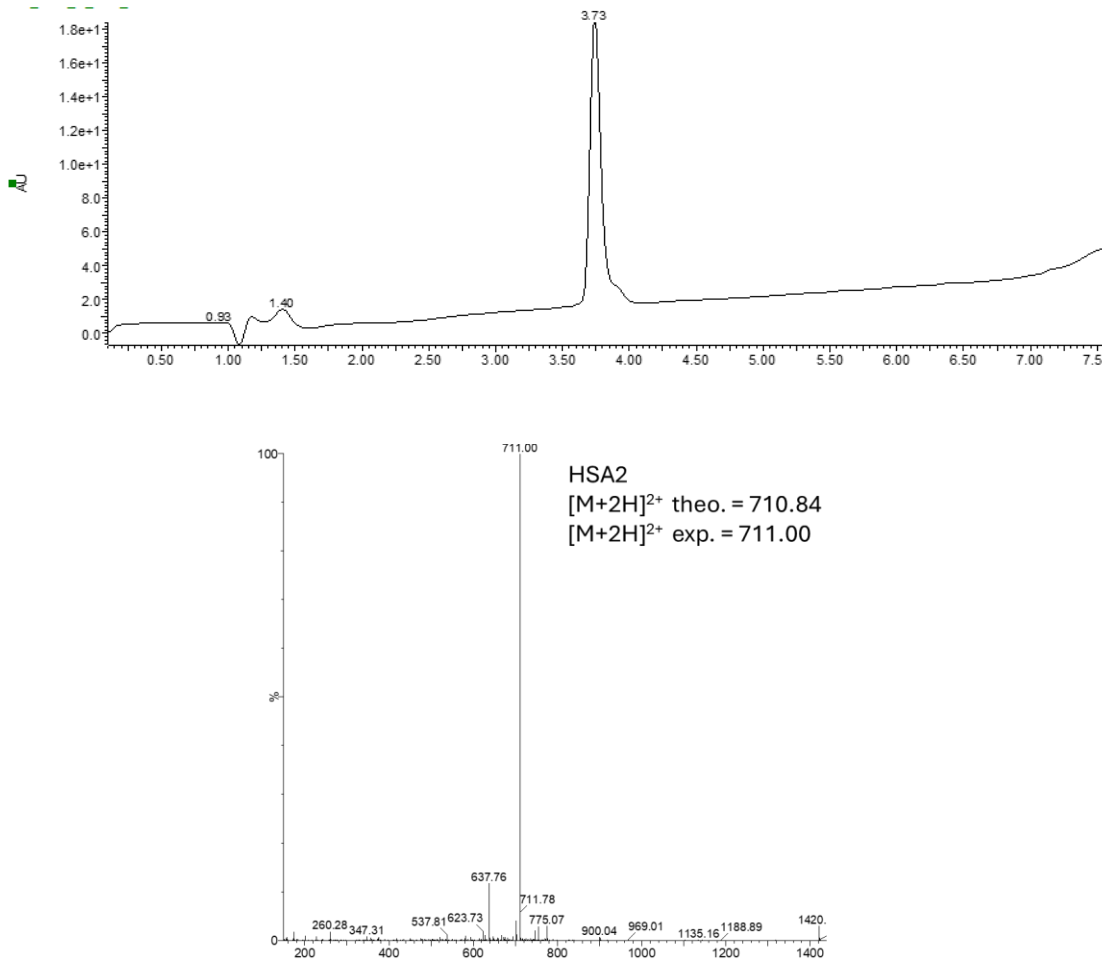

Fig.8: A) RP-HPLC (Alliance Chromatography system (Waters, Milford Massachusetts, USA)) of HSA2: C18 column Waters Acquity BEH (130 Å, 1.7 µm, 2.1 50 mm); temperature 35°C; flow, 0.6 ml/min; eluent, 0.1% (v/v) TFA in H2O (A) and 0.1% (v/v) TFA in CH3CN (B); λ, 215 nm, rt = 3.73 min; gradient, 20–80% B in 5 min. B) ESI-MS spectrum (ESI-MS Micromass ZQ (Waters, Milford Massachusetts, USA)) of HSA2, (m/z): $[M+H]^{2+}$ exp: 711.00

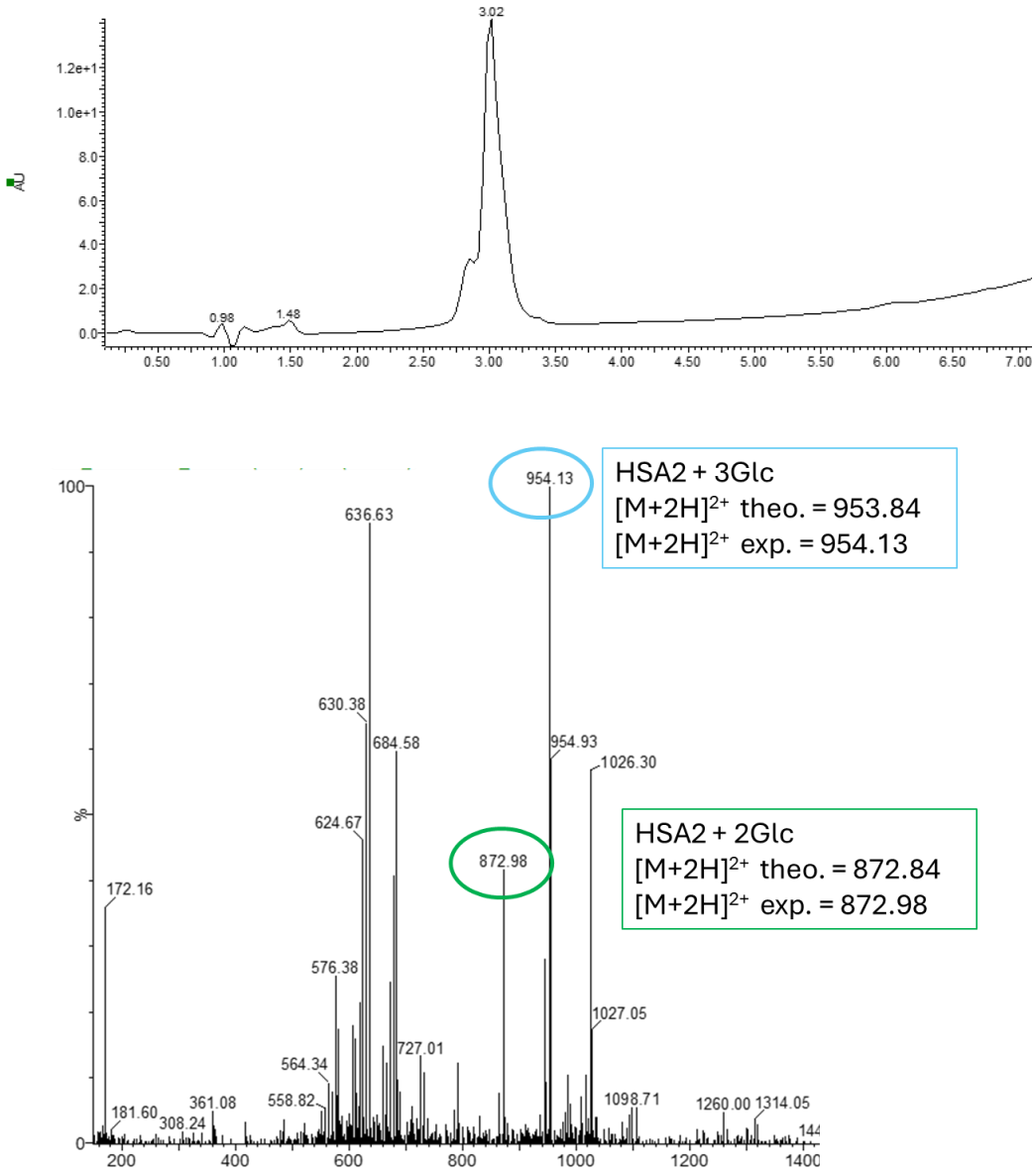

Fig.9: A) RP-HPLC (Alliance Chromatography system (Waters, Milford Massachusetts, USA)) of glycated HSA1: C18 column Waters Acquity BEH (130 Å, 1.7 µm, 2.1 50 mm); temperature 35°C; flow, 0.6 ml/min; eluent, 0.1% (v/v) TFA in H2O (A) and 0.1% (v/v) TFA in CH3CN (B); λ, 215 nm, rt = 3.02 min, gradient, 30–80% B in 5 min. B) ESI-MS spectrum (ESI-MS Micromass ZQ (Waters, Milford Massachusetts, USA)) of glycated HSA1, (m/z) of HSA2+2Glc: $[M+H]^{2+}$ exp: 872.98, (m/z) HSA1+3Glc: $[M+H]^{2+}$ exp: 954.13.

3.3 Boronate affinity chromatography

A key part of the present research project involved designing, synthesizing, and evaluating boronate-functionalized solid supports for the selective enrichment of early glycation products, particularly Amadori-type peptides, potential markers of diabetes.

As discussed in 3.1 paragraph, two classes of solid supports were investigated: ChemMatrix® Rink resin (CMXRR), a synthetic PEG-based resin characterized by high swelling capacity and mechanical stability, and ω-aminohexyl–agarose resin (AGRR), a hydrophilic, polysaccharide-based support. Both were functionalized with either mono- or di-substituted phenylboronic acid (PhB) moieties in para or meta orientation to yield a total of eight resins (R_1–R_8). (see Table 1)

The loading capacities of the functionalized resins, determined by elemental analysis and UV quantification, ranged from 0.15 to 0.52 mmol g^{-1}. This variability in loading values reflected differences in substitution patterns, steric effects during coupling, and the chemical nature of the support matrix. The bi-functionalized variants exhibited higher nominal loading, as expected, but their spatial configuration and flexibility were hypothesized to influence their accessibility for cis-diol recognition.

3.3.1 Boronate affinity chromatography: from peptide mixture to complex biological mixtures

To evaluate the capture efficiency and selectivity of the 8 eight functionalized solid supports, a systematic screening was conducted using a set of synthetic peptides representative of glycated, non-glycated, and glycosylated sequences. (Table 2).

No	Name	Sequence	MW (g/mol)
P1	Amadori Peptide 1	Ac-YNKSW**K**((N$^{\varepsilon}$-DeoxyFru)FEHSNFNDVC-OH	2236
P2	Non - Amadori Peptide 1	Ac-YNKSWKFEHSNFNDVC-OH	1930
P3	Scrambled Peptide 1 Amadori GCD-59	Ac-VSENDK(N$^{\varepsilon}$-DeoxyFru)YNFHKSWNFC-OH	2236
P4	Surrogate Calibrator Gluticol GCD-59	Ac-NKAWK(N$^{\varepsilon}$-DeoxyFru)FEHANFNDC(OH)-PEG	5940
P5	Ser^{7}(Glc)]CSF114	H-TPRVERS^{7}(β-D-Glc)GHSVFLAPYGWMVK-OH	2579
P6	Asn^{7}(Gal)]CSF114	H-TPRVERN^{7}(β-D-Gal)GHSVFLAPYGWMVK-OH	2606
P7	[(N$^{\varepsilon}$-1-DeoxyFru)]CSF114	H-TPRVERK^{7}(N$^{\varepsilon}$-DeoxyFru)GHSVFLAPYGWMVK-OH	2621
P8	Asn^{7}(Glc)]CSF114	H-TPRVERN^{7}(β-D-Glc)GHSVFLAPYGWMVK-OH	2606

Table2: List of the Amadori CD59 peptides and the glycosylated peptides used as a matrix for capturing.

These model peptides were selected to mimic clinically relevant glycated sites identified in the extracellular domain of CD59, a glycoprotein implicated in diabetes-related pathophysiology.

All resins, R1-R8, were tested with a mixture of single peptides, more complex mixtures, and sera from patients affected by T2DM, at the optimal pH for boronate–diol complex formation. Capture efficiencies were measured by UV absorbance of unbound fractions and confirmed through LC–MS analysis of eluates.

3.3.1.1 Screening of Meta-Substituted resins

The first screening experiments focused on the comparative evaluation of meta-substituted resins (R2, R4, R6, R8), differing by units of boronate attached (mono- versus bi-functionalized) and by the support, CMXRR or AGRR.

The primary parameters considered to evaluate the efficiency in enrichment were the selectivity toward mimic Amadori peptides versus glycosylated or non-modified peptides, the global capture efficiency and lastly the reproducibility.

The results revealed an overall better performance, with a good compromise in efficiency and selectivity, of the mono-substituted *meta*-resins, Ac-Lys(*m*-PhB)-CMXRR (R4) and Ac-Lys(*m*-PhB)-AGRR (R8).

In particular, R4 and R8 exhibited strong enrichment for Amadori peptides P1, P3, and P8, with capture yields ranging from 31–45%, while maintaining minimal non-specific binding toward unmodified or glycosylated analogues (≤10%). In contrast, the bi-functionalized analogues (R2, R6) showed reduced selectivity, tracible to steric hindrance and the simultaneous presence of two closely spaced boronic acid sites that hindered optimal interaction with the peptide-bound fructosyl moiety.

Interestingly, it was noted that resin architecture also impacted in the peptide retention. The PEG-based CMXRR support consistently yielded slightly higher capture efficiencies compared to the hydrophilic agarose support, supposedly

due to its enhanced swelling properties and greater accessibility of boronate groups within the polymeric network.

Peptide-dependent effects were observed, as well. Longer peptides such as P4 (MW ≈ 6000 Da) displayed markedly lower binding (<15%), attributed to steric exclusion and conformational rigidity. These findings highlight the need for proteolytic digestion of biological samples prior to affinity capture to ensure accessibility of glycated sites.

3.3.1.2 Para vs Meta Orientation: structural influence

To explore the role of boronic acid substitution pattern on binding performance, a second comparative experiment was conducted between the most effective meta resins (R4 and R8) and their corresponding para-analogues (R3 and R7).

The results demonstrated a distinct dependence on positional isomerism and resin backbone.

For the CMXRR resins, the *meta*-analogue (R4) outperformed the *para* form (R3), with average capture efficiencies for Amadori peptides of 37% versus 28%, respectively. Conversely, in the AGRR resins, the *para*-analogue (R7) exhibited slightly higher efficiency compared to the *meta-analogue* (R8), but at the expense of selectivity.

These results and the ones after the first set of experiment, confirmed that both the chemical microenvironment of the boronate moiety and the polymeric architecture of the support jointly dictate the effectivess of binding. In fact, CMXRR support, a PEG-based matrix, most likely provided greater flexibility and solvent exposure, allowing the *meta*-substituted boronate group to engage in

more favorable orientation for cyclic ester formation with the fructosyl diol. The agarose matrix, by contrast, imposes more steric and hydrogen-bonding constraints, favoring the *para* configuration for accessibility.

From a mechanistic perspective, the higher performance of R4 is consistent with previous findings indicating that boronic acids with electron-withdrawing substituents or spatially unconstrained binding pockets exhibit enhanced complexation rates with cis-diols under mildly alkaline conditions.[139]

Overall, R4 emerged as the most balanced resin in terms of selectivity and efficiency, capturing Amadori peptides with high yield (≈40%) while minimizing nonspecific adsorption (<10%).

3.3.1.3 Comparative evaluation with Commercial supports

To assess the performance of the resins produced further experiments compared R4 with a commercially available *m*-aminophenylboronic acid–agarose resin (PBA-agarose, Sigma-Aldrich A8530).

Two sets of solutions were employed, the first was an equimolar mixture of [(1-deoxyfructosyl)Lys^{7}]CSF114 (P7) and [(Asn^{7}-Glc)]CSF114 (P8), the second were mixtures containing only 5% (*w:w*) P7 relative to P8 to study the selectivity under competitive conditions.

From the first set, under equimolar conditions, the performances of both resins were comparable, suggesting a functional boronate activity. However, under competitive low-abundance conditions, only R4 retained significant selectivity for the deoxy-fructosylated peptide.

This difference underscores the critical influence of the resin backbone on selectivity, as suggested by the previous set of experiments.

3.3.1.4 Application to Complex Biological Samples

To validate the applicability of the R4 resin in realistic biological contexts, experiments were extended to human serum samples from individuals with normal glucose tolerance (NGT) and, type 2 diabetes mellitus (T2DM).

As first it was decided to test the selectivity of R4 by gradually enhanced the complexity of the peptides mixture, shifting form single peptides or multi synthetic peptides mixture, to a tryptic digested of Human Serum Albumin (HSA).

Prior to boronate affinity chromatography, the HSA has been glycated by Boratynsky's strategy, as described in 3.2.1, and enzymatically digested via trypsin. The resulting complex, varying peptide mixture undergoes boronate affinity capture under previously optimized conditions.

The flow through and eluted fractions have been analysed via HPLC-ESI-MS, enabling detection and relative quantification of Amadori peptides.

Here below the resalting deconvoluted spectra for glycated HSA, from which it was possible to confirm the high complexity of the starting mixture (Fig.10), the enrichment via affinity chromatography proved a distinct difference between the flow through (Fig.11) and eluted fractions (Fig.12)

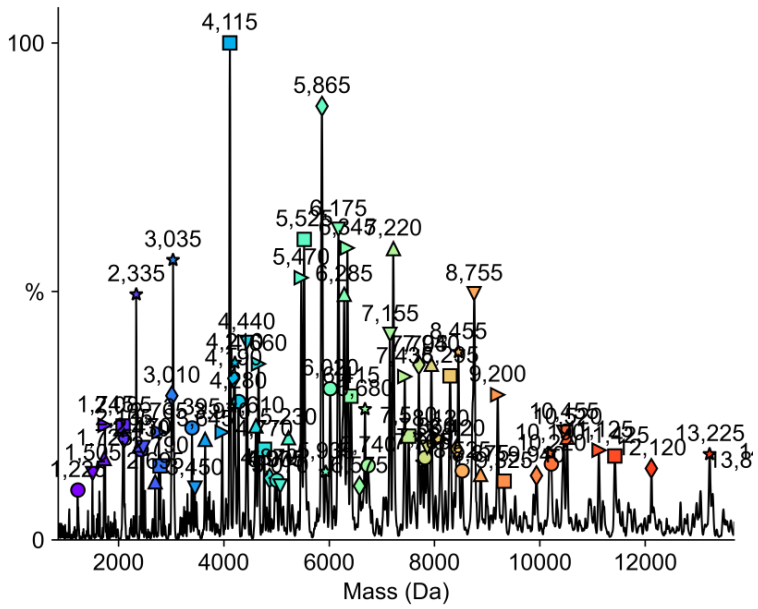

Fig.10: Deconvoluted MS spectra ESI-MS Micromass ZQ (Waters, Milford Massachusetts, USA)of tryptic digested HSA, prior enrichment.

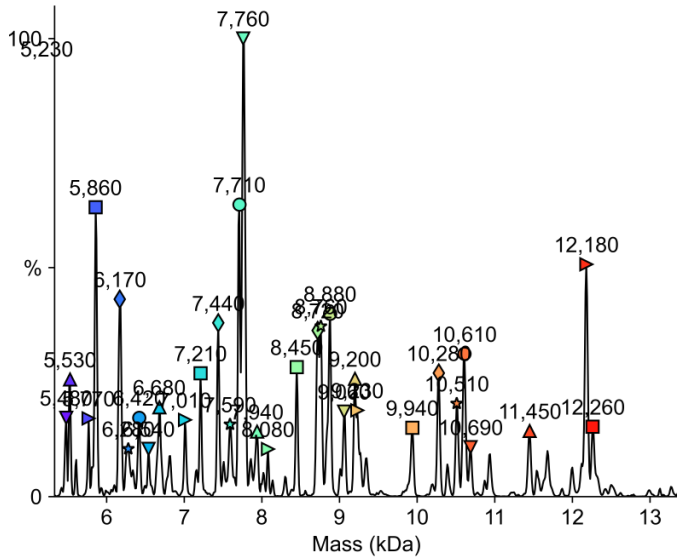

Fig.11: Deconvoluted MS spectra ESI-MS Micromass ZQ (Waters, Milford Massachusetts, USA) of digested HSA fragments not trapped in the BAMs.

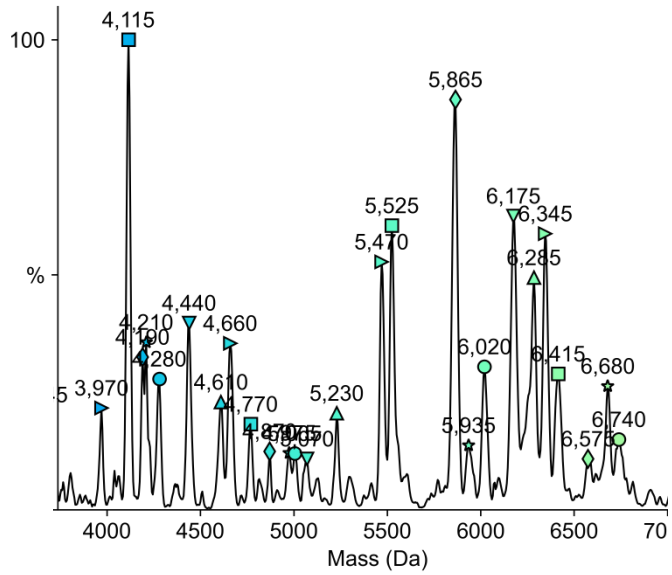

Fig.12: Deconvoluted MS spectra ESI-MS Micromass ZQ (Waters, Milford Massachusetts, USA) of digested HAS fragments eluted.

Same DoE has been applied for sera of patients affected by T2DM. Also, for them a tryptic digestion was required prior chromatography. And again, the affinity with R4 showed a good performance in simplifying the mixtures and trapping specific fragments, as it shown in the spectra down below. (Fig. 13-15)

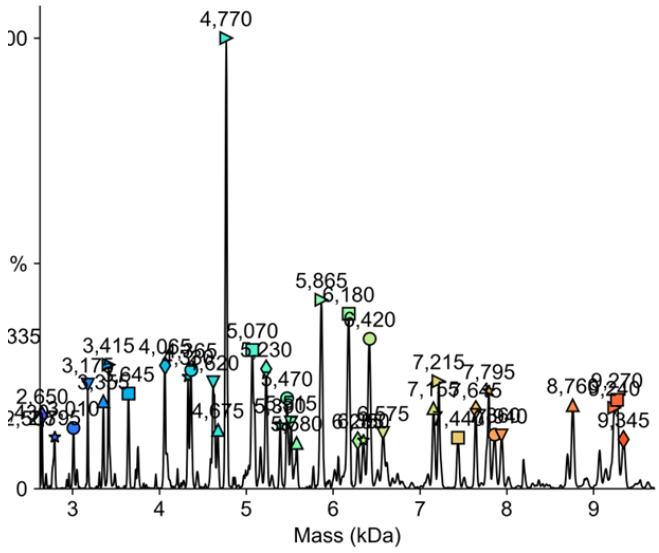

Fig.13: Deconvoluted MS spectra ESI-MS Micromass ZQ (Waters, Milford Massachusetts, USA) of diabetic sera, prior affinity chromatography.

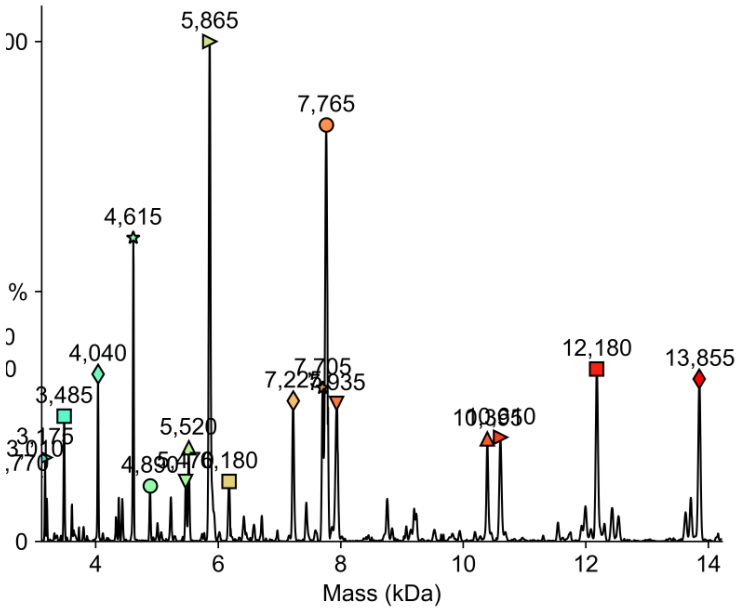

Fig.14: Deconvoluted spectra ESI-MS Micromass ZQ (Waters, Milford Massachusetts, USA).of non-retained peptides fragments.

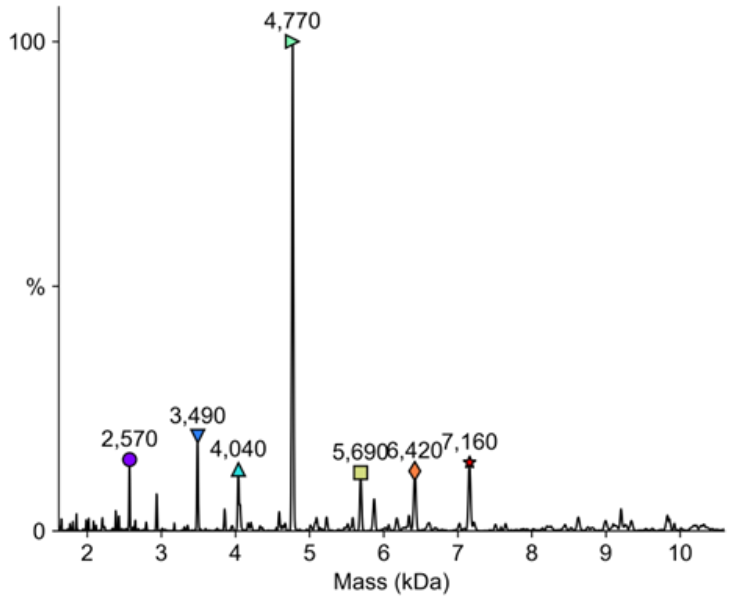

Fig.15: Deconvoluted MS spectra ESI-MS Micromass ZQ (Waters, Milford Massachusetts, USA).of enriched fragments.

The R4 resin demonstrated robust performance in complex matrices, yielding reproducible enrichment of glycated peptides even at low abundance. Comparative profiling revealed elevated levels of Amadori-modified peptides derived from abundant serum proteins, particularly HSA.

This trend was maintained with the progressive increase in protein glycation observed during hyperglycemic states.

3.4 Mass Spectrometry

For the study and characterization of specific biomarker of glycated peptides in patient affected by diabetes (T2DM), the spectrometer of choice has been the LTQ XL™ mass spectrometer by Thermo Scientific.

This system is a quadrupole based linear ion trap (LIT) mass spectrometer designed for rapid multi MS scan with high sensitivity. In Fig. it is shown the schematic representation of the parts that make up the instrumentation.

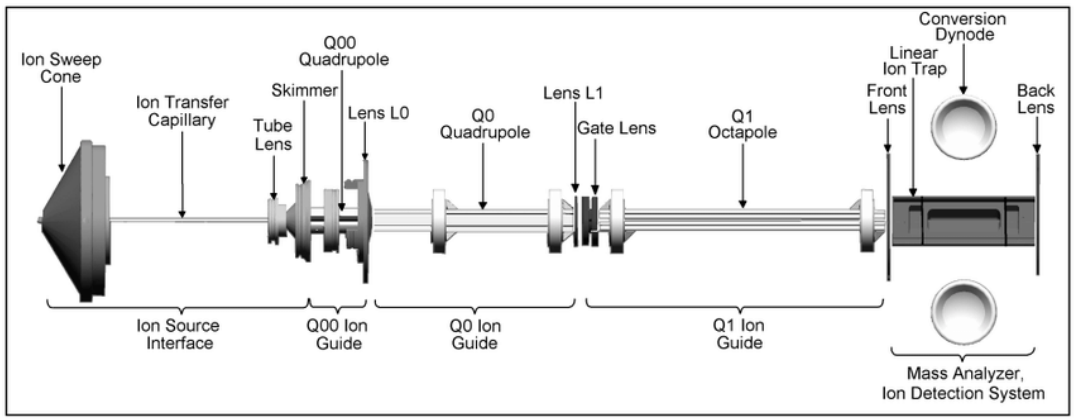

Fig.16: Schematic representation of the LTQ XL mass spectrometer, showing Ion source, the three quadrupoles (Q00, Q0, Q1) and, the ion trap.

3.4.1 MS^n for glycated peptides

The LTQ XL high ion-storage capacity and fast scan speed make it well suited to data-dependent acquisition (DDA) during LC–MS analyses. Its ability to perform MS^3 is especially advantageous for Amadori peptides, where secondary fragmentation of neutral-loss ions enhances structural confidence.

As first approach to a multi-scan MS DoE it was decided to test HSA1 glycated by Boratynsky strategy (see paragraph 3.2.1)

Before showing the spectra obtained, some additional experimental considerations were necessary:

1. Employing moderate normalized collision energies (NCE), typically at 25–30%. A low NCE usually provide the best balance between fragmentation efficiency and spectral clarity. In fact, these energies generate high sequence informative ions form peptide backbone with minimal internal fragmentation or loss of labile side-chain modifications (as sugar moieties).
2. Consider the limitation connected to the low-mass cut-off, which is typical of ion-trap analyzers. They exclude fragment ions below m/z 100 from detection, ions below this threshold cannot be stabilized during resonance excitation.
3. Recognizing that multiply charged precursor ions (typically 2+, 3+, 4+) tend to produce mainly singly charged fragments following CID. This reflects the redistribution of available protons during fragmentation: since a single proton is sufficient to stabilize a small product ion, one fragment usually carries a single positive charge while the complementary fragment retains the remainder. In ion-trap instruments, this behavior is accentuated by trapping dynamics and detection bias toward singly charged species, which simplifies the resulting spectra and facilitates sequence interpretation.
4. Control and regulate the number of ions entering into the trap, ensuring consistent signal intensity and preventing space-charge effects. Overfilling the trap can distort ion motion, broaden peaks, and suppress detection of low-abundance species.

As proof-of-concept the HSA1 glycated bearing three units of glucose was analyzed in MS/MS scan mode. The results in Fig.17 and Fig.18.

After full MS scan the parent ion corresponding to the second charge, $[M+2H^+]^{2+}$ 1129.68 was isolated and through CID fragmentated in wide band mode. It was possible to identify the presence of diagnostic neutral-loss series of −36, −54 Da corresponding primarily to the loss of two or three water molecules.

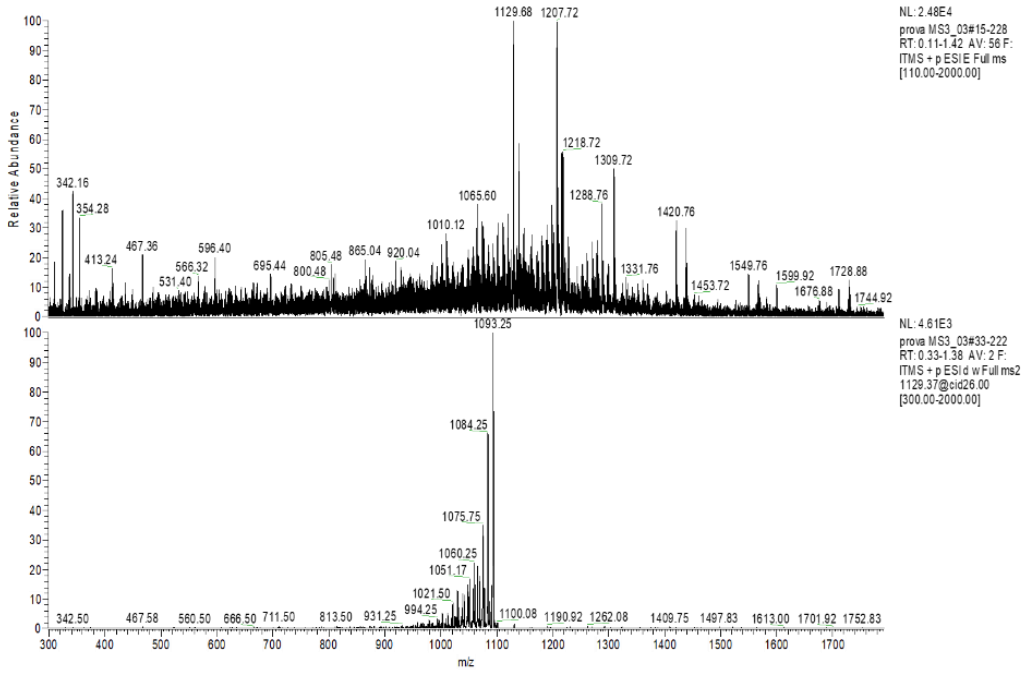

Fig.17: MS spectra (LTQ XL™ mass spectrometer, Thermo Scientific); direct infusion of HSA1 glycated peptide, MS full $[M+2H^+]^{2+}$: 1129,68 corresponding to the HSA1+3Glc.

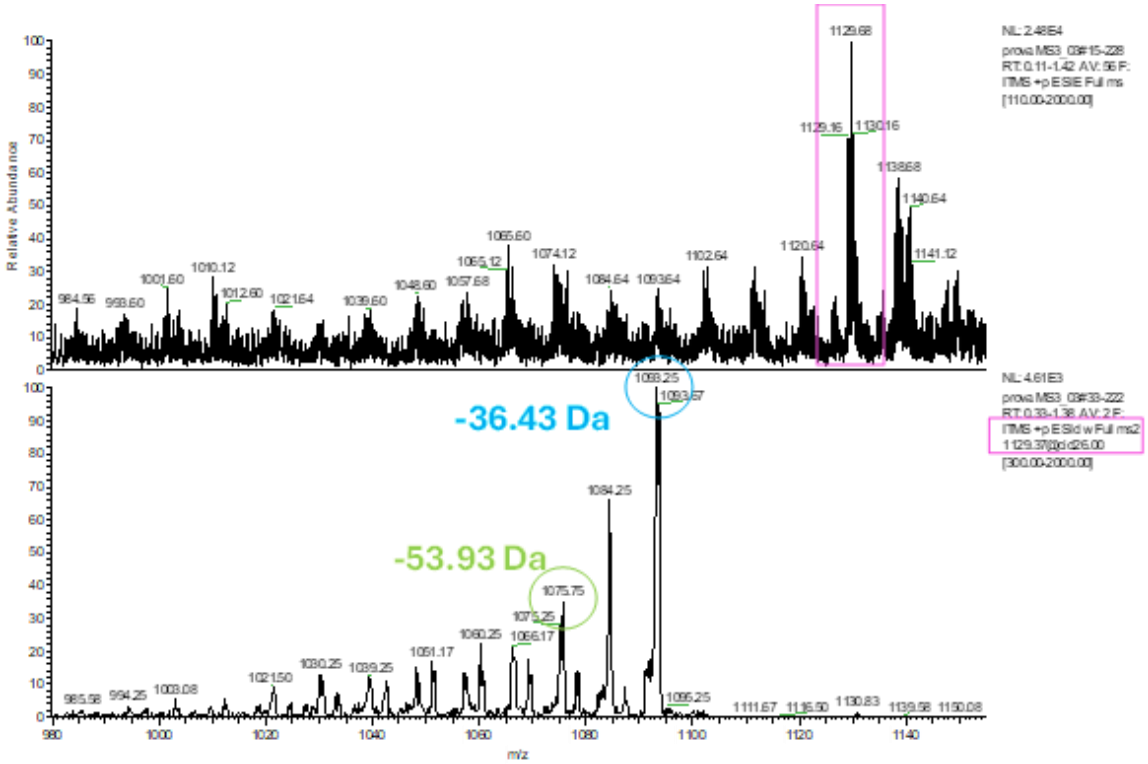

Fig.18: MS spectra (LTQ XL™ mass spectrometer, Thermo Scientific); direct infusion of HSA1 glycated, MS/MS scan in wide band, parent ion:1129,68, peaks corresponding to the loss of 3 and 4 molecules of water.

MS spectrometry results offer an unparalleled combination of selectivity, sensitivity, and structural detail for the study of peptide/protein glycation. It was possible to recognize the typical finger-print of an Amadori compound.

The LTQ XL™ linear ion-trap exemplifies how sensitive, rapid, and flexible MS instrumentation can be applied to biomedical questions such as the identification of glycation biomarkers in T2DM.

4. Conclusion and future perspectives

Glycation and the formation of advanced glycation end-products (AGEs) represent fundamental, non-enzymatic processes linking chronic hyperglycemia to cellular dysfunction, inflammation, and vascular complications in diabetes mellitus. Despite extensive biochemical knowledge, the analytical characterization of glycated species has remained challenging due to their structural heterogeneity, low abundance, and variable physicochemical properties. Conventional bulk assays, including spectrophotometric or immunochemical techniques, lack the molecular specificity required for site-resolved glycation profiling.

Consequently, developing selective enrichment tools and high-resolution analytical workflows is essential to bridge the gap between biochemical insight and clinical translation.

In this context, the present research aimed to design and validate a new generation of boronate-functionalized solid supports tailored for the selective capture of early glycation products, especially Amadori peptides, representing promising markers of short-term glycemic control.

Building upon the well-established affinity of boronic acids for cis-diols, this study systematically investigated how ligand architecture, substitution pattern, and polymeric backbone influence binding selectivity and efficiency. The ultimate goal was to integrate such tailored boronate-affinity materials into a robust analytical platform coupled to high-resolution tandem mass spectrometry (MS/MS and MS^3), enabling the identification and characterization of glycated peptides directly from complex biological matrices such as serum.

A panel of eight boronate-functionalized resins was synthesized and characterized, differing by both the nature of the polymeric support—ChemMatrix® Rink Resin (CMXRR) and ω-aminohexyl–agarose (AGRR)—and by the substitution pattern of the phenylboronic acid moieties (*para* or *meta*) as well as the degree of functionalization (mono- versus bi-substituted). This design enabled a systematic exploration of how electronic and steric factors influence the interaction between the boronate ligand and the diol-bearing Amadori adducts. Elemental analysis and UV quantification confirmed successful functionalization, with loadings ranging from 0.15 to 0.52 mmol g^{-1} depending on resin type and coupling efficiency.

A rational series of screening experiments was performed using synthetic model peptides that mimicked glycated, glycosylated, and non-modified sequences. The results revealed that mono-substituted *meta*-phenylboronic acid derivatives, Ac-Lys(*m*-PhB)–ChemMatrix® (R4) and Ac-Lys(*m*-PhB)–Agarose (R8), displayed the most favorable balance between selectivity and binding capacity. In contrast, bi-functionalized variants tended to exhibit steric hindrance and diminished selectivity. Notably, the polymeric backbone exerted a marked influence on performance: the PEG-based ChemMatrix® support (R4) consistently outperformed its agarose counterpart, most likely due to superior swelling, flexibility, and solvent accessibility of the active boronate sites. These findings underscored the cooperative role of electronic, steric, and microenvironmental factors in dictating boronate–diol complexation efficiency.

Subsequent experiments compared the optimized in-house resin (R4) to commercial m-aminophenylboronic acid–agarose (PBA–agarose). Under equimolar conditions, both materials showed comparable binding capacity; however, under competitive low-abundance scenarios, only R4 retained

significant selectivity for Amadori peptides. This superior performance under realistic analytical conditions confirmed the critical impact of resin architecture and highlighted R4 as a highly selective platform for analytical glycation studies.

Building on these results, the optimized workflow was applied to increasingly complex peptide mixtures, including tryptic digests of human serum albumin and serum samples from patients affected by type 2 diabetes mellitus (T2DM). Boronate-affinity enrichment with R4 followed by LC–ESI–MS analysis revealed distinct simplification of complex spectra and enhanced detection of glycated peptides. The deconvoluted MS profiles of enriched fractions demonstrated clear enrichment of Amadori-modified fragments, confirming both the selectivity and robustness of the material when applied to biological matrices. These findings validate the feasibility of coupling boronate-affinity chromatography with high-resolution mass spectrometry for selective profiling of glycated peptides directly from serum samples.

The introduction of multi-stage tandem mass spectrometry (MS^n) further enhanced structural characterization. Using an LTQ XL™ linear ion trap, data-dependent acquisition enabled rapid multi-scan analysis of glycated peptides, including MS^3 experiments. In particular, the controlled fragmentation of the model peptide HSA1 bearing three glucose units provided clear diagnostic patterns of sequential neutral losses (−18 Da, −36 Da, −54 Da, −84 Da), corresponding to stepwise elimination of water and formaldehyde molecules. These spectral fingerprints are consistent with the characteristic fragmentation cascade of Amadori compounds, confirming successful detection and structural assignment of glycation sites. The ability to perform MS^3 scans greatly improved confidence in site localization, enabling differentiation between

isomeric glycated forms and validating the analytical power of the developed workflow.

Collectively, the results obtained in this work demonstrate that carefully engineered boronate-functionalized supports, in combination with advanced MS-based detection, provide a powerful and selective strategy for the study of early glycation events. The optimized resin (R4) achieved high selectivity (≈40% capture yield) with minimal nonspecific adsorption (<10%), outperforming commercial materials and maintaining reproducibility in complex biological samples. Furthermore, the integration of multi-scan mass spectrometry enabled unambiguous identification of Amadori modifications, offering molecular-level insight into glycation chemistry and paving the way for quantitative biomarker applications.

From a broader perspective, this work establishes a methodological framework that bridges synthetic chemistry, affinity materials design, and analytical glycoproteomics. The proof-of-concept validation on HSA and serum samples supports the translational potential of this approach for identifying clinically relevant glycated peptide markers in diabetes. Beyond its immediate analytical implications, the workflow developed here could be adapted to other biomolecular contexts, including oxidative or carbonyl stress-related modifications, and extended toward quantitative proteomic platforms for precision medicine.

In conclusion, the study advances the state of the art in glycation analysis by demonstrating that rationally designed boronate supports can provide both high selectivity and compatibility with downstream mass spectrometric workflows. The combination of boronate-affinity capture and multi-MS scanning represents

a synergistic platform capable of dissecting the complexity of protein glycation at unprecedented resolution. The preliminary MS^3 data obtained herein not only confirm the robustness of the workflow but also highlight its potential for uncovering novel glycation biomarkers that could refine the monitoring of short-term glycemic dynamics in T2DM. Future developments will focus on expanding validation to larger patient cohorts, optimizing quantitative LC–MS/MS assays, and exploring miniaturized or sensor-based implementations of the boronate-affinity concept. Together, these advances lay the foundation for translating analytical innovation into clinically meaningful glycation diagnostics.

5. Experimental part

5.1 ChemMatrix® Rink resin and Agarose Rink resin functionalization with boronate units

5.1.1 Synthesis of p-PhB-Lys(p-PhB)-ChemMatrix® Rink resin (Resin **1**) and m-PhB-Lys(m-PhB)-ChemMatrix® Rink resin (Resin **2**)

The ChemMatrix® Rink resin (1.035 g, loading 0.60 mmol/mg) was weighted in a plastic syringe with a filter and swelled in DMF for 30 min. Fmoc-Lys-Fmoc-OH was used in 3-fold excess and activated with HBTU (3 eq) and DIPEA (6 eq) in DMF for the coupling on the resin. The coupling mixture was stirred for 40 min at 25°C. After the coupling reaction, the resin was filtered and washed with DMF (3 x 10 ml) and DCMX (5 x 10 ml). The reaction was monitored by Kaiser test. After Fmoc-deprotection from N-terminus and ε-amino group of lysine by 20% piperidine in DMF (v/v), the resin was washed with DMF (3 x 10 ml) and with DCMX (5 x 10 ml). A solution of 4-carboxyphenylboronic acid (p-PhB-OH, 6 eq, to obtain Resin 1) and of 3-carboxyphenylboronic acid (m-PhB-OH, 6 eq, to obtain Resin 2), HBTU (6 eq) and DIPEA (12 eq) dissolved in DMF (10 ml) was added to the syringe containing the functionalised resin Lys-CMXRR. The reaction was stirred for 40 min at 25 °C. Once reactions were complete, the resins were washed with: DMF (7 × 5 min) and DCMX (3 × 5 min). Each coupling was checked by Kaiser test and repeated if necessary. The resins were then dried under vacuum for 3 days. Both p-PhB-Lys(p-PhB)-NH 2 and m-PhB-Lys(m-PhB)-NH 2 were cleaved in 3 h using a mixture of TFA/H2O/TIS (95:2.5:2.5) (v:v:v). The solution was evaporated under a gentle stream of nitrogen and then lyophilised and used to evaluate final loading. Resin 1: p-PhB-Lys(p-PhB)-CMXRR: obtained 3.001g; loading: 0.462 mmol/g. Resin 2: m-PhB-Lys(m-PhB)—CMXRR: obtained 0.533g; loading 0.289 momol/g.

5.1.2 Synthesis of Ac-Lys(p-PhB)-ChemMatrix® Rink resin (Resin **3**) and Ac-Lys(m-PhB)-ChemMatrix® Rink resin (Resin **4**)

Ac-Lys(p-PhB)-CMXRR was obtained by coupling Fmoc-Lys(Mtt)-CMXRR with 4-carboxyphenylboronic acid and after Fmoc-deprotection the N α amino function was acetylated with Ac 2 O to obtain resin 3. The same procedure was followed for the synthesis of Ac-Lys(m-PhB)-CMXRR (resin 4), using 3-carboxyphenylboronic acid. The ChemMatrix® Rink resin (0.508 g for Resin 3, 0.496 g for Resin 4, loading 0.60 mmol/mg) was weighted in a plastic syringe with a filter and swelled in DMF for 30 min. The Fmoc-Lys(Mtt)-OH coupling was performed as described for Fmoc-Lys(Fmoc)-OH (see paragraph 3.4.3.1). In order to remove the Mtt protecting group a solution of TFA/TIS/DCMX (1%, 5%, 94%, v:v:v) was added to the resin Fmoc-Lys-CMXRR, refreshing four times the solution. A solution of phenylboronic acid (PhB-OH, 3 eq), HBTU (3 eq), and DIPEA (6 eq) dissolved in DMF (10 ml) was added to the syringe containing Fmoc-Lys-CMXRR. The Resin 3 was obtained coupling 4-carboxyphenylboronic acid (p-PhB-OH) and the Resin 4 was obtained coupling 3-carboxyphenylboronic acid (m-PhB-OH). The reaction was stirred for 40 min at
25 °C. Once reactions were complete, the resins were washed with: DMF (7 × 5 min) and DCMX (3 × 5 min). The N α -amino functions of Resin 3 and Resin 4 were acetylated adding a solution of acetic anhydride (AcO 2 , 10 eq) and DIPEA (10 eq) in DMF and stirred for 1 h. The resins were filtered and washed with DMF (3 x 10 ml) and DCMX (5 x 10 ml). The reactions were monitored by Kaiser Test. The resin was then dried under vacuum for 3 days. A small quantity of Ac-Lys(p-PhB)-NH 2 and Ac-Lys(m-PhB)-NH 2 were cleaved with a TFA/H2O/TIS (95:2.5:2.5) (v:v:v) solution for 3h a r.t. The solution was evaporated under a gentle stream of nitrogen and then lyophilised and used to evaluate final loading. Resin 3: Ac-

Lys(p-PhB)-CMXRR: obtained 0.549 g; loading: 0.354 mmol/g. Resin 4: Ac-Lys(m-PhB)-CMXRR: obtained 0.487 g; loading: 0.151 mmol/g.

5.1.3 Synthesis of p-PhB-Lys(p-PhB)-Agarose Rink resin (Resin **5**) and m-PhB-Lys(m-PhB)-Agarose Rink resin (Resin **6**)

The Agarose gel (Affigel 102® BioRad, 5 ml, loading 15µmol/ml) was placed in a plastic syringe with a filter and swelled in a DMF/H 2 O solution (65:35, v:v) for 30 min. The Fmoc-Rink Linker coupling (3eq) on the resin was performed with HATU (3eq) and DIPEA (6eq) for 2h at 25 °C. The resin was filtered and washed with DMF and H2O. The reaction was monitored by Kaiser test and coupling was repeated with fresh solution. After Fmoc deprotection by a 20% piperidine solution in DMF (v:v), a solution of Fmoc-Lys(Fmoc)-OH (3eq), HATU (3eq), and DIPEA (6eq) dissolved in DMF was added. The coupling reaction was stirred for 2h at 25 °C. After then, the resins were washed with DMF and H 2 O in order to remove the soluble side-products and the excess of reagents. In order to perform the coupling reaction with p-PhB-OH to obtain Resin 6 or m-PhB-OH to obtain Resin 7, the Fmoc protecting groups were removed by 20% piperidine solution in DMF (v:v). A solution of 4-carboxyphenylboronic acid (p-PhB-OH, 6 eq, to obtain Resin 6) and of 3-carboxyphenylboronic acid (m-PhB-OH, 6 eq, to obtain Resin 7), HATU (6 eq) and DIPEA (12 eq), was dissolved in DMF (10 ml), then added to the syringe containing the functionalized resin Lys-AGRR. The reaction was stirred for 40 min at 25 °C. Once reactions were complete, the resins were washed with: DMF (7 × 5 min) and H2O (3 × 5 min). Each coupling was checked by Kaiser test and repeated if necessary. Both p-PhB-Lys(p-PhB)-NH 2 and m-PhB-Lys(m-PhB)-NH 2 were cleaved in 3 h using a mixture of TFA/H 2 O/TIS (95:2.5:2.5, v:v:v). The solution was evaporated under a gentle stream of

nitrogen and then lyophilised and used to evaluate final loading. Resin 5: p-PhB-Lys(p-PhB)-AGRR: loading 6.5 μmol/ml. Resin 6: m-PhB-Lys(m-PhB)-AGRR: loading 7.4 μmol/ml.

5.1.4 Synthesis of Ac-Lys(p-PhB)-Agarose Rink resin (Resin 7) and Ac-Lys(m-PhB)-Agarose Rink resin (Resin 8)

The Agarose gel (Affigel 102® BioRad, 5 ml, loading 15 μmol/ml) was placed in a plastic syringe with a filter and swelled in a DMF/H 2 O solution (65:35, v:v) for 30 min. The Fmoc-Rink Linker coupling (3eq) on the resin was performed with HATU (3eq) and DIPEA (6eq) for 2h at 25 °C. The resin was filtered and washed with DMF and H 2 O. The reaction was monitored by Kaiser test and the solution was refreshed to repeat the coupling (Scheme 4). After Fmoc-linker deprotection by a 20% piperidine solution in DMF (v:v), Fmoc-Lys(ivDde)-OH (3eq), HATU (3eq), and DIPEA (6eq) dissolved in DMF were added to the resin for 2h at 25 °C. The Fmoc-Lys(ivDde)-AGRR was washed with DMF and H 2 O in order to remove the soluble side-products and the excess of reagents. To remove the Fmoc group on α-amino Lys function, 20% piperidine solution in DMF (v:v) was added and successively the free amino group was acetylated with acetic anhydride (AcO 2 , 10eq) and DIPEA (10eq) in DMF and stirred for 1 h to obtain Ac-Lys(ivDde)-AGRR. The ivDde protecting group was removed with a 2% hydrazine monohydrate solution in DMF(v:v), refreshing three times. A solution of 4-carboxyphenylboronic acid (p-PhB-OH, 3eq, to obtain Resin 7) and of 3-carboxyphenylboronic acid (m-PhB-OH, 3eq, to obtain Resin 8), HATU (3eq) and DIPEA (6eq) dissolved in DMF (10 ml) was added to the syringe containing the Ac-Lys-AGRR. The reactions were stirred for 40 min at 25 °C (Scheme 6). Once reactions were complete, the resins were washed with: DMF (7 × 5 min) and H 2

O (3 × 5 min). Each coupling was checked by Kaiser test and repeated if necessary. Small amounts of Ac-Lys(p-PhB)-NH2 and Ac-Lys(m-PhB)-NH 2 were cleaved with a TFA/H 2 O/TIS solution (95:2.5:2.5, v:v:v) for
3h a r.t. The solution was evaporated under a gentle stream of nitrogen, lyophilised and used to evaluate final loading. Resin 7: Ac-Lys(p-PhB)-AGRR: loading: 4.3 μmol/ml; Resin 8: Ac-Lys(m-PhB)-AGRR: obtained loading: 3.2 μmol/ml.

5.1.5 Loading of the new functionalized phenylboronate resins

The calibration curve was calculated plotting peak area average (y) against concentration of standards (x). A stock solution was prepared weighting 6.64 mg (4 × 10 -5 mol) of 4-carboxyphenylboronic acid (Sigma Aldrich, M=165.94 g/mol) dissolved in 10 ml H 2 O/MeCN (1:1, v/v, conc. 4 mM). Eight working solutions for calibration curve plotting, were prepared by serial dilution of the initial sample (0.1 mM, 0.05 mM, 0.02 mM, 10 μM, 5 μM, 2 μM, 1 μM). H2O/MeCN (1:1, v/v) solution was used as blank sample. The samples were measured at λ 236 nm by UV-Vis Spectroscopy, using Cary 4000 UV-Vis Spectrophotometer (Palo Alto, California, USA) with quartz cells. Curves with correlation coefficients (R^2) 0.998 were generated.

5.2 Synthesis of glycated peptides

5.2.1 Solid-phase peptide synthesis by microwave automated synthesizer

5.2.1.1 Procedure for Microwave-assisted automatic SPPS

The synthesis of ERQIKKQTALVELVK (HSA1) and SSAKQRLKCASLQ (HSA2) was carried out on a Liberty Blue™ automatic synthesizer equipped with a Teflon

reaction vessel. A Fmoc/tBu orthogonal protection strategy was used while microwaves were applied both in coupling and deprotection steps. Nitrogen bubbling ensured thorough mixing during all the reactions.

The resins Fmoc-Lys(Boc)-wang resin and Fmoc-Gln(Trt)-wang resin (loading 0.6 mmol/g), was weighed and put in the reaction vessel for 15 min to allow swelling. In the meantime, amino acid building blocks solution, coupling and deprotection solutions were prepared with the following concentrations, based on a 0.025 scale synthesis: amino acid building block 0.2 M, Piperidine 20% in DMF , Oxyma Pure 0.5 M, DIC 0.25 M.

Following peptide synthesis, the final deprotection was carried out manually. The resin was initially swollen in fresh DMF for 10 minutes and subsequently filtered under vacuum. A 20% piperidine solution in DMF was then added for 5 minutes, after which the solution was removed by vacuum filtration. A second portion of 20% piperidine in DMF was applied for 10 minutes, followed by filtration. The resin was finally washed sequentially with fresh DMF and DCMX and subsequently dried under vacuum.

Cleavage was carried out with the following mixtures: 92.5:2.5:2.5 TFA:TIS:H_2O 92.5:2.5:2.5:2.5 H_2O:DODT:TIS:H_2O. For each 100 mg of resin 1 mL cleavage solution was used, with an excess of 1 mL. The resin was mixed for 2h at room temperature. After the resin was filtered and the liquid collected, the addition of cold diethyl ether caused the peptide to precipitate. To enhance this process, the falcons were placed at -20°C for 20 minutes. Afterwards, centrifugation was performed at 4°C for 5 minutes at 4000 rpm. The cold diethyl ether was drained, and the process was repeated twice. Finally, the filtered product was lyophilized.

5.2.1.2 Boratyński protocol reaction for peptide glycation

A mixture of 1:1:1 (*v:v:v)* of synthetic peptides (20 mg/mL in H_2O):D-glucose (40mg/mL in H_2O):0.1M phosphate buffer pH8. Then the solution was freeze dried until complete lyophilization, then they were heated for 40 min at 104 °C.

5.3 Boronate affinity chromatography: from peptide to complex biological mixtures

5.3.1 General procedure of capturing of glycated peptides by the new functionalized resin (R1 – R8)

The general procedure optimised for PhB-Lys(PhB)-CMXRR described in Molecules 2020, 25, 755, p. 8 – DOI 10.3390/molecules25030755 was applied with each functionalised resin R1 – R8 to capture separately equimolar concentrations of all synthetic peptides P2–P8.

After 1h of capturing reaction, the filtrate and washing solutions were collected (flow through, FT). Subsequent cleavage in acidic conditions led to the filtrate with captured peptides (eluted), which together with washing solutions was combined into the final solution. Both fractions were then lyophilized. Each lyophilized sample was dissolved in H2O (1.0 mL). FT and eluted solutions were then analysed by UV-HPLC, to calculate the yield of capturing by the following formula: Abs eluted/(Abs eluted+Abs FT) * 100%

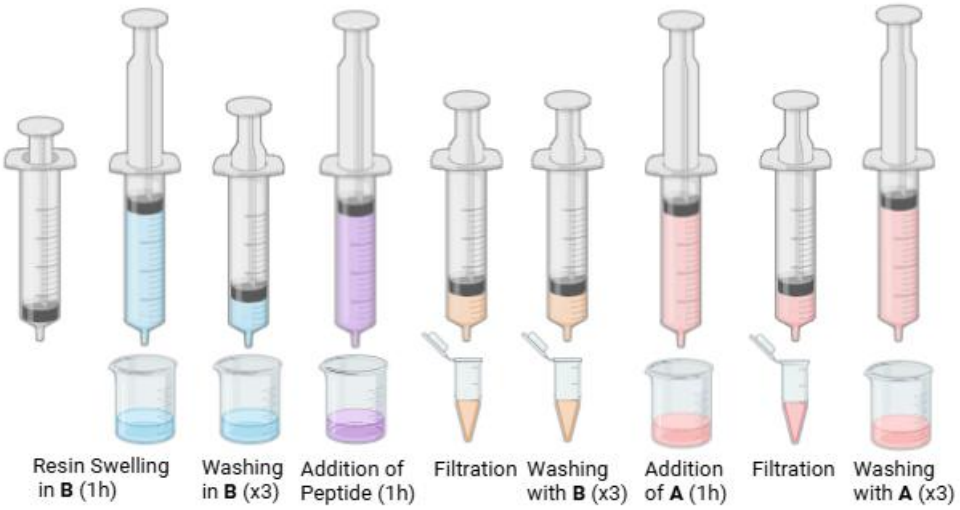

Fig.19: Procedure of capturing and cleaving peptides by the Resin

5.3.2 Experiment 1: Screening of meta-PhB-functionalized resins CMXRR (R2, R4) Resin and meta AGRR resin (R6, R8)

Basic solutions ad hoc containing the equimolar concentrations of each peptide sequences P1-P8 was prepared and used following the general capturing protocol described above with each meta resin R2, R4, R6, R8. All the fractions (FT and eluted from resins) were collected, lyophilized, and analyzed by LC-UV-MS.

5.3.3 Experiment 2: Comparison of selected para CMXRR Resin (R3) and para AGRR resin (R7)

Selected resins R3 and R7 were used to capture the equimolar concentrations of each one separately peptide sequences P1-P8 following the general capturing protocol described in 5.3.1

5.3.4 Experiment 3: Capturing comparison of Ac-Lys(m-PhB)-CMXRR(R4) and PBA-agarose resins

Two ad hoc aqueous solutions, containing the equimolar concentrations of [Lys7(1-deoxyFru)]CSF114 (P8) and Asn7(Glc)CSF114 (P9) peptides with same concentration, or 5% w/w P8:P9, were prepared and used following the general capturing protocol described above. All the fractions (FT and released from PBA-agarose (A8530), (R4) Ac-Lys(m-PhB)-CMXRR and (R8) Ac-Lys(m-PhB)-AGRR resins) were collected, lyophilized, and analyzed by LC-UV-MS to check the capturing efficiency towards Amadori and non-Amadori peptides in different concentrations. One ad hoc aqueous solution containing the equimolar concentrations of complex mixture of different non-Amadori peptides (μmol/mL), including two Amadori peptides P1 and P8, at the same concentration (μmol/mL), was prepared and used following the general capturing protocol described above. All the fractions uncaught and released were collected, lyophilized, and analyzed by LC-UV-MS to calculate the yield of capturing.

5.4 Trypsin/Chymiotrypsin Digestion Protocol

The protein and sera samples were denatured and reduced in 50 mM ammonium bicarbonate buffer pH 7.8. Disulfide bonds were reduced using tris(2-

carboxyethyl)phosphine (TCEP) and alkylated with iodoacetamide to prevent reformation. Digestion was performed by adding trypsin at a 1:25 enzyme-to-protein ratio (w/w), followed by incubation at 37°C for 12 hours. The reaction was terminated by lowering the pH to <4 with formic acid. For chymotrypsin digestion, analogous conditions were employed, with pH adjusted to 7.8 and the enzyme-to-protein ratio optimized accordingly.

5.5 LC-MS Analysis

The elution of peptides/tryptic digested peptide mixtures followed a linear gradient from 10%B to 60%B over 25 minutes, at a flow rate of 0.4 mL/min and a column temperature of 35°C, with detection at 214 nm and injection of 10µg of protein on the column. The desalting step was performed with a gradient starting with 100% 0.1% FA in H_2O for 2 minutes, then gradually shifting to 50% acetonitrile over 0.5 minutes. This was maintained isocratically for the next 2.5 minutes, followed by a final ramp to 100% ACN over the last 2 minutes. The flow rate was set to 0.5 mL/min, with injection volumes ranging from 1 to 5 µL.

For mass spectrometric detection, the LTQ XL (Thermo Scientific) mass spectrometer was employed, running in positive ion mode. Full mass spectra were collected within an m/z range from 150 to 2000, applying in-source collision-induced dissociation (CID) at 80 eV.

Appendix 1 - LTQ XL™ mass spectrometer

For the study and characterization of specific biomarker of glycated peptides in patient affected by diabetes (T2DM), the spectrometer of choice has been the LTQ XL™ mass spectrometer by Thermo Scientific.

This system is a quadrupole based linear ion trap (LIT) mas spectrometer designed for rapid multi MS scan with high sensitivity. In Fig.1 it is shown the schematic representation of the parts that make up the instrumentation.

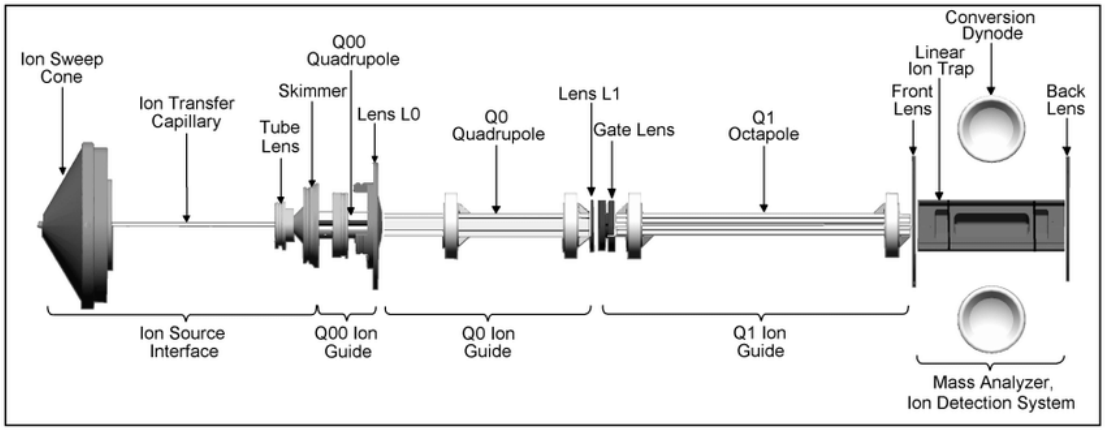

Fig.1: Schematic representation of the LTQ XL mass spectrometer, showing Ion source, the three quadrupoles (Q00, Q0, Q1) and, the ion trap.

Electrospray ion source and inlet system

Peptides eluting from the LC column are nebulized under an applied potential (2–4 kV). The aerosol enters the instrument through a heated capillary, which aids desolvation, and passes through a tube-lens/skimmer assembly that focuses the ions and removes neutral contaminants.

Ion optics and RF guides

A series of multipole RF ion guides transmit ions through differentially pumped regions, maintaining ion current while progressively reducing pressure from atmospheric (~1 mbar) to high-vacuum (~10^{-5} mbar) levels.

Linear ion trap analyzer

Ions are radially confined by oscillating RF fields between parallel rods and axially trapped by DC end electrodes. During an MS scan, ions are accumulated, then sequentially ejected according to their m/z dependent resonance frequency and detected. For tandem MS, a selected precursor is isolated in a narrow m/z window and subjected to resonant CID with helium as collision gas. The trap can perform multiple stages (MS^n) of fragmentation, which is particularly valuable for confirming glycation sites.

List of Symposium Proceedings- PhD student Margherita Marino

[**1**] Marino M., Paolo Rovero, Walter Mier, Hendrik Rusche, Anna Maria Papini. *"Innovative liquid chromatographic-mass spectometric technologies to purify and identify biologically active antibody-drug conjugates"* *h*ttps://doi.org/10.17952/37EPS.2024.P2136

[2] F. Nuti, M. Marino, P. Ledwon, R. Latajka, A. Lapolla, M. Chorev, P. Rovero, A.M. Papini. *"A fishing technology of glycated peptides"*https://doi.org/10.17952/37EPS.2024.P2186

List of Publications- PhD student Margherita Marino

[1] F. Nuti, M. Marino, P. Ledwon, R. Latajka, A. Lapolla, M. Chorev, P. Rovero, A.M. Papini. *"A strategy to trap glycated peptides in human sera of patient affected by diabetes"* Internal revision.

[2] Book chapter: "Preparation, purification and characcterization of Antibody Drug Conjugates", book Antibody Drug Conjugate, Topics in Medical Chemistry. Internal revision.

List of *oral communications* at conferences - PhD student Margherita Marino

- [OR121] Marino M., Paolo Rovero, Walter Mier, Hendrik Rusche, Anna Maria Papini.

*"Antibody-drug conjugates: a strategy of purification and characterization".*54th International Symposium on High Performance Liquid Phase Separations and Related Techniques (HPLC2025), Bruges (Belgium), June 15-19, 2025. Flash oral presentation.

The PhD student M. Marino attended the Symposium from remote and presented the oral communication.

- [OR63] **Marino, M.**, Papini A.M. Innovative liquid chromatographic-mass spectrometric technologies to purify and identify biologically active antibody-drug conjugates.PiCSU2025 PhD in chemical sciences at UNIFI, Sesto Fiorentino (Italy), January 14-17 Flash oral presentation.

The PhD student M. Marino attended the Symposium from remoteand presented the oral communication.

- [OR02] **Marino, M.**, Papini A.M. "*Innovative liquid chromatographic-mass spectrometric technologies to purify and identify glycated and glycosylated proteins in biological fluids*". PiCSU2024 PhD in chemical sciences at UNIFI, Sesto Fiorentino (Italy), January 23-26. Flash oral presentation.

The PhD student M. Marino attended the Symposium from remote and presented the oral communication.

List of *poster communications* at conferences - PhD student Margherita Marino

- [BIO-23] Marino M., Paolo Rovero, Walter Mier, Hendrik Rusche, Anna Maria Papini.

"Antibody-drug conjugates: a strategy of purification and characterization".54th International Symposium on High Performance Liquid Phase Separations and Related Techniques (HPLC2025), Bruges (Belgium), June 15-19, 2025. Poster Communication BIO-23

The PhD student M. Marino personally attended the Symposium and presented the poster session.

- [P16] Marino M., Paolo Rovero, Walter Mier, Hendrik Rusche, Anna Maria Papini.

"Innovative liquid chromatographic-mass spectometric technologies to purify and identify
biologically active antibody-drug conjugates" 2nd Internation Mass School, Ion Mobility Mass Spectrometry, Erice (Italy), September 09-14 2024. Poster communication

The PhD student M. Marino personally attended the Symposium and presented the poster session.

- [P2136] Marino M., Paolo Rovero, Walter Mier, Hendrik Rusche, Anna Maria Papini.

"Innovative liquid chromatographic-mass spectometric technologies to purify and identify
biologically active antibody-drug conjugates" 37th European Peptide Symposium and 14th International Peptide symposium, Firenze (Italy), August 25-29 2024. Poster communication

The PhD student M. Marino personally attended the Symposium and presented the poster session.

- [P2186] F. Nuti, M. Marino, P. Ledwon, R. Latajka, A. Lapolla, M. Chorev, P. Rovero, A.M. Papini. *"A fishing technology of glycated peptides"* 37th European Peptide Symposium and 14th International Peptide symposium, Firenze (Italy), August 25-29 2024. Poster communication

- [POS11] Marino M., Paolo Rovero, Hendrik Rusche, Anna Maria Papini.

"Innovative liquid chromatographic-mass spectrometric technologies to purify and identify glycated and glycosylated proteins in biological fluids" PiCSU2023 PhD in chemical sciences at UNIFI, Sesto Fiorentino (Italy), January 25-27. . Poster communication

The PhD student M. Marino personally attended the Symposium and presented the poster session.

6. Bibliography

(1) Breedveld, F. Therapeutic Monoclonal Antibodies. *The Lancet* **2000**, *355* (9205), 735–740. https://doi.org/10.1016/S0140-6736(00)01034-5.

(2) Leavy, O. Therapeutic Antibodies: Past, Present and Future. *Nat. Rev. Immunol.* **2010**, *10* (5), 297–297. https://doi.org/10.1038/nri2763.

(3) Chames, P.; Van Regenmortel, M.; Weiss, E.; Baty, D. Therapeutic Antibodies: Successes, Limitations and Hopes for the Future. *Br. J. Pharmacol.* **2009**, *157* (2), 220–233. https://doi.org/10.1111/j.1476-5381.2009.00190.x.

(4) Nelson, A. L.; Dhimolea, E.; Reichert, J. M. Development Trends for Human Monoclonal Antibody Therapeutics. *Nat. Rev. Drug Discov.* **2010**, *9* (10), 767–774. https://doi.org/10.1038/nrd3229.

(5) Weiner, G. J. Building Better Monoclonal Antibody-Based Therapeutics. *Nat. Rev. Cancer* **2015**, *15* (6), 361–370. https://doi.org/10.1038/nrc3930.

(6) Singh, R.; Chandley, P.; Rohatgi, S. Recent Advances in the Development of Monoclonal Antibodies and Next-Generation Antibodies. *ImmunoHorizons* **2023**, *7* (12), 886–897. https://doi.org/10.4049/immunohorizons.2300102.

(7) Xu, Z.; Ismanto, H. S.; Zhou, H.; Saputri, D. S.; Sugihara, F.; Standley, D. M. Advances in Antibody Discovery from Human BCR Repertoires. *Front. Bioinforma.* **2022**, *2*, 1044975. https://doi.org/10.3389/fbinf.2022.1044975.

(8) Buss, N. A.; Henderson, S. J.; McFarlane, M.; Shenton, J. M.; De Haan, L. Monoclonal Antibody Therapeutics: History and Future. *Curr. Opin. Pharmacol.* **2012**, *12* (5), 615–622. https://doi.org/10.1016/j.coph.2012.08.001.

(9) Vidarsson, G.; Dekkers, G.; Rispens, T. IgG Subclasses and Allotypes: From Structure to Effector Functions. *Front. Immunol.* **2014**, *5*. https://doi.org/10.3389/fimmu.2014.00520.

(10) Vermeer, A. Adsorption of IgG onto Hydrophobic Teflon. Differences between the Fab and Fc Domains. *Biochim. Biophys. Acta BBA - Gen. Subj.* **2001**, *1526* (1), 61–69. https://doi.org/10.1016/S0304-4165(01)00101-5.

(11) Types of Antibodies: Structure, Isotypes, and Functions.

(12) Hinkle, J. D.; D'Ippolito, R. A.; Panepinto, M. C.; Wang, W.-H.; Bai, D. L.; Shabanowitz, J.; Hunt, D. F. Unambiguous Sequence Characterization of a Monoclonal Antibody in a Single Analysis Using a Nonspecific Immobilized Enzyme Reactor. *Anal. Chem.* **2019**, *91* (21), 13547–13554. https://doi.org/10.1021/acs.analchem.9b02666.

(13) Jay, J. W.; Bray, B.; Qi, Y.; Igbinigie, E.; Wu, H.; Li, J.; Ren, G. IgG Antibody 3D Structures and Dynamics. *Antibodies* **2018**, *7* (2), 18. https://doi.org/10.3390/antib7020018.

(14) Lu, J.; Chu, J.; Zou, Z.; Hamacher, N. B.; Rixon, M. W.; Sun, P. D. Structure of FcγRI in Complex with Fc Reveals the Importance of Glycan Recognition for High-Affinity IgG Binding. *Proc. Natl. Acad. Sci.* **2015**, *112* (3), 833–838. https://doi.org/10.1073/pnas.1418812112.

(15) Kiyoshi, M.; Caaveiro, J. M. M.; Kawai, T.; Tashiro, S.; Ide, T.; Asaoka, Y.; Hatayama, K.; Tsumoto, K. Structural Basis for Binding of Human IgG1 to Its High-Affinity Human Receptor FcγRI. *Nat. Commun.* **2015**, *6* (1), 6866. https://doi.org/10.1038/ncomms7866.

(16) Davies, A. M.; Sutton, B. J. Human IgG4: A Structural Perspective. *Immunol. Rev.* **2015**, *268* (1), 139–159. https://doi.org/10.1111/imr.12349.

(17) Mach, J.-P. Introduction to Monoclonal Antibodies. *Cancer Immun.* **2012**, *12*, 11.

(18) Nissim, A.; Chernajovsky, Y. Historical Development of Monoclonal Antibody Therapeutics. In *Therapeutic Antibodies*; Chernajovsky, Y., Nissim, A., Eds.; Starke, K., Series Ed.; Handbook of Experimental Pharmacology; Springer Berlin Heidelberg: Berlin, Heidelberg, 2008; Vol. 181, pp 3–18. https://doi.org/10.1007/978-3-540-73259-4_1.

(19) Zamani, M. R.; Šácha, P. Immune Checkpoint Inhibitors in Cancer Therapy: What Lies beyond Monoclonal Antibodies? *Med. Oncol.* **2025**, *42* (7), 273. https://doi.org/10.1007/s12032-025-02822-1.

(20) Pander, G.; Uhl, P.; Kühl, N.; Haberkorn, U.; Anderl, J.; Mier, W. Antibody–Drug Conjugates: What Drives Their Progress? *Drug Discov. Today* **2022**, *27* (10), 103311. https://doi.org/10.1016/j.drudis.2022.06.011.

(21) Chatzantoni, K.; Mouzaki, A. Anti-TNF-α Antibody Therapies in Autoimmune Diseases. *Curr. Top. Med. Chem.* **2006**, *6* (16), 1707–1714. https://doi.org/10.2174/156802606778194217.

(22) Nakahara, H.; Nishimoto, N. Anti-Interleukin-6 Receptor Antibody Therapy in Rheumatic Diseases. *Endocr. Metab. Immune Disord. - Drug Targets* **2006**, *6* (4), 373–381. https://doi.org/10.2174/187153006779025694.

(23) Marshall, M. J. E.; Stopforth, R. J.; Cragg, M. S. Therapeutic Antibodies: What Have We Learnt from Targeting CD20 and Where Are We Going? *Front. Immunol.* **2017**, *8*, 1245. https://doi.org/10.3389/fimmu.2017.01245.

(24) *Handbook of Therapeutic Antibodies*, Second edition.; Dübel, S., Reichert, J. M., Eds.; Wiley Blackwell: Weinheim, Germany, 2014.

(25) Chen, J.; Gao, K.; Wang, R.; Nguyen, D. D.; Wei, G.-W. Review of COVID-19 Antibody Therapies. *Annu. Rev. Biophys.* **2021**, *50* (1), 1–30. https://doi.org/10.1146/annurev-biophys-062920-063711.

(26) Yang, L.; Liu, W.; Yu, X.; Wu, M.; Reichert, J. M.; Ho, M. COVID-19 Antibody Therapeutics Tracker: A Global Online Database of Antibody Therapeutics for

the Prevention and Treatment of COVID-19. *Antib. Ther.* **2020**, *3* (3), 205–212. https://doi.org/10.1093/abt/tbaa020.
(27) Onrust, S. V.; Lamb, H. M.; Barman Balfour, J. A. Rituximab: *Drugs* **1999**, *58* (1), 79–88. https://doi.org/10.2165/00003495-199958010-00009.
(28) Ajina, R.; AlDeghaither, D.; Jablonski, S.; Weiner, L. M. Cancer Immunotherapy. In *Comprehensive Medicinal Chemistry III*; Elsevier, 2017; pp 32–65. https://doi.org/10.1016/B978-0-12-409547-2.12426-6.
(29) Weiner, G. J. Rituximab: Mechanism of Action. *Semin. Hematol.* **2010**, *47* (2), 115–123. https://doi.org/10.1053/j.seminhematol.2010.01.011.
(30) Salles, G.; Barrett, M.; Foà, R.; Maurer, J.; O'Brien, S.; Valente, N.; Wenger, M.; Maloney, D. G. Rituximab in B-Cell Hematologic Malignancies: A Review of 20 Years of Clinical Experience. *Adv. Ther.* **2017**, *34* (10), 2232–2273. https://doi.org/10.1007/s12325-017-0612-x.
(31) Johnson, P. W. M.; Glennie, M. J. Rituximab: Mechanisms and Applications. *Br. J. Cancer* **2001**, *85* (11), 1619–1623. https://doi.org/10.1054/bjoc.2001.2127.
(32) Schmiedel, J.; Blaukat, A.; Li, S.; Knöchel, T.; Ferguson, K. M. Matuzumab Binding to EGFR Prevents the Conformational Rearrangement Required for Dimerization. *Cancer Cell* **2008**, *13* (4), 365–373. https://doi.org/10.1016/j.ccr.2008.02.019.
(33) Socinski, M. A. Antibodies to the Epidermal Growth Factor Receptor in Non–Small Cell Lung Cancer: Current Status of Matuzumab and Panitumumab. *Clin. Cancer Res.* **2007**, *13* (15), 4597s–4601s. https://doi.org/10.1158/1078-0432.CCR-07-0335.
(34) Matuzumab Mechanism of Action.
(35) Kim, T. Technology Evaluation: Matuzumab, Merck KGaA. *Curr. Opin. Mol. Ther.* **2004**, *6* (1), 96–103.
(36) Nahta, R.; Esteva, F. J. Trastuzumab: Triumphs and Tribulations. *Oncogene* **2007**, *26* (25), 3637–3643. https://doi.org/10.1038/sj.onc.1210379.
(37) Cesca, M. G.; Vian, L.; Cristóvão-Ferreira, S.; Pondé, N.; De Azambuja, E. HER2-Positive Advanced Breast Cancer Treatment in 2020. *Cancer Treat. Rev.* **2020**, *88*, 102033. https://doi.org/10.1016/j.ctrv.2020.102033.
(38) Gemmete, J. J.; Mukherji, S. K. Trastuzumab (Herceptin): Fig 1. *Am. J. Neuroradiol.* **2011**, *32* (8), 1373–1374. https://doi.org/10.3174/ajnr.A2619.
(39) Baselga, J. Clinical Trials of Herceptin® (Trastuzumab). *Eur. J. Cancer* **2001**, *37*, 18–24. https://doi.org/10.1016/S0959-8049(00)00404-4.

(40) Boekhout, A. H.; Beijnen, J. H.; Schellens, J. H. M. Trastuzumab. *The Oncologist* **2011**, *16* (6), 800–810. https://doi.org/10.1634/theoncologist.2010-0035.
(41) Carter, P. J.; Rajpal, A. Designing Antibodies as Therapeutics. *Cell* **2022**, *185* (15), 2789–2805. https://doi.org/10.1016/j.cell.2022.05.029.
(42) Tiller, K. E.; Tessier, P. M. Advances in Antibody Design. *Annu. Rev. Biomed. Eng.* **2015**, *17* (1), 191–216. https://doi.org/10.1146/annurev-bioeng-071114-040733.
(43) Bauer, J.; Rajagopal, N.; Gupta, P.; Gupta, P.; Nixon, A. E.; Kumar, S. How Can We Discover Developable Antibody-Based Biotherapeutics? *Front. Mol. Biosci.* **2023**, *10*, 1221626. https://doi.org/10.3389/fmolb.2023.1221626.
(44) Graff, C. P.; Wittrup, K. D. Theoretical Analysis of Antibody Targeting of Tumor Spheroids: Importance of Dosage for Penetration, and Affinity for Retention. *Cancer Res.* **2003**, *63* (6), 1288–1296.
(45) Du, J.-J.; Zhang, R.-Y.; Jiang, S.; Xiao, S.; Liu, Y.; Niu, Y.; Zhao, W.-X.; Wang, D.; Ma, X. Applications of Cell Penetrating Peptide-Based Drug Delivery System in Immunotherapy. *Front. Immunol.* **2025**, *16*, 1540192. https://doi.org/10.3389/fimmu.2025.1540192.
(46) Heitz, F.; Morris, M. C.; Divita, G. Twenty Years of Cell-penetrating Peptides: From Molecular Mechanisms to Therapeutics. *Br. J. Pharmacol.* **2009**, *157* (2), 195–206. https://doi.org/10.1111/j.1476-5381.2009.00057.x.
(47) Moreno-Vargas, L. M.; Prada-Gracia, D. Exploring the Chemical Features and Biomedical Relevance of Cell-Penetrating Peptides. *Int. J. Mol. Sci.* **2024**, *26* (1), 59. https://doi.org/10.3390/ijms26010059.
(48) Gori, A.; Lodigiani, G.; Colombarolli, S. G.; Bergamaschi, G.; Vitali, A. Cell Penetrating Peptides: Classification, Mechanisms, Methods of Study, and Applications. *ChemMedChem* **2023**, *18* (17), e202300236. https://doi.org/10.1002/cmdc.202300236.
(49) Koren, E.; Torchilin, V. P. Cell-Penetrating Peptides: Breaking through to the Other Side. *Trends Mol. Med.* **2012**, *18* (7), 385–393. https://doi.org/10.1016/j.molmed.2012.04.012.
(50) Lindgren, M.; Langel, Ü. Classes and Prediction of Cell-Penetrating Peptides. In *Cell-Penetrating Peptides*; Langel, Ü., Ed.; Methods in Molecular Biology; Humana Press: Totowa, NJ, 2011; Vol. 683, pp 3–19. https://doi.org/10.1007/978-1-60761-919-2_1.
(51) Pooga, M.; Hällbrink, M.; Zorko, M.; Langel, U. Cell Penetration by Transportan. *FASEB J.* **1998**, *12* (1), 67–77. https://doi.org/10.1096/fasebj.12.1.67.

(52) Jeang, K.-T.; Xiao, H.; Rich, E. A. Multifaceted Activities of the HIV-1 Transactivator of Transcription, Tat. *J. Biol. Chem.* **1999**, *274* (41), 28837–28840. https://doi.org/10.1074/jbc.274.41.28837.

(53) Futaki, S.; Suzuki, T.; Ohashi, W.; Yagami, T.; Tanaka, S.; Ueda, K.; Sugiura, Y. Arginine-Rich Peptides. *J. Biol. Chem.* **2001**, *276* (8), 5836–5840. https://doi.org/10.1074/jbc.M007540200.

(54) Esteruelas, G.; Ettcheto, M.; Haro, I.; Herrando-Grabulosa, M.; Gaja-Capdevila, N.; Gomara, M. J.; Navarro, X.; Espina, M.; Souto, E.; Camins, A.; García, M. L.; Sánchez-López, E. Novel Tissue-Specific Multifunctionalized Nanotechnological Platform Encapsulating Riluzole Against Motor Neuron Diseases. *Int. J. Nanomedicine* **2025**, *Volume 20*, 2273–2288. https://doi.org/10.2147/IJN.S479819.

(55) Hahn, K. R.; Kwon, H. J.; Moon, S. M.; Kim, W.; Hwang, I. K.; Kim, D. W.; Yoo, D. Y. Therapeutic Potential of Cell-Permeable PEP-1-Srxn1 in Mitigating Oxidative and Ischemic Damage in the Hippocampus. *Neurochem. Int.* **2025**, *187*, 105988. https://doi.org/10.1016/j.neuint.2025.105988.

(56) Nam, S. H.; Park, J.; Koo, H. Recent Advances in Selective and Targeted Drug/Gene Delivery Systems Using Cell-Penetrating Peptides. *Arch. Pharm. Res.* **2023**, *46* (1), 18–34. https://doi.org/10.1007/s12272-022-01425-y.

(57) Sun, Z.; Huang, J.; Fishelson, Z.; Wang, C.; Zhang, S. Cell-Penetrating Peptide-Based Delivery of Macromolecular Drugs: Development, Strategies, and Progress. *Biomedicines* **2023**, *11* (7), 1971. https://doi.org/10.3390/biomedicines11071971.

(58) Huang, L.; Li, A.; Liu, H.; Ji, S.; Fei, H. Exploring Structure-Directed Immunogenic Cytotoxicity of Arginine-Rich Peptides for Cytolysis-Induced Immunotherapy of Cancer. *Bioorg. Med. Chem.* **2024**, *116*, 117984. https://doi.org/10.1016/j.bmc.2024.117984.

(59) Nakase, I.; Tadokoro, A.; Kawabata, N.; Takeuchi, T.; Katoh, H.; Hiramoto, K.; Negishi, M.; Nomizu, M.; Sugiura, Y.; Futaki, S. Interaction of Arginine-Rich Peptides with Membrane-Associated Proteoglycans Is Crucial for Induction of Actin Organization and Macropinocytosis. *Biochemistry* **2007**, *46* (2), 492–501. https://doi.org/10.1021/bi0612824.

(60) Ma, M.; Li, X.; Jing, M.; Zhang, P.; Zhang, M.; Wang, L.; Liang, X.; Jiang, Y.; Li, J.; He, J.; Wang, X.; Lin, M.; Wang, L.; Fan, J. Enhanced Tumor-Targeted Delivery of Arginine-Rich Peptides via a Positive Feedback Loop Orchestrated by Piezo1/Integrin B1 Signaling Axis. *Adv. Sci.* **2024**, *11* (42), 2409081. https://doi.org/10.1002/advs.202409081.

(61) Kosuge, M.; Takeuchi, T.; Nakase, I.; Jones, A. T.; Futaki, S. Cellular Internalization and Distribution of Arginine-Rich Peptides as a Function of

Extracellular Peptide Concentration, Serum, and Plasma Membrane Associated Proteoglycans. *Bioconjug. Chem.* **2008**, *19* (3), 656–664. https://doi.org/10.1021/bc700289w.

(62) Duca, S.; Nikoi, N. D.; Berrow, M.; Barber, L.; Slope, L. N.; Peacock, A. F. A.; De Cogan, F. Oligoarginine Peptide Structure and Its Effect on Cell Penetration in Ocular Drug Delivery. *Heliyon* **2024**, *10* (15), e35109. https://doi.org/10.1016/j.heliyon.2024.e35109.

(63) Jones, S. W.; Christison, R.; Bundell, K.; Voyce, C. J.; Brockbank, S. M. V.; Newham, P.; Lindsay, M. A. Characterisation of Cell-penetrating Peptide-mediated Peptide Delivery. *Br. J. Pharmacol.* **2005**, *145* (8), 1093–1102. https://doi.org/10.1038/sj.bjp.0706279.

(64) Akram, F.; Ali, A. M.; Akhtar, M. T.; Fatima, T.; Shabbir, I.; Ul Haq, I. The Journey of Antibody-Drug Conjugates for Revolutionizing Cancer Therapy: A Review. *Bioorg. Med. Chem.* **2025**, *117*, 118010. https://doi.org/10.1016/j.bmc.2024.118010.

(65) Jain, N.; Smith, S. W.; Ghone, S.; Tomczuk, B. Current ADC Linker Chemistry. *Pharm. Res.* **2015**, *32* (11), 3526–3540. https://doi.org/10.1007/s11095-015-1657-7.

(66) Zhu, M.; Zhou, L.; Hu, S.; Miao, Q.; Gong, J.; Zhang, N.; Zhang, G.; Wang, M.; Wang, J.; He, H.; Wang, Y. Rational Design and Systemic Appraisal of an EGFR-Targeting Antibody–Drug Conjugate LR-DM1 for Pancreatic Cancer. *J. Med. Chem.* **2022**, *65* (10), 7141–7153. https://doi.org/10.1021/acs.jmedchem.1c01920.

(67) Spicer, C. D.; Pashuck, E. T.; Stevens, M. M. Achieving Controlled Biomolecule–Biomaterial Conjugation. *Chem. Rev.* **2018**, *118* (16), 7702–7743. https://doi.org/10.1021/acs.chemrev.8b00253.

(68) Lehot, V.; Kuhn, I.; Nothisen, M.; Erb, S.; Kolodych, S.; Cianférani, S.; Chaubet, G.; Wagner, A. Non-Specific Interactions of Antibody-Oligonucleotide Conjugates with Living Cells. *Sci. Rep.* **2021**, *11* (1), 5881. https://doi.org/10.1038/s41598-021-85352-w.

(69) Schlein, E.; Syvänen, S.; Rokka, J.; Gustavsson, T.; Rossin, R.; Robillard, M.; Eriksson, J.; Sehlin, D. Functionalization of Radiolabeled Antibodies to Enhance Peripheral Clearance for High Contrast Brain Imaging. *Mol. Pharm.* **2022**, *19* (11), 4111–4122. https://doi.org/10.1021/acs.molpharmaceut.2c00536.

(70) Wu, G.; Gao, Y.; Liu, D.; Tan, X.; Hu, L.; Qiu, Z.; Liu, J.; He, H.; Liu, Y. Study on the Heterogeneity of T-DM1 and the Analysis of the Unconjugated Linker Structure under a Stable Conjugation Process. *ACS Omega* **2019**, *4* (5), 8834–8845. https://doi.org/10.1021/acsomega.9b00430.

(71) Strop, P.; Liu, S.-H.; Dorywalska, M.; Delaria, K.; Dushin, R. G.; Tran, T.-T.; Ho, W.-H.; Farias, S.; Casas, M. G.; Abdiche, Y.; Zhou, D.; Chandrasekaran, R.; Samain, C.; Loo, C.; Rossi, A.; Rickert, M.; Krimm, S.; Wong, T.; Chin, S. M.; Yu, J.; Dilley, J.; Chaparro-Riggers, J.; Filzen, G. F.; O'Donnell, C. J.; Wang, F.; Myers, J. S.; Pons, J.; Shelton, D. L.; Rajpal, A. Location Matters: Site of Conjugation Modulates Stability and Pharmacokinetics of Antibody Drug Conjugates. *Chem. Biol.* **2013**, *20* (2), 161–167. https://doi.org/10.1016/j.chembiol.2013.01.010.

(72) Hwang, D.; Tsuji, K.; Park, H.; Burke, T. R.; Rader, C. Site-Specific Lysine Arylation as an Alternative Bioconjugation Strategy for Chemically Programmed Antibodies and Antibody–Drug Conjugates. *Bioconjug. Chem.* **2019**, *30* (11), 2889–2896. https://doi.org/10.1021/acs.bioconjchem.9b00609.

(73) Fu, Z.; Li, S.; Han, S.; Shi, C.; Zhang, Y. Antibody Drug Conjugate: The "Biological Missile" for Targeted Cancer Therapy. *Signal Transduct. Target. Ther.* **2022**, *7* (1), 93. https://doi.org/10.1038/s41392-022-00947-7.

(74) Wagh, A.; Song, H.; Zeng, M.; Tao, L.; Das, T. K. Challenges and New Frontiers in Analytical Characterization of Antibody-Drug Conjugates. *mAbs* **2018**, *10* (2), 222–243. https://doi.org/10.1080/19420862.2017.1412025.

(75) Rahban, M.; Ahmad, F.; Piatyszek, M. A.; Haertlé, T.; Saso, L.; Saboury, A. A. Stabilization Challenges and Aggregation in Protein-Based Therapeutics in the Pharmaceutical Industry. *RSC Adv.* **2023**, *13* (51), 35947–35963. https://doi.org/10.1039/D3RA06476J.

(76) Díaz-Tejeiro, C.; López De Sá, A.; Poyatos-Racionero, E.; Ballestín, P.; Bartolomé, J.; Calvo, E.; Moreno, V.; Moris, F.; Pérez-Segura, P.; Gyorffy, B.; Pandiella, A.; Ocaña, A. Understanding the Preclinical Efficacy of Antibody–Drug Conjugates. *Int. J. Mol. Sci.* **2024**, *25* (23), 12875. https://doi.org/10.3390/ijms252312875.

(77) Nguyen, T. D.; Bordeau, B. M.; Balthasar, J. P. Mechanisms of ADC Toxicity and Strategies to Increase ADC Tolerability. *Cancers* **2023**, *15* (3), 713. https://doi.org/10.3390/cancers15030713.

(78) Ravasco, J. M. J. M.; Faustino, H.; Trindade, A.; Gois, P. M. P. Bioconjugation with Maleimides: A Useful Tool for Chemical Biology. *Chem. – Eur. J.* **2019**, *25* (1), 43–59. https://doi.org/10.1002/chem.201803174.

(79) Sikora, K.; Jaśkiewicz, M.; Neubauer, D.; Migoń, D.; Kamysz, W. The Role of Counter-Ions in Peptides—An Overview. *Pharmaceuticals* **2020**, *13* (12), 442. https://doi.org/10.3390/ph13120442.

(80) Van Der Meer, J.; Dorssers, L.; Zabel, P. Antibody-Linked Polymerase Assay on Protein Blots: A Novel Method for Identifying Polymerases

Following SDS-Polyacrylamide Gel Electrophoresis. *EMBO J.* **1983**, *2* (2), 233–237. https://doi.org/10.1002/j.1460-2075.1983.tb01411.x.
(81) Maalouf, M.; Carstensen, N.; Wolter, M.; Sievers-Engler, A.; Lämmerhofer, M. Temperature-Controlled Transition between Non-Denaturing and Denaturing Analysis of Patisiran on a Mixed-Mode SAX Stationary Phase Utilizing Two-Dimensional Liquid Chromatography. *J. Chromatogr. A* **2025**, *1761*, 466396. https://doi.org/10.1016/j.chroma.2025.466396.
(82) Kosarev, E. L.; Muranov, K. O. Chromatography+RECOVERY=superresolution Chromatography. *Nucl. Instrum. Methods Phys. Res. Sect. Accel. Spectrometers Detect. Assoc. Equip.* **2003**, *502* (2–3), 764–767. https://doi.org/10.1016/S0168-9002(03)00576-X.
(83) Maalouf, M.; Carstensen, N.; Wolter, M.; Sievers-Engler, A.; Lämmerhofer, M. Temperature-Controlled Transition between Non-Denaturing and Denaturing Analysis of Patisiran on a Mixed-Mode SAX Stationary Phase Utilizing Two-Dimensional Liquid Chromatography. *J. Chromatogr. A* **2025**, *1761*, 466396. https://doi.org/10.1016/j.chroma.2025.466396.
(84) Understanding HPLC Instrumentation: Principles & Uses.
(85) Goyon, A.; D'Atri, V.; Bobaly, B.; Wagner-Rousset, E.; Beck, A.; Fekete, S.; Guillarme, D. Protocols for the Analytical Characterization of Therapeutic Monoclonal Antibodies. I – Non-Denaturing Chromatographic Techniques. *J. Chromatogr. B* **2017**, *1058*, 73–84. https://doi.org/10.1016/j.jchromb.2017.05.010.
(86) Tosoh TSKgel G4000SWXL.
(87) Tosoh TSKgel HIC-ADC Butyl Column.
(88) SkillPak™ 5 mL TOYOPEARL® Phenyl-650-M.
(89) Tosoh Bioscience TSKgel CM-STAT.
(90) User Guide Eshmuno® CMX Chromatography Resin.
(91) Buffer Conditions Eshmuno® CMX Chromatography Resin.
(92) Koehnlein, W.; Holzgreve, A.; Schwendner, K.; Skudas, R.; Schelter, F. Purification of Hydrophobic Complex Antibody Formats Using a Moderately Hydrophobic Mixed Mode Cation Exchange Resin. *J. Chromatogr. A* **2023**, *1687*, 463696. https://doi.org/10.1016/j.chroma.2022.463696.
(93) Fekete, S.; Veuthey, J.-L.; Beck, A.; Guillarme, D. Hydrophobic Interaction Chromatography for the Characterization of Monoclonal Antibodies and Related Products. *J. Pharm. Biomed. Anal.* **2016**, *130*, 3–18. https://doi.org/10.1016/j.jpba.2016.04.004.
(94) Agilent Technologies. LC-HandBook Complete.

(95) Bornfeldt, K. E.; Tabas, I. Insulin Resistance, Hyperglycemia, and Atherosclerosis. *Cell Metab.* **2011**, *14* (5), 575–585. https://doi.org/10.1016/j.cmet.2011.07.015.
(96) Kahn, S. E. The Importance of the β-Cell in the Pathogenesis of Type 2 Diabetes Mellitus. *Am. J. Med.* **2000**, *108* (6), 2–8. https://doi.org/10.1016/S0002-9343(00)00336-3.
(97) Taylor, R. Insulin Resistance and Type 2 Diabetes. *Diabetes* **2012**, *61* (4), 778–779. https://doi.org/10.2337/db12-0073.
(98) Sami, A.; Javed, A.; Ozsahin, D. U.; Ozsahin, I.; Muhammad, K.; Waheed, Y. Genetics of Diabetes and Its Complications: A Comprehensive Review. *Diabetol. Metab. Syndr.* **2025**, *17* (1), 185. https://doi.org/10.1186/s13098-025-01748-y.
(99) Chandrasekaran, P.; Weiskirchen, R. The Role of Obesity in Type 2 Diabetes Mellitus—An Overview. *Int. J. Mol. Sci.* **2024**, *25* (3), 1882. https://doi.org/10.3390/ijms25031882.
(100) Roman, G.; Pantea Stoian, A. Cardiovascular Risk/Disease in Type 2 Diabetes Mellitus. In *Type 2 Diabetes - From Pathophysiology to Cyber Systems*; Pantea Stoian, A., Ed.; IntechOpen, 2021. https://doi.org/10.5772/intechopen.97422.
(101) Murray, C. J. L. Findings from the Global Burden of Disease Study 2021. *The Lancet* **2024**, *403* (10440), 2259–2262. https://doi.org/10.1016/S0140-6736(24)00769-4.
(102) Naghavi, M.; Kyu, H. H.; A, B.; Aalipour, M. A.; Aalruz, H.; Ababneh, H. S.; Abafita, B. J.; Abaraogu, U. O.; Abbafati, C.; Abbasi, M.; Abbaspour, F.; Abbastabar, H.; Abd Al Magied, A. H. A.; Abd ElHafeez, S.; Abdalla, A. N.; Abdalla, M. A.; Abdallah, E. M.; Abdeeq, B. A.; Abdel Razeq, N. M. I.; Abdelgalil, A. A.; Abdel-Hameed, R.; Abdelmasseh, M.; Abdelnabi, M.; Abdel-Rahman, W. M.; Abdous, A.; Abdrabou, M. M.; Abdul Aziz, J. M.; Abdulah, D. M.; Abdullahi, A.; Abdul-Rahman, T.; Abebe Getahun, H.; Abedi, A.; Abedi, A.; Abedi, P.; Abejew, A. A.; Abeldaño Zuñiga, R. A.; Abid, S. U. A.; Abidi, S. H.; Abie, A.; Abiodun, O. O.; Aboagye, R. G.; Abohashem, S.; Abolhassani, H.; Abonie, U. S.; Abourashed, N. M.; Abouzid, M.; Abramov, D.; Abreu, L. G.; Abtahi, D.; Abu Farha, R. K.; Abuadas, F. H. A.; Abubakar, A. K.; Abu-Elala, N.; Abu-Gharbieh, E.; Abuhammad, S.; Abuhelwa, A. Y.; Abukhadijah, H. J.; Abu-Rmeileh, N. M.; Aburuz, S.; Abushanab, D.; Accrombessi, M. M. K.; Acharya, A. B.; Acharya, A.; Adal, O.; Adams, L. C.; Adamu, A. A.; Addo, I. Y.; Adeagbo, O. A.; Adebisi, T. A.; Adedeji, I. A.; Adedokun, K. A.; Adegbile, O. E.; Adegoke, N. A.; Adeleke, O. T.; Adema, B. G.; Aden, B.; Adesina, I. A.; Adesina, M. A.; Adetunji, J. B.; Adewuyi, H. O.;

Adeyeoluwa, T. E.; Adhana, M. T.; Adhikary, R. K.; Adiga, U.; Adl Parvar, T.; Adnan, M.; Adnani, Q. E. S.; Adoma, P. O.; Adzigbli, L. A.; Adzrago, D.; Affinito, G.; Afifi, A. M.; Afoakwah, C.; Afolabi, A. A.; Afolabi, R. F.; Afrăsânie, V.-A.; Afzal, S.; Agafari, G. B.; Agampodi, S. B.; Agampodi, T. C.; Aggarwal, N.; Aghaalikhani, M.; Aghajanian, S.; Aghamir, S. M. K.; Agide, F. D.; Agostinis Sobrinho, C.; Agrawal, A.; Agyemang-Duah, W.; Ahadi, M.; Ahinkorah, B. O.; Ahmad, A.; Ahmad, D.; Ahmad, F.; Ahmad, I.; Ahmad, K.; Ahmad, K.; Ahmad, S.; Ahmad, T.; Ahmad, W.; Ahmadi, N. S.; Ahmed, A.; Ahmed, A.; Ahmed, G. S.; Ahmed, H.; Ahmed, J.; Ahmed, L. A.; Ahmed, M. F.; Ahmed, M. S.; Ahmed, M. S.; Ahmed, M. B.; Ahmed, M.; Ahmed, S.; Ahmed, S. M.; Ahmed, S. A.; Aimagambetova, G.; Ajami, M.; Aji, B.; Akbarialiabad, H.; Akbarifard, S.; Akeju, O.; Akhigbe, R. E.; Akhmedullin, R.; Akinkuotu, O. A.; Akkaif, M. A.; Akosile, W.; Akrami, A. E.; Akyea, R. K.; Al Amiry, A.; Al Awaidy, S.; Al Hasan, S. M.; Al Homsi, A.; Al Nawayseh, M. K.; Al Omari, O.; Al Ta'ani, Z.; Al Thaher, Y.; Al Zaabi, O. A. M.; Al Zoubi, M. A. M.; Al-Abbadi, M. A.; Alalwan, T. A.; Al-Aly, Z.; Alam, K.; Alam, M.; Alam, M. K.; Alam, M.; Al-Amer, R. M.; Alamrew, A.; Alansari, A.; Alanzi, T. M.; Al-Ashwal, F. Y.; Albashtawy, M.; Aldhaleei, W. A.; Aldossary, M. S.; Aldridge, R. W.; Aleidi, S. M.; Alemayehu, B. A.; Alemnew, F.; Alemu, M. B.; Alene, K. A.; Al-Eyadhy, A.; Alfalki, A. M.; Algahtani, F. D.; Algammal, A. M.; Al-Habbal, K.; Alhaji, N. B.; Al-Hajj, S.; Alhalaiqa, F. N.; Al-Hanawi, M. K.; Alhasan, K. A.; Alhumaidi, A.; Alhumaydhi, F. A.; Ali, A.; Ali, H. M.; Ali, I.; Ali, L.; Ali, M.; Ali, M. D.; Ali, M. U.; Ali, R.; Ali, S.; Ali, S. S.; Ali, W.; Alicandro, G.; Al-Iede, M.; Alif, S. M.; Alinejad Rokny, H.; Alipour, M.; Al-Jabi, S. W.; Aljofan, M.; Aljohani, M. S.; Aljunid, S. M.; Alkhatib, A.; Alkhawam, M.; Allebeck, P.; Allemailem, K. S.; Allouh, M. Z.; Almagharbeh, W. T.; Al-Marwani, S.; Almasri, N. A.; Almazan, J. U.; Al-Mekhlafi, H. M.; Almidani, O.; Almobayed, A.; Alnawafleh, K. A.; Alniss, H. Y.; Alocious Sukumar, M. B.; Alomari, M. A.; Alosta, M. R.; Alqahtani, J. S.; Alqahtani, S. A.; Alqudimat, M. R.; Al-Qudimat, A. R.; Alrimawi, I.; Alrousan, S. M.; Al-Sabah, S. K.; Alsabri, M. A.; Altaany, Z.; Altaf, A.; Al-Tammemi, A. B.; Al-Tawfiq, J. A.; Althobiani, M. A.; Altirkawi, K. A.; Alvarez-Galvez, J.; Alvis-Guzman, N.; Alvis-Zakzuk, N. J.; Alwafi, H.; Al-Wardat, M.; Al-Worafi, Y. M.; Aly, H.; Alyahya, M. S. I.; Alzahrani, H.; Alzoubi, K. H.; Al-Zubairi, A. S.; Amafah, E. J.; Amafah, J.; Amani-Beni, R.; Amer, F.; Amidi, B.; Amin, A.; Amin, T. T.; Amindarolzarbi, A.; Amini, S.; Amini-Salehi, E.; Aminzare, M.; Amiri, S.; Amlag, J. O.; Amugsi, D. A.; Amusa, G. A.; Anagnostakis, F.; Ananda, R. A.; Anaraki, N.; Ancuceanu, R.; Anderlini, D.; Anderson, D. B.; Anh, N. H.; Anjorin, A.-A. A.; Ankomah, S. E.; Annadurai, K.; Ansari, S.; Ansari-Moghaddam, A.; Antony, C. M.; Antriyandarti, E.; Anuoluwa, B. S.; Anuoluwa, I. A.; Anvari, S.; Anwar, S.; Anwar, S. L.; Anwer, R.;

Anwer, S.; Anyasodor, A. E.; Appiah, F.; Arab, J. P.; Arabi, H.; Arabloo, J.; Arafat, M.; Araki, D. T.; Aravkin, A. Y.; Areda, D.; Aregu, G. M.; Arias De La Torre, J.; Arjmand, G.; Armocida, B.; Ärnlöv, J.; Arockiaraj, J.; Arooj, M.; Artamonov, A. A.; Arumugam, A.; Arumuganainar, D.; Aryal, U. R.; Aryntayeva, N.; Asadi Anar, M.; Asaduzzaman, M.; Asdaq, S. M. B.; Asemahagn, M. A. A.; Asemu, M. T.; Asgary, S.; Asghari-Jafarabadi, M.; Ashraf, S. A.; Ashraf, T.; Ashrafi, M.; Ashrafizadeh, M.; Asiamah-Asare, B. K. Y.; Aslani, S.; Asri, Y.; Assembekov, B.; Athari, S. S.; Atreya, A.; Atta, J. A.; Atwan, Z. A.; Aurangzeb, K.; Ausloos, M.; Avan, A.; Avelar, N. C. P.; Awan, S. J.; Awotidebe, A. W.; Ayana, L. A. A.; Ayatollahi, H.; Ayipo, Y. O.; Ayyoubzadeh, S. M.; Azadnajafabad, S.; Azadnia, A.; Azam, J. M.; Azarboo, A.; Azene, Z. N.; Azhar, G. S.; Azimi, A.; Azimi, F.; Aziz, M. Y.; Aziz, S. A.; Azizan, A.; Azzam, A. Y.; Babu, G. R.; Bae, Y.; Bagga, A.; Bagheri, N.; Bagheri, S.; Baghizadeh, E.; Baghizadeh, F.; Baghizadeh, S.; Baghlaf, K. K.; Bahmanziari, N.; Bai, R.; Baklola, M. I.; Bako, A. T.; Balcha, W. F.; Balkis, M.; Balmori-de-la-Miyar, J.; Balooch Hasankhani, M.; Baltatu, O. C.; Bandyopadhyay, S.; Banik, P. C.; Barengo, N. C.; Barker-Collo, S. L.; Barqawi, H. J.; Barrow, A.; Barteit, S.; Barua, L.; Bashar, M. A.; Bashir, S.; Basile, G.; Basri, R.; Bassat, Q.; Bastan, M.-M.; Batiha, A.-M.; Batra, K.; Bauckneht, M.; Bayat, M.; Bayat Tork, M. A.; Beaney, T.; Bedi, N.; Beeraka, N. M.; Beghi, M.; Behjati, J.; Bekele, B. K.; Belay, A. N.; Belay, D. M.; Belayneh, A. G.; Belayneh, M.; Belete, A. C.; Belge Bilgin, G.; Bello, M. B.; Bello, O. O.; Bello, U. M.; Belo, L.; Beloukas, A.; Bendardaf, R.; Bensenor, I. M.; Bente Kamal Tune, S. N.; Bergami, M.; Berhie, A. Y.; Berihun, A. A.; Bermudez, A. N. C.; Bernstein, R. S.; Bertolacci, G. J.; Bertuccio, P.; Bettencourt, P. J. G.; Bhadoria, A. S.; Bhagavathula, A. S.; Bhala, N.; Bhandari, B.; Bhangdia, K.; Bhanushali, C.; Bhardwaj, N.; Bhardwaj, P.; Bhargava, A.; Bhaskar, S.; Bhat, A.; Bhattacharjee, P.; Bhattacharjee, S.; Bhatti, G. K.; Bhatti, J. S.; Bhuiyan, M. A.; Bhutta, Z. A.; Bhuyan, S. S.; Bi, H.; Biadgilign, S. K.; Bievel-Radulescu, R.; Binsaleh, N. K.; Bisignano, C.; Biswas, A.; Biswas, B.; Biswas, M. S.; Bitar, A. N.; Bitew, M.; Bizzozero-Peroni, B.; Bjørge, T.; Bodolica, V.; Bogale, E. K.; Bohn, L.; Bolarinwa, O. A.; Bolourinejad, P.; Bonny, A.; Boppana, S. H.; Borhany, H.; Borran, M.; Bose, S.; Bosoka, S. A.; Botero Carvajal, A.; Boufous, S.; Boxe, C.; Braithwaite, D.; Brant, L. C.; Brauer, M.; Breitborde, N. J. K.; Breitner, S.; Brenner, H.; Brewer, E. D.; Bringas Vega, M. L.; Brown, J.; Browne, A. J.; Brugha, T.; Bugiardini, R.; Bulamu, N. B.; Bunare, T. S.; Buonsenso, D.; Burns, R. A.; Busari, A. O.; Busch, F.; Bustanji, Y.; Butt, N. S.; Butt, Z. A.; C J, S.; Cai, T.; Cairns, R.; Çakmak Barsbay, M.; Calina, D.; Cámera, L. A.; Campos, L. A.; Campos-Nonato, I.; Cao, F.; Cao, S.; Capodici, A.; Cárdenas, R.; Carreras, G.; Carrero, J. J.; Carugno, A.; Carvalho, A. F.; Carvalho, F.;

Carvalho, M.; Carvalho-e-Silva, A. P.; Castaldelli-Maia, J. M.; Castañeda-Orjuela, C. A.; Castelpietra, G.; Catalá-López, F.; Catapano, A. L.; Cattaruzza, M. S.; Cegolon, L.; Cembranel, F.; Cenderadewi, M.; Cercy, K. M.; Cerin, E.; Chacón-Uscamaita, P. R.; Chakraborty, C.; Chakraborty, S.; Chandan, J. S.; Chandika, R. M.; Chandradasa, M.; Chandrasekaran, B.; Chattu, V. K.; Chatzimavridou-Grigoriadou, V.; Chaudhary, A. A.; Chaudhuri, S.; Chaurasia, A.; Chen, A.-T.; Chen, C. S.; Chen, G.; Chen, H.; Chen, H.; Chen, H.; Chen, H.; Chen, R.; Chen, S.; Chen, S.; Chen, X.; Cheng, H.; Cheung, K. C.; Chew, N. W.; Chi, G.; Chichagi, F.; Chihara, I.; Chimed-Ochir, O.; Ching, P. R.; Chirinos-Caceres, J. L.; Cho, D. Y.; Cho, W. C. S.; Chong, B.; Chong, Y. Y.; Chou, H. I.; Chowdhury, E. K.; Chowdhury, S.; Christensen, H.; Chuang, T.-W.; Chukwu, I. S.; Chung, E.; Chung, S.-C.; Chung, S.; Chutiyami, M.; Cicero, A. F. G.; Clark, C. C. T.; Cohen, F.; Columbus, A.; Conde, J.; Congly, S. E.; Conrad, N.; Cooper, L. T.; Corlateanu, A.; Cortese, S.; Cortesi, P. A.; Cosma, C.; Cousin, E.; Cowart, E. J.; Criqui, M. H.; Crist, A.; Cruz, J. A.; Cruz-Martins, N.; Cui, X.; Culbreth, G. T.; Cullen, P.; Cunningham, M.; Dababo, N.; Dabbagh, A.; Dadras, O.; Dahiru, T.; Dai, X.; Dai, Z.; Dalakoti, M.; Dalal, K.; Dalla Costa, G.; D'Amico, E.; Daniel, R. A.; D'Anna, L.; Danpanichkul, P.; Danso, S. E.; Darcho, S. D.; Dardas, L. A.; Dare, C.; Darouei, B.; Darvishi Cheshmeh Soltani, R.; Das, S. K.; Dávila-Cervantes, C. A.; Davis Weaver, N.; Davletov, D.; Davletov, K.; De La Hoz, F. P.; De La Torre-Luque, A.; Dee, E. C.; Deekonda, S.; Deen, A.; Degenhardt, L.; Dehesh, P.; Delbari, P.; Delgado-Ortiz, L.; Delsoz, M.; Demetriades, A. K.; Denova-Gutiérrez, E.; Derese, T. N.; Dergaa, I.; Deribe, K.; Derseh, H. A.; Dervenis, N.; Dervišević, E.; Desai, H. D.; Desta, A. A.; Devanbu, V. G. C.; Devarakonda, P. K.; Dewan, S. M. R.; Dhali, A.; Dhama, K.; Dharmagadda, S.; Dhimal, M. L.; Dhimal, M.; Dhungel, B.; Di Pumpo, M.; Dias Da Silva, D.; Diaz, D.; Diaz, L. A.; Didehvar, K.; Dilipan, E.; Dillard, L. K.; Ding, X.; Doaei, S.; Dohare, S.; Dokova, K. G.; D'Oria, M.; Dorostkar, F.; Dorsey, E. R.; Doshi, O. P.; Doshmangir, L.; Dowou, R. K.; Dresse, M. T.; Driscoll, T. R.; Dsouza, A. C.; Du, J.; Dube, J.; Dubno, J. R.; Dumbili, E. W.; Dumith, S. C.; Duncan, B. B.; Duraes, A. R.; Durojaiye, O. C.; Dutta, A. K.; Dutta, S.; Dutta, S.; Ebohon, O.; Eboreime, E.; Ebraheim, L. L. M.; Ebrahimi, A.; Ebrahimi, M. H.; Ed-Dra, A.; Edvardsson, D.; Efendi, F.; Eftekhari, B.; Eghbali, F.; Eighaei Sedeh, A.; Eikemo, T. A.; Eini, E.; Ekholuenetale, M.; Ekundayo, T. C.; El Arab, R. A.; El Omri, A.; El Sayed Zaki, M.; Eladl, M. A.; Elahi, R.; El-Ashker, S.; Elbeshbeishy, R.; Elemam, N. M.; ElGohary, G. M. T.; Elhadi, M.; Elhoumed, M.; El-Huneidi, W.; Elmeligy, O. A. A.; Elmonem, M. A.; Elmorsi, R.; Elnaem, M. H.; ELNahas, G.; Elshaer, M.; Elsohaby, I.; Eltahawy, A. S.; Emagneneh, T.; Endriyas, M.; Erkhembayar, R.;

Esezobor, C. I.; Eshetu, D.; Eslami, M.; Eslami, N.; Espírito Santo, R. C. D.; Estep, K.; Eyawo, O.; Eze, U. A.; Ezenwankwo, E.; Fadavian, H.; Fagbamigbe, A. F.; Fagbule, O. F.; Fahim, A.; Fahimi, S.; Fahira, A.; Fakhradiyev, I. R.; Fakhri-Demeshghieh, A.; Falzone, L.; Fan, Q.; Farahmand, M.; Faramarzi, A.; Fareed, M.; Farhana, Z.; Faria, L.; Farinha, C. S. E. S.; Faris, M. E. M.; Faro, A.; Farooq, S. M. Y.; Farrokhpour, H.; Farshad, F.; Farsi, F.; Fasina, F. O.; Fasina, M. M.; Fatehizadeh, A.; Fathi, D.; Fatima, Z.; Fayaz, M.; Fazeli, P.; Feigin, V. L.; Feizkhah, A.; Fekadu, G.; Fekadu, G.; Femoe, U. M.; Ferdous, T. R.; Fereshtehnejad, S.-M.; Fernandez-Jimenez, R.; Ferrara, P.; Ferrari, A. J.; Ferreira, N.; Fetensa, G.; Feyisa, B. R.; Finnemore, A.; Fiorilla, C.; Fischer, F.; Fitriana, I.; Fogacci, F.; Folayan, M. O.; Fomenkov, A. A.; Fonzo, M.; Force, L. M.; Fortuna, D.; Foschi, M.; Fotouhi, M.; Fowobaje, K. R.; Franklin, R. C.; Freitas, A.; Fu, J.; Fukumoto, T.; Fukunaga, A.; Fuller, J. E.; G, S.; Gaal, P. A.; Gadanya, M. A.; Gadeka, D. D.; Gafane-Matemane, L. F.; Gajdács, M.; Galali, Y.; Galiyeva, D.; Gallus, S.; Ganapathy, D.; Ganesan, B.; Gangachannaiah, S.; Gao, X.; Gao, Y.; Garba, B.; Garcia-Argibay, M.; Garcia-Azorin, D.; Gardner, W. M.; Gastélum Espinoza, W. P.; Gatzioufas, Z.; Gautam, P.; Gautam, R. K.; Gaye, B.; Ge, H.-H.; Gebre, F. S.; Gebregergis, M. W.; Gebrehiwot, M.; Gelchu, M.; Gelibter, S.; George, N. S.; Getacher, L.; Getahun, G. K.; Gete, K. Y.; Gething, P. W.; Ghadiri, K.; Ghadirian, F.; Ghaffari Jolfayi, A.; Ghamkhar, A.; Ghasemi Assl, S.; Ghassemi, F.; Ghazy, R. M.; Ghoba, S.; Gholamalizadeh, M.; Gholami, Z.; Gholizadeh, N.; Ghorbani, Z.; Ghotbi, E.; Ghuge, A.; Gialluisi, A.; Giannakis, K.; Gilani, S. A.; Gill, T. K.; Giri, B. R.; Girmay, A. A.; Girombelli, A.; Göbölös, L.; Goel, A. K.; Goel, A.; Goel, R. K.; Goh, L. H.; Gohari, K.; Golechha, M.; Golestani, A.; Golinelli, D.; Golmohammadi, M.; Gong, W.; Goulart, A. C.; Grada, A.; Graham, S. M.; Grivna, M.; Guan, S.-Y.; Guarducci, G.; Gubari, M. I. M.; Gudeta, M. D.; Guha, A.; Guicciardi, S.; Gulati, S.; Gunturu, S.; Guo, C.; Guo, X.; Guo, Z.; Guo, Z.; Gupta, B.; Gupta, G.; Gupta, L.; Gupta, R.; Gutiérrez, R. A.; Gutiérrez-Murillo, R. S.; Guzman-Esquivel, J.; Habteyes, A. T.; Habteyohannes, A. D.; Hadaro, T. S.; Hadi, N. R.; Hadian, Z.; Hafiz, A.; Hafsia, S.; Haghdoost, F.; Haghtalab, A.; Hai Nam, N.; Haile, A.; Haile, D.; Halder, P.; Haller, S.; Halwani, R.; Hama Aziz, K. H.; Hamad, I. M.; Hamadeh, R. R.; Hamidi, S.; Hamilton, E. B.; Hammoud, A.; Han, C.; Han, H.; Hanif, A.; Hanifi, N.; Hankey, G. J.; Hanna, F.; Haque, A.; Haque, M. N.; Haque, O. I.; Hargono, A.; Hariandja, A. M. A.; Haro, J. M.; Harris, A. A.; Hasaballah, A. I.; Hasan, F.; Hasan, M. K.; Hasan, T.; Hasani, H.; Hasanpour-Dehkordi, A.; Hashempur, M. H.; Hashim, N. T.; Hasnain, A.; Hassan, A. M.; Hassan, A.; Hassan, I. N.; Hassan, I.; Hassan, N.; Hassan Ahmed, O.; Hassan Wada, Y.; Hassan Zadeh Tabatabaei, M. S.; Hassanipour, S.; Hathagoda, L.

W.; Haubold, J.; Havmoeller, R. J.; Hay, S. I.; Hbid, Y.; He, J.; Hebert, J. J.; Heidari, G.; Heidari, M.; Heydari, M.; Hezam, K.; Hiraike, Y.; Horita, N.; Hossain, A.; Hossain, L.; Hossain, M. B.; Hossain, M. M.; Hossain, M. S.; Hossain, M. B.; Hosseini, F. S.; Hosseinzadeh, M.; Hostiuc, M.; Hostiuc, S.; Hotez, P. J.; Hotwani, P.; Hoven, H.; Hu, C.; Hu, Y.; Huang, J.; Huang, W.; Huang, Y.; Huang, Y.; Huang, Z.; Huda, M. H.; Humayun, A.; Husain, W.; Hushmandi, K.; Hussain, J.; Hussein, N. R.; Husseiny, M. I.; Iannone, L. F.; Ibitoye, S. E.; Ibrahim, K. S.; Ibrahim, R.; Ibrahim, R.; Ibrahim, U. I.; Ibrayeva, A.; Ida, F.; Ikuta, K. S.; Ilesanmi, O. S.; Ilic, I. M.; Ilic, M. D.; Ilyas, M. H.; Imam, M. T.; Imani, M.; Imoh, L. C.; Inok, A.; Iqbal, M.; Iqbal, M.; Irham, L. M.; Isa, M. A.; Iskandar, B.; Iskander, T. R.; Islam, M. R.; Islam, M. S.; Islam, M. S.; Islam, S. M. S.; Islami, F.; Ismail, F.; Ismail, N. E.; Ismoldayev, Y.; Isola, G.; Iwagami, M.; Iyamu, I. O.; J, V.; Jaafari, J.; Jacob, L.; Jacobsen, K. H.; Jadidi, A.; Jadidi-Niaragh, F.; Jafari, M.; Jafarinia, M.; Jafarzadeh, A.; Jaffar, S.; Jahrami, H.; Jairoun, A. A.; Jaiswal, V.; Jaka, S.; Jakovljevic, M.; Jalilzadeh Yengejeh, R.; Jalloh, M.; Jamal, A.; Jamal, Q. M. S.; Jamaluddin, J.; James, J.; Jamil, H.; Jamil, S.; Jamora, R. D. G.; Jamshidi, M.; JamshidiRastabi, S.; Janardhanan, R.; Jani, C. T.; Jarrahi, E.; Javaheri, T.; Javaid, S. S.; Javanmardi, A.; Javidnia, J.; Jawaid, T.; Jawell Odah Abed, Q.; Jayapal, S. K.; Jayaram, S.; Jayasinghe, R. D.; Jayasinghe, Y. A.; Jee, S. H.; Jeganathan, J.; Jena, D.; Jeong, S.; Jeswani, B. M.; Jha, V.; Ji, J. S.; Jiang, M.; Jin, W.; Jomehzadeh, N.; Jonas, J. B.; Joo, T.; Jor, A.; Joseph, A.; Joseph, N.; Joshi, M.; Joy, G.; Jozwiak, J. J.; Jürisson, M.; K, V.; Kaambwa, B.; Kabir, A.; Kabir, Z.; Kadel, R.; Kadir, D. H. H.; Kakkar, A. K.; Kakodkar, P. V.; Kalani, R.; Kalavani, K.; Kaliyadan, F.; Kalra, S.; Kamal, M. M.; Kamal, M.; Kamarajah, S. K.; Kamath, R.; Kamenova, S.; Kamireddy, A.; Kamorudeen, R. T.; Kamtam, D. N.; Kamyari, N.; Kamyshnyi, O.; Kanaan, M.; Kanaan, S. F.; Kang, J.; Kanmodi, K. K.; Kannan S, S.; Kantar, R. S.; Kar, D.; Kar, S. K.; Karakasis, P.; Karami, J.; Karasneh, R. A.; Karimi, M. A.; Karimi, S. E.; Karimi Behnagh, A.; Karobari, M. I.; Karpiński, T. M.; Katamreddy, A.; Kauppila, J. H.; Kaushal, K.; Kazemi, F.; Kazemi Rad, N.; Kazemian, S.; Kebede, H. K.; Kebede, Y. T.; Keflie, T. S.; Kempegowda, S. N.; Kerai, S.; Kerr, J. A.; Keshri, V. R.; Keshtkar, K.; Kesse-Guyot, E.; Khademi, R.; Khader, Y. S.; Khalid, S.; Khalifa, H. O.; Khalifeh, A. H.; Khalil, A. A.; Khalili, A.; Khalili, P.; Khalilian, A.; Khalili-Tanha, G.; Khalis, M.; Khamesipour, F.; Khan, A.; Khan, F.; Khan, G.; Khan, I. W.; Khan, M.; Khan, M. A. S.; Khan, M. J.; Khan, M. H.; Khan, M. M.; Khan, M. U.; Khan, M. U.; Khan, S. A.; Khan, S.; Khan, S.; Khan, U.; Khan, Y. S.; Khan, Z.; Khanal, V.; Khanmohammadi, S.; Khasbage, S. U.; Khashim, Z.; Khatab, K.; Khatatbeh, H.; Khatatbeh, M. M.; Khatib, M. N.; Khatri, K.; Khayat Kashani, H. R.; Kheirallah, K. A.; Khokhar, S. K.; Khoshnaw,

N. S. H.; Khosla, A. A.; Khosravi, A.; Khosravi, F.; Khosravi, S.; Khosrowjerdi, M.; Khuman, P. R.; Kifle, Z. D.; Kim, H. J.; Kim, J.; Kim, K.; Kim, M. S.; Kim, Y. J.; Kimokoti, R. W.; Kinati, T.; Kinfu, Y.; Kini B, S.; Kirk, M.; Kisa, A.; Kisa, S.; Kissimova-Skarbek, K.; Kitaw, T. A.; Kivimäki, M.; Km, A. B.; Km, S.; Knudsen, A. K. S.; Kobyliak, N.; Kocarnik, J. M.; Kochhar, S.; Kodali, P. B.; Kokkorakis, M.; Kolahi, A.-A.; Kolieghu Tcheumeni, D. G.; Kolves, K.; Komesuor, J.; Kompani, F.; Kondybayeva, A.; Koomson, I.; Koren, G.; Kormoker, T.; Korshunov, V. A.; Korzh, O.; Kosen, S.; Kostev, K.; Koul, P. A.; Kretchy, I. A.; Kretchy, J.-P.; Krishan, K.; Kua, C.-H.; Kuanar, A.; Kuate Defo, B.; Kuddus, M.; Kuitunen, I.; Kulimbet, M.; Kulshreshtha, S.; Kumar, D.; Kumar, D.; Kumar, J.; Kumar, K.; Kumar, M.; Kumar, N.; Kumar, N.; Kumar, T.; Kumar, T.; Kumar, V.; Kumar, V.; Kumaran, S.; Kunjavara, J.; Kunutsor, S. K.; Kurmanova, A.; Kurmi, O. P.; Kurniasari, M. D.; Kurpad, K. P.; Kusnali, A.; Kustanti, C. Y.; Kusuma, D.; Kutluk, T.; Kuttybayev, A.; Kyei, E. F.; Kyei, G. K.; Kyei-Arthur, F.; Kytö, V.; L C, P.; La Vecchia, A.; La Vecchia, C.; Lachi, A.; Ladan, M. A.; Lagat, A. K.; Lahariya, C.; Lai, D. T. C.; Lakanova, B.; Lakhani, A.; Lallukka, T.; Lám, J.; Landires, I.; Langguth, B.; Laplante-Lévesque, A.; Lara-Castor, L.; Lasrado, S.; Latief, K.; Latif, A.; Latif, M.; Lau, J.; Lauriola, P.; Lawan, A.; Lawanson, T.; Lawford, H. L. S.; Lazarus, E. R.; Le, D. Q.; Le, D. T.; Le, T. T. T.; Ledda, C.; Lee, I.; Lee, P. H.; Lee, S. W.; Lee, Y. H.; Leigh, J.; Leivaditis, V.; Lennon, M. J.; Leonardi, M.; Leong, E.; Letafatkar, N.; Li, C.; Li, H.; Li, J.; Li, J.; Li, M.-C.; Li, S.; Li, W.; Li, W.; Li, Z. A.; Li, Z.; Lian, Y.; Liao, C.; Lim, S. S.; Lin, J.; Lin, Q.; Lin, S.; Lindholm, D.; Linehan, C.; Ling, Y.; Linn, S.; Liu, H.; Liu, J.; Liu, X.; Liu, X.; Liu, X.; Liu, Z.; Liu, Z.; Llanaj, E.; Loftus, M. J.; Lohner, V.; López-Gil, J. F.; Lopukhov, P. D.; Lorkowski, S.; Lozano, R.; Luan, S.; Lubinda, J.; Lucas, T.; Lucchetti, G.; Lugo, A.; Lunevicius, R.; Luo, H.; Luo, L.; Luo, S.; Lv, L.; Lytras, M. D.; Lytvyak, E.; Ma, K. S.-K.; Ma, Z. F.; Maalman, R. S.-E.; Maass, K. L.; Mabrok, M.; Machairas, N.; Machoy, M.; Madinezad, S. A.; Madureira-Carvalho, A. M.; Maffia, P.; Mahalingam, S.; Mahamed, S. A.; Mahmood, N. H.; Mahmood, S. A. I.; Mahmoudi, A.; Mai, M. T.; Mai Xuan, H.; Maiti, R.; Majdan, M.; Makram, A. M.; Makram, O. M.; Malekpour, M.-R.; Malekzadeh, R.; Malhotra, H. S.; Malik, A. A.; Malik, F.; Malta, D. C.; Mangdow, M.; Manikkath, J.; Manla, Y.; Mannan, F.; Mansoor, F.; Mansourian, M.; Mansournia, M. A.; Mantovani, L. G.; Mao, C.; Maqbool, T.; Marasini, B. P.; Marateb, H. R.; Maravilla, J. C.; Marques, A.; Martinez-Guerra, B. A.; Martinez-Piedra, R.; Martini, D.; Martini, S.; Martins-Melo, F. R.; Martorell, M.; März, W.; Marzo, R. R.; Marzouk, S.; Mashudi, S.; Masi, S.; Mathangasinghe, Y.; Mathieson, S.; Mathioudakis, A. G.; Mathur, M.; Mathur, N.; Mattiello, R.; Maude, R. J.; Maulik, P. K.; May, M. L.; Mayeli, M.; Mazidi, M.; Mazzotti, A.;

Mbachu, I. I.; McKee, M.; McPhail, M. A.; McPhail, S. M.; Mediratta, R. P.; Meena, J.; Mehari, M.; Mehboob, R.; Mehrotra, R.; Mehta, V.; Mekene Meto, T.; Meles, H. N.; Melese, A.; Melwani, S.; Memetova, A.; Mendoza, W.; Menezes, G. A.; Menezes, R. G.; Mengistie, E. A.; Mensah, G. A.; Meo, S. A.; Mercogliano, M.; Meretoja, A.; Meretoja, T. J.; Mestrovic, T.; Mettananda, C. D. K.; Mettananda, S.; Metwally, M. M. M.; Mhlanga, A.; Miazgowski, T.; Michalek, I. M.; Michelerio, A.; Mideksa, H. S.; Mihretie, K. M.; Miller, T. R.; Minervini, G.; Ming, W.; Mini, G.; Mirghafourvand, M.; Mirica, A.; Mirkheshti, A.; Mirshahvalad, S. A.; Mirutse, M. K.; Mirzaei, M.; Mishra, A.; Mishra, A.; Mishra, V.; Mitchell, P. B.; Mitra, S.; Mittal, C.; Mobayen, M.; Moberg, M. E.; Modi, S.; Mohamed, A. I.; Mohamed, H. M.; Mohamed, J.; Mohamed, M. G.; Mohamed, N. S.; Mohamed Ahmed, K. A. H.; Mohammad, T.; Mohammadi, A.; Mohammadi, M. R.; Mohammadian-Hafshejani, A.; Mohammadzadeh, I.; Mohammed, A.; Mohammed, A. S.; Mohammed, H.; Mohammed, O.; Mohammed, S.; Mohammed, S.; Mohammed, Y.; Mohseni, M.; Mok, T.; Mokari-Yamchi, A.; Mokdad, A. H.; Molinaro, S.; Mollaei, A.; Momani, S.; Monasta, L.; Monazzami, A.; Mondal, H.; Montalti, M.; Moradi, Y.; Moradi-Joo, M.; Moradi-Lakeh, M.; Moraga, P.; Morawska, L.; Moreira, R. S.; Morsy, M. M.; Mosaddeghi Heris, R.; Mosser, J. F.; Mossialos, E.; Motavvef, M.; Mougin, V.; Mousavi, A.; Mousavi, S. Z.; Mousavi Khaneghah, A.; Mousavi Kiasary, S. M. S.; Movo, A.; Mowafy, H. L.; Mozahheb Yousefi, K.; Mrejen, M.; Mubarak, R.; Mubarik, S.; Mudenda, S.; Mughal, F.; Muhammad, S. A.; Muhtar, M. S.; Mujica, O. J.; Mukherjee, S.; Mukherjee, S.; Mukhopadhyay, A.; Muktadir, M. A.; Mulatu, S.; Mulita, F.; Mulugeta, C.; Mulwa, D. F.; Muñoz Laguna, J.; Munshi, A.; Murillo-Zamora, E.; Mushtaq, A.; Mustapha, M. T.; Muthu, S.; Muthupandian, S.; Muvunyi, C. M.; Myung, W.; Nabavi, A.; Naddafi, F.; Nafei, A.; Nagarajan, A. J.; Naik, G. R.; Naik, G.; Nainu, F.; Nair, S.; Najmuldeen, H. H. R.; Nakhostin Ansari, N.; Nambi, G.; Nanditha, N. G. A.; Nangia, V.; Nansseu, J. R.; Naqid, I. A.; Narayana, A. I.; Nargus, S.; Narimani Davani, D.; Nartey, Y.; Nascimento, B. R.; Nascimento, G. G.; Naser, A. Y.; Nashwan, A. J.; Nasiri, H.; Nassar, M.; Natto, Z. S.; Nauman, J.; Navaratna, S. N. K.; Nayak, B. P.; Nayak, S. G.; Nayak, V. C.; Naz, S.; Nazri-Panjaki, A.; Nchanji, G. T.; Nduaguba, S. O.; Nega, A. T.; Negassa, M. T.; Negesse, C. T.; Negoi, I.; Negoi, R. I.; Negru, A. G.; Nejjari, C.; Nepal, S.; Nesbit, O. D.; Netsere, H. B.; Ng, M.; Nguefack-Tsague, G.; Ngunjiri, J. W.; Nguyen, C. T.; Nguyen, D.; Nguyen, H.-D. T.; Nguyen, N. P.; Nguyen, T. P.; Nguyen, V. T.; Ngwa, A. M.; Niazi, R. K.; Nieddu, L.; Nigatu, Y. T.; Nikoobar, A.; Niranjan, V.; Nisro, A. M.; Nnaji, C. A.; Nomura, S.; Noor, S. T. A.; Noorafrooz, M.; Noreen, M.; Noroozi, M.; Noubiap, J. J.; Nouri, M.; Noyes, T.; Nriagu, V. C.; Nri-Ezedi, C. A.; Nshimiyimana, J. C.;

Nugen, F.; Nunemo, M. H.; Nurfatimah, N.; Nurrika, D.; Nyadanu, S. D.; Nyande, F. K.; Oancea, B.; Odat, R. M.; Oddi, F. M.; Odetokun, I. A.; Odukoya, O. O.; Oduro, J. K.; Oduro, M. S.; Ogundeko-Olugbami, O. T.; Ogunkoya, A.; Ogunmiluyi, O. E.; Oh, I.-H.; Oh, S.; Okati-Aliabad, H.; Okeke, S. R.; Okeke-Obayemi, D. O.; Okekunle, A. P.; Okesanya, O. J.; Okonji, O. C.; Ola, B. A.; Olabisi, O. I.; Olalusi, O. V.; Olatubi, M. I.; Oliveira, A. B.; Oliveira, G. M. M.; Olorukooba, A. A.; Oludoye, O. O.; Olum, R.; Olusanya, B. O.; Olusanya, J. O.; Oluwole, O. G.; Omage, F. B.; Omer, G. L.; Omonisi, A. E.; Ong, K. L.; Onie, S.; Onwujekwe, O. E.; Opesemowo, O. A. G.; Opio, J. N.; Opitz, M.; Oradova, A. S.; Ordak, M.; Orish, V. N.; Ornello, R.; Orscelik, A.; Ortiz, A.; Ortiz-Prado, E.; Osborne, A.; Ostroff, S. M.; Ostrominski, J. W.; Osuagwu, U. L.; Osuolale, O.; Othman, E. H.; Otoiu, A.; Oumer, A.; Ouner, J. J.; Ouyahia, A.; Owolabi, M. O.; Owusu, I. A.; Oyebanji, O. A.; Oyebola, K.; Oyelade, T.; Oyeniran, K. A.; Oyeyemi, O. T.; Ozsahin, I.; P A, M.; Pacheco-Barrios, K.; Padron-Monedero, A.; Padubidri, J. R.; Paija, D. M.; Pak, A.; Pakbaz, Y.; Pal, P. K.; Palicz, T.; Palladino, R.; Paluvai, T.; Pan, F.; Panda, S. K.; Panda-Jonas, S.; Pande Katare, D.; Pandi-Perumal, S. R.; Pando-Robles, V.; Pandya, A.; Pangaribuan, H. U.; Panos, G. D.; Panos, L. D.; Pantazopoulos, I.; Pantea Stoian, A.; Paolino, G.; Papa, M. V.; Papadimopoulos, I.; Papadopoulou, P.; Parhizkar Roudsari, P.; Parikh, R. R.; Park, C.; Park, S.; Parmar, A.; Passera, R.; Patel, J.; Patel, M.; Patel, N. N.; Patel, S. K.; Patel, S.; Patil, B. S. U.; Patil, S.; Patoulias, D.; Patra, A.; Patthipati, V. S.; Pawar, S.; Pawar, S.; Pazoki Toroudi, H.; Pearce, N.; Peden, A. E.; Pedersini, P.; Pekarcikova, J.; Penberthy, L.; Pepito, V. C. F.; Peprah, E. K.; Peprah, P.; Perdigão, J.; Pereira, G.; Perez Chacon, G.; Perianayagam, A.; Perico, N.; Perna, S.; Pesudovs, K.; Petakh, P.; Petcu, I.-R.; Peter, O. J.; Petermann-Rocha, F. E.; Petri, W. A.; Pham, H. N.; Pham, H. T.; Pham, T. T.; Philip, A. K.; Phillips, M. R.; Piracha, Z. Z.; Pirera, E.; Piroozkhkah, M.; Pirouzpanah, S.; Pisoni, E.; Plotnikov, E.; Podder, I.; Poddighe, D.; Polibin, R. V.; Poluru, R.; Pon Avudaiappan, A.; Ponkilainen, V. T.; Popa, I.; Popovic, D. S.; Porntaveetus, T.; Pourasghary, S.; Pourbabaki, R.; Pourghazi, F.; Pourtaheri, N.; Prada, S. I.; Pradhan, J.; Pradipta, R. O.; Prashant, A.; Prates, E. J. S.; Pritchett, N.; Priya, H.; Pugliese, N. R.; Puvvula, J.; Qasim, N. H.; Qattea, I.; Qi, X.; Qi, Z.; Qiao, Y.; Quazi, Z. S.; Rabiee, N.; Rabiei, R.; Rachmat, B.; Radhakrishnan, R. A.; Radhakrishnan, V.; Radojčić, M. R.; Radpour, N.; Raeisi Shahraki, H.; Rafati, L.; Rafique, I.; Raghuveer, P.; Rahim, F.; Rahim, H. M.-A.; Rahimi, S.; Rahimi-Movaghar, V.; Rahman, F. M.; Rahman, M.; Rahman, M. M.; Rahman, M. H. U.; Rahman, M. M.; Rahman, M.; Rahmani, A. M.; Rahmani, S.; Rahmati, M.; Rahmatpour Rokni, G.; Rahmoune, H.; Raimondo, D.; Raimondo, I.; Raina, S. K.; Raj, J. P.; Raja, A.; Rajaa, S.; Rajabi,

E.; Rajendran, G.; Rajendran, J.; Rajendran, V.; Rajindrajith, S.; Rajpoot, P. L.; Rajput, P.; Ramadan, M. M.; Ramadan, M.; Ramadhan, K.; Ramasamy, C.; Ramasamy, S. K.; Ramezani, Z.; Ramezani Farani, M.; Ramírez-Vélez, R.; Rana, J.; Rana, K.; Rana, S. S.; Ranabhat, C. L.; Rancic, N.; Rani, S.; Ranjbar Noei, F.-; Rao, C. R.; Rao, K.; Rao, M.; Rasella, D.; Rashedi, S.; Rashedi, V.; Rashid, M.; Rashidi, M.-M.; Rasouli, M. A.; Rasouli-Saravani, A.; Rasul, A.; Rathish, D.; Rauf, A.; Rauniyar, S. K.; Rautalin, I.; Ravangard, R.; Rawaf, D. L.; Rawal, L.; Rawassizadeh, R.; Razi, B.; Reategui-Rivera, C. M.; Redwan, E.; Rehman, A. U.; Rehman, F. U.; Rehman, W.; Reifels, L.; Reile, R.; Remuzzi, G.; Reshmi, B.; Restaino, S.; Reyes, L. F.; Rezaei, M.; Rezaei, N.; Rezaei, N.; Rezaeian, M.; Rezazadeh Eidgahi, D.; Rhee, T. G.; Rias, Y. A.; Ribeiro, A. L. P.; Ribeiro Da Silva, T. M.; Rickard, J.; Rizvi, M. R.; Robinson-Oden, H. E.; Rocha, H. A. L.; Rocha-Gomes, J. R.; Rodrigues, M.; Rodrigues Da Silva, T. P.; Rodriguez, J. A. B.; Roever, L.; Rohloff, P.; Rohmah, I.; Röhr, S.; Rojas-Rueda, D.; Rolfzen, M. L.; Romadlon, D. S.; Romoli, M.; Ronfani, L.; Root, K. T.; Rosenblad, E.; Roshanshad, A.; Rostamian, M.; Roth, G. A.; Rotimi, K.; Rout, H. S.; Rouzbahani, H.; Rouzbahani, R.; Rowlands, J. V.; Roy, A.; Roy, B.; Roy, P.; Roy, S.; Roy, S.; Roy, S.; Royapuram Parthasarathy, P.; Rubagotti, E.; Rumisha, S. F.; Russo, M.; Rwegerera, G. M.; Saad, A. M. A.; Sabbatucci, M.; Saber-Ayad, M. M.; Sabour, S.; Sachdev, P. S.; Sadat Rafiei, S. K.; Saddik, B. A.; Sadee, B. A.; Sadegh, T.; Sadeghi, E.; Sadeghi, E.; Sadeghi-Ghyassi, F.; Saeed, M.; Saeed, U.; Saeedi, M.; Safdarian, M.; Safi, S.; Safi, S. Z.; Sagar, R.; Sagharichi, M.; Saghazadeh, A.; Sagoe, D.; Saha, I.; Saha, N.; Saheb Sharif-Askari, F.; Saheb Sharif-Askari, N.; Sahebkar, A.; Sahu, K. S.; Saif, Z.; Sajadi, S. M.; Sajib, M. R. U. Z.; Sajid, M. R.; Salabat, D.; Salamati, P.; Salaroli, L. B.; Saleh, M. A.; Salehi, L.; Salehi, M.; Salem, M. R.; Salem, M. Z. Y.; Salemcity, A. J.; Salihu, D.; Salimi, S.; Sallam, M.; Samadi Kafil, H.; Samaranayake, J. E.; Samargandy, S.; Sami, W.; Samodra, Y. L.; Samy, A. M.; Sangle, S. G.; Sanjari, E.; Sankar, S.; Sanmarchi, F.; Sanna, F.; Santomauro, D. F.; Santos, I. S.; Santos, L. H. C. C.; Santric-Milicevic, M. M.; Sanyaolu, A.; Sao Jose, B. P.; Sapkota, K. P.; Saraswathy, S. Y. I.; Sarikhani, Y.; Sarma, H.; Sarmadi, M.; Sarode, G. S.; Sarode, S. C.; Sartorius, B.; Sarveazad, A.; Sassano, M.; Sathya Narayanan, M. K.; Satpathy, M.; Sattarpour, R.; Sattin, D.; Savabi Far, M.; Sawhney, M.; Saxena, S. G.; Saya, G. K.; Sayeed, A.; Schinckus, C.; Schmidt, J. C.; Schmidt, M. I.; Schneider, R. D.; Schuermans, A.; Schumacher, A. E.; Schutte, A. E.; Schwarz, G.; Schwebel, D. C.; Schwendicke, F.; Sebastian, S. A.; Sedigh, A.; Seedat, S.; Šekerija, M.; Selvamani, M.; Selvaraj, V.; Semenova, Y.; Semreen, M. H.; Sendeku, F. W.; Sengupta, P.; Senol, Y. C.; Senthilkumaran, S.; Sepanlou, S. G.; Serván-Mori, E.; Sethi, Y.; Seyed

Alshohadaei, S. M.; Seylani, A.; Sha'aban, A.; Shafie, M.; Shafieioun, A.; Shaharudin, S.; Shahbaz, M.; Shahid, S.; Shahid, S. A.; Shahini, E.; Shahrahmani, F.; Shahsavari, H. R.; Shahwan, M. J.; Shaikh, M. A.; Shakeri, A.; Shakerimoghaddam, A.; Shalash, A. S.; Shamim, M. A.; Shams, F.; Shams-Beyranvand, M.; Shamsi, A.; Shamsutdinova, A.; Shan, D.; Shan, S.; Shanawaz, M.; Sharifan, A.; Sharifi Rad, J.; Sharma, A.; Sharma, B. K.; Sharma, B.; Sharma, G.; Sharma, K.; Sharma, K.; Sharma, M.; Sharma, R. K.; Sharma, U.; Sharma, V.; Shastry, S.; Shayan, M.; Shehu Bappah, B.; Sheida, F.; Sheidaei, A.; Sheikhy, A.; Shenoy, R. R.; Sherchan, S. P.; Shetty, B. S. K.; Shetty, S.; Shi, F.; Shi, F.; Shiani, A.; Shibesh, B. F.; Shibuya, K.; Shiferaw, D.; Shimels, T.; Shimul, M. M. H.; Shin, M.-J.; Shiri, R.; Shirkoohi, R.; Shittu, A.; Shitu, A. O.; Shiue, I.; Shivarov, V.; Shlobin, N. A.; Shoaib, A.; Shojaei, S.; Shool, S.; Shorofi, S. A.; Shrestha, S.; Shuaibu, S. A.; Shuval, K.; Siavashpour, Z.; Sibuyi, N. R. S.; Siddig, E. E.; Siddiqi, A. K.; Silva, D. A. S.; Silva, J. P.; Silva, L. M. L. R.; Simkhada, P. P.; Simonetti, B.; Singh, A.; Singh, A.; Singh, B. B.; Singh, B.; Singh, B. P.; Singh, H.; Singh, H.; Singh, J. A.; Singh, J.; Singh, K.; Singh, M.; Singh, N. P.; Singh, P.; Singh, P. S.; Singh, P.; Singh, R. K.; Singh, S.; Singh, S.; Singh, S.; Singh, S.; Sinha, M. K.; Sinto, R.; Sirota, S. B.; Siyoum, D. F.; Skhvitaridze, N.; Skryabina, A. A.; Sleet, D. A.; SobhZahedi, M.; Soheili, M.; Sohel, M.; Sohrabi, S.; Solanki, S.; Solbana, L. K.; Solikhah, S.; Soliman, S. S. M.; Song, W.; Sood, A.; Sood, P.; Soraneh, S.; Sorensen, R. J. D.; Soriano, J. B.; Sousa, F.; Sousa, M. A.; Soyiri, I. N.; Soylu, C.; Spartalis, M.; Sreeramareddy, C. T.; Srinivasamurthy, S. K.; Sriram, S.; Srivastav, P.; Srivastava, D. B.; Stafford, L. K.; Stanaway, J. D.; Stanikzai, M. H.; Steckling-Muschack, N.; Stein, D. J.; Steiner, C.; Steinmetz, J. D.; Steiropoulos, P.; Stephan, B. C. M.; Stevanović, A.; Stockfelt, L.; Straube, S.; Stubbs, J. L.; Stubbs, P.; Subasi, O.; Subedi, N.; Suhag, A.; Sujon, H.; Sukaew, T.; Sulaiman, S. K.; Suleiman, A. G.; Suleiman Odidi, M.; Suleman, M.; Sullman, M. J. M.; Sultan Meo, A.; Sun, H. Z.; Sun, J.; Sun, M.; Sun, X.; Sun, X.; Sun, Z.; Sun, Z.; Sundaragiri, S.; Sundaram, T.; Sundström, J.; Sunkersing, D.; Sunny, S.; Suresh, V.; Susianti, H.; Swain, C. K.; Swart, V. M.; Syaiful, D. A.; Symons, T. L.; Szarpak, L.; Szeto, M. D.; T Y, S. S.; Tabaee Damavandi, P.; Tabarés-Seisdedos, R.; Tabatabaei, F. S.; Tabatabaei, S. S.; Tabatabaei, S. M.; Tabatabaeizadeh, S.-A.; Tabatabai, S.; Tabche, C.; Tabish, M.; Tabuchi, T.; Tadesse, G. F.; Taghizadeh-Hesary, F.; Taha, Z. M.-A.; Taiba, J.; Tajabadi, S.; Talaat, I. M.; Tampa, M.; Tamuzi, J. L.; Tan, K.-K.; Tanashat, M.; Tang, H.; Tanveer, M.; Tareke, A. A.; Taridashti, S.; Tarigan, I. U.; Tariku, M. K.; Tariq, S.; Tazhiyeva, A. Y.; Temedie-Asogwa, T.; Temsah, M.-H.; Teramoto, M.; Tesfu, A. A.; Teshager, N. W.; Tessema, G. A.; Tewari, J.; Teymouri, A.; Thakur, C. K.;

Thankappan, K. R.; Thapar, R.; Tharwat, I.; Tharwat, S.; Thayakaran, R.; Thiruvengadam, M.; Thomas, M. S.; Tian, W.; Ticoalu, J. H. V.; Tleshev, M.; Tomo, S.; Tonelli, M.; Topor-Madry, R.; Touvier, M.; Tovani-Palone, M. R.; Trabelsi, K.; Tran, Q. T. H.; Tran, T. Q. M.; Tran, T. H.; Tran Minh Duc, N.; Trico, D.; Trihandini, I.; Tripathi, M.; Tripathi, T.; Tromans, S. J.; Truong, Q. X. N.; Truyen, T. T. T. T.; Tse, G.; Tseriotis, V.-S.; Tsermpini, E. E.; Tudor Car, L.; Tumurkhuu, M.; Tuo, Z.; Tusa, B. S.; Tye, S. C.; Tyrovolas, S.; Udoakang, A. J.; Ullah, A.; Ullah, H.; Ullah, S.; Umair, M.; Umar, H. O.; Umar, L.; Umar, M.; Umar, M.; Umar, S. S.; Undurraga, E. A.; Unnikrishnan, B.; Upadhya, D.; Upadhyay, E.; Uppal, D.; Urso, D.; Usman, J. S.; Uzor, K. J.; Uzunçıbuk, H.; Vadagam, P.; Vaithinathan, A. G.; Valdez, P. R.; Valenti, M.; Vally, Z.; Van Den Eynde, J.; Varasteh, J.; Varghese, J.; Varma, P.; Vasankari, T. J.; Vasishta, S.; Vasudevan, S. S.; Vaysi, A.; Vaziri, S.; Venketasubramanian, N.; Verma, M.; Verma, M.; Verma, P.; Veroux, M.; Verras, G.-I.; Vidale, S.; Vijayageetha, M.; Villa, S.; Villafañe, J. H.; Villani, L.; Villarreal-Zegarra, D.; Violante, F. S.; Visaga Ambi, S.; Vitorino, L. M.; Vlassov, V.; Vollset, S. E.; Vongpradith, A.; Vos, T.; Vosoughi, M.; Vounzoulaki, E.; Vu, L.; Vujcic, I. S.; Vyas, K. D.; Wada, H. T.; Waheed, Y.; Wahid, M.; Wahidin, M.; Walde, M. T.; Walia, M.; Wan, J.-Y.; Wander, A.; Wang, F.; Wang, F.; Wang, J.; Wang, L.; Wang, Q.; Wang, R.; Wang, S.; Wang, W.; Wang, X.; Wang, X.; Wang, Y.; Wang, Y.; Wang, Y.; Wang, Y.; Wang, Y.-P.; Wang, Z.; Wani, T. A.; Wanjau, M. N.; Waqar, A. B.; Waqas, M.; Ward, J. W.; Ward, P.; Wassie, T. H.; Watson, S.; Weerasekara, I.; Wei, F.-L.; Wei, X.; Weintraub, R. G.; Weiss, D. J.; Weiss, E. J.; Wells, K. M.; Werdecker, A.; Westerman, R.; Wiangkham, T.; Wibowo, Y. C.; Wickramasinghe, D. P.; Wickramasinghe, N. D.; Wiebe, S.; Wilandika, A.; Willeit, P.; Wilson, S.; Wireko, A. A.; Wiysonge, C. S.; Woday, A. T.; Wojtyniak, B.; Woldehana, N. A.; Woldeyes, D. H.; Wolf, A. W.; Wonde, T. E.; Wong, Y. J.; Worede, D. T.; Workicho, A.; Worku, M. C.; Wu, A.-M.; Wu, C.; Wu, F.; Wu, J. F.; Wu, J.; Wu, P.; Wu, Z.; Wubie, Y. M.; Wulandari, R. D.; Xia, Z.; Xiao, G.; Xiao, L.; Xiao, N.; Xie, W.; Xu, S.; Xu, S.; Xu, X.; Xu, Y. Y.; Yadav, M. K.; Yadav, V.; Yadollahi, M.; Yahoo (Syed), S.; Yahya, G.; Yamagishi, K.; Yan, G.; Yang, H.; Yano, Y.; Yao, H.; Yao, L.; Yarahmadi, A.; Yaribeygi, H.; Yasin, H.; Yassin, M. A.; Yasufuku, Y.; Yaya, S.; Ye, P.; Yeganeh, M.; Yekdeş, A. C.; YektaKooshali, M. H.; Yergaliyev, K. A.; Yesuf, S. A.; Yezli, S.; Yi, S.; Yin, D.; Yip, P.; Yismaw, M. B.; Yismaw, Y. E.; Yon, D. K.; Yonemoto, N.; Yoon, S.-J.; Younis, M. Z.; Yousefi, S.; Yousuf, A.; Yu, C.; Yu, Y.; Yuan, H.; Yuh, F. H.; Yunus, G.; Yunusa, U.; Zadey, S.; Zadnik, V.; Zafar, M.; Zaghampour, M.; Zainal Abidin, E.; Zakham, F.; Zaki, N.; Zamagni, G.; Zamora, N.; Zandam, H.; Zanghì, A.; Zar, H. J.; Zarea, K.; Zawiah, M.; Zeariya, M. G. M.; Zenebe, A. M.; Zensen, S.; Zepro, N. B.; Zeru, E. M.; Zhan,

T.; Zhan, Y.; Zhang, B.; Zhang, C. J. P.; Zhang, H.; Zhang, J. M. F.; Zhang, K.; Zhang, L.; Zhang, M.; Zhang, X.; Zhang, X.-H.; Zhang, Y.; Zhang, Z.; Zhangelova, S. B.; Zhao, H.; Zhao, J.; Zhao, J.; Zhao, Y.; Zhao, Z.; Zhong, A.; Zhong, C. C.; Zhou, J.; Zhou, J.; Zhu, B.; Zhumagaliuly, A.; Zielińska, M.; Zoghi, G.; Zoromba, M. A.; Zou, Z.; Zrieq, R. M.; Zuhlke, L. J.; Zuhriyah, L.; Zumla, A.; Zyoud, A. H.; Zyoud, S. H.; Zyoud, S. H.; Wool, E. E.; Murray, C. J. L. Global Burden of 292 Causes of Death in 204 Countries and Territories and 660 Subnational Locations, 1990–2023: A Systematic Analysis for the Global Burden of Disease Study 2023. *The Lancet* **2025**, *406* (10513), 1811–1872. https://doi.org/10.1016/S0140-6736(25)01917-8.

(103) Hellwig, M.; Henle, T. Baking, Ageing, Diabetes: A Short History of the Maillard Reaction. *Angew. Chem. Int. Ed.* **2014**, *53* (39), 10316–10329. https://doi.org/10.1002/anie.201308808.

(104) Ahmad, A.; Imran, M.; Ahsan, H. Biomarkers as Biomedical Bioindicators: Approaches and Techniques for the Detection, Analysis, and Validation of Novel Biomarkers of Diseases. *Pharmaceutics* **2023**, *15* (6), 1630. https://doi.org/10.3390/pharmaceutics15061630.

(105) Phuong-Nguyen, K.; McNeill, B. A.; Aston-Mourney, K.; Rivera, L. R. Advanced Glycation End-Products and Their Effects on Gut Health. *Nutrients* **2023**, *15* (2), 405. https://doi.org/10.3390/nu15020405.

(106) Rabbani, N.; Thornalley, P. J. Protein Glycation – Biomarkers of Metabolic Dysfunction and Early-Stage Decline in Health in the Era of Precision Medicine. *Redox Biol.* **2021**, *42*, 101920. https://doi.org/10.1016/j.redox.2021.101920.

(107) Martin, M. S.; Jacob-Dolan, J. W.; Pham, V. T. T.; Sjoblom, N. M.; Scheck, R. A. The Chemical Language of Protein Glycation. *Nat. Chem. Biol.* **2025**, *21* (3), 324–336. https://doi.org/10.1038/s41589-024-01644-y.

(108) Zhong, Q.; Xiao, X.; Qiu, Y.; Xu, Z.; Chen, C.; Chong, B.; Zhao, X.; Hai, S.; Li, S.; An, Z.; Dai, L. Protein Posttranslational Modifications in Health and Diseases: Functions, Regulatory Mechanisms, and Therapeutic Implications. *MedComm* **2023**, *4* (3), e261. https://doi.org/10.1002/mco2.261.

(109) Twarda-Clapa, A.; Olczak, A.; Białkowska, A. M.; Koziołkiewicz, M. Advanced Glycation End-Products (AGEs): Formation, Chemistry, Classification, Receptors, and Diseases Related to AGEs. *Cells* **2022**, *11* (8), 1312. https://doi.org/10.3390/cells11081312.

(110) Bronowicka-Szydełko, A.; Gostomska-Pampuch, K.; Kuzan, A.; Pietkiewicz, J.; Krzystek-Korpacka, M.; Gamian, A. Effect of Advanced Glycation End-Products in a Wide Range of Medical Problems Including

COVID-19. *Adv. Med. Sci.* **2024**, *69* (1), 36–50. https://doi.org/10.1016/j.advms.2024.01.003.
(111) Ashraf, J. Mohd.; Ahmad, S.; Choi, I.; Ahmad, N.; Farhan, Mohd.; Tatyana, G.; Shahab, U. Recent Advances in Detection of AGEs: Immunochemical, Bioanalytical and Biochemical Approaches: Technological Progress in Age Detection. *IUBMB Life* **2015**, *67* (12), 897–913. https://doi.org/10.1002/iub.1450.
(112) Maruthur, N. M.; Li, M.; Halushka, M. K.; Astor, B. C.; Pankow, J. S.; Boerwinkle, E.; Coresh, J.; Selvin, E.; Kao, W. H. L. Genetics of Plasma Soluble Receptor for Advanced Glycation End-Products and Cardiovascular Outcomes in a Community-Based Population: Results from the Atherosclerosis Risk in Communities Study. *PLOS ONE* **2015**, *10* (6), e0128452. https://doi.org/10.1371/journal.pone.0128452.
(113) Petrica, L.; Vlad, A.; Gluhovschi, G.; Zamfir, A.; Popescu, C.; Gadalean, F.; Dumitrascu, V.; Vlad, D.; Popescu, R.; Velciov, S.; Gluhovschi, C.; Bob, F.; Milas, O.; Ursoniu, S. Glycated Peptides Are Associated with Proximal Tubule Dysfunction in Type 2 Diabetes Mellitus. *Int. J. Clin. Exp. Med.* **2015**, *8* (2), 2516–2525.
(114) Raghavan, C. T. Advanced Glycation End Products in Neurodegenerative Diseases. *J. Mol. Neurosci.* **2024**, *74* (4), 114. https://doi.org/10.1007/s12031-024-02297-1.
(115) Turk, Z. Glycation and Age in Diabetes and Complications. *EJIFCC* **2002**, *13* (5), 210–214.
(116) Chaudhuri, J.; Bains, Y.; Guha, S.; Kahn, A.; Hall, D.; Bose, N.; Gugliucci, A.; Kapahi, P. The Role of Advanced Glycation End Products in Aging and Metabolic Diseases: Bridging Association and Causality. *Cell Metab.* **2018**, *28* (3), 337–352. https://doi.org/10.1016/j.cmet.2018.08.014.
(117) Vlassara, H.; Uribarri, J. Advanced Glycation End Products (AGE) and Diabetes: Cause, Effect, or Both? *Curr. Diab. Rep.* **2014**, *14* (1), 453. https://doi.org/10.1007/s11892-013-0453-1.
(118) Frolov, A.; Blüher, M.; Hoffmann, R. Glycation Sites of Human Plasma Proteins Are Affected to Different Extents by Hyperglycemic Conditions in Type 2 Diabetes Mellitus. *Anal. Bioanal. Chem.* **2014**, *406* (24), 5755–5763. https://doi.org/10.1007/s00216-014-8018-y.
(119) Kisugi, R.; Kouzuma, T.; Yamamoto, T.; Akizuki, S.; Miyamoto, H.; Someya, Y.; Yokoyama, J.; Abe, I.; Hirai, N.; Ohnishi, A. Structural and Glycation Site Changes of Albumin in Diabetic Patient with Very High Glycated Albumin. *Clin. Chim. Acta* **2007**, *382* (1–2), 59–64. https://doi.org/10.1016/j.cca.2007.04.001.

(120) Furusyo, N.; Hayashi, J. Glycated Albumin and Diabetes Mellitus. *Biochim. Biophys. Acta BBA - Gen. Subj.* **2013**, *1830* (12), 5509–5514. https://doi.org/10.1016/j.bbagen.2013.05.010.
(121) Furusyo, N.; Koga, T.; Ai, M.; Otokozawa, S.; Kohzuma, T.; Ikezaki, H.; Schaefer, E. J.; Hayashi, J. Plasma Glycated Albumin Level and Atherosclerosis: Results from the Kyushu and Okinawa Population Study (KOPS). *Int. J. Cardiol.* **2013**, *167* (5), 2066–2072. https://doi.org/10.1016/j.ijcard.2012.05.045.
(122) English, E.; Lenters-Westra, E. HbA1c Method Performance: The Great Success Story of Global Standardization. *Crit. Rev. Clin. Lab. Sci.* **2018**, *55* (6), 408–419. https://doi.org/10.1080/10408363.2018.1480591.
(123) Kaiafa, G.; Veneti, S.; Polychronopoulos, G.; Pilalas, D.; Daios, S.; Kanellos, I.; Didangelos, T.; Pagoni, S.; Savopoulos, C. Is HbA1c an Ideal Biomarker of Well-Controlled Diabetes? *Postgrad. Med. J.* **2021**, *97* (1148), 380–383. https://doi.org/10.1136/postgradmedj-2020-138756.
(124) Siricharoenthai, P.; Phupong, V. Diagnostic Accuracy of HbA1c in Detecting Gestational Diabetes Mellitus. *J. Matern. Fetal Neonatal Med.* **2020**, *33* (20), 3497–3500. https://doi.org/10.1080/14767058.2019.1576169.
(125) Xiong, W.; Zeng, Z.-H.; Xu, Y.; Li, H.; Lin, H. Circulating Glycated Albumin Levels and Gestational Diabetes Mellitus. *World J. Diabetes* **2024**, *15* (8), 1802–1810. https://doi.org/10.4239/wjd.v15.i8.1802.
(126) Gan, T.; Liu, X.; Xu, G. Glycated Albumin Versus HbA1c in the Evaluation of Glycemic Control in Patients With Diabetes and CKD. *Kidney Int. Rep.* **2018**, *3* (3), 542–554. https://doi.org/10.1016/j.ekir.2017.11.009.
(127) Gan, L.; Du, X.; Wei, Y.; Hu, Z. Sources of Advanced Glycation End Products in the Human Body: A Mini Review. *Int. J. Food Sci. Technol.* **2025**, *60* (1), vvaf119. https://doi.org/10.1093/ijfood/vvaf119.
(128) Zhang, M.; Xu, W.; Deng, Y. A New Strategy for Early Diagnosis of Type 2 Diabetes by Standard-Free, Label-Free LC-MS/MS Quantification of Glycated Peptides. *Diabetes* **2013**, *62* (11), 3936–3942. https://doi.org/10.2337/db13-0347.
(129) Qiu, H.; Jin, L.; Chen, J.; Shi, M.; Shi, F.; Wang, M.; Li, D.; Xu, X.; Su, X.; Yin, X.; Li, W.; Zhou, X.; Linhardt, R. J.; Wang, Z.; Chi, L.; Zhang, Q. Comprehensive Glycomic Analysis Reveals That Human Serum Albumin Glycation Specifically Affects the Pharmacokinetics and Efficacy of Different Anticoagulant Drugs in Diabetes. *Diabetes* **2020**, *69* (4), 760–770. https://doi.org/10.2337/db19-0738.
(130) Thornalley, P. J.; Battah, S.; Ahmed, N.; Karachalias, N.; Agalou, S.; Babaei-Jadidi, R.; Dawnay, A. Quantitative Screening of Advanced Glycation

Endproducts in Cellular and Extracellular Proteins by Tandem Mass Spectrometry. *Biochem. J.* **2003**, *375* (3), 581–592. https://doi.org/10.1042/bj20030763.

(131) Zhang, Q.; Tang, N.; Brock, J. W. C.; Mottaz, H. M.; Ames, J. M.; Baynes, J. W.; Smith, R. D.; Metz, T. O. Enrichment and Analysis of Nonenzymatically Glycated Peptides: Boronate Affinity Chromatography Coupled with Electron-Transfer Dissociation Mass Spectrometry. *J. Proteome Res.* **2007**, *6* (6), 2323–2330. https://doi.org/10.1021/pr070112q.

(132) Soboleva, A.; Vikhnina, M.; Grishina, T.; Frolov, A. Probing Protein Glycation by Chromatography and Mass Spectrometry: Analysis of Glycation Adducts. *Int. J. Mol. Sci.* **2017**, *18* (12), 2557. https://doi.org/10.3390/ijms18122557.

(133) Thornalley, P. J.; Battah, S.; Ahmed, N.; Karachalias, N.; Agalou, S.; Babaei-Jadidi, R.; Dawnay, A. Quantitative Screening of Advanced Glycation Endproducts in Cellular and Extracellular Proteins by Tandem Mass Spectrometry. *Biochem. J.* **2003**, *375* (3), 581–592. https://doi.org/10.1042/bj20030763.

(134) Jeanethe Anguizola. AFFINITY CHROMATOGRAPHIC STUDIES OF DRUG-PROTEIN BINDING IN PERSONALIZED MEDICINE. **2013**.

(135) Beisswenger, P. J.; Howell, S.; Mackenzie, T.; Corstjens, H.; Muizzuddin, N.; Matsui, M. S. Two Fluorescent Wavelengths, 440_{ex} /520_{em} Nm and 370_{ex} /440_{em} Nm, Reflect Advanced Glycation and Oxidation End Products in Human Skin Without Diabetes. *Diabetes Technol. Ther.* **2012**, *14* (3), 285–292. https://doi.org/10.1089/dia.2011.0108.

(136) Monnier, V. M.; Kohn, R. R.; Cerami, A. Accelerated Age-Related Browning of Human Collagen in Diabetes Mellitus. *Proc. Natl. Acad. Sci.* **1984**, *81* (2), 583–587. https://doi.org/10.1073/pnas.81.2.583.

(137) Baynes, J. W. The Role of AGEs in Aging: Causation or Correlation. *Exp. Gerontol.* **2001**, *36* (9), 1527–1537. https://doi.org/10.1016/S0531-5565(01)00138-3.

(138) Meerwaldt, R.; Links, T.; Graaff, R.; Thorpe, S. R.; Baynes, J. W.; Hartog, J.; Gans, R.; Smit, A. Simple Noninvasive Measurement of Skin Autofluorescence. *Ann. N. Y. Acad. Sci.* **2005**, *1043* (1), 290–298. https://doi.org/10.1196/annals.1333.036.

(139) Springsteen, G.; Wang, B. A Detailed Examination of Boronic Acid–Diol Complexation. *Tetrahedron* **2002**, *58* (26), 5291–5300. https://doi.org/10.1016/S0040-4020(02)00489-1.

(140) Lacina, K.; Skládal, P.; James, T. D. Boronic Acids for Sensing and Other Applications - a Mini-Review of Papers Published in 2013. *Chem. Cent. J.* **2014**, *8* (1), 60. https://doi.org/10.1186/s13065-014-0060-5.
(141) Yan, J.; Fang, H.; Wang, B. Boronolectins and Fluorescent Boronolectins: An Examination of the Detailed Chemistry Issues Important for the Design. *Med. Res. Rev.* **2005**, *25* (5), 490–520. https://doi.org/10.1002/med.20038.
(142) Liu, Z.; He, H. Synthesis and Applications of Boronate Affinity Materials: From Class Selectivity to Biomimetic Specificity. *Acc. Chem. Res.* **2017**, *50* (9), 2185–2193. https://doi.org/10.1021/acs.accounts.7b00179.
(143) The Development of the Boronate Affinity Chromatography and Biotime's Success, 2022.
(144) Szarek, W. A.; Martin, O. R.; Rafka, R. J.; Cameron, T. S. Structure–Sweetness Relationships for Fructose Analogs. Part II. Synthesis and Properties of 1,6-Dihydroxy-2-Hexanone, a Simple Analog of the Ketohexoses, and X-Ray Structure Determination of the Corresponding Dianhydrides. *Can. J. Chem.* **1985**, *63* (6), 1222–1227. https://doi.org/10.1139/v85-208.
(145) James, T. D. Saccharide-Selective Boronic Acid Based Photoinduced Electron Transfer (PET) Fluorescent Sensors. In *Creative Chemical Sensor Systems*; Schrader, T., Ed.; Topics in Current Chemistry; Springer Berlin Heidelberg: Berlin, Heidelberg, 2007; Vol. 277, pp 107–152. https://doi.org/10.1007/128_2007_110.
(146) Xiao, H.; Chen, W.; Smeekens, J. M.; Wu, R. An Enrichment Method Based on Synergistic and Reversible Covalent Interactions for Large-Scale Analysis of Glycoproteins. *Nat. Commun.* **2018**, *9* (1), 1692. https://doi.org/10.1038/s41467-018-04081-3.
(147) Zhu, R.; Song, E.; Hussein, A.; Kobeissy, F. H.; Mechref, Y. Glycoproteins Enrichment and LC-MS/MS Glycoproteomics in Central Nervous System Applications. In *Neuroproteomics*; Kobeissy, F. H., Stevens, S. M., Eds.; Methods in Molecular Biology; Springer New York: New York, NY, 2017; Vol. 1598, pp 213–227. https://doi.org/10.1007/978-1-4939-6952-4_9.
(148) Zhu, R.; Zacharias, L.; Wooding, K. M.; Peng, W.; Mechref, Y. Glycoprotein Enrichment Analytical Techniques. In *Methods in Enzymology*; Elsevier, 2017; Vol. 585, pp 397–429. https://doi.org/10.1016/bs.mie.2016.11.009.
(149) Fang, G.; Wang, H.; Bian, Z.; Sun, J.; Liu, A.; Fang, H.; Liu, B.; Yao, Q.; Wu, Z. Recent Development of Boronic Acid-Based Fluorescent Sensors. *RSC Adv.* **2018**, *8* (51), 29400–29427. https://doi.org/10.1039/C8RA04503H.

(150) Goldberg, D.; Bentwich, I.; Haran, Y.; Getter, T. Design and Synthesis of Novel Di-Boronic Acid-Based Chemical Glucose Sensors. *ACS Omega* **2025**, *10* (11), 10812–10825. https://doi.org/10.1021/acsomega.4c06237.
(151) Ansari, N. A.; Rasheed, Z. Non-enzymatic glycation of proteins: from diabetes to cancer. *Biomeditsinskaya Khimiya* **2010**, *56* (2), 168–178. https://doi.org/10.18097/pbmc20105602168.
(152) Cao, L.; Qu, Y.; Zhang, Z.; Wang, Z.; Prytkova, I.; Wu, S. Intact Glycopeptide Characterization Using Mass Spectrometry. *Expert Rev. Proteomics* **2016**, *13* (5), 513–522. https://doi.org/10.1586/14789450.2016.1172965.
(153) Welsh, K. J.; Kirkman, M. S.; Sacks, D. B. Role of Glycated Proteins in the Diagnosis and Management of Diabetes: Research Gaps and Future Directions. *Diabetes Care* **2016**, *39* (8), 1299–1306. https://doi.org/10.2337/dc15-2727.
(154) Berger, M. T.; Hemmler, D.; Walker, A.; Rychlik, M.; Marshall, J. W.; Schmitt-Kopplin, P. Molecular Characterization of Sequence-Driven Peptide Glycation. *Sci. Rep.* **2021**, *11* (1), 13294. https://doi.org/10.1038/s41598-021-92413-7.
(155) Ruan, E. D.; Wang, H.; Ruan, Y.; Juárez, M. Study of Fragmentation Behavior of Amadori Rearrangement Products in Lysine-Containing Peptide Model by Tandem Mass Spectrometry. *Eur. J. Mass Spectrom.* **2013**, *19* (4), 295–303. https://doi.org/10.1255/ejms.1237.
(156) Fedorova, M.; Frolov, A.; Hoffmann, R. Fragmentation Behavior of Amadori-peptides Obtained by Non-enzymatic Glycosylation of Lysine Residues with ADP-ribose in Tandem Mass Spectrometry. *J. Mass Spectrom.* **2010**, *45* (6), 664–669. https://doi.org/10.1002/jms.1758.
(157) Barnaby, O. S.; Cerny, R. L.; Clarke, W.; Hage, D. S. Quantitative Analysis of Glycation Patterns in Human Serum Albumin Using 16O/18O-Labeling and MALDI–TOF MS. *Clin. Chim. Acta* **2011**, *412* (17–18), 1606–1615. https://doi.org/10.1016/j.cca.2011.05.012.
(158) Kumari, N.; Vaishnav, M. S.; Srikanta, S.; Krishnaswamy, P. R.; Bhat, N. Exploring Glycated Sites in Human Serum Albumin: Impact of Sample Processing Techniques on Detection and Analysis. *Anal. Methods* **2024**, *16* (30), 5239–5247. https://doi.org/10.1039/D4AY00503A.
(159) Wa, C.; Cerny, R. L.; Clarke, W. A.; Hage, D. S. Characterization of Glycation Adducts on Human Serum Albumin by Matrix-Assisted Laser Desorption/Ionization Time-of-Flight Mass Spectrometry. *Clin. Chim. Acta* **2007**, *385* (1–2), 48–60. https://doi.org/10.1016/j.cca.2007.06.011.

(160) Lapolla, A.; Molin, L.; Traldi, P. Protein Glycation in Diabetes as Determined by Mass Spectrometry. *Int. J. Endocrinol.* **2013**, *2013*, 1–11. https://doi.org/10.1155/2013/412103.
(161) Sun, W.; Wu, S.; Wang, X.; Zheng, D.; Gao, Y. A Systematical Analysis of Tryptic Peptide Identification with Reverse Phase Liquid Chromatography and Electrospray Ion Trap Mass Spectrometry. *Genomics Proteomics Bioinformatics* **2004**, *2* (3), 174–183. https://doi.org/10.1016/S1672-0229(04)02023-6.
(162) Stefanowicz, P.; Kapczynska, K.; Jaremko, M.; Jaremko, Ł.; Szewczuk, Z. A Mechanistic Study on the Fragmentation of Peptide-derived Amadori Products. *J. Mass Spectrom.* **2009**, *44* (10), 1500–1508. https://doi.org/10.1002/jms.1639.
(163) Zhang, Q.; Petyuk, V. A.; Schepmoes, A. A.; Orton, D. J.; Monroe, M. E.; Yang, F.; Smith, R. D.; Metz, T. O. Analysis of Non-enzymatically Glycated Peptides: Neutral-loss-triggered MS^3 versus Multi-stage Activation Tandem Mass Spectrometry. *Rapid Commun. Mass Spectrom.* **2008**, *22* (19), 3027–3034. https://doi.org/10.1002/rcm.3703.
(164) Frolov, A.; Hoffmann, R. Identification and Relative Quantification of Specific Glycation Sites in Human Serum Albumin. *Anal. Bioanal. Chem.* **2010**, *397* (6), 2349–2356. https://doi.org/10.1007/s00216-010-3810-9.
(165) Kumar, S. Developments, Advancements, and Contributions of Mass Spectrometry in Omics Technologies. In *Advances in Protein Molecular and Structural Biology Methods*; Elsevier, 2022; pp 327–356. https://doi.org/10.1016/B978-0-323-90264-9.00021-0.
(166) Dudley, E.; Bond, A. E. Phosphoproteomic Techniques and Applications. In *Advances in Protein Chemistry and Structural Biology*; Elsevier, 2014; Vol. 95, pp 25–69. https://doi.org/10.1016/B978-0-12-800453-1.00002-6.
(167) Hunt, D. F.; Yates, J. R.; Shabanowitz, J.; Winston, S.; Hauer, C. R. Protein Sequencing by Tandem Mass Spectrometry. *Proc. Natl. Acad. Sci.* **1986**, *83* (17), 6233–6237. https://doi.org/10.1073/pnas.83.17.6233.
(168) Neagu, A.-N.; Jayathirtha, M.; Baxter, E.; Donnelly, M.; Petre, B. A.; Darie, C. C. Applications of Tandem Mass Spectrometry (MS/MS) in Protein Analysis for Biomedical Research. *Molecules* **2022**, *27* (8), 2411. https://doi.org/10.3390/molecules27082411.
(169) Sakurai, Toru.; Ito, Hiroyuki.; Matsuo, Takekiyo. MS/MS and MS/MS/MS Analyses in a Multisector Time-of-Flight Mass Spectrometer. *Anal. Chem.* **1994**, *66* (14), 2313–2317. https://doi.org/10.1021/ac00086a017.
(170) Halket, J. M.; Waterman, D.; Przyborowska, A. M.; Patel, R. K. P.; Fraser, P. D.; Bramley, P. M. Chemical Derivatization and Mass Spectral Libraries in

Metabolic Profiling by GC/MS and LC/MS/MS. *J. Exp. Bot.* **2005**, *56* (410), 219–243. https://doi.org/10.1093/jxb/eri069.

(171) Kijewska, M.; Nuti, F.; Wierzbicka, M.; Waliczek, M.; Ledwoń, P.; Staśkiewicz, A.; Real-Fernandez, F.; Sabatino, G.; Rovero, P.; Stefanowicz, P.; Szewczuk, Z.; Papini, A. M. An Optimised Di-Boronate-ChemMatrix Affinity Chromatography to Trap Deoxyfructosylated Peptides as Biomarkers of Glycation. *Molecules* **2020**, *25* (3), 755. https://doi.org/10.3390/molecules25030755.

(172) Qiu, H.-Y.; Hou, N.-N.; Shi, J.-F.; Liu, Y.-P.; Kan, C.-X.; Han, F.; Sun, X.-D. Comprehensive Overview of Human Serum Albumin Glycation in Diabetes Mellitus. *World J. Diabetes* **2021**, *12* (7), 1057–1069. https://doi.org/10.4239/wjd.v12.i7.1057.

(173) Al-Harthi, S.; Lachowicz, J. I.; Nowakowski, M. E.; Jaremko, M.; Jaremko, Ł. Towards the Functional High-Resolution Coordination Chemistry of Blood Plasma Human Serum Albumin. *J. Inorg. Biochem.* **2019**, *198*, 110716. https://doi.org/10.1016/j.jinorgbio.2019.110716.

(174) Lapolla, A.; Fedele, D.; Reitano, R.; Aricò, N. C.; Seraglia, R.; Traldi, P.; Marotta, E.; Tonani, R. Enzymatic Digestion and Mass Spectrometry in the Study of Advanced Glycation End Products/Peptides. *J. Am. Soc. Mass Spectrom.* **2004**, *15* (4), 496–509. https://doi.org/10.1016/j.jasms.2003.11.014.

(175) Kańska, U.; Boratyński, J. Thermal Glycation of Proteins by D-Glucose and D-Fructose. *Arch. Immunol. Ther. Exp. (Warsz.)* **2002**, *50* (1), 61–66.

La borsa di dottorato cofinanziata con risorse dell'Unione europea-*NextGeneration EU*
4.1 Borse PNRR patrimonio Culturale – *CUP B12B22000660007* Investimento 3.3 "Introduzione di dottorati innovativi che rispondono ai fabbisogni di innovazione delle imprese e promuovono l'assunzione dei ricercatori dalle imprese.